

**NANOCOMPOSITE MATERIALS PRECURSOR TO CHITOSAN  
IN THE DEVELOPMENT OF SENSORS: DETECTION OF  
MICRO-POLLUTANTS AND HEAVY METAL TOXIC IONS  
FROM AQUEOUS SOLUTIONS**

**A THESIS SUBMITTED IN PARTIAL FULFILMENT OF THE  
REQUIREMENTS FOR THE DEGREE OF DOCTOR OF  
PHILOSOPHY**

**SARIKOKBA**

**MZU REGISTRATION NUMBER: 2010616**

**Ph.D. REGISTRATION NUMBER: MZU/Ph.D./1176 OF 25.10.2018**



**DEPARTMENT OF CHEMISTRY  
SCHOOL OF PHYSICAL SCIENCES  
SEPTEMBER, 2022**

NANOCOMPOSITE MATERIALS PRECURSOR TO CHITOSAN IN  
THE DEVELOPMENT OF SENSORS: DETECTION OF MICRO-  
POLLUTANTS AND HEAVY METAL TOXIC IONS FROM  
AQUEOUS SOLUTIONS

BY  
SARIKOKBA  
Department of Chemistry

Under the supervision of  
Prof. DIWAKAR TIWARI

Submitted  
In partial fulfilment of the requirement of the Degree of Doctor of  
Philosophy in  
Chemistry of Mizoram University, Aizawl.



**MIZORAM UNIVERSITY**  
**Department of Chemistry**  
(A DST-FIST Supported Department)  
**Tanhril, Aizawl, Mizoram. PIN: 796004**

---

*Prof. Diwakar Tiwari, Dean (SPS)*

**Thesis Certificate**

This is to certify that the thesis entitled '*Nanocomposite materials precursor to chitosan in the development of sensors: Detection of micro-pollutants and heavy metal toxic ions from aqueous solutions*' submitted by **Mr. Sarikokba** for the degree of **Doctor of Philosophy** in the Mizoram University, Aizawl, Mizoram, embodies the record of original investigations carried out by him under my supervision. He has been duly registered and the thesis presented is worthy of being considered for the award of the Ph.D. degree. This work has not been submitted for any degree in any other university.

Dated: 22<sup>nd</sup> September, 2022.

(DIWAKAR TIWARI)

Supervisor

**Declaration of the Candidate**  
**Mizoram University**  
**September, 2022**

I, SARIKOKBA, hereby declare that the subject matter of this thesis is the record of work done by me, that the contents of this thesis did not form basis of the award of any previous degree to me or to the best of my knowledge to anybody else, and that the thesis has not been submitted by me for any research degree in any other University/Institute.

This is being submitted to the Mizoram University for the degree of Doctor of Philosophy in Chemistry.

Dated: 22<sup>nd</sup> September, 2022.

(SARIKOKBA)  
Candidate

(Prof. MUTHUKUMARAN)  
Head

(Prof. DIWAKAR TIWARI)  
Supervisor

## ACKNOWLEDGEMENT

I have great pleasure to express my heartfelt gratitude to my mentor and supervisor, *Prof. Diwakar Tiwari*, Department of Chemistry, Mizoram University. His dedication, genuine interest, and, most of all, his overwhelming attitude to assist his students had been solely responsible for the completion of my work. He is always ready to provide a fresh perspective and scholarly advice during my entire tenure. I admire his timely advice, scrutiny, and scientific approach, which have greatly aided me in completing this work.

I sincerely thank and give respect to *Prof. Muthukumaran, R.*, Head, Department of Chemistry, MZU, and other faculty members viz., *Dr. Zodinpuia Pachuau*, *Dr. N. Mohondas Singh*, *Dr. Ved Prakash Singh*, and *Dr. A. Bimolini Devi*, for their constant encouragement and useful advice they have offered me throughout my academic career in the University.

My heartfelt thanks go to *Dr. Lalhmunsiana* for his incentive and helpful suggestions in completing my research works.

I am grateful for the close cooperation and support I received from all of my colleagues in the Department of Chemistry. I'd like to thank *Dr. J. Lalmalsawm*, *Dr. R. Malsawmdawgnzela*, *Dr. Levia Lalthazuala*, *Ms. Ngainunsiami*, *Mr. CVL Hmingmawia*, *Mr. Ricky Lalawmpuia*, *Mr. Himangshu Dihingia*, *Ms. Melody Lalhrualthuangi*, *Ms. Swagata Goswami* and *Mr. Lalruatkima Ralte* for assisting me with my laboratory work. I owe a deep sense of gratitude to the assistance of *Mr. Brojendro Singh Shagolsem*, Sr. Laboratory Technician, and *Mr. John Vanlalhruaia*, Technical Assistant, Chemistry Department.

It is my privilege to thank my parents and all of my family members for their love and support during my tenure for the degree, as well as their comforts and prayers; I can't repay them entirely, but I thank and appreciate them from the bottom of my heart.

After all, I thank Almighty God for blessing me with health, strength, and knowledge to accomplish this work. Without his grace and mercy, this work would not have been possible.

(SARIKOKBA)

## TABLE OF CONTENTS

|                                                                       | Page No.  |
|-----------------------------------------------------------------------|-----------|
| Title of the Thesis                                                   | i         |
| Certificate                                                           | ii        |
| Declaration of the Candidate                                          | iii       |
| Acknowledgements                                                      | iv        |
| Table of Contents                                                     | v         |
| List of Figures                                                       | ix        |
| List of Tables                                                        | xiv       |
| <b>CHAPTER 1</b>                                                      |           |
| <b>1. INTRODUCTION</b>                                                | <b>1</b>  |
| <b>1.1. BACKGROUND</b>                                                | <b>1</b>  |
| <b>1.2. FATE OF POLLUTANTS AND THEIR TOXICITY</b>                     | <b>5</b>  |
| 1.2.1. Lead (Pb (II))                                                 | 5         |
| 1.2.2. Bisphenol A (BPA)                                              | 6         |
| 1.2.3. Triclosan (TCS)                                                | 9         |
| <b>1.3. REVIEW OF LITERATURE</b>                                      | <b>10</b> |
| <b>1.4. SCOPE OF PRESENT INVESTIGATION</b>                            | <b>19</b> |
| <b>CHAPTER 2</b>                                                      |           |
| <b>2. METHODOLOGY</b>                                                 | <b>21</b> |
| <b>2.1. CHITOSAN AND REAL WATER SAMPLES</b>                           | <b>21</b> |
| <b>2.2. CHEMICALS AND APPARATUS</b>                                   | <b>21</b> |
| <b>2.3. INSTRUMENTS</b>                                               | <b>27</b> |
| <b>2.4. ELECTROCHEMICAL METHODS</b>                                   | <b>29</b> |
| 2.4.1 Cyclic voltammetry                                              | 29        |
| 2.4.2. Pulse voltammetry technique                                    | 30        |
| 2.4.3. Electrochemical impedance spectroscopy                         | 32        |
| <b>2.5. MATERIALS PREPARATION</b>                                     | <b>33</b> |
| 2.5.1. Preparation of plant leave extracts ( <i>Psidium guajava</i> ) | 33        |

|                                                                            |    |
|----------------------------------------------------------------------------|----|
| 2.5.2. Leave extract Phytochemical analysis                                | 34 |
| 2.5.3. Composite/nanocomposite material synthesis                          | 35 |
| 2.5.4. Composite material synthesis                                        | 35 |
| 2.5.5. Casting solution preparation and nanocomposite material             |    |
| Synthesis                                                                  | 36 |
| <b>2.6. MATERIALS CHARACTERIZATION</b>                                     | 37 |
| <b>2.7. ELECTRODES FABRICATION</b>                                         | 39 |
| 2.7.1. Glassy carbon electrode (GCE)                                       | 39 |
| <b>2.8. PROCEDURES FOR ELECTROCHEMICAL METHOD</b>                          | 40 |
| 2.8.1. Electrodes electrochemical characterization                         | 40 |
| 2.8.2. Electrochemical determination of pollutants                         | 41 |
| <br><b>CHAPTER 3</b>                                                       |    |
| <b>3. RESULTS AND DISCUSSION</b>                                           | 44 |
| <b>3.1. MATERIALS CHARACTERIZATION</b>                                     | 44 |
| 3.1.1. Phytochemical analysis of <i>Psidium guajava</i> leaves extract     | 45 |
| 3.1.2. UV-Vis spectroscopic analysis of Ag(NPs)                            | 45 |
| 3.1.3. FT-IR analysis for synthesized materials                            | 44 |
| 3.1.4. Surface morphology of solids                                        | 51 |
| <b>3.2. ELECTROCHEMICAL CHARACTERISATION OF FABRICATED</b>                 |    |
| <b>GLASSY CARBON ELECTRODES</b>                                            | 56 |
| 3.2.1. Cyclic voltammetry (CV) studies                                     | 56 |
| 3.2.2. Electrochemical impedance spectroscopy (EIS) analysis of fabricated |    |
| Electrodes                                                                 | 62 |

**3.3. ELECTROCHEMICAL DETERMINATION OF Pb (II) USING CHTMS  
COMPOSITE MATERIAL** 64

|                                                                                      |    |
|--------------------------------------------------------------------------------------|----|
| 3.3.1. Electrochemical behaviour of Pb (II) at different modified GCE<br>under DPASV | 64 |
| 3.3.2. Optimization of experimental parameters                                       | 67 |
| 3.3.3. Effect of pH                                                                  | 67 |
| 3.3.4. Effect of deposition potential                                                | 68 |
| 3.3.5. Effect of Deposition time                                                     | 68 |
| 3.3.6. Electrochemical determination of Pb (II)                                      | 70 |
| 3.3.7. Effect of Interfering ions                                                    | 74 |
| 3.3.8. Reproducibility and stability study                                           | 75 |
| 3.3.9. Real sample analysis                                                          | 76 |
| 3.3.10. Conclusion                                                                   | 81 |

**3.4. ELECTROCHEMICAL DETERMINATION OF Pb (II) USING  
CHTMS+Ag(NPs) NANOCOMPOSITE MATERIAL** 81

|                                                                                      |    |
|--------------------------------------------------------------------------------------|----|
| 3.4.1. Electrochemical behaviour of Pb (II) at different modified GCE<br>under DPASV | 81 |
| 3.4.2. Optimization of the stripping parameters                                      | 83 |
| 3.4.3. Electrochemical determination of Pb (II)                                      | 86 |
| 3.4.4. Effect of interfering ions in Pb (II) detection                               | 89 |
| 3.4.5. Reproducibility and stability study                                           | 90 |
| 3.4.6. Real sample analysis                                                          | 91 |
| 3.4.7. Conclusion                                                                    | 95 |

**3.5. ELECTROCHEMICAL DETERMINATION OF BISPHENOL A** 95

|                                                                                                    |    |
|----------------------------------------------------------------------------------------------------|----|
| 3.5.1. Electro oxidation of BPA using CHMTS/GCE                                                    | 95 |
| 3.5.2. Electrochemical behaviour of BPA using the fabricated<br>electrodes under the DPASV studies | 99 |
| 3.5.3. Optimization of the experimental parameters                                                 | 95 |
| 3.5.4. Effect of pH                                                                                | 99 |



|                                                                                   |     |
|-----------------------------------------------------------------------------------|-----|
| 3.5.5. Effect of deposition potential and time                                    | 100 |
| 3.5.6. Electrochemical determination of BPA                                       | 102 |
| 3.5.7. Effect of co-existing ions                                                 | 105 |
| 3.5.8. Reproducibility and stability study                                        | 106 |
| 3.5.9. Real water implications                                                    | 108 |
| 3.5.10. Conclusions                                                               | 113 |
| <b>3.6. ELECTROCHEMICAL DETERMINATION OF TRICLOSAN (TCS)</b>                      | 114 |
| 3.6.1. Electro oxidation of TCS toward CHMTS/GCE under CV study                   | 114 |
| 3.6.2. Differential Pulse Anodic Stripping Voltammetry (DPASV) study of Triclosan | 115 |
| 3.6.3. Experimental parameters Optimization                                       | 116 |
| 3.6.4. Effect of pH                                                               | 116 |
| 3.6.5. Effect of deposition potential and time                                    | 116 |
| 3.6.6. Concentration dependence studies                                           | 119 |
| 3.6.7. Interfering ions study                                                     | 121 |
| 3.6.8. Reproducibility and stability of fabricated electrode                      | 123 |
| 3.6.9. Real implication and recovery rate study                                   | 124 |
| 3.6.10. Conclusion                                                                | 128 |

## **CHAPTER 4**

|                                        |     |
|----------------------------------------|-----|
| <b>4. CONCLUSIONS</b>                  | 129 |
| <b>REFERENCES</b>                      | 135 |
| <b>BRIEF BIO-DATA OF THE CANDIDATE</b> |     |
| <b>PARTICULARS OF THE CANDIDATE</b>    |     |
| <b>LIST OF PUBLICATIONS</b>            |     |
| <b>CONFERENCES AND SEMINAR</b>         |     |

## **PUBLISHED JOURNAL PAPERS**

### **LIST OF FIGURES**

#### **Figure**

**1.1.** Structure of bisphenol A(BPA)

**1.2.** Structure of Triclosan (TCS)

**1.3.** Structure of chitosan and cellulose

**2.1.** Potential sweep from initial potential to switching potential completed first segment and sweep to the final potential which represent the second segment representing one cycle in cyclic voltammetry study

**2.2.** Extraction of phytochemicals from *Psidium guajava* leaves; (a) *Psidium guajava* chopped leaves; (b) grinded leaves was stirred with 60 mL of double distilled water for 30 minutes; and (c) leave extract, filtered using Whatman filter paper (pore size 11µm)

**2.3.** (a) Setup and synthesis of silane grafted chitosan and synthesized composite material; (b) CHTMS solid; (c) CHMTS solid; (d) Casting solution for CHTMS; (e) Casting solution for CHMTS; (f) Synthesized CHTMS+Ag(NPs), Casting solution

**2.4.** Fabrication of GCE (a) GCE along with polishing pad and solution; (b) Sonicating after polishing the GCE for two minutes each using ethanol and double distilled water; (c) simple drop casting method was followed; (d) drying the fabricated GCE at 40°C for 30 minutes; (e) Fabricated GCE is ready for experiment

**3.1.** UV visible absorption spectrum of the CHTMS, AgNO<sub>3</sub> and CHTMS+Ag(NPs) and inset CHTMS and CHTMS+Ag(NPs) solutions

**3.2.** FTIR analysis of CH, CHMTS, CHTMS and CHTMS+Ag(NPs) materials

**3.3.** X-ray diffraction pattern of CHTMS and CHTMS+Ag(NPs) materials

**3.4.** N<sub>2</sub> adsorption-desorption isotherms for the solids CH, CHTMS and CHMTS materials

**3.5.** The SEM micrograph of (a) CH (Chitosan); (b) CHTMS; (c) CHMTS; and (d) CHTMS+Ag(NPs) materials

**3.6.** EDX spectra of (a) CH; (b) CHMTS; (c) CHTMS; and (d) CHTMS+Ag(NPs) materials

**3.7.** TEM micrograph of (a) Chitosan (CH); (b) CHMTS; (c) CHTMS; (d) CHTMS+Ag(NPs); (e) d-spacing of Ag(NPs); and (f) Average particle size distribution using the histogram for CHTMS+Ag(NPs) solid

**3.8.** Cyclic voltammograms of [Fe(CN)<sub>6</sub>]<sup>3-/4-</sup> (0.002 M; 0.1 M acetate buffer pH 4.5) obtained at a scan rate of 100 mV/s using the bare GCE, CH/GCE, CHTMS/GCE, CHMTS/GCE and CHTMS+Ag(NPs)/GCE

**3.9.** Scan rate studies for redox couple [Fe(CN)<sub>6</sub>]<sup>3-/4-</sup> (0.002 M; 0.1 M acetate buffer; pH 4.5) using the bare GCE, CH/GCE, CHTMS/GCE, CHMTS/GCE and CHTMS+Ag(NPs)

**3.10.** Plots of scan rate ( $v^{1/2}$ ) vs I<sub>p</sub> (peak current; anodic peak current) using different electrodes i.e., bare GCE, CH/GCE, CHTMS/GCE, CHMTS/GCE and CHTMS+Ag(NPs)/GCE (0.002 M [Fe(CN)<sub>6</sub>]<sup>3-/4-</sup> (0.1 M acetate buffer; pH 4.5)

**3.11.** Nyquist plots of bare GCE, CH/GCE, CHTMS/GCE, CHMTS/GCE and CHTMS+Ag(NPs) with Z<sub>fit</sub> modified GCE using the standard probe of [Fe(CN)<sub>6</sub>]<sup>3-/4-</sup> (0.002 M; 0.1 M acetate buffer at pH 4.5) [Inset: Fitted equivalent circuit]

**3.12.** DPASV curves obtained for Pb (II) (50.0 µg/L at pH 4.5; acetate buffer (0.1 M)) using the bare GCE; and CHTMS/GCE (Deposition potential: -0.9 V; Scan rate: 100 mV/s; and Deposition time: 180.0 sec; Pulse amplitude: 0.05 V; Step potential: 0.0001 V; Modulation time: 0.05 sec; and Time interval: 0.5 sec]

**3.13.** Parametric studies carried out at 50.0 µg/L Pb (II) (0.1 M acetate buffer; pH 4.5); (a) The oxidative peak current of Pb (II) as a function of pH; (b) The oxidative peak

current of Pb (II) as a function of deposition potential; and (c) The oxidative peak current of Pb (II) as a function of deposition time [Pulse amplitude: 0.05 V; Step potential: 0.0001 V; Modulation time: 0.05 sec; and time interval: 0.5 sec]

**3.14.** (a) The DPASV of Pb (II) as a function of Pb (II) concentrations; (b) Calibration line obtained for the oxidative peak current of Pb (II) as a function of Pb (II) concentration (Acetate buffer (0.1 M; pH 4.5); deposition potential: -0.9 V; deposition time: 180.0 sec; Pulse amplitude: 0.05 V; Step potential: 0.0001 V; Modulation time: 0.05 sec; and time interval: 0.5 sec)

**3.15.** The detection of Pb (II) in presence of several interfering ions using the CHTMS/GCE ([Pb (II): 50.0 µg/L; [Interfering ion]: 500.0 µg/L; acetate buffer (0.1 M; pH 4.5); Pulse amplitude = 0.05 V; Step potential= 0.0001 V; Modulation time= 0.05 sec; and time interval= 0.5 sec)

**3.16.** Real water sample spiked with Pb (II) having concentrations from 5.0 to 40.0 µg/L (Acetate buffer 0.1 M; pH 4.5), (a) DPASV of Pb (II) using the ground water; and (b) DPASV of Pb (II) using spring water; calibration lines obtained for (c) ground water; and (d) spring water samples. [Deposition potential = -0.9 V; Accumulation time = 180.0 sec.; Pulse amplitude = 0.05 V; Step potential= 0.0001 V; Modulation time= 0.05 sec; and time interval= 0.5 sec]

**3.17.** DPASV curves obtained for Pb (II) (50.0 µg/L at pH 4.5; acetate buffer (0.1 M)) using the (a) bare GCE; (b) CHTMS/GCE; and (c) CHTMS+Ag(NPs)/GCE (Deposition potential: -0.9 V; Scan rate: 100 mV/s; and Deposition time: 180.0 sec; Pulse amplitude: 0.05 V; Step potential: 0.0001 V; Modulation time: 0.05 sec.; and Time interval: 0.5 sec]

**3.18.** Parametric studies carried out at 50.0 µg/L Pb (II) (0.1 M acetate buffer; pH 4.5); (a) The oxidative peak current of Pb (II) as a function of pH; (b) The oxidative peak current of Pb (II) as a function of deposition potential; and (c) The oxidative peak current of Pb (II) as a function of deposition time [Pulse amplitude: 0.05 V; Step potential: 0.0001 V; Modulation time: 0.05 sec; and time interval: 0.5 sec]

**3.19.** (a) The DPASV of Pb (II) as a function of Pb (II) concentrations; (b) Calibration line obtained for the oxidative peak current of Pb (II) as a function of Pb (II) concentration (Acetate buffer (0.1 M; pH 4.5); deposition potential: -0.9 V; deposition time: 180.0 sec; Pulse amplitude: 0.05 V; Step potential: 0.0001 V; Modulation time: 0.05 sec; and time interval: 0.5 sec)

**3.20.** The detection of Pb (II) in presence of several interfering ions using the CHTMS+Ag(NPs)/GCE ([Pb (II): 50.0 µg/L; [Interfering ion]: 500.0 µg/L; acetate buffer (0.1 M; pH 4.5); Pulse amplitude = 0.05 V; Step potential= 0.0001 V; Modulation time= 0.05 sec; and time interval= 0.5 sec)

**3.21.** Real water sample spiked with Pb (II) having concentrations from 5.0 to 20.0 µg/L (Acetate buffer 0.1 M; pH 4.5), (a) DPASV of Pb (II) using the spring water; and (b) DPASV of Pb (II) using ground water; calibration lines obtained for (c) spring water; and (d) ground water samples. [Deposition potential = -0.9 V; Accumulation time = 180.0 sec; Pulse amplitude = 0.05 V; Step potential= 0.0001 V; Modulation time= 0.05 sec; and time interval= 0.5 sec]

**3.22.** Cyclic voltammograms of BPA (20.0 mg/L; phosphate buffer (0.1 M); pH 10.0) using the CHMTS/GCE and blank (Scan rate: 100 mV/s)

**3.23.** DPASV curves obtained for BPA (180.0 µg/L at pH 10.0; phosphate buffer (0.1 M)) using the bare GCE, CH/GCE and CHMTS/GCE (Deposition potential: 0.2 V; Scan rate: 100 mV/s; and Deposition time: 180.0 sec; Pulse amplitude: 0.05 V; Step potential: 0.0001 V; Modulation time: 0.05 sec; and Time interval: 0.5 sec]

**3.24.** Parametric studies carried out at 180.0 µg/L BPA (0.1 M phosphate buffer; pH 10.0); (a) The oxidative peak potential (Primary axis) as a function of pH and the oxidative peak current of BPA at different pH values (Secondary axis); (b) The oxidative peak current of BPA as a function of deposition potential; and (c) The oxidative peak current of BPA as a function of deposition time [Pulse amplitude: 0.05 V; Step potential: 0.0001 V; Modulation time: 0.05 sec; and time interval: 0.5 sec]

**3.25.** (a) The DPASV of BPA as a function of BPA concentrations; (b) Calibration line obtained for the oxidative peak current of BPA as a function of BPA concentration

(Phosphate buffer (0.1 M; pH 10.0); deposition potential: 0.2 V; deposition time: 180.0 sec; Pulse amplitude: 0.05 V; Step potential: 0.0001 V; Modulation time: 0.05 sec; and time interval: 0.5 sec)

**3.26.** The detection of BPA in presence of several interfering ions using the CHMTS/GCE ([BPA: 180.0  $\mu\text{g/L}$ ; [Interfering ion]: 1.8. mg/L; phosphate buffer (0.1 M; pH 10.0); Pulse amplitude = 0.05 V; Step potential= 0.0001 V; Modulation time= 0.05 sec; and time interval= 0.5 sec)

**3.27.** (a) Reproducibility studies using the CHMTS/GCE at 180.0  $\mu\text{g/L}$  BPA, for repeated detection of BPA; and (b) Stability of fabricated CHMTS/GCE at varied duration of time i.e., from 0 to 48 hrs

**3.28.** Real water sample spiked with BPA having concentrations from 160.0 to 200.0  $\mu\text{g/L}$  (Phosphate buffer 0.1 M; pH 10.0), (a) DPASV of BPA using the spring water; and (b) DPASV of BPA using Chite river water; calibration lines obtained for (c) spring water; and (d) Chite river water samples. [Deposition potential = 0.2 V; Accumulation time = 180.0 sec.; Pulse amplitude = 0.05 V; Step potential= 0.0001 V; Modulation time= 0.05 sec; and time interval= 0.5 sec]

**3.29.** Cyclic voltammograms of TCS (20.0 mg/L; phosphate buffer (0.1 M); pH 8.0) using the CHMTS/GCE and blank (Scan rate: 100 mV/s)

**3.30.** DPASV curves obtained for TCS (200.0  $\mu\text{g/L}$  at pH 8.0; phosphate buffer (0.1 M)) using the bare GCE, CH/GCE and CHMTS/GCE (Deposition potential: 0.2 V; Scan rate: 100 mV/s; and Deposition time: 180.0 sec; Pulse amplitude: 0.05 V; Step potential: 0.0001 V; Modulation time: 0.05 sec; and Time interval: 0.5 sec]

**3.31.** Parametric studies carried out at 200.0  $\mu\text{g/L}$  TCS (0.1 M phosphate buffer; pH 8.0); (a) The oxidative peak potential (Primary axis) as a function of pH and the oxidative peak current of TCS at different pH values (Secondary axis); (b) The oxidative peak current of TCS as a function of deposition potential; and (c) The oxidative peak current of TCS as a function of deposition time [Pulse amplitude: 0.05 V; Step potential: 0.0001 V; Modulation time: 0.05 sec; and time interval: 0.5 sec]

**3.32.** (a) The DPASV of TCS as a function of TCS concentrations; (b) Calibration line obtained for the oxidative peak current of TCS as a function of TCS concentration (Phosphate buffer (0.1 M; pH 8.0); deposition potential: 0.2 V; deposition time: 180.0 sec; Pulse amplitude: 0.05 V; Step potential: 0.0001 V; Modulation time: 0.05 sec; and time interval: 0.5 sec)

**3.33.** The detection of TCS in presence of several interfering ions using the CHMTS/GCE ([TCS: 200.0 µg/L; [Interfering ion]: 2000.0 µg/L; phosphate buffer (0.1 M; pH 8.0); Pulse amplitude = 0.05 V; Step potential= 0.0001 V; Modulation time= 0.05 sec; and time interval= 0.5 sec.)

**3.34:** (a) Reproducibility studies using the CHMTS/GCE at 200.0 µg/L TCS, for repeated detection of TCS; and (b) Stability of fabricated CHMTS/GCE at varied duration of time i.e., from 0 to 48 hrs

**3.35:** Real water sample spiked with TCS having concentrations from 160.0 to 200.0 µg/L (Phosphate buffer 0.1 M; pH 8.0), (a) DPASV of TCS using the Chite river water; and (b) DPASV of TCS using ground; calibration lines obtained for (c) Chite river water; and (d) Ground water samples. [Deposition potential = 0.2 V; Accumulation time = 180.0 sec.; Pulse amplitude = 0.05 V; Step potential= 0.0001 V; Modulation time= 0.05 sec.; and time interval= 0.5 sec.]

## **LIST OF TABLES**

### **Table**

**2.1.** Details of all chemicals used in present dissertation.

**3.1.** Phytochemical screening results. (+)= present

**3.2.** Prominent IR-IR peak of the CH, CHMTS, CHTMS and CHTMS+Ag(NPs) solids

**3.3.** Surface area, pore size and pore volume of CH, CHMTS and CHTMS materials were obtained from the BET analysis

**3.4.** Electroactive surface area of GCE, CH/GCE, CHTMS/GCE, CHMTS/GCE and CHTMS+Ag(NPs)/GCE obtained by using the Randle-Sevick equation

**3.5.** The obtained EIS parameters estimated for the best fitted electrical circuit model of the Nyquist plots for bare GCE, CH/GCE, CHTMS/GCE, CHMTS/GCE and CHTMS+Ag(NPs)/GCE working electrodes

**3.6.** The comparison of LOD obtained for Pb (II) using the CHTMS/GCE with other studies

**3.7.** Calculation of %RSD (relative standard deviation) in different time duration of prepared electrode in the determination of Pb (II) 50.0  $\mu\text{g/L}$  from aqueous solution

**3.8.** Analysis of real water sample using different analytical methodes

**3.9.** The recovery of Pb (II) in the spiked spring water and ground water using CHTMS/GCE

**3.10.** The comparison of LOD obtained for Pb (II) using the CHTMS+Ag(NPs)/GCE with other studies

**3.11.** Calculation of %RSD (relative standard deviation) in different time duration of prepared electrode in the determination of Pb (II) 50.0  $\mu\text{g/L}$  from aqueous solution

**3.12.** The recovery of Pb (II) in the spiked spring water and ground water using CHTMS+Ag(NPs)/GCE

**3.13.** The comparison of LOD obtained for BPA using the CHMTS/GCE with other studies

**3.14.** Analysis of real water samples using different analytical methods

**3.15.** The recovery of BPA in the spiked spring water and Chite river water using CHMTS/GCE

**3.16.** The comparison of LOD obtained for TCS using the CHMTS/GCE with other studies



**3.17.** The recovery of TCS in the spiked Chite river water and ground water using CHMTS/GCE

**4.1.** LOD values of several contaminants obtained with modified electrodes compared to MCL levels established by WHO and the US-EPA

**CHAPTER 1**  
**INTRODUCTION**

## **1. INTRODUCTION**

### **1.1. BACKGROUND**

Water is one of the most precious natural resources and is abundant as well on the earth's surface covering more than 70%. However, the availability of fresh and drinkable water is under tremendous stress. Living beings on the earth need water for their survival, in addition the agriculture, industry etc. requires a large fraction of water. Therefore, the reclamation and reuse of water is essential for its sustainable use. Moreover, water security is one of the important aspects at present that needs to be addressed in ways. The safe discharge of industrial effluent to the water bodies is a serious aspect given a global concern to keep available water safe and fresh (Gleick, 2002; Greenlee et al., 2009).

Existence of water in pure form is colourless, odourless and tasteless and considered as a universal solvent that dissolves many substances. Because of this, natural water is contaminated easily and cause severe health and ecological imbalances. Certain compounds/elements found in water are essential for living being but their presence beyond the permissible level causes adverse effects to the human health and the environment in general (Hossain, 2015).

Further, population explosion and globalization led high demand for safe drinking water in developing countries (Narain, 2009). Access to safe drinking water is a constitutional right since water is essential for life. The clean and fresh water significantly improves human health and prevents several waterborne diseases. Therefore, providing safe and clean water to the human population is an urgent need the hour. Water quality parameters are laid down by several regulatory bodies are updated time-to-time to safeguard the humanity on this planet (Gleick, 2002). Unsanitary conditions prevails with several waterborne diseases and highly vulnerable towards infants, young children or even elderly persons. Accessibility of clean and safe drinking water is of the foremost importance in maintaining good hygiene and a clean environment. Packaged water and ice have followed guideline laid down by the concerned bodies such as USEPA (United States Environmental Protection Agency), CDC (Centre for Disease Control), and WHO (World Health Organization), for safety to human consumption. Moreover, different water quality measures are recommended

for the use of water for different purposes. For example: water quality parameters for washing contact lenses, renal dialysis, use in pharmaceutical industries and food production processing industries are quite different from the quality of agricultural water (Gleick, 2002; World Health Organization, 2008).

Contamination of ground and surface water with several heavy metal toxic ions and micro-pollutants is a severe global concern. These pollutants are either non-biodegradable, or seemingly persistent/recalcitrant in aquatic environments, which lead to serious concern to the human health and marine life (Gumpu et al., 2015; Pruden et al., 2006).

Rapid growth of population and the need for land and resources, urbanisation and industrialisation are the visible changes, which leads to consequences like polluting the aquatic environment generated through municipal waste, industrial waste, chemical uses in agricultural and farm land, runoff from mining fields etc. The highly persistent and non-biodegradable pollutants when discarded into the environment without following the treatment protocols, eventually enter into the aquatic environment. Some heavy metals are essential to the human body at trace levels however, it poses serious health effects at higher levels (Valko et al., 2005). Metal ions including Pb (II), Cr (III), Cd (II), Hg (II), As (III), pose a serious threat toward human life, and are known for their acute toxicity. However, these metals ions are often present in industrial waste/effluent and entering into the water bodies; posing potential threat to aquatic ecosystems and polluting the surface or ground waters. Consequently enters directly or indirectly to the food chains causing several biological disorders to humans as well to live stocks (Duruibe et al., 2007). Ingestion/accumulation of heavy metal toxic ions such as As(III), Pb(II) and Cd(II) in the human body causing skin, bladder, kidney or lung cancers based on the individual toxic ions (Huff et al., 2007; Martinez et al., 2011; Phillips & Arlt, 2009; Ruiz-Manríquez et al., 1998; Steenland & Boffetta, 2000).

The anthropogenic/natural substances, *viz.*, pharmaceuticals (PHCs), personal care products (PCPs), hormones, antibiotics, pesticides, industrial chemicals, etc., are called emerging micropollutants and pose serious environmental and health concerns (Kim & Zoh, 2016). In a line, the EDCs, which are the exogenous agent that interferes

with the synthesis secretion, transport, binding action, or elimination of natural hormones in the body that are responsible for the maintenance of homeostasis, reproduction and development, and or behavior (USEPA) is a global concern for its removal from wastewaters (Luo et al., 2014). These micro-pollutants are persistent and not efficiently removed in conventional wastewater treatment plants. Hence, these micro-pollutants escape from the treatment plants and are entered into the water bodies. The level of micro-pollutants in surface waters is detected at ng/L to mg/L, which is serious and alarming to human health (Bolong et al., 2009; Schwarzenbach et al., 2006). Micro-pollutants even at low concentrations in the aquatic environment is a serious concern because it causes long term effects when exposed. Moreover, short term effects of these pollutants are known such as disturbance of normal endocrine receptor function and antibiotic resistance gene due to continued intake of antibiotics (Pruden *et al.*, 2006).

Pharmaceuticals are discharged into the aquatic environment from pharmaceutical industries. In addition, human urine and faeces contribute to be significant rise of pharmaceuticals in the municipal waste and sewage wastewater since *Ca.* 70% of ingested drug compounds are excreted through urine or faeces (Daughton & Ruhoy, 2009; Landry & Boyer, 2013). Wide range of drugs which are consumed everyday worldwide such as diclofenac, ibuprofen, 17  $\beta$ -estradiol, indomethacin and naproxen (Anti-inflammatory drugs), metoprolol and propranolol ( $\beta$ -blockers), carbamazepine (antiepileptic), antimicrobial drug are detected in surface water from trace level to  $\mu\text{g/L}$  concentrations (Kim & Zoh, 2016).

Runoff from farm/agricultural lands using pesticides for controlling pests; creates a serious challenge as it leads to continuous addition of harmful chemicals into the aquatic system. Herbicide chemicals such as atrazine, diuron insecticides viz., diazinon, paraoxon, aldicarb, and fungicides such as clotrimazole and tebuconazole are widely used synthetic chemicals as pesticides and detected in the water bodies at low levels (Campanale et al., 2021; Rajmohan et al., 2020). These chemicals are highly toxic and sometimes permanently hinders the activity of acetylcholinesterase (AChE) in the central and peripheral nervous system, resulting in accumulation of neurotransmitter acetylcholine in the body (Quinn, 1987). Atrazine, which is a known

endocrine disrupting compound; also known to be a potential carcinogenic type C compound (Kucka et al., 2012; Lin & Chu, 2011; Xing et al., 2012). Similarly, the oral lethal dose of paraoxon is 5 mg/kg for humans and mammals (Roda et al., 1994).

Although the micro-pollutants are priority hazardous substances, however; there is no such acceptable limit laid down by the regulatory bodies viz., EPA or WHO for several compounds. However, due to the toxicity or genotoxicity of these compounds, a complete removal/elimination from water bodies is important to safeguard the aquatic environment (Roda et al., 1994).

Determination of heavy metal toxic ions and micro-pollutants from the complex matrix like blood sample, saliva, serum, natural water, waste water, food, air, soil, etc., required selective and sensitive analytical tools for their *on site* detection. Highly sophisticated modern instruments like atomic absorption spectroscopy (AAS) (Bansod et al., 2017; Gong et al., 2016), inductively coupled plasma, mass spectroscopy (ICP-MS) (Gong et al., 2016), X-ray fluorescence spectrometry (XRF) (Sitko et al., 2015), neutron activation analysis (NAA), inductively coupled plasma-optical emission spectrometry (ICP-OES) (Losev et al., 2015), liquid chromatography-mass spectrometry (LC-MS) (Yan et al., 2015), gas chromatography-mass spectrometry (GC-MS), high-performance liquid chromatography (HPLC), enzyme-linked immunosorbent assay (ELISA), fluorescence and chemiluminescence (Tian et al., 2020), are known sophisticated analytical tools; determines efficiently these contaminants in different matrix. The instruments are highly sensitive and selective for the analytes, however; they showed with several disadvantages viz., high input cost, sophisticated and costly instruments, cumbersome in instrument handling, requirement of highly trained technician to run the system and most importantly they lack with *on-site* detection of analyte (Yi et al., 2013). Therefore, the development of miniaturized, robust, simple and cost-effective sensors for *on-site* detection of these pollutants is essential to safeguard the environment and hence the ecosystem. The electrochemical techniques are suitable alternatives since they require low detection limit, cost effectiveness, are easy to operate, no complicated sample preparations and useful in *on site* detection (Yan et al., 2015).

## **1.2. FATE OF POLLUTANT AND THEIR TOXICITY**

Increased level of heavy metal toxic ions and micro-pollutants in the aquatic environment poses serious environmental concerns due to their persistence in the environment subsequently the ecological imbalances. The non-biodegradable heavy metal toxic ions are mostly deposited in sediments, and excessive exposure or intake above the permissible limit causes several health effects (Kim et al., 2015). Similarly, continuous intake of micro-pollutants leads to the development of antibiotic resistance in humans and disruption of normal biochemical function (Gumpu et al., 2015; Pruden et al., 2006). The occurrence and fate of heavy metal toxic ion Pb (II) and micro-pollutants, bisphenol A (BPA) and triclosan (TCS) are summarized below.

### **1.2.1. Lead (Pb (II))**

Lead is ubiquitous in the environment and since Roman era lead is known as a highly toxic element. Lead is highly malleable, poor conductive, ductile, low melting point, soft and corrosion resistive (Oprea, 2002). These properties attracted extensive usage in everyday life activities resulting in lead contamination/accumulation in the environment (Wani et al., 2015). Because of acute toxicity of lead, the use of lead in many countries is discontinued. However, still it is used in various applications like leaded pipe, solders, grids, battery manufacturing and recycling, refining etc. which leads to excessive exposure of lead to humans. Lead is also known for occupational toxin and continued exposure leads to serious biological complications both in adults and children. Children are more susceptible towards lead exposure because of their soft tissues compared to adults. It was reported that exposure of children to lead even at low level concentrations leads to behavioural problem, mental retardation and decrease in IQ levels (Flora et al., 2012; Wani et al., 2015).

Anthropogenic activities primarily introduce lead into the environment. (Zhang et al., 2013). The EPA and WHO recommended the maximum acceptable limit in drinking water is 15.0 µg/L and 10.0 µg/L respectively (Awual, 2016). According to CDCD (Centre of Disease Control and Prevention), children with lead levels of 10.0 µg/dL and above were considered as “level of concern” (Ettinger et al., 2019; Gilbert & Weiss, 2006). Long term exposure to lead leads to anemia, damage of the central

nervous system, blood pressure in both old and middle-aged people, kidney and liver damage in both children and adult. It is also reported that excessive lead exposure causes miscarriage and declined fertility in human (Moneim et al., 2011; Gidlow, 2004; Wani et al., 2015). Similarly, absorption of lead through ingestion and lead particle through respiratory tract leads to disruption of biochemical function and accumulate in bones, kidney which causes serious damage to central nervous system, renal function even at low lead concentrations (Moneim et al., 2011; Lin et al., 2003).

Most of the lead in the environment is found in the uppermost humus rich surface layer of the soils because lead forms complexations with organic matter. Lead is least mobile toxic metal ion in the soil under non acidic or neutral or basic pH conditions, which is attributed to binding of lead with organic matter (An et al., 2001; Mielke & Reagan, 1998; Gumpu et al., 2015; Krishna & Govil, 2004). Furthermore, industrial emission, burning of fossil fuels and use of leaded gasoline in aviation industries leads to the atmospheric deposition of lead in the soil, which is very common in urban soil (Bindler, 2011; Hernberg, 2000; Masiol & Harrison, 2014). Additional sources of lead contamination includes acid metal plating, used ammunition, leaded paints, ceramic, toys, tetraethyl lead manufacturing plant, dying industries, glass industries etc. (An et al., 2001).

### **1.2.2. Bisphenol A (BPA)**

Among the synthetic EDCs, bisphenol A (BPA) is having widespread applications hence, extensively produced with the annual production of 3.8 million tons. BPA is an organic synthetic compound ( $C_{15}H_{16}O_2$ , IUPAC Name: 4,4'-(propane-2,2-diyl) diphenol) (Cf Figure 1.1), having a molar mass of 228.29 g/mol. BPA is white crystalline solid and readily soluble in fats but poorly soluble in water (low solubility, 200 mg/dm<sup>3</sup> at 25°C) (Michałowicz, 2014). BPA is the precursor material for the production of synthetic polymers including polycarbonate plastic and epoxy resins. It is also used in production of food containers, water packaging bottles, toys etc. It is also used in flame retardants materials, dental products, plasticizer, coatings, water



pipes, impact safety material, medical devices, thermal papers, electronic devices, food cane linings etc. (Flint et al., 2012; Tian et al., 2020).

Increasing level of BPA concentration in the natural environment is only due to anthropogenic activities. Degradation of BPA containing products like polycarbonate and epoxy resin, results in releasing BPA into the ecosystem and food (Vandenberg et al., 2012). BPA is often detected in the atmosphere and the highest concentration ( $4.55 \text{ ng/m}^3$ ) was found in the Indian urban states of Chennai and Mumbai, which was due to the combustion of plastic products contained with BPA (Praveen et al., 2020). BPA usually exists a low level in surface waters but study in 16 major rivers of Taiwan showed that contamination has significantly increased from  $0.01\text{-}44.65 \text{ }\mu\text{g/L}$  in surface water, and  $0.37\text{-}491.54 \text{ }\mu\text{g/kg}$ , due to the mixing of industrial effluents originated from the BPA producing industries (Lee et al., 2013). Urbanization contributes in releasing BPA in the environment, which results in atmospheric fallout, sewer overflow or runoff and slowly increasing the concentration of BPA in the aquatic system (Cladière et al., 2013). The contamination of groundwater was substantial due to dumping of BPA containing products and waste in the landfills, and the leachates contaminates the groundwater (Michałowicz, 2014). Contaminated food and drinking water with BPA are the main source of BPA exposure to humans. Polycarbonate and epoxy resin contain BPA and are widely used in manufacturing food containers and tin food containers which leads to exposure of food toward BPA. It is believed that everyday intake of BPA is estimated to be  $0.48 \text{ to } 1.6 \text{ }\mu\text{g/kg/body weight/day}$  through the alimentary canal (Vandenberg et al., 2007). Release of BPA from polycarbonate and epoxy resins were reported and the sources of BPA contamination are food stored in tin cans and water bottles, usage of polycarbonate containers (Colin et al., 2014; Yonekubo et al., 2008). The occupational manpower engaged in the BPA producing or related factories are inhaling-BPA in the form of dust which has occurred through the BPA containing products. Moreover, the workers are also exposed through the dermal routes (Michałowicz, 2014).

BPA is a well known xenoestrogen, which disrupts the endocrine function. The behaviour of BPA and natural estrogen- $17\text{-}\beta$  estradiol are similar, which results in mimicking the normal estrogen- $17\text{-}\beta$  estradiol function and binding with estrogen

receptors, which disrupt the entire estrogen function (Iso et al., 2006). BPA also shows interaction with the arylhydrocarbon receptor (AHR) affecting follicle growth in mice (Ziv-Gal et al., 2013). Not only affecting estrogenic function, it affects the function of androgens, thyroid hormones, prolactin, insulin and causing immunotoxic, hepatotoxic, mutagenic and carcinogenic effects (Hassan et al., 2012; Michałowicz, 2014; Wetherill et al., 2007). Obesity, heart disease and diabetic are closely related to the BPA exposure (Michałowicz, 2014). BPA showed less toxicity towards plants and microorganism that includes fungi, bacteria and algae, since they convert BPA to its metabolites such as carboxylic/polycarboxylic acids and  $\beta$ -hydroxybutyric acid, which exhibit less toxicity compared to BPA (Chai et al., 2005; Louati et al., 2019). In mammal's, the biotransformation (oxidation) of BPA produces more toxic metabolites i.e., cytochrome P450 monooxygenase, which is highly toxic and shows excessive estrogenicity. Some species of bacteria and fungi which use BPA for the carbon and energy, minimized the concentration of BPA from the surrounding environment. Hence, those species that degrade or minimise BPA concentration from the terrestrial environment are used for removing BPA from the environment (Li et al., 2012; Michałowicz, 2014).

Because of the toxicity and several health hazards due to BPA exposures, Canada is the first country to restrict the sale and advertising products containing BPA and prohibited the import of polycarbonate baby bottles containing BPA (Government of Canada, 2010). In Taiwan, BPA has designated BPA as a Class 4 toxic substance under Toxic Chemical Substances Control Act (Taiwan, 2009). Class 4 toxic substances are substances that create concern toward environment pollution and endangering human health (U.S. Environmental Protection Agency, 2010). Other countries like the European Union (EU), China and Malaysia also banned the use of BPA in certain products (United States Environmental Protection Agency, 2010). In India the use of BPA is prohibited in baby feeding bottles and Sippy cups by Bureau of Indian Standards (BSI) (*Indian Standards Referred in Government Regulations - Bureau of Indian Standards*, n.d.)

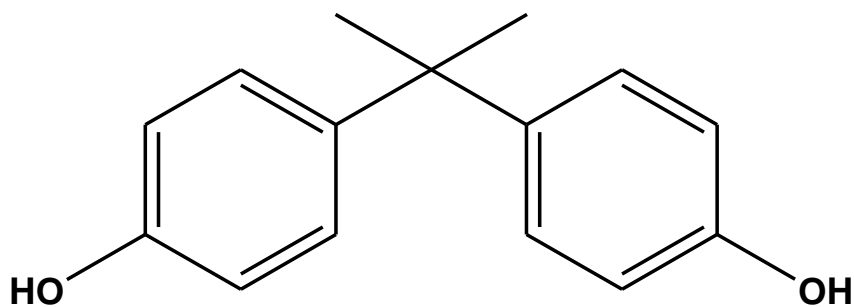


**Figure 1.1:** Structure of bisphenol A (BPA)

### 1.2.3. Triclosan (TCS)

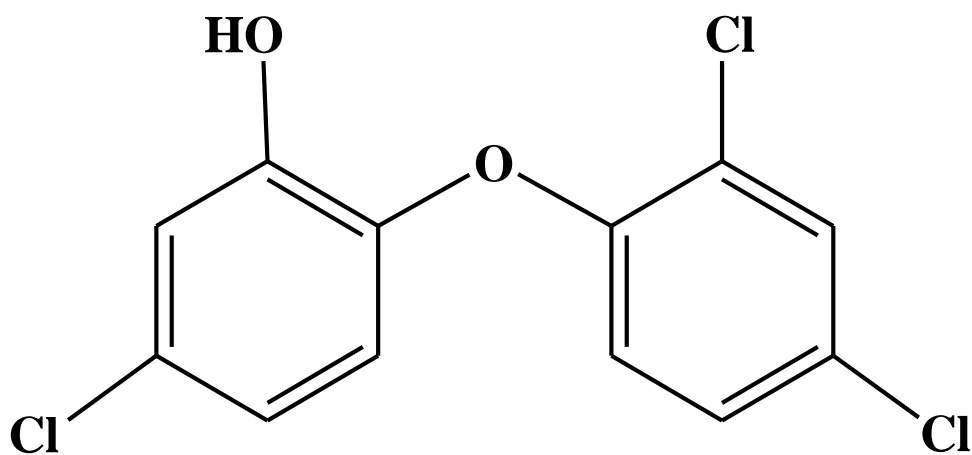


**Figure 1.2:** Structure of Triclosan (TCS)

2,2,4'-trichloro-2'-hydroxydiphenyl ether also known as triclosan (TCS) or irgasan (*Cf* Figure 1.2) is having widespread use in personal care products (Ishibashi et al., 2004). Triclosan is having poor solubility in water, but readily soluble in alkali solution and nonpolar organic solvents (Bhargava & Leonard, 1996). It is a stable, lipophilic compound, non-ionic, broad-spectrum antibacterial and antimicrobial agent. Because of these excellent properties, TCS is incorporated in personal care products,

such as toothpaste, hand sanitizer, mouthwash, disinfectants, deodorants, shampoo, soap, detergents etc. (Morrall et al., 2004; Motia et al., 2019; Saljooqi et al., 2020; Yazdankhah et al., 2006) and the typical concentration in the range of 0.1 to 0.3% of product weight (Montaseri & Forbes, 2016). The content of TCS should not exceed 0.3% in the product, which is regulated by European Community Cosmetic Directive or the US Food and Drug Agency (USFDA) in Europe and the USA, respectively (Motia et al., 2019; Rodricks et al., 2010). The presence of TCS in this product is low, the usage is ubiquitous, resulting in the TCS being detected in the waste water, rivers and lakes, causing ill effects to the environment and human health (Zhao et al., 2013).

Much attention was given towards the degradation of TCS in aqueous medium however, the release of hazardous dioxin-type by-products resulted in the degradation of TCS, showing additional contamination of the aquatic environment (Yueh & Tukey, 2016). The irradiation of TCS with UV light causes the cyclization of the compound, which forms a more toxic compound compared to TCS. The dioxin derivatives are formed which are potential carcinogens (Yueh & Tukey, 2016). Dioxins are phenolic compounds such as 2, 8-dichlorodibenzo-p-dioxin, 2, 4-dichlorophenol and 2, 4, 6-trichlorophenol, also regarded as potential EDCs (Sankoda et al., 2011).

TCS is a disrupting endocrine compound (Sankoda et al., 2011), affecting hyperthyroid function (Cullinan et al., 2012). Enhanced exposure of TCS induces skin irritation (Anderson et al., 2016), decreases the oestrogen levels in placenta during pregnancy (Jung et al., 2012), reduces neural stem cell in the rat brain (Park et al., 2016), and significant rise in the body mass index in children and adult (Lankester et al., 2013). It occurs in human blood (Allmyr et al., 2008), plasma (Zhang et al., 2006), breast milk (Allmyr et al., 2008) and urine (Calafat et al., 2008). Therefore, based on the severe environmental and health concerns, the development of sensitive and selective sensors for low level detection and monitoring of TCS could help in safeguarding the human health and environment in general.

### **1.3. Review of Literature**

Nano bio-composite materials are used in various areas, including biomedical, environmental engineering, agricultural sciences, materials sciences, electronics and

devices, and biological sciences. However, the biocomposite materials are promising in the environmental remediation and the sensor studies because of several novel properties viz., the natural and environmental friendly, low cost, enhanced stability, abundance in nature, biocompatibility, biodegradability, easy fabricability for optimum use etc. (Sarikokba et al., 2020). A review already published demonstrating the use of nano bio-composites materials precursor to the chitosan in the development of electrochemical sensors for various potential and emerging pollutants in aqueous medium (Sarikokba et al., 2020).

Chitosan is a known biopolymer that showed promising applications in the field of biomedical sciences. Rouget demonstrated the deacetylation of chitin to chitosan in the nineteenth century, it paved the way for various applications of compounds in allied and medical sciences. Chitosan is a polysaccharide biopolymer made by the partial alkaline N-deacetylation of chitin (Casadidio et al., 2019). Chitin is a protein, which is primarily isolated from the shells of shrimp and crabs. Chitosan is found in the Zygomycetes fungal cell walls and insect cuticles (Raafat et al., 2008).

Chitosan is a natural biopolymer that is the second most prevalent in nature after cellulose. Similarly, it is extensively derived from natural products such as insect and arthropod exoskeletons, or as a by-product of the seafood processing industry (Crini & Badot, 2008; Lachhimpui et al., 2017). The unique properties of chitosan viz., biocompatibility, biodegradability, bio-renewable and non-toxic nature, low cost, etc., finds a suitable material for varied medical applications (Shukla et al., 2013). Chitosan has linear  $\beta$ -(1 $\rightarrow$ 4) glycosidic linkages, hence, showed a similar structure as cellulose (Cf Figure 1.3). Glycosidic linkage connects the two chitosan units, 2-acetamido-d-glucose and 2-amino-d-glucose. Chitosan is produced by hydration or enzymatic hydrolysis in the presence of chitin deacetylase by removing an acetate moiety from chitin (Shukla et al., 2013; Suh & Matthew, 2000).

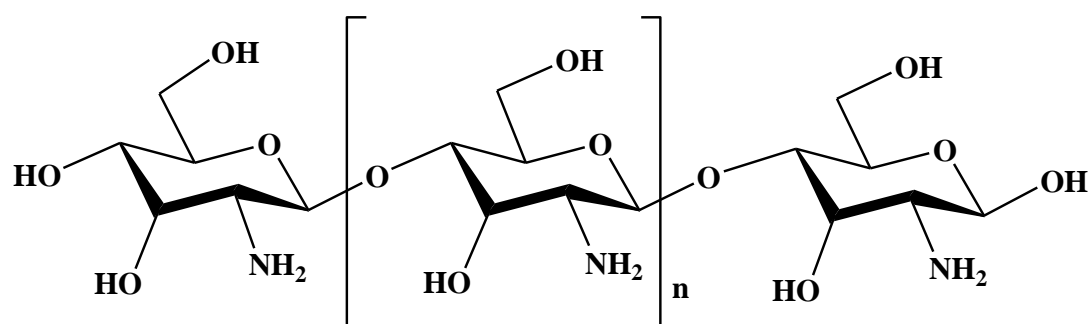
In general, the amino and hydroxyl groups in chitosan compound make it suitable for a wide range of applications, and it is recognised to have polycationic properties, compared to other natural polymers (Agrawal et al., 2010). The glycosidic linkages, enables the material's molecular weight and viscosity. Chitosan is highly pH sensitive and rapidly dissolves in an acidic environment (Lalhmunsiana et al., 2016). The degree of deacetylation and molecular weight of chitosan determines its physical

and chemical properties. At lower pH chitosan showed lower mechanical strength and poor settling ability, which limits its wider applications (Shukla et al., 2013). However, introducing suitable inorganic or organic functionalized materials, the physical and chemical properties of chitosan could be altered (Jiménez-Gómez & Cecilia, 2020). Chemical modification of chitosan by introducing the suitable functional groups such as carboxylic, hydroxyl showed varied applications in various field of research (Shukla et al., 2013). The crosslinking agent is reported in the literature for chemical modification of chitosan for sensor development. In a line, the glutaraldehyde, which has a carboxylic group in their chemical structure, crosslinked with the chitosan and showed promising in electrochemical determination of Cr (VI), glucose and hydrogen peroxide (Miao et al., 2001; Miao & Tan, 2000, 2000; Song et al., 2018). Similarly, the diepoxy compound [1,2:7,8-diepoxyoctane (DEO)] was crosslinked with the chitosan matrix and possessed high removal capacity for Cr (VI) in acidic medium (Vakili et al., 2018). Furthermore, the sodium tripolyphosphate (TPP) and gloxal were utilized to crosslink with the chitosan polymer (Gupta & Rastogi, 2008; Nasution et al., 2018). Further, the materials showed enhanced swelling properties, hydrophilicity, higher mechanical strength, pore size dimension and also possessed enhanced stability even at lower pH values (Song et al., 2018).

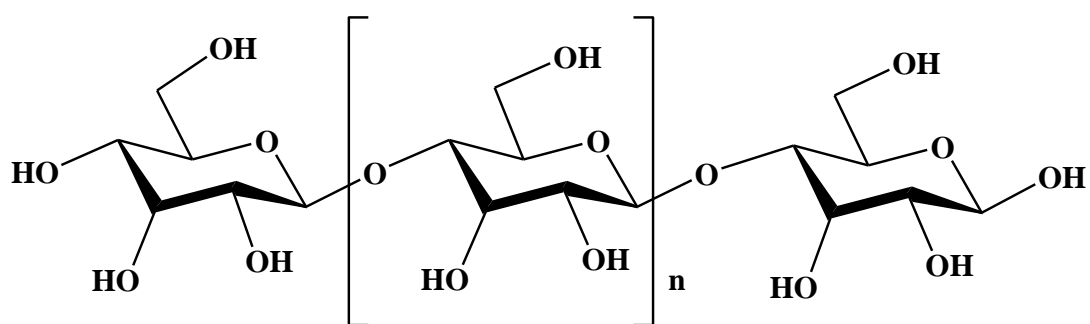
Inorganic polymeric compounds such as isocyanatopropyltriethoxysilane (ICPTES) were grafted with the chitosan polymeric chain using the sol gel process. The synthesized material possessed multifunctional groups and showed promise in photoluminance features (Silva et al., 2005). Similarly, the grafting of chitosan using silane (trimethoxyoctylsilane and 3-mercaptopropyl trimethoxysilane) are useful materials in the removal of arsenate from aqueous solutions applied under the batch and column reactor operations (Lalhmunsiam et al., 2016; Lalhmunsiam et al., 2016).

Furthermore, chitosan has outstanding film-forming capacity, good adhesion, high permeability and nontoxicity make it useful for a wide range of applications, including sensor development through the fabrication of selective electrodes for a variety of pollutants. It also facilitates electron transfer reactions because of swelling and hydrophilic nature (Batra & Pundir, 2013; Ling et al., 2009)].

The importance of nano bio-composite materials in the fabrication of a variety of electrodes provides a way of developing suitable electrochemical sensors for different analytes having the concern in the field of environmental engineering, food technology or even in the medical sciences. The latest research examines the problems and opportunities of employing nano bio-composites in the fabrication of microelectrodes for trace detection of heavy metal toxic ion (lead) and some micropollutants (bisphenol A and triclosan). Future study is included to pave the way for nano composites' possible implications in miniaturized device development.



**Chitosan**



**Cellulose**

**Figure 1.3:** Structure of chitosan and cellulose

### 1.3.1. Electrochemical Detection of Heavy metal toxic ion, Pb (II)

Pb (II) is one of the most toxic heavy metal ions that is not essential for life sustenance. Pb (II) is readily bioaccumulation and causes severe health concerns, which includes the failure of the nervous system (Priya et al., 2017; Zuo et al., 2017). The detection and removal of Pb (II) at the trace level from the environment is essential in order to safeguard the human being or the marine life in aquatic environments. Several techniques are available for the efficient and low level detection of Pb (II) in aqueous medium however, the electrochemical technique is promising due to its simplicity, low cost, fast in analysis and feasible in real time analysis (Sarikokba et al., 2020). In electrochemical techniques, the role of working electrodes (GCE) is crucial for sensitive and selective detection of pollutants. Therefore, the fabrication of working electrodes with suitable and advanced materials show high sensitivity with low detection limit for Pb (II) detection in aqueous medium (Mourya et al., 2021; Nodehi et al., 2021). Chitosan is regarded as an excellent substrate material in fabrication or modification of working electrodes due to its useful properties such as film forming ability, swelling ability and forming chelates with metal ions (Sarikokba et al., 2020). Therefore, the chitosan stabilized gold nanoparticles (Au(NPs)) and was employed in the determination of Pb (II) from aqueous medium (Çiftçi *et al.*, 2014). The in situ synthesis enabled synthesizing the composite material (hep/CS-rGO) contained with the chitosan, reduced graphene oxide and heparin. The glassy carbon electrode surface was modified with the nanocomposite material. The modified electrode showed significantly enhanced oxidative peak current for Pb (II) under the square wave anodic stripping voltammetry (SWASV) (Priya *et al.*, 2017).

Furthermore, the simultaneous determination of Pb (II) and Cd (II) was carried out using bismuth doped carbon xerogel nanocomposite incorporated with the chitosan matrix (Chi-(Bi-CX)). The synthesized material exhibited high surface area and meso-to-macropores with an average diameter of *Ca* 60 nm (Fort et al., 2015). Nanocomposite material based on reduced graphene oxide (rGO) and chitosan (CS) was obtained, which was synthesized using chitosan as a reducing agent for graphene oxide (GO) to form rGO-CS and the nanocomposite was drop casted onto the glassy carbon electrode (rGO-CS/GCE). Further, the electro-polymerization of L-lysine was conducted using the cyclic voltammetry which resulted with fabrication of the rGO-



CS/PLL/GCE electrode. The electrode was then employed in simultaneous determination of Cd (II), Pb (II) and Cu (II), which showed an enhanced electrocatalytic activity toward the metal ions and achieved the limit of detection for Cd (II) 0.01  $\mu\text{g/L}$ , Pb (II) 0.02  $\mu\text{g/L}$  and Cu (II) 0.02  $\mu\text{g/L}$  (Guo et al., 2017).  $\text{Co}_3\text{O}_4/\text{rGO}/\text{chitosan}$  nanocomposite was synthesized by in-situ growth of  $\text{Co}_3\text{O}_4$  onto the rGO followed by the reduction using hydrazine. The material was utilised in fabricating the GCE and employed in trace determination of Pb (II) under optimised experimental conditions. The electrooxidation of Pb (II) shows good linearity within a wide concentration range i.e., from 1.0 to 200.0 nM with the limit of detection of 0.35 nM for Pb (II). The high sensitivity in Pb (II) detection was achieved due to the good electrical conductivity and high surface area of rGO and sorption of Pb (II) toward the electrode surface (Zuo et al., 2017).

Simultaneous quantification of Cd (II) and Pb (II) using  $\text{Fe}_3\text{O}_4/\text{multiwalled carbon nanotube}/\text{laser scribed graphene}$  composites functionalized with chitosan modified glassy carbon electrode ( $\text{Fe}_3\text{O}_4/\text{MWCNTs}/\text{LSG}/\text{CS}/\text{GCE}$ ) was conducted using the square wave anodic stripping voltammetry (SWASV). The nanocomposite material shows significantly enhanced surface area, improved conductivity, excellent absorption ability as compared to the bare GCE. The fabricated GCE shows a favourable sensing platform and provides a good calibration line within the concentration range 1.0 to 200.0  $\mu\text{g/L}$ . Further, the limit of detection is found 0.1  $\mu\text{g/L}$  for Cd (II) and 0.07  $\mu\text{g/L}$  for Pb (II) (Xu et al., 2019).

### **1.3.2. Electrochemical Detection of Micro-pollutants**

#### **1.3.3. Bisphenol A (BPA)**

Literature survey reveals that a variety of materials are employed to fabricate the glassy carbon electrode and utilized for the low level detection of bisphenol A in aqueous solutions (Gugoasa, 2019). The hydroxyl group of the bisphenol A is readily oxidized which makes possible for electrochemical determination of BPA in aqueous solutions (Tian et al., 2020).

The composite materials chitosan- $\text{Fe}_3\text{O}_4$  (CS- $\text{Fe}_3\text{O}_4$ ) was impregnated onto the GCE and employed in the detection of bisphenol A under the amperometry method

(Yu et al., 2011). The XPS analysis confirmed the presence of Fe<sub>2</sub>O<sub>4</sub> nanoparticles. Moreover, the lone pair electrons of nitrogen (N) of chitosan was interacting with the 3d orbital of the Fe atom of Fe<sub>3</sub>O<sub>4</sub> and forming a coordinate bond (Deng et al., 2003; Yu et al., 2011). The electrochemical method was employed for quantitative determination of BPA in plastic samples and showed reasonably high recovery rate (Yu et al., 2011). The hydrothermal method was used to synthesis nano molybdenum disulphide (MoS<sub>2</sub>) and introduced into the chitosan and decorated with the gold nanoparticle to obtain the nanocomposite material (MoS<sub>2</sub>-chitisan-Au). The material was used in fabrication of GCE and utilized in low level detection BPA using cyclic voltammetry. A two electro-oxidation of BPA was observed in electrochemical study where oxidative peak current show good linearity with the concentration of BPA, having the linear equation of  $i_p \text{ (mA)} = 88.87 + 29.79 \log C \text{ (mM)}$  ( $R^2$ : 0.9896) and LOD of 5.0 nmol/L (Huang et al., 2014).

Similarly, composite material MnO<sub>2</sub>NWs-rGO (MnO<sub>2</sub> nanowires-decorated reduced graphene oxide composite) was employed in fabricating the GCE and applied in sensitive determination of BPA. The electrode showed excellent electrocatalytic activity, sensitivity, stability, and selectivity towards the BPA detection using the CV and chronocoulometry (CC) studies. The second derivative linear sweep voltammetry (SDLSV) was employed in the BPA detection which showed reasonably good linearity with the concentration of BPA (studied concentration range, 0.02–20  $\mu$ M and 20–100  $\mu$ M) with the LOD of 6.0 nM. Further, the BPA was detected in the plastic samples and showed a reasonably high recovery rate of BPA (Tian et al., 2020). Graphene was obtained by the soft chemistry synthesis that involves graphite oxidation and chemical reduction process. The graphene was introduced onto the GCE surface using a facile drop cast method. The electrode was electrochemically characterised using the potassium ferricyanide redox probe under the CV. The determination of BPA under optimised experimental conditions showed a good linearity within the BPA concentration range of  $5 \times 10^{-8} \text{ mol L}^{-1}$  to  $1 \times 10^{-6} \text{ mol L}^{-1}$  and the LOD was found  $4.689 \times 10^{-8} \text{ M}$  (Ntsendwana et al., 2012). Exfoliated graphite (EG) electrode was fabricated and employed in the determination of BPA under square wave voltammetric technique, where oxidative peak current exhibits linearity within the BPA concentration range from 1.56  $\mu$ M to 50  $\mu$ M. Further, the LOD was found 0.76  $\mu$ M (Ndlovu et al., 2012).

Furthermore, the nitrogen doped graphene sheet (N-GS) and chitosan (CS) was utilized for electrochemical determination of BPA. The nanocomposite materials (CS/N-GS) showed enhanced electron transport ability and electrocatalytic activity compared to the bare graphene. The nanocomposite modified electrode shows enhanced electrical signal towards the BPA with the limit of detection of  $5.0 \times 10^{-9}$  mol/L (Fan et al., 2012). The stacked graphene nanofibers and gold nanoparticles composite material (AuNPs/SGNF/GCE) modified GCE was used for the electrooxidation of BPA. The nanocomposite material caused a decrease in oxidative overpotential and an increase in peak oxidative current of BPA. Linear sweep voltammetry was employed in the determination of BPA with the LOD  $3.5 \times 10^{-8}$  M (Niu et al., 2013).

#### **1.3.4. Triclosan (TCS)**

Triclosan (TCS) is one of the widely used compounds in the personal care products due to its antibacterial properties. TCS is feeble soluble in water but solubility is significantly increased in alkaline and nonpolar organic solvents (Bhargava & Leonard, 1996; Saljooqi et al., 2020). TCS is often detected in river, lake, and wastewater samples. The UV light irradiation caused for cyclization of triclosan to generate more toxic dioxane derivatives (i.e., 2, 8-dichlorodibenzo-p-dioxin, 2, 4-dichlorophenol and 2, 4, 6-trichlorophenol), which are found to be highly toxic compounds (Sankoda et al., 2011). Triclosan is a known endocrine disrupting compound, which alters the hyperthyroid function (Ley et al., 2017). An excess intake of TCS causes severe skin irritations (Anderson et al., 2016) and during pregnancy exposure of TCS reduces the production of estrogen in placenta (Jackson et al., 2018; Sankoda et al., 2011; Yueh & Tukey, 2016). Furthermore, TCS contained with hydroxyl and phenolic groups, which are readily oxidised hence, provide oxidative peak current that facilitates in electrochemical detection of triclosan utilizing the efficient working electrodes (Fan et al., 2012).

The functionalized graphene nano plates using  $\beta$ -cyclodextrin ( $\beta$ -CD/GNP) utilized in fabricating the GCE and employed in the trace detection of TCS. Owing to the large surface area and fast electron transfer reactions at the nanocomposite surface, the electro-oxidation of TCS shows good linearity of oxidative peak current

within the BPA concentrations 2.0  $\mu\text{M}$  to 100  $\mu\text{M}$ . The method provides the detection limit of 0.6  $\mu\text{M}$  (Li et al., 2014). Similarly, poly (diallyldimethylammonium chloride) functionalised graphene doped with palladium nanoparticles (PDDA-Gr/PdNPs) was obtained using one-pot synthesis. Further, the nanocomposite material exhibits good electron transfer ability and catalytic activity in the detection of TCS at a wide concentration range and the limit of detection was found 3.5 nM. Moreover, the nanocomposite electrode showed good reproducibility, long term stability and applicability in real sample analysis in the BPA detections (Wu et al., 2017a). The reduced graphene oxide (rGO) was functionalized with the polyoxometalate (POM) in aqueous solutions and decorated with the gold nanoparticles (AuNPs/POM/rGO). The nanomaterial was further employed in the trace determination of TCS in aqueous medium (Yola et al., 2015).

Facile synthesis of  $\text{Fe}_3\text{O}_4\text{@Au-PPy/GO}$  nanocomposite was carried out utilizing the nanostructured  $\text{Fe}_3\text{O}_4\text{@Au}$ , graphene oxide (GO) and the polymer polypyrrole (PPy). The material was used in fabricating the GCE and utilised in the determination of TCS (Saljooqi et al., 2020). Chitosan was used as a host material, for one-pot synthesis of carbon nanodots (CNDs) and chitosan (CS) composite film (CNDs/CS). The composite material possessed high surface area 0.261  $\text{cm}^2$  and the electrocatalytic activity enabled for efficient electro-oxidation of TCS. The electrode showed the limit of detection of 9.2 nM for the TCS (Dai et al., 2012a). The graphene quantum dots (GQD) supported by chitosan show an enhanced electro-oxidation of TCS and MePa (methylparaben). Further, the limit of detection was found 0.03 and 0.04  $\mu\text{mol/L}$  for TCS and MePa, respectively. The GQD favoured the electrooxidation of TCS efficiently at the electrode surface, due to the rapid and efficient charge transfer reactions occurring at the electrode surface (Santana & Spinelli, 2020).

Similarly, the MWCNT (Multiwall Carbon Nanotube) modified GCE was assessed in sensitive detection of TCS and the electro-oxidation of TCS involves a one electron irreversible oxidation process. The fabricated electrode show enhanced electrochemical response in TCS detection and a reasonably good linearity of oxidative peak current with TCS concentration (50.0  $\mu\text{g/L}$  to 1.75  $\text{mg/L}$ ) was achieved with the limit of detection of TCS 16.5  $\mu\text{g/L}$  (Yang et al., 2009).

#### 1.4. SCOPE OF PRESENT INVESTIGATION

The natural activity largely through the industrial activity viz., mining/metallurgical, paints, leaded pipes, solders etc. causes for elevated level of Pb (II) in the terrestrial environment. The intake of Pb (II) caused for several severe health effects hence, the permissible limit of Pb (II) in the drinking water is prescribed as low as 10  $\mu\text{g/L}$  (World Health Organisation (WHO)). On the other hand, the micropollutants such as bisphenol A (BPA) and TCS is posing serious health problems. These micropollutants are often detected at  $\mu\text{g/L}$  to  $\text{ng/L}$  in the aquatic environment hence, showed greater concerns for the environmentalist for their detection at low levels. Therefore, the present investigation focuses on the development of simple, cost effective, portable electrochemical sensor for the trace and efficient detection of emerging water contaminants viz., Pb (II) and micropollutants viz., bisphenol A (BPA) and triclosan (TCS). The miniaturized device development with efficient *on-site* detection is the demand of the hour. The electrochemical technique, which utilizes the use of advanced materials, paves the way for development of miniaturized devices. Therefore, the present investigation synthesizes the advanced composite and nanocomposite materials precursor to the chitosan and silanes. The chitosan is used as a base and natural polymeric material to functionalize it with a variety of silanes. Chitosan has abundance of amino and hydroxyl groups enabling it for possible grafting of silanes. Moreover, the chitosan shows good film forming and swelling abilities easing the fabrication of thin film electrodes. The silanes (3-mercaptopropyl trimethoxysilane (MTS) and trimethoxyoctylsilane (TMS)) are preferentially are to be grafted with the chitosan (CH). Further, the functionalized chitosan materials i.e., the trimethoxyoctylsilane grafted chitosan (CHTMS) was decorated with silver nanoparticle (Ag(NPs)) in a greener route utilising (*Psidium guajava*) leave extract as reducing agent for synthesizing nanocomposite material (CHTMS+Ag(NPs)). The natural phytochemicals utilized in the synthesis of silver nanoparticles is an endeavour to obtain the greener synthetic route. Further, these advanced materials were utilized in the fabrication of thin film electrodes viz., CHTMS/GCE, CHMTS/GCE and CHTMS+Ag(NPs) fabricated glassy carbon electrodes were then utilized in the trace

detection of these emerging water contaminants. The fabrication of thin-film electrodes is conducted with simple and facile methods. The electrode stability for repeated and prolonged applications is a greater challenge in real implications of the electrode. Moreover, the real water implications demonstrate the selectivity of the electrode in the real implications. The present investigation extensively demonstrated the stability and selectivity of devised electrodes in the sensitive and trace detection of pollutants.

Therefore, extensive laboratory results are useful input data in the development of miniaturized devices for trace, efficient and *on site* monitoring of Pb (II), bisphenol A and triclosan in aqueous solution.

## **CHAPTER 2**

### **METHODOLOGY**

## **2. METHODOLOGY**

### **2.1. CHITOSAN AND REAL WATER SAMPLES**

Chitosan which is used as a substrate for synthesis of composite/nanocomposite material were procured from HIMEDIA having the degree of deacetylation is  $\geq 75\%$ . Real water samples used in real matrix study were collected from three different locations within the Aizawl City, Mizoram, India. River water sample, collected from Chite river, Falkand Veng, (GPS (Global position system) coordinates: N23.73916, E092.74136), whereas, ground water and spring water was collected from Mizoram University campus, Aizawl, India and their GPS coordinates are: N23.73255, E092.66342 and N23.73255, E092.66342, respectively. Prior to the experiment, the real water samples were filtered using Whatman filter paper (pore size 11  $\mu\text{m}$ ) to remove any sediment or suspended particles from the water. The physico-chemical parameters of the collected real water samples were analysed using different analytical instruments such as pH, salinity, conductivity, resistivity, total dissolved solid and oxidation-reduction potential was studied using a multiparameter probe (Hanna, model: HI98194, USA). Similarly, the presence of phosphate, nitrate, sulphate and fluoride was studied using multiparameter instrument (Hanna, model: Hi83300, USA). The presence of NPOC (Non-purgeable Organic Carbon) and IC (inorganic carbon) was obtained using TOC analyser. Various elements present in the water samples are studied using an AAS (Atomic absorption spectrometer). For real matrix study, the collected water samples were used to prepare the supporting electrolyte (0.1 M acetate buffer/phosphate buffer), whose pH was adjusted. Furthermore, the prepared electrolyte solutions were spiked with known concentrations of Pb (II), bisphenol A and triclosan.

### **2.2. CHEMICALS AND APPARATUS**

Chemicals procured were of analytical grade and used without further purification. Details of all the chemicals are listed in Table 2.1. Glassy carbon plate (1 mm thick, type 1: CAS no. 7440-44-0; Alfa Aesar, Thermo Fishere Scientific, USA) was used for investigation of surface morphology (SEM analysis)



**Table 2.1:** Details of all chemicals used in present dissertation.

| Sl. No. | Chemicals                         | IUPAC Name                                               | Formula                                          | Company                          | CAS No./ID |
|---------|-----------------------------------|----------------------------------------------------------|--------------------------------------------------|----------------------------------|------------|
| 1       | Silver nitrate                    | Silver nitrate                                           | $\text{AgNO}_3$                                  | HiMedia Chemicals, Mumbai India. | 7761-88-8  |
| 2       | Chloroform                        | Trichloromethane                                         | $\text{CHCl}_3$                                  | HiMedia Chemicals, Mumbai India. | 67-66-3    |
| 3       | Glycine                           | 2-Aminoethanoic acid                                     | $\text{C}_2\text{H}_5\text{NO}_2$                | HiMedia Chemicals, Mumbai India. | 56-40-6    |
| 4       | Lead acetate                      | Lead acetate                                             | $\text{Pb}(\text{C}_2\text{H}_3\text{O}_2)_2$    | HiMedia Chemicals, Mumbai India. | 6080-56-4  |
| 5       | Ethylene diamine tetraacetic acid | 2,2',2'',2'''-(Ethane 1,2-diyl)dinitrilotetraacetic acid | $\text{C}_{10}\text{H}_{16}\text{N}_2\text{O}_8$ | HiMedia Chemicals, Mumbai India  | 60-00-4    |
| 6       | Chitosan                          | (1,4)-2-Amino-2-desoxy- beta-D-glucan                    | $(\text{C}_6\text{H}_{11}\text{NO}_4)_n$         | HiMedia Chemicals,               | 9012-76-4  |

|    |                                                 |                                                       |                                                     |                                           |                    |
|----|-------------------------------------------------|-------------------------------------------------------|-----------------------------------------------------|-------------------------------------------|--------------------|
|    |                                                 |                                                       |                                                     | Mumbai<br>India.                          |                    |
| 7  | Sodium<br>phosphate<br>dibasic<br>heptahydrate  | Disodium;<br>dihydrogen<br>phosphate;<br>heptahydrate | $\text{Na}_2\text{HPO}_4 \cdot 7\text{H}_2\text{O}$ | HiMedia<br>Chemicals,<br>Mumbai<br>India. | 7558-<br>79-4      |
| 8  | Sodium<br>phosphate<br>monobasic<br>monohydrate | Sodium<br>dihydrogen<br>phosphate                     | $\text{NaH}_2\text{PO}_4 \cdot \text{H}_2\text{O}$  | HiMedia<br>Chemicals,<br>Mumbai<br>India. | 10049-<br>21-5.    |
| 9  | Ferric chloride                                 | Iron<br>trichloride<br>hexahydrate                    | $\text{FeCl}_3 \cdot 6\text{H}_2\text{O}$           | HiMedia<br>Chemicals,<br>Mumbai<br>India. | 10025<br>-77-<br>1 |
| 10 | Sodium<br>acetate<br>anhydrous                  | Sodium<br>acetate                                     | $\text{CH}_3\text{COONa}$                           | HiMedia<br>Chemicals,<br>Mumbai<br>India. | 127-09-3           |
| 11 | Acetic acid                                     | Acetic acid                                           | $\text{CH}_3\text{COOH}$                            | HiMedia<br>Chemicals,<br>Mumbai<br>India. | 64-19-7            |
| 12 | Trimethoxy(o<br>ctyl)silane                     | Trimethoxy(o<br>ctyl)silane                           | $\text{C}_{11}\text{H}_{26}\text{O}_5\text{Si}_2$   | Sigma<br>Aldrich,<br>USA.                 | 3069-40-<br>7      |

|    |                                     |                                           |                                                                |                      |            |
|----|-------------------------------------|-------------------------------------------|----------------------------------------------------------------|----------------------|------------|
| 13 | (3-Mercaptopropyl) trimethoxysilane | (3-Mercaptopropyl) trimethoxysilane       | $\text{HS}(\text{CH}_2)_3\text{Si}(\text{OCH}_3)_3$            | Sigma Aldrich, USA.  | 4420-74-0  |
| 14 | Bisphenol A                         | 4,4'-(propane-2,2-diyl) diphenol          | $(\text{CH}_3)_2\text{C}(\text{C}_6\text{H}_4\text{OH})_2$     | Merck, Mumbai, India | 80-05-7    |
| 15 | Triclosan                           | 5-chloro-2-(2,4-dichlorophenoxy)phenol    | $\text{C}_{12}\text{H}_7\text{Cl}_3\text{O}_2$                 | Merck, Mumbai, India | 3380-34-5  |
| 16 | Lead nitrate                        | Lead nitrate                              | $\text{Pb}(\text{NO}_3)_2$                                     | Merck, Mumbai, India | 10099-74-8 |
| 17 | Potassium ferricyanide              | Potassium hexacyanoferate (III)           | $\text{K}_3[\text{Fe}(\text{CN})_6]$                           | Merck, Mumbai, India | 13746-66-2 |
| 18 | Potassium ferrocyanide              | Potassium hexacyanoferate (II) trihydrate | $\text{K}_4[\text{Fe}(\text{CN})_6] \cdot 3\text{H}_2\text{O}$ | Merck, Mumbai, India | 14459-95-1 |
| 19 | Potassium chloride                  | Potassium chloride                        | KCl                                                            | Merck, Mumbai, India | 7447-40-7  |

|    |                              |                              |                                                      |                      |            |
|----|------------------------------|------------------------------|------------------------------------------------------|----------------------|------------|
| 20 | Copper sulphate              | Copper sulphate              | $\text{CuSO}_4$                                      | Merck, Mumbai, India | 7758-98-7  |
| 21 | Ethyl alcohol                | Ethanol                      | $\text{C}_2\text{H}_5\text{OH}$                      | Merck, Mumbai, India | 64-17-5    |
| 22 | Glutardialdehyde             | Pentanedial                  | $\text{C}_5\text{H}_8\text{O}_2$                     | Merck, Mumbai, India | 111-30-8   |
| 23 | Cadmium nitrate tetrahydrate | Cadmium nitrate tetrahydrate | $\text{Cd}(\text{NO}_3)_2 \cdot 4\text{H}_2\text{O}$ | Merck, Mumbai, India | 10022-68-1 |
| 24 | Zinc sulphate                | Zinc sulphate                | $\text{ZnSO}_4$                                      | Merck, Mumbai, India | 7446-20-0  |
| 25 | Chromium chloride            | Chromium chloride            | $\text{CrCl}_3$                                      | Merck, Mumbai, India | 10049-05-5 |
| 26 | Methanol                     | Methanol                     | $\text{CH}_3\text{OH}$                               | Merck, Mumbai, India | 67-56-1    |
| 27 | Sodium hydroxide             | Sodium hydroxide             | $\text{NaOH}$                                        | Merck, Mumbai, India | 1310-73-2  |
| 28 | N,N-dimethylformamide        | N,N-dimethylformamide        | $\text{C}_3\text{H}_7\text{NO}$                      | Merck, Mumbai, India | 68-12-2    |

|    |                    |                    |                                  |                      |           |
|----|--------------------|--------------------|----------------------------------|----------------------|-----------|
| 29 | Nickel chloride    | Dichloronickel     | $\text{Cl}_2\text{Ni}$           | Merck, Mumbai, India | 7718-54-9 |
| 30 | Oxalic acid        | Oxalic acid        | $\text{C}_2\text{H}_2\text{O}_4$ | Merck, Mumbai, India | 144-62-7  |
| 31 | Sodium chloride    | Sodium chloride    | $\text{NaCl}$                    | Merck, Mumbai, India | 7647-14-5 |
| 32 | Hydroquinone       | Benzene-1,4-diol   | $\text{C}_6\text{H}_6\text{O}_2$ | Merck, Mumbai, India | 123-31-9  |
| 33 | Phenol             | Phenol             | $\text{C}_6\text{H}_6\text{O}$   | Merck, Mumbai, India | 108-95-2  |
| 34 | Sodium nitrate     | Sodium nitrate     | $\text{NaNO}_3$                  | Merck, Mumbai, India | 7631-99-4 |
| 35 | Magnesium sulphate | Magnesium sulphate | $\text{MgSO}_4$                  | Merck, Mumbai, India | 7487-88-9 |
| 36 | Sulphuric acid     | Sulphuric acid     | $\text{H}_2\text{SO}_4$          | Merck, Mumbai, India | 7664-93-9 |

Water purification system (Arium Mini Plus UV Lab) was used to obtain the purified water having the water resistivity (at 25°C) is  $18.2 \text{ M}\Omega \times \text{cm}$  &  $< 20 \text{ }\mu\text{S/cm}$ .

Double distilled water is employed to prepare all the solutions. Acetate buffer and phosphate buffer solutions were prepared using the known methods described elsewhere (Po & Senozan, 2001). The standard analyte solutions were diluted using the stock solution and their pH was adjusted using 0.1 M HCl or NaOH solutions. All interfering ion solutions were prepared using 1000 ppm AAS standard solutions.

### 2.3. INSTRUMENTS

All weighing was performed using an electronic balance (HPB220, Wensar, India). All the solutions pH were adjusted using Microprocessor pH meter (Labtronics, India). Collecting solid samples using centrifuge (REMI-23, Vasai, India) having RPM of 6900. Sonicator (LMUS-4, Wensar, India) was used for sonication of electrodes after polishing. A UV-Visible spectrophotometer (UV-1800, Shimadzu, Japan) was used for analysing silver nanoparticles in the fixed wavelength of 200 nm to 600 nm. The characterisation of chitosan (CH) and composite materials (CHMTS and CHTMS) and nanocomposite (CHTMS+Ag(NPs)) material was done using Fourier Transform Infra-Red Spectrometer (FT-IR, IR Affinity-1S, Shimadzu, Japan) within the wavenumber of 500 to 4000  $\text{cm}^{-1}$ .

X-Ray diffraction (XRD) instrument (PANalytical, X'Pert PRO MPD, Netherland) was utilised to obtain the diffraction pattern of CH, CHMTS, CHTMS and CHTMS+Ag(NPs) materials with the set operation condition: scan rate 0.033 of 2 $\theta$  illumination, and generator 30 mA, 40 kV. Anode material Cu  $K_{\alpha 1}$  and  $K_{\alpha 2}$  radiations were utilised, which have the wavelengths of 1.5406 and 1.54443 Å. Surface area, pore size and pore volume of CH, CHMTS and CHTMS material were obtained using Brunauer-Emmett-Teller (BET) analyses (Micromeritics, ASAP 2000 V2.04, USA) based on N<sub>2</sub> adsorption and desorption isotherm.

The surface morphology of the CH, CHMTS, CHTMS and CHTMS+Ag(NPs) materials were obtained using a Field Emission Scanning Electron Microscope/Energy dispersive X-Ray (FESEM/EDX: JEOL JSM 7100F; Oxford Xmax, Japan), Operation condition: SEI Resolution used: 15 kV, Magnification: 10 - 1000000, Accelerating

Voltage: 0.2 - 30kV, Probe Current: 1pA- 400nA and Electron Gun used: In-lens Schottky field emission gun and High Resolution Transmission Electron Microscopic (HRTEM: JEOL, JEM 2100; Oxford Xtreme, Japan) operated at an Acceleration voltage: 200 kV, Magnification: X40K, Emission current (status): 113  $\mu$ A, Spot size (diameter): TEM Spot 1, Alpha 3, Current density: 0.3 pA/cm<sup>2</sup>, Experiment time: 0.3 sec. M.

TOC analyser (TOC-VCPH/CPN, Shimadzu, Japan) was used to analyse the NPOC and IC of the real water sample collected from different locations in Mizoram. The instrument is operated at high temperature catalytic oxidation of pollutants (680°C combustion) and a non-dispersive infra-red (NDIR) detector was used to analyse the generated CO<sub>2</sub>.

Similarly, the water samples were subjected for elemental analysis such as Cu, Ca, Zn, Pb, Ni, Fe, Mn utilising Atomic Absorption Spectrometer (AAS) (Model: AA-7000, Shimadzu, Japan). Calibration of AAS was done using standards (1000 ppm) of all the elements procured from Merck, Mumbai, India, and made three different concentrations through serial dilution for each element and calibrated using the prepared concentration for each elemental analysis.

Multiparameter photometer (Hanna, model: Hi83300, USA) was used for analysing nitrate, phosphate, sulphate and fluoride along with Multiparameter waterproof meter (probe) (Hanna, model: HI98194, USA), which determines *on site* the pH, ORP (Oxidation-Reduction Potential), conductivity, resistivity, TDS (Total Dissolved Solid) and salinity of the real water sample.

Electrochemical characterisation of the test solutions was carried out using cyclic voltammetry (CV) and electrochemical impedance spectroscopy (EIS). Whereas, the electrochemical measurement (detection of pollutants) was carried out by differential pulse anodic stripping voltammetry (DPASV) using electrochemical workstation (Biologic Instruments, Model SP-200, France). All the experiment was conducted using reference electrode Ag/AgCl/KCl (3.5M) (BaSi, USA, Model: RE-5B, France), platinum electrode was used as counter electrode (outer diameter-6 mm, inner diameter 1.6 mm; Model: A-002013, France) and working electrode as glassy

carbon electrode (GCE) (outer diameter – 6 mm, inner diameter - 3 mm; Model: A-002421, France). The electrochemical data were analysed using inbuilt computer software ECLab®.

## **2.4. ELECTROCHEMICAL METHODS**

### **2.4.1. Cyclic Voltammetry**

Cyclic voltammetry is an electroanalytical technique where a potentiostat applies a triangular potential waveform to an electrochemical system and measures the resulting current. The triangular waveform is made up of this potential sweep, sweeping the potential linearly as a function of time. The current is measured as a function of time but ends up plotting the current as a function of the applied potential and the plot represents current on the Y-axis and potential on the X-axis and this gives a cyclic voltammogram. This triangular waveform has several parameters such as it has an initial potential, which is the starting point of the experiment. It starts at the point where sweep the potential, then sweep it to the switching potential, which defines the end of the first segment of triangular potential waveform and then the final potential, which defines the second segment of linear sweep completing the triangular waveform representing one cycle (*Cf* Figure 2.1). The cyclic voltammetry consists of one or multiple cycles. Initial potential, switching potential and final potential and the number of segments is adjusted depending on electrochemical systems. In fact, there are a wide variety of potential waveforms that can be created just based on adjusting the parameters. The classical triangular potential waveform is not strictly the only waveform used in cyclic voltammetry. In classical triangular potential waveform consists of two segments, if it only consists of one segment it is referred as linear sweep voltammetry. The final parameter adjusted in a cyclic voltammetry is the slope of the linear sweep, which is referred as the sweep rate or the scan rate and it is measured of how fast the sweep is conducted or in other words the potential as a function of time.



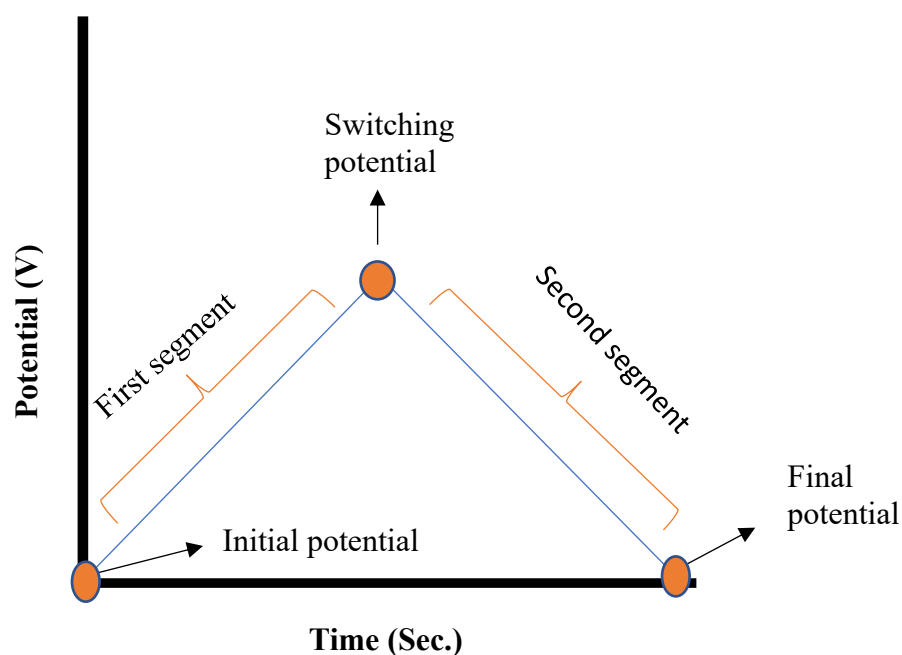


**Figure 2.1:** Potential sweep from initial potential to switching potential completed first segment and sweep to the final potential, which represent the second segment representing one cycle in cyclic voltammetry study.

#### 2.4.2. Pulse voltammetry techniques

In pulse technique, the difference between the charging current decay and faradaic currents rates of decay, which usually follows a potential step or pulse fashion. Exponential decay was observed in a charging current whereas, for faradaic current (diffusion controlled current) decay as a function of  $1/(\text{time})^{1/2}$ . The charging current decay is much faster compared to faradaic current decay. After the potential step, the charging current becomes insignificant after a time of  $5R_uC_{dl}$  ( $R_uC_{dl}$  is the electrochemical cell, time constant ranging from  $\mu\text{s}$  to  $\text{ms}$ ). Since only the faradaic current is present beyond this point (charging current), monitoring the current at the end of a potential pulse allows for the separation of the faradaic and charging currents.

Important parameters for pulse technique include pulse amplitude, pulse width and sampling period. Pulse voltammetry is of three types as:

#### ***Normal pulse voltammetry (NPV)***

In this type of technique, a series of potential pulses are applied, which have the same width and increase amplitude. The potential keeps coming back to its initial value after every pulse. The measurement of current is done at the end of each pulse. The duration of pulses is usually 1 to 200 ms and the interval is of several seconds. Normal pulse voltammogram is of sigmoidal shape.

#### ***Differential Pulse Voltammetry (DPV)***

In this type of technique, the potential form comprises a small pulse of the same amplitude of 10-100 mV and this pulse is superimposed on each other in a stair-case wave fashion. The measurement of the current is done twice after each pulse period. Firstly, it is measured at the starting of the applied pulse and then at the end of the same pulse. The differential pulse voltammogram shows differentiations between the measured current for every pulse.

#### ***Square wave voltammetry (SWV)***

It is one of the most advanced, fast and sophisticated techniques. The potential form of SWV comprises a symmetrical square wave pulse having the same amplitude (ESW). This pulse is superimposed in a stair-case wave fashion. In SWV, the potential changes from a small potential step i.e.,  $dE$ . In this technique the current is measured two times at the end of every cycle. Oxidative current i.e., forward current is produced when the measurement of current is done at the end of half cycle of oxidation. Similarly, the reductive current i.e., the backward current produced and the measurement of the current is done at the end of the half cycle of reduction. From subtraction between the backward and forward current is the net current in SWV.

### 2.4.3. Electrochemical impedance spectroscopy (EIS)

Electrochemical impedance spectroscopy (EIS) is an electrochemical technique that measures the impedance of a system depending on the frequency of AC (alternating current) potentials. The impedance is an electrical parameter used in real world circuit elements that exhibit complex behaviours, unlike the ideal resistor. Similar to resistance, impedance is also a measure of the circuit's potential to resist the current flow. However, it is not limited by the ideal resistor properties such as independence of frequency, fulfilment of Ohm's law at all levels of voltage and current, and lastly, the phase coherence of current and voltage signals through the resistor. While resistance is the ratio of voltage/potential and current for a direct current (DC) system, the impedance is the ratio of voltage/potential and current for AC systems. Usually, it is measured by the application of an AC potential to an electrochemical cell and then measuring the current through the cell. Assuming that we apply a sinusoidal potential excitation, the response to this potential is an AC signal. This current signal is analysed as a sum of sinusoidal functions (a Fourier series). Electrochemical impedance is normally measured using a small excitation signal so that the response of the cell is pseudo-linear. In a linear (or pseudo-linear) system, the current response to a sinusoidal potential will be a sinusoid at the same frequency but shifted in phase. Therefore, it behaves like a wave, and because of this nature, it is necessary to define impedance with two parameters which are (i) total impedance ( $Z$ ) and (ii) phase shift ( $\Phi$ ). These are expressed in the impedance spectra in the form of Nyquist plots and Bode plots. The expression for  $Z(\omega)$  (where  $\omega$  is angular velocity of current;  $\omega = 2\pi\nu$ ; where  $\nu$  is the frequency) is made up of two components - real and imaginary components. In the Bode plot, the impedance is plotted against log frequency on the X-axis and absolute impedance values ( $|Z|=Z_0$ ) and phase-shift on the Y-axis. A "Nyquist Plot" is obtained by plotting the real component on the X-axis and the imaginary component on the Y-axis of the graph. The Y-axis is negative in this plot, and each point on the Nyquist Plot represents the impedance at a given frequency. Fitting EIS data to an equivalent electrical circuit model is a common method of analysing EIS data. The majority of the circuit elements in the model are standard electrical components such as resistors, capacitors, and

inductors. In EIS experiments of real samples, capacitors frequently do not behave ideally. Rather, they function as a constant phase element. These circuit components relate to certain electrochemical properties such as solution resistance, double layer capacitance, polarization resistance, charge transfer resistance, etc. which are important factors in the impedance of electrolytic cells. Thus, by fitting experimental EIS data collected from electrolytic cells to a suitable electrical circuit model, the values of these electrochemical parameters are optimized by the least square fitting method and accordingly the equivalent circuit is obtained.

## 2.5. MATERIALS PREPARATION

### 2.5.1. Preparation of plant leaf extracts (*Psidium guajava*)

Fresh and matured leave of guava (*Psidium guajava*) was collected from the Mizoram University, India, campus premises and washed thoroughly using distilled water for removing foreign material and using oven it was dried at 50°C. After drying, leaves were chopped into smaller pieces. The chopped leaf was weight 5 gm and grinded using mortar and pestle to form a paste and dispensed in double distilled water of around 60 mL under stirred and kept stirring for 30 minutes at room temperature. The solution mixture was filtered using Whatman filter paper (pore size 11µm) after 30 minutes of stirring Figure 2.2. After filtration of the leaf extract it was stored in a polyethylene bottle and kept in the refrigerator for further usage.

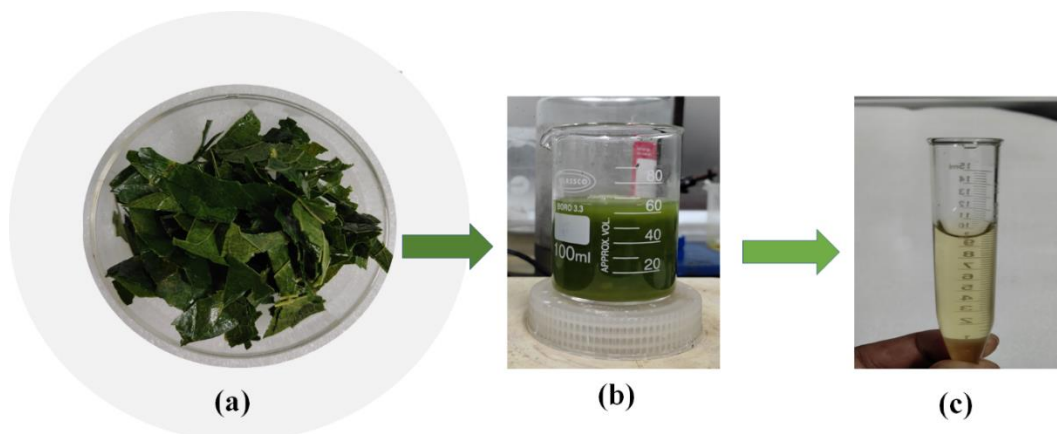


**Figure 2.2:** Extraction of phytochemicals from *Psidium guajava* leaves; (a) *Psidium guajava* chopped leaves; (b) grinded leaves was stirred with 60 mL of double distilled water for 30 minutes; and (c) leave extract, filtered using Whatman filter paper (pore size 11µm).

### 2.5.2. Leave extract phytochemical analysis

Different phytochemicals present in *Psidium guajava* leaves extract were analysed qualitatively. Several test was conducted using the standard phytochemical method such as, test for alkaloids, glycosides, steroids (Chandraker et al., 2020), flavonoid (Rattanachaikunsopon & Phumkhachorn, 2010), saponins (Adeyemi et al., 2009), quinones (Vaidyanathan & Kiruba, 2014), tannin (Mailoa et al., 2014) and terpenoids (Biswas et al., 2013) were carried out and positive results were confirmed for these phytochemicals.

**Alkaloids Test:** The mixture of 2 mL of leaves extract and 2 mL of 10% aqueous hydrochloric acid was agitated for 20 minutes. Wagner's reagent was added in small amounts to 1 mL of the mixed solution, which produced a white precipitate that showed the presence of alkaloids.

**Glycosides Test:** Add 2-3 drops of Molisch's reagent to 1 mL of the leaves extract and few drops of concentrated H<sub>2</sub>SO<sub>4</sub> added slowly to the reaction mixture. The creation of a ring (brownish) at the junction of the solution mixture verifies the presence of glycosides.

**Steroids Test:** Chloroform 2mL was dispensed in 2 mL of the leaves extract. And add 2 mL of chloroform, which forms the lowest layer of the solution mixture and indicates the presence of steroids in the leaves extract, to the solution mixture slowly.

**Flavonoid Test:** A test tube containing 3 mL of filtered leaves extract was mixed with 1 mL of 10% NaOH, the liquid became yellow, indicating the presence of flavonoids.

**Saponin Test:** Shaking vigorously after adding 5 mL of the leaves extract to 5 mL of distilled water causes foam to develop, indicating the presence of saponin.

**Quinone Test:** When a few drops of concentrated  $\text{H}_2\text{SO}_4$  are added to 1 mL of leaf extract, the liquid changes colour from clear to yellowish brown, indicating the presence of quinone.

**Tannin Test:** Shake vigorously after adding 2 mL of a 5% ferric chloride solution to 1 mL of the leaf extract. The presence of tannin in the leaf extract was confirmed by the observation of a dark green coloration.

**Terpenoids Test (Salkowski test):** To create a mixed solution, 5 mL of the leaves extract was placed in a test tube along with 2 mL of chloroform. 3 mL of concentrated  $\text{H}_2\text{SO}_4$  was added to the solution mixture slowly. This will create a layer that is reddish brown in colour at the interface, indicating that terpenoids are present in the leaf extract.

### **2.5.3. Composite/nanocomposite material synthesis**

#### **2.5.4. Composite material synthesis**

Chitosan (CH) (degree of deacetylation  $\geq 75\%$ ) was used as a substrate material. The 30 gm of chitosan was taken in a three neck round bottom flask and dispensed using 300 mL of N, N-dimethylformamide under constant stirring in a magnetic stirrer. After complete dispensed of chitosan in N, N-dimethylformamide, 30 mL of trimethoxyoctylsilane/3-mercaptopropyl trimethoxysilane was slowly introduced using micropipette dropper under constant stirring and under nitrogen atmosphere. The flask was sealed and stirred for 48 hours under a nitrogen atmosphere at  $105^\circ\text{C}$  and refluxed using the condenser. After 48 hours the heating was stopped and a mixture of 90 mL acetic acid and 180 mL of ethanol was added into the reaction mixture under constant stirring and again sealed the flask and stirred for another 24 hours under nitrogen atmosphere at room temperature Figure 2.3 (a). The formation of gel was observed and it was clearly dispersed in the reaction mixture, which was then collected using centrifugation at 4000 RPM (Revolution Per Minutes). The composite gel was washed with methanol 10 times and dried in a hot air oven at  $50^\circ\text{C}$  for 12 hours. The dried composite material was grinded into its powder form using mortar and pestle and sieved the grinded composite material using 100 nm BSS (British

standard sieve) sieve to make into powder form. The powder was used for characterization as well as for preparation of casting solution. The powder was stored in an airtight polyethylene container and labelled as CHTMS (chitosan-trimethoxyoctylsilane) and CHMTS (chitosan-3-mercaptopropyl trimethoxysilane) Figure 2.3. (b &c).

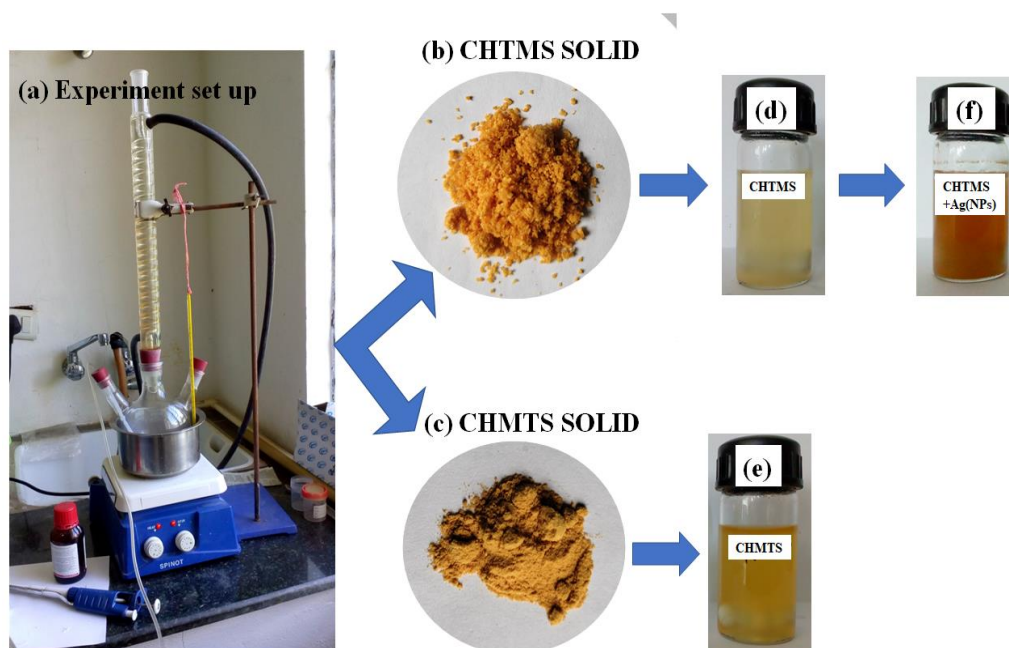


**Figure 2.3:** (a) Setup and synthesis of silane grafted chitosan and synthesized composite material; (b) CHTMS solid; (c) CHMTS solid; (d) casting solution for CHTMS; (e) casting solution for CHMTS; (f) Synthesized CHTMS+Ag(NPs), casting solution.

## 2.5.5. Casting solution preparation and nanocomposite material synthesis:

### 2.5.5.1. Casting solution preparation for composite material

50 mg of (CHTMS/CHMTS) composite material in a powder form was dispensed with 10 mL of 1% acetic acid solution to obtain 0.5% composite material stock solution. The solution mixture stirred for 12 hours using a magnetic stirrer. The

solid was completely dissolved and after the dissolution, the pH of the solution mixture was adjusted to 5.1 by adding freshly prepared 0.1 M NaOH. The solution mixture was collected using a centrifuge at 4000 RPM, and dispensed the sample in 10 mL of double distilled water, which was used as a casting solution as shown in Figure. 2.3 (d & e) form fabricating GCE.

#### **2.5.5.2. Synthesis of nanocomposite material and casting solution preparation (CHTMS+Ag(NPs))**

10 mL of solution mixture pH 5.1 (*from casting solution preparation*), freshly prepared 10 mL of AgNO<sub>3</sub> (30 mM) solution was vigorously mixed and stirred for 1 hours. After 1 hour of stirring 0.2 mL of *Psidium guajava* leaf extract was added and stirred the solution mixture for another 3 hours at 60°C under reflux. The solution colour was gradually changed from pale yellow to deep yellow. Further, the formation of silver nanoparticles was confirmed using the UV-visible measurements. The UV-Vis spectra were recorded within the wavelength range 200 nm to 600 nm. The nanocomposite material (CHTMS+Ag(NPs)) was collected using centrifugation at 4000 RPM and washed with double distilled water several times to remove any unreacted AgNO<sub>3</sub>.

#### **2.5.5.3. Preparation of Casting solution for CHTMS+Ag(NPs)**

After washing the collected sample was dispensed in 10 mL of double distilled water to form the final nanocomposite (CHTMS+Ag(NPs)) casting solution for fabricating GCE Figure 2.3 (f).

### **2.6. MATERIALS CHARACTERIZATION**

UV Visible spectrophotometer was used to confirm the formation of Ag(NPs) within the nanocomposite material (CHTMS+Ag(NPs)). The solution mixture of synthesized CHTMS+Ag(NPs) along with the bare composite and silver nitrate solutions were subjected to the UV-Vis Spectra. The UV-Vis spectra were recorded within the wavelength of 200 to 600 nm. Bare chitosan (CH), composite materials (CHTMS, CHMTS) and nanocomposite material (CHTMS+AgNPs) were



characterised using FT-IR Spectrometer. The FT-IR analysis enabled us to identify the functional groups present in the solids. The FT-IR spectra was recorded within the wavenumber of 500 to 4000  $\text{cm}^{-1}$ . Similarly, the XRD (X-Ray Diffraction) pattern of CHTMS and CHTMS+Ag(NPs) was obtained. Further, the XRD pattern was enabled us to identify the Ag(NPs) in the CHTMS+Ag(NPs) material. The diffraction peaks of CHTMS+Ag(NPs) material was used to estimate the crystallite size of solids under the powder X-ray diffraction results using the Scherrer formula (2.1)

$$d = \frac{0.9\lambda}{\beta \cos \theta} \quad \dots(2.1)$$

where 'd' is the crystallite size,  $\lambda$  is the wavelength of X-ray radiation source,  $\beta$  is the full width at half maximum (FWHM) of the XRD peak at diffraction angle  $\theta$  (Govindan et al., 2012).

The BET (Brunauer-Emmett-Teller) analyses of CH, CHTMS and CHMTS was conducted using the powder samples. The surface area, pore size and pore volume of the materials were obtained with the  $\text{N}_2$  adsorption and desorption isotherms.

Surface morphology study along with elemental mapping of the materials i.e., CH, CHTMS, CHMTS and CHTMS+Ag(NPs) was studied using glassy carbon plate (1 mm thick) which was polished first using 0.005  $\mu\text{m}$  alumina slurry rubbing solution and washed with double distilled water, followed by polishing using 1  $\mu\text{m}$  diamond rubbing solution and sonicated using ethanol and double distilled water for 2 minutes and dried in a hot air oven at 40°C for 30 minutes. Further, the dried and clean glassy carbon plate was casted using 0.02 mL casting solution of CH, CHMTS, CHTMS and CHTMS+Ag(NPs) and dried in the hot air oven at 40°C for 30 minutes. The casted glassy carbon sheets were then subjected for the field emission scanning electron microscope/energy dispersive X-Ray analysis (FE-SEM/EDX). HRTEM (high resolution transmission electron microscope) micrographs were obtained for CH, CHTMS, CHMTS and CHTMS+Ag(NPs) using the powder samples of these solids. The TEM micrographs enabled us to optimize the nanoparticle size and distribution. Further, using J software the average particle size was estimated and the d-spacings of the nanoparticle was calculated by Gatan digital micrograph software.

## **2.7. ELECTRODES FABRICATION**

### **2.7.1. GCE**

Fabrication of GCE was done using a straightforward drop casting technique. First, GCE (outer diameter – 6 mm, inner diameter - 3 mm) was polished using GCE polishing pad along with 0.005  $\mu\text{m}$  alumina slurry solution and washed with double distilled water and further polished using 1  $\mu\text{m}$  diamond rubbing solution and washed again with double distilled and sonicated in ethanol and double distilled water for 2 minutes each using ultrasonic cleaner sonicator to remove any impurities on the electrode surface and washed with double distilled water and dried in hot air oven at 40°C for 30 minutes Figure 2.4 (a&b). The clean and dried GCE was drop casted using the prepare casting solution, only 0.02 mL of casting solution was drop casted and dried in the hot air oven for 30 minutes at 40°C. After drying the fabricated electrode is ready for experiment in case of micropollutant detection study. Whereas for heavy metal detection study GCE was drop casted with CHTMS and CHTMS+Ag(NPs) casting solution and dried in the hot air oven and after drying the fabricated electrode (CHTMS/GCE and CHTMS+Ag(NPs)/GCE) was again crosslinked using 0.1% glutaraldehyde solution for 5 minutes each and washed with double distilled water to remove any uncross linked glutaraldehyde solution on the surface of the fabricated electrode and further dried the fabricated electrode in the hot air oven at 40°C for 30 minutes. After drying the fabricated electrode is ready for experiment Figure 2.4 (d &e).

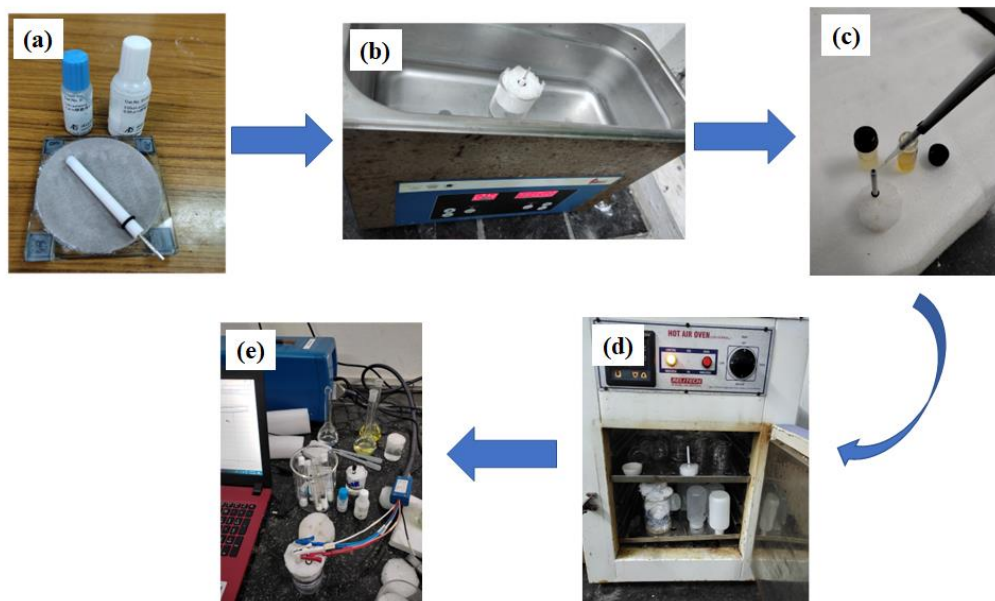


**Figure 2.4:** Fabrication of GCE (a) GCE along with polishing pad and solution; (b) Sonicating after polishing the GCE for two minutes each using ethanol and double distilled water; (c) simple drop casting method was followed; (d) drying the fabricated GCE at 40°C for 30 minutes; (e) Fabricated GCE is ready for experiment.

## 2.8. PROCEDURES FOR ELECTROCHEMICAL METHODE

### 2.8.1 Electrodes electrochemical characterization

First, cyclic voltammograms were recorded in presence of 20.0 mg/L bisphenol A (BPA) and triclosan (TCS). The voltammograms were recorded using supporting electrolyte phosphate buffer solution of pH 10.0 and 8.0 for BPA and TCS, with fixed potential window of -0.1 to 1.0 V (Ag/AgCl) and scan rate of 100 mV/s utilising CHMTS/GCE working electrode. While the scan rate study was conducted for bare GCE, CH/GCE, CHMTS/GCE, CHTMS/GCE and CHTMS+Ag(NPs)/GCE at varying scan rate of 20 to 150 mV/s at potential window of -0.5 to 0.1 V using the 0.002 M standard redox couple  $[\text{Fe}(\text{CN})_6]^{3-/4-}$  and the supporting electrolyte of 0.1 M acetate buffer solution. With the increase of scan rate, the peak current increases linearly and obtains a straight-line equation from the calibration curve which is a diffusion control process and follows Randles-Sevcik equation (2.2).

$$I_p = 2.69 \times 10^5 \times n^{2/3} \times v^{1/2} \times D^{1/2} \times C \times A \quad \dots(2.2)$$

where  $I_p$  is the peak current (mA);  $n$  is the number of electrons involved in redox process,  $D$  is the Diffusion coefficient of  $[\text{Fe}(\text{CN})_6]^{3-/4-}$  in aqueous media and equal to  $6.70 \times 10^{-7} \text{ cm}^2/\text{s}$ ,  $v$  is the scan rate (mV/s),  $C$  is the concentration of electroactive species (M), and  $A$  is the electroactive surface area of working electrode ( $\text{mm}^2$ ) (Marken et al., 2002).

For EIS characterisation, the fabricated electrodes CH/GCE, CHTMS/GCE, CHMTS/GCE and CHTMS+Ag(NPs) along with bare GCE were studied. The impedance spectra were collected for all the employed between 80 kHz and 100 MHz in the redox couple solution at 6 point per decade with sinusoidal amplitude of 10.0 mV. The best equivalent circuit  $R_1+Q_2/(R_2+W_2)$  was obtained for all the working electrode, where  $R_1$  stands for solution resistance ( $R_s$ ),  $Q_2$  for double layer capacitance ( $C_{dl}$ ) at solution and electrode interface,  $R_2$  for charge transfer resistance ( $R_{ct}$ ), and  $W_2$  for Warburg impedance ( $Z_w$ ) in the Randle's circuit, respectively, provided the best fit for the obtained Nyquist plot. Using the built-in programme EClab and the least square fitting approach, equivalent circuit fitting and electrical parameter evolution for each impedance spectrum are carried out.

### 2.8.2. Electrochemical determination of pollutants

For determination of heavy meatal toxic ion Pb (II), CHTMS and CHTMS+Ag(NPs) material were used for fabricating GCE and employed in differential pulse anodic stripping voltammetry study. The supporting electrolyte use was 0.1 M acetate buffer solution. Before conducting the detection experiment, the optimisation of experimental parameters was carried out such as pH, deposition potential, deposition time. The pH was studied from 3.4 to 5.5 in acetate buffer solution containing 50.0  $\mu\text{g/L}$  Pb (II). And for deposition potential study was conducted from -0.6 to -1.0 where deposition time study was conducted from 60.0 to 240.0 second. And other conditions such as pulse amplitude of 50 mV, scan increment of 10 mV, and pulse width of 50 ms. were remained constant for all the experiment. Under optimised condition behaviour of different fabricated electrode such as bare GCE,

CH/GCE, CHTMS/GCE and CHTMS+Ag(NPs)/GCE were studied. Concentration study was carried out from 5.0 to 80.0  $\mu\text{g/L}$ . while interfering study was conducted with the increase of 10 fold interfering ions compared to 50.0  $\mu\text{g/L}$  Pb (II), such interfering are Cd (II), Cr (II), Cu (II), Ni (II), Zn (II), glycine, oxalic acid and Ethylenediamine tetraacetic acid. Reproducibility study was conducted upon continuous detection (10 time) of 50.0  $\mu\text{g/L}$  Pb (II) and stability study was conducted using time duration of 0 to 48 hours where detection was done after 12 hour each and the fabricated electrode was stored at room temperature. Real water sample analysis was conducted using groundwater and spring water which was spiked with Pb (II) varying concentration of 5.0, 10.0, 20.0, 30.0 and 40.0  $\mu\text{g/L}$ . While recovery rate study was conducted using the spiked concentration in the real water sample. Whereas, for micropollutant determination study supporting electrode is 0.1 M phosphate buffer solution. The fabricated electrode CHMTS/GCE was employed for determination of bisphenol A (BPA) and triclosan (TCS). Electrochemical behaviour of the CHMTS/GCE was subjected to CV study to know the reversibility of the pollutant. Where differential pulse anodic voltammetry was used for electrochemical behaviour of pollutants toward bare GCE, CH/GCE and CHMTS/GCE. Optimisation of experimental parameter for BPA and TCS was studied at different concentration such as for BPA 180.0  $\mu\text{g/L}$  and for TCS is 200.0  $\mu\text{g/L}$ . pH optimisation was done in phosphate buffer solution at different pH from 6.0 to 10.0. Deposition potential was studied from 0.15 to 0.35 V for BPA and for TCS is from 0.2 to 0.5 V. And time study is from 90.0 to 210.0 second for BPA whereas, for TCS is from 60.0 to 180.0 second. Under the optimised experimental condition electrochemical determination of BPA and TCS was carried out from 140.0 to 200.0  $\mu\text{g/L}$  concentration. For interfering study 10 fold increase in interfering ion was employed in determination of BPA and TCS. Such interfering ions are phenol, hydroquinone, oxalic acid, glycine, Ethylenediamine tetraacetic acid,  $\text{Cl}^-$ ,  $\text{NO}_3^-$ ,  $\text{Mg}^{+2}$ ,  $\text{Na}^+$ . For reproducibility and stability, study continuous determination of BPA (180.0  $\mu\text{g/L}$ ) and TCS (200.0  $\mu\text{g/L}$ ) in variation of time i.e., 0 to 48 hours. Real matrix study was conducted using spring water, river water and ground water which is spiked with varying concentrations of BPA and TCS. And the recovery rate study was conducted using the spiked concentration in a real water sample. For calculating limit of detection (LOD) and limit of quantification

(LOQ) the standard equation was used i.e.,  $LOD = 3 \times SD/m$  and  $LOQ = 10 \times SD/m$ , where SD is the standard deviation of six replicate of blank sample, ' $m$ ' is the mean slope of the calibration line (Uhrovčík, 2014). Furthermore, RSD (relative standard deviation) was calculated using the equation  $percent\ RSD = s \times 100/m$ , where ' $s$ ' denotes the standard deviation and ' $m$ ' is the mean of the data (Gao et al., 2013)

**CHAPTER 3**  
**RESULTS AND DISCUSSION**

### 3. RESULTS AND DISCUSSION

#### 3.1. MATERIALS CHARACTERIZATION

##### 3.1.1. Phytochemical analysis of *Psidium guajava* leaves extract

The presence of numerous phytochemicals in *Psidium guajava* leaves extract were investigated using the standard qualitative tests. The results are shown in Table 3.1. It is evident that the alkaloids, glycosides, steroids, flavonoids, quinones, tannin, and terpenoids show positive test results. This confirmed the presence of these phytochemicals in the leaf extract. The presence of flavonoids reduces the Ag<sup>+</sup> ions and stabilizes the nanoparticles by capping the reduced nanoparticles (Kalainila et al., 2014).

**Table 3.1:** Phytochemical screening results. (+)= present

| Phytochemicals | Results |
|----------------|---------|
| Alkaloids      | +       |
| Glycosides     | +       |
| Steroids       | +       |
| Flavonoids     | +       |
| Saponin        | +       |
| Quinones       | +       |
| Tannin         | +       |
| Terpenoids     | +       |



### 3.1.2. UV-Visible spectroscopic analysis of Ag(NPs)

A UV-visible spectra demonstrates the formation of Ag(NPs). Therefore, UV-Visible spectra of the CHTMS, AgNO<sub>3</sub> and CHTMS+Ag(NPs) are shown in Figure 3.1 CHTMS+Ag(NPs) showed a strong SPR (surface plasmon resonance) peak at 440 nm, confirming the presence of Ag(NPs) with the CHTMS material. The SPR peak of CHTMS+Ag(NPs) sample occurred due to the reduction of Ag<sup>+</sup> to Ag<sup>0</sup> by the phytochemicals present in the leaf extract whereas no absorption peak appeared for CHTMS and AgNO<sub>3</sub> (Chen et al., 2014). Further, the Figure 3.1 (inset) shows an apparent colour of the CHTMS and CHTMS+Ag(NP) solutions. A distinct colour change with the CHTMS+Ag(NP), clearly inferred the presence of Ag(NPs) in the composite.

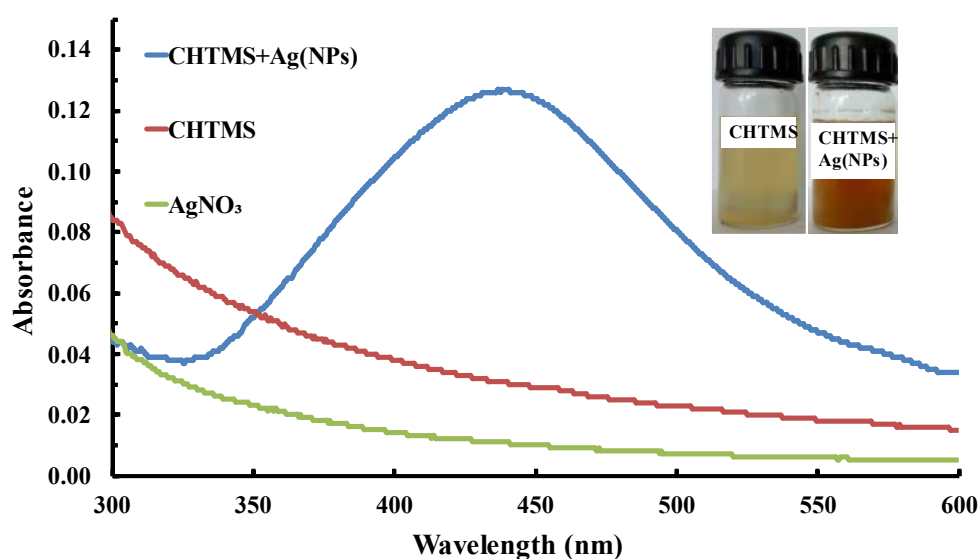


**Figure 3.1:** UV visible absorption spectra of the CHTMS, AgNO<sub>3</sub> and CHTMS+Ag(NPs) and inset CHTMS and CHTMS+Ag(NPs) solutions.

### 3.1.3. FT-IR analysis for synthesized materials

The FT-IR spectra of bare chitosan (CH), chitosan-trimethoxyoctylsilane (CHMTS), chitosan-3-mercaptopropyl trimethoxysilane (CHTMS) and

CHTMS+Ag(NPs) materials are shown in Figure 3.2 and the identified FT-IR vibration bands are included in Table 3.2. All these materials show the prominent FT-IR bands of alkyl, amide, N-H, O-H stretching vibrations, chitosan glycosidic linkages (-C-O-C-) (*Cf* Table 3.2). In CH, the stretching vibration of N-H and O-H appear in the region between 3000-3500  $\text{cm}^{-1}$ , which is almost diminished in CHTMS, CHMTS and CHTMS+Ag(NPs) materials. The alkyl vibrational band is observed around the wave number of 2916 and 2877  $\text{cm}^{-1}$ , whereas the amide peaks occurred around 1651 and 1558  $\text{cm}^{-1}$  in the CH. However, the amide band is shifted from 1558 to 1544  $\text{cm}^{-1}$  in CHMTS material while in CHTMS, the amide band is shifted from 1558 to 1543, respectively. This inferred the grafting of silane molecules with the amino group of chitosan (Lalhmunsiam et al., 2016). Whereas, in CHTMS+Ag(NPs) material the amide band was further shifted from 1543 to 1566  $\text{cm}^{-1}$  with reduced vibrational intensity of N-H band (Prakash et al., 2012). The -CH stretching bands were observed at 2916 and 2877  $\text{cm}^{-1}$  is associated with the propyl group introduced within the chitosan using the trimethoxyoctylsilane and 3-mercaptopropyl trimethoxysilane. Stretching vibrations around 1000-1100  $\text{cm}^{-1}$ , 900-950  $\text{cm}^{-1}$  and 700-800  $\text{cm}^{-1}$  were assigned to the presence of Si-O-Si, Si-OH and Si-O-Si in the CHMTS, CHTMS and CHTMS+Ag(NPs) (Lalhmunsiam et al., 2016). These results revealed that the silanes viz., the trimethoxyoctylsilane and 3-mercaptopropyl trimethoxysilane are successfully grafted with the chitosan matrix.

**Table 3.2:** Prominent FT-IR peaks of the CH, CHMTS, CHTMS and CHTMS+Ag(NPs) solids.

| FT-IR<br>Vibrational<br>bands | CH<br>( $\text{cm}^{-1}$ ) | CHMTS<br>( $\text{cm}^{-1}$ ) | CHTMS<br>( $\text{cm}^{-1}$ ) | CHTMS+Ag(NPs)<br>( $\text{cm}^{-1}$ ) |
|-------------------------------|----------------------------|-------------------------------|-------------------------------|---------------------------------------|
| Alkyl bond                    | 2870,<br>2924              | 2870, 2924                    | 2870, 2924                    | 2870, 2924                            |

|                                            |               |              |              |                                          |
|--------------------------------------------|---------------|--------------|--------------|------------------------------------------|
| Amide bond                                 | 1651,<br>1558 | 1558 to 1544 | 1558 to 1543 | 1543 to 1566<br>(Decreased<br>intensity) |
| -NH and -OH<br>stretching<br>vibrations    | 3363          | Diminished   | Diminished   | Diminished                               |
| -C-O-C-<br>glycosidic<br>linkage           | 1100-<br>1000 | 1100-1000    | 1100-1000    | 1100- 1000                               |
| Stretching<br>vibration of<br>Si-O-Si bond |               | 800-700      | 800-700      | 800-700                                  |
| Vibration of<br>Si-OH                      |               | 900-950      | 900-950      | 900-950                                  |

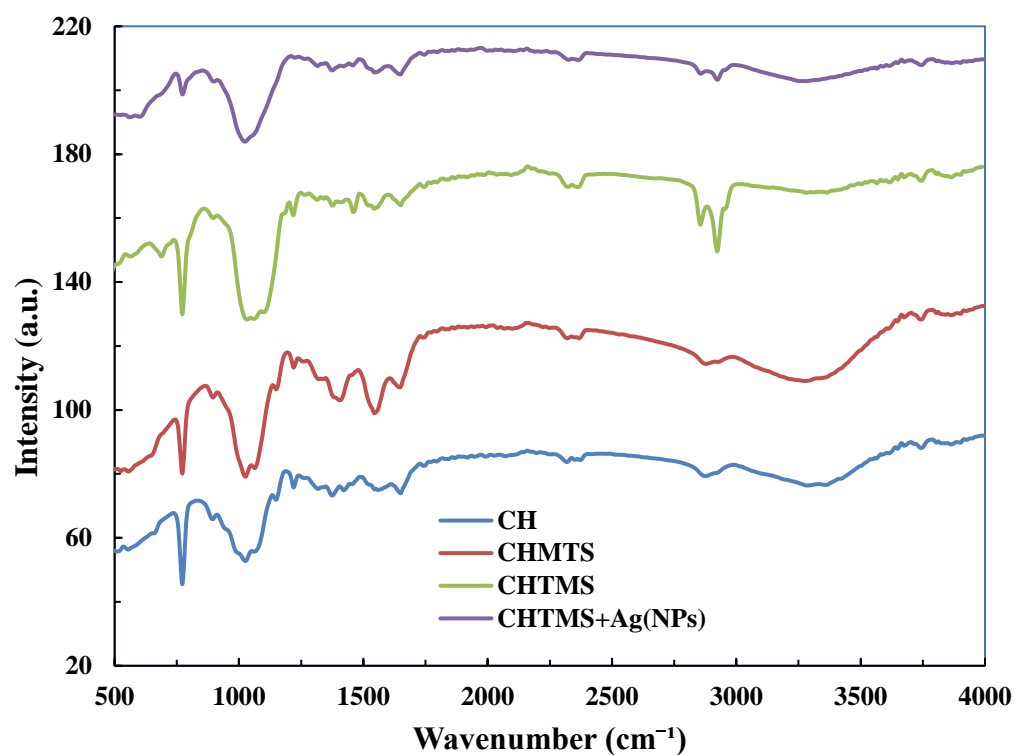


**Figure 3.2:** FT-IR spectra of CH, CHMTS, CHTMS and CHTMS+Ag(NPs) materials.

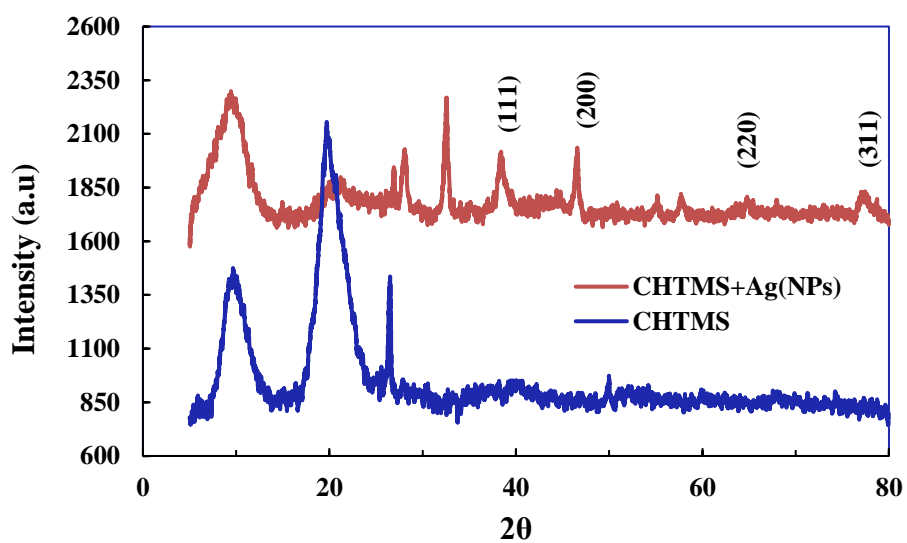


**Figure 3.3:** X-ray diffraction pattern of CHTMS and CHTMS+Ag(NPs) materials.

The X-ray diffraction pattern of the CHTMS and CHTMS+Ag(NPs) are shown in Figure 3.3. The XRD pattern shows two diffraction peaks at  $2\theta$  value of 9.5 and 20.26 in both the samples, which confirmed the semi-crystalline nature of chitosan. The higher degree of deacetylation of chitosan shows high degree of crystallinity; this is due to chains of chitosan with high degree of deacetylation are more flexible and with fewer large acetyl side groups (Yuan et al., 2011). The additional diffraction peaks appeared with the CHTMS+Ag(NPs) solid at the  $2\theta$  values of 38.38, 46.59, 64.79 and 77.43, which ascribed to the diffraction from the (111), (200), (220) and (311) planes of the Ag(NPs) (JCPDS card no. 04-0783). In addition, some additional peaks appeared in the XRD pattern which is, possibly, due to the some organic compounds/proteins present in the nanoparticle synthesis (Kalaivani et al., 2018; Prakash et al., 2012). Further, the mean crystallite size of the Ag(NPs) was obtained using the Scherrer Equation (2.1) (Govindan et al., 2012) and the calculated crystallite size was 28.17 nm.

The specific surface area, pore size and pore volume of CH, CHTMS and CHMTS are obtained by the BET analyser with nitrogen adsorption and desorption isotherms and the results are returned in Figure 3.4. The  $N_2$  adsorption and desorption isotherms show that all these materials follow type IV isotherm with an H3-type hysteresis loop, which consists of mesopores with slit-shaped pores (Cao et al., 2015; Rusmin et al., 2015). The surface area, pore size and pore volume of CH, CHMTS and CHTMS were returned in Table 3.3. CH has a surface area of  $0.172 \text{ m}^2/\text{g}$ , whereas the surface area of CHMTS and CHTMS was increased to  $1.013 \text{ m}^2/\text{g}$  and  $0.795 \text{ m}^2/\text{g}$  which is due to the grafting of silane within the chitosan matrix. The pore size of CH was larger i.e., 48.75 nm compared to CHMTS and CHTMS i.e., 35.21 nm and 35.12 nm, respectively. This is because grafted silane preferably occupied the pores of CH, resulting in decrease in pore size. However, the pore volume was increased from  $0.0024 \text{ cm}^3/\text{g}$  (for CH) to  $0.0097 \text{ cm}^3/\text{g}$  (for CHMTS) and  $0.0057 \text{ cm}^3/\text{g}$  (for CHTMS). Similar results were obtained by grafting of chitosan with 3-aminopropyltriethoxysilane resulting in enhanced surface area (Lalhmunsiana et al., 2016). Similarly, a significant increase in the surface area of composite material

(chitosan/nano- $\text{Al}_2\text{O}_3$  i.e.,  $38 \text{ m}^3/\text{g}$ ) was obtained compared to the bare chitosan (Zavareh et al., 2015).

**Table 3.3:** Surface area, pore size and pore volume of the CH, CHMTS and CHTMS materials obtained from the BET analysis.

| Materials | Surface area<br>( $\text{m}^2/\text{g}$ ) | Pore size<br>(nm) | Pore volume<br>( $\text{cm}^3/\text{g}$ ) |
|-----------|-------------------------------------------|-------------------|-------------------------------------------|
| CH        | 0.172                                     | 48.75             | 0.0024                                    |
| CHMTS     | 1.013                                     | 35.21             | 0.0097                                    |
| CHTMS     | 0.795                                     | 35.12             | 0.0057                                    |

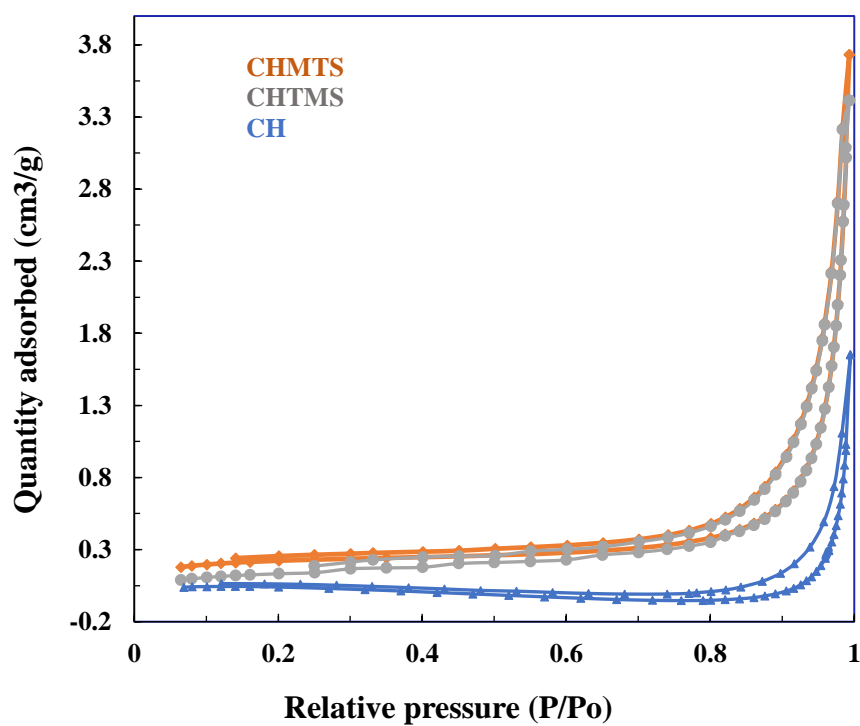


**Figure 3.4:** N<sub>2</sub> adsorption-desorption isotherms for the solids CH, CHTMS and CHMTS materials.

#### **3.1.4. Surface morphology of solids**

Surface morphology of CH and CHMTS, CHTMS and CHTMS+Ag(NPs) were studied using the scanning electron microscope (SEM) images of these solids and shown in Figure 3.5. The SEM image of bare CH shows a heterogeneous and porous surface where the pores are randomly distributed on the surface of chitosan. The polymer is dense and very disordered on the surface (*Cf* Figure 3.5 (a)). However, the SEM image of CHTMS composite material shows a very dense surface structure. The surface is heterogeneous and disordered but pores and surface are predominantly occupied by the silane molecules (trimethoxyoctylsilane) (*Cf* Figure 3.5 (b)). Moreover, perhaps, the silica is visible on the surface as white illuminations. Similarly, the material composite material CHMTS (i.e., 3-mercaptopropyl trimethoxysilane grafted chitosan) shows heterogeneous and dense surface structure. Silanes are predominantly occupied the surface and pores of the chitosan. Previously, it was reported that the grafting of silanes with chitosan caused for more dense and heterogeneous surface structure of solids (Lalhmunsiam et al., 2016). Finally, the SEM image of (CHTMS+Ag(NPs)) solid is shown in Figure 3.5 (d). It is evident from the SEM image that the Ag(NPs) are distinctly distributed onto the surface of composite CHTMS material. No agglomeration of Ag(NPs) is observed on the solid surface (Prakash et al., 2012).

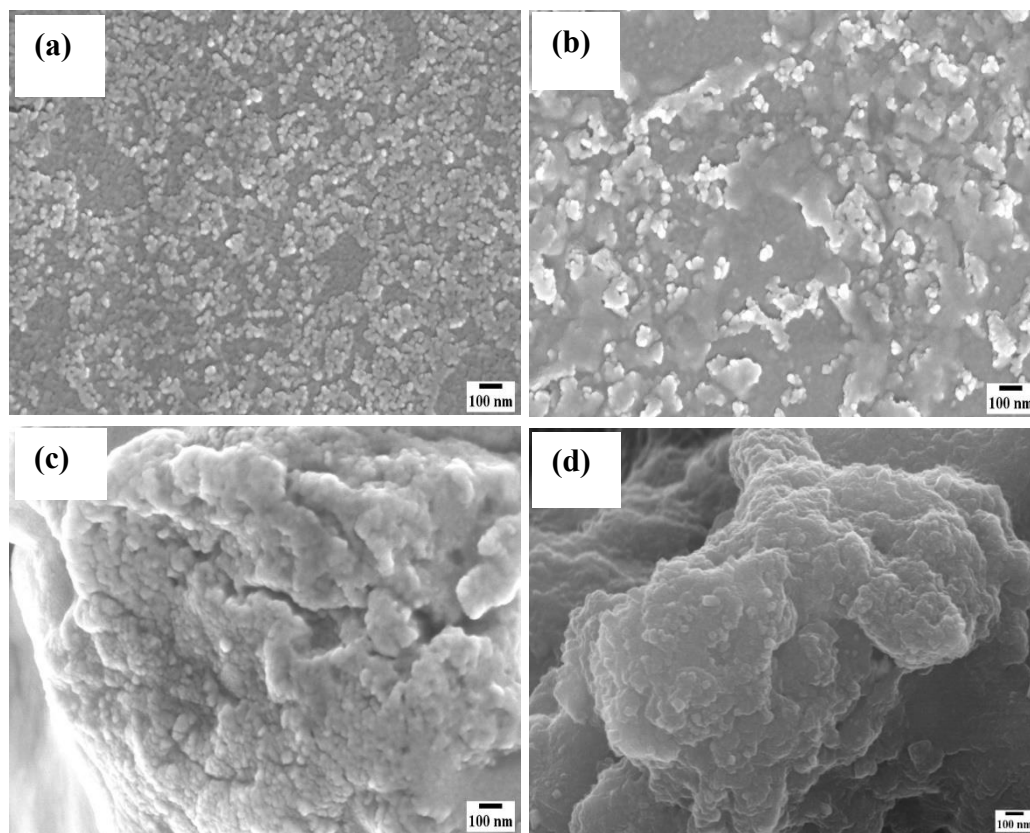


**Figure 3.5:** The SEM micrographs of (a) CH (Chitosan); (b) CHTMS; (c) CHMTS; and (d) CHTMS+Ag(NPs) materials.

Furthermore, Figure 3.6 (a-d), shows the energy dispersive X-ray spectra of these solids i.e., bare chitosan (CH), CHMTS, CHTMS and CHTMS+Ag(NPs). The EDX spectra of these solids show the distinct peaks of C, N, O, and S elements in all these solids. This inferred the presence of these elements in all the solids. However, an additional peak due to the presence of Si is appeared in the composite materials viz., CHMTS, CHMTS and CHTMS+Ag(NPs), further confirmed the presence of silane with the chitosan (*Cf* Figure 3.6 (b, c and d)). Further, the nanocomposite solid CHTMS+Ag(NPs) possessed an EDX peak due to the presence of Ag, inferred the decoration of composite materials with the Ag(NPs) (*Cf* Figure 3.6 (d)) (Murugan et al., 2017).



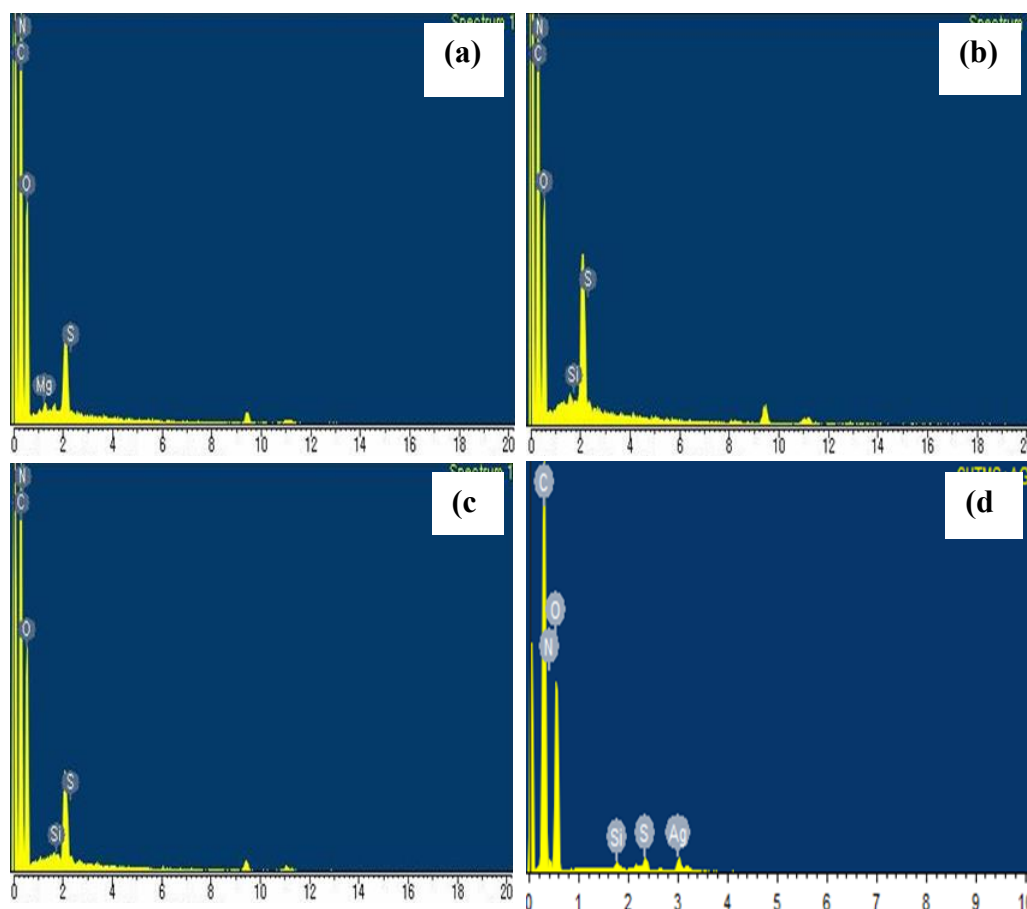


**Figure 3.6:** EDX spectra of (a) CH; (b) CHMTS; (c) CHTMS; and (d) CHTMS+Ag(NPs) materials.

The TEM micrographs of the chitosan and composite materials are shown in Figure 3.7 (a-e). Chitosan shows a dense and heterogeneous surface. Moreover, some linings are visible in the TEM micrographs possibly due to the arrangement of polymeric molecules within the chitosan network (*Cf* Figure 3.7 (a)). On the other hand, the CHMTS and CHTMS materials showed similar heterogeneous and dense surface structure. However, the darker spots indicated that the silanes occupied the surface of chitosan (*Cf* Figure 3.7 (b & c)). This inferred the grafting of silane within the chitosan network. Moreover, the grafted silane is aggregated on the surface and forms a denser material compared to the bare chitosan. Further, the TEM image of (CHMTS+Ag(NPs)) solid showed a distinct presence of small sized silver nanoparticles on the surface of composite CHTMS material. The Ag(NPs) are not

aggregated and almost spherical in shape (Cf Figure 3.7 (d)). Furthermore, the Ag(NPs) showed visible and clear fringes with the TEM micrograph ((Cf Figure 3.7 (e)), and Gatan Digital micrograph which was utilized to obtain the d-spacing and found to be 0.37 nm. Additionally, the average particle size distribution of Ag(NPs) was obtained using the Image J software and shown in Figure 3.7 (f). The average particle size histogram inferred that the mean diameter of the Ag(NPs) was 22.32 nm. The results inferred that the greener and *in situ* decoration of Ag(NPs) enabled to obtain spherical and small sized Ag(NPs) which were not aggregated on the surface of composite material (Uddin et al., 2017).

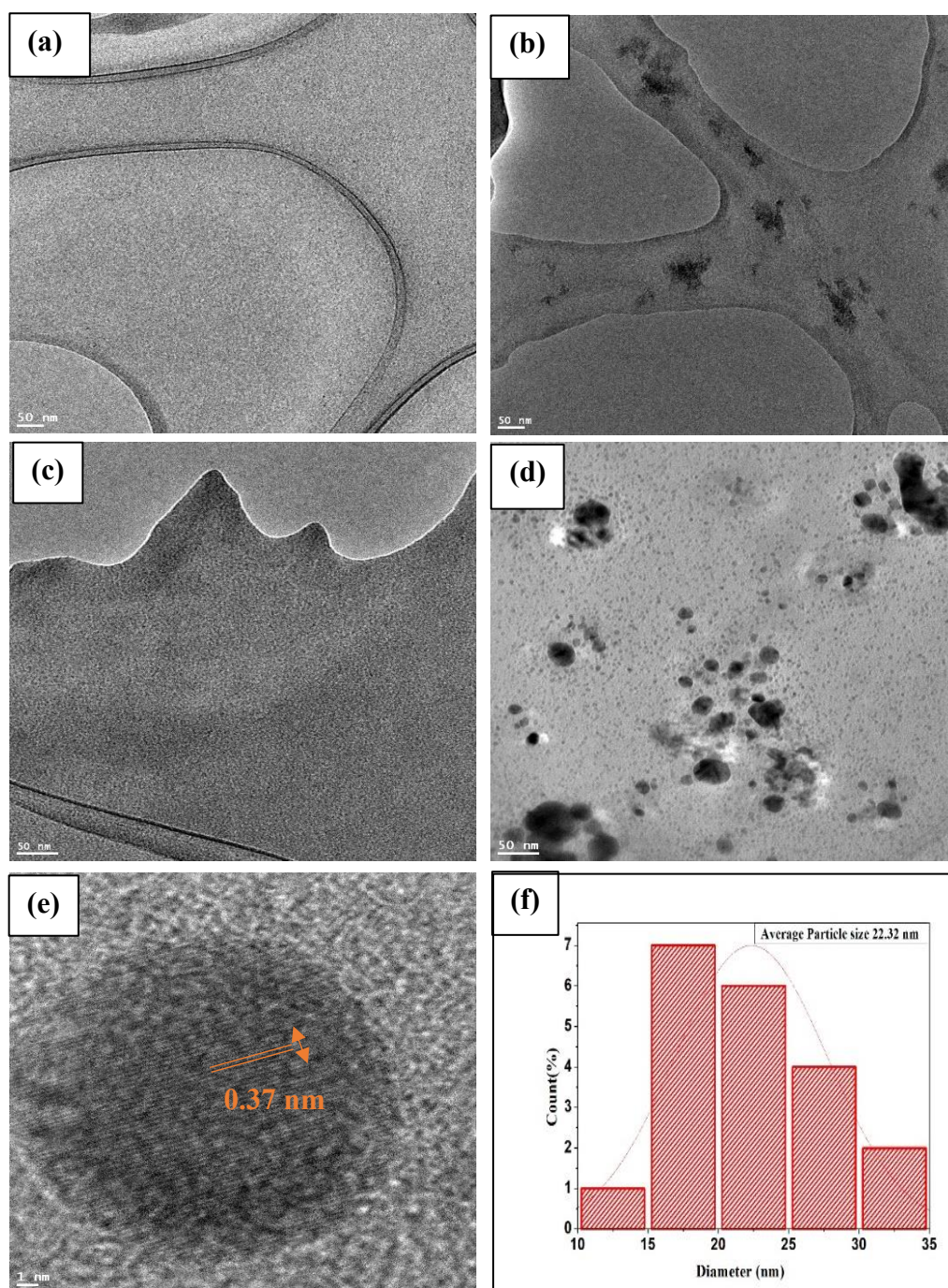


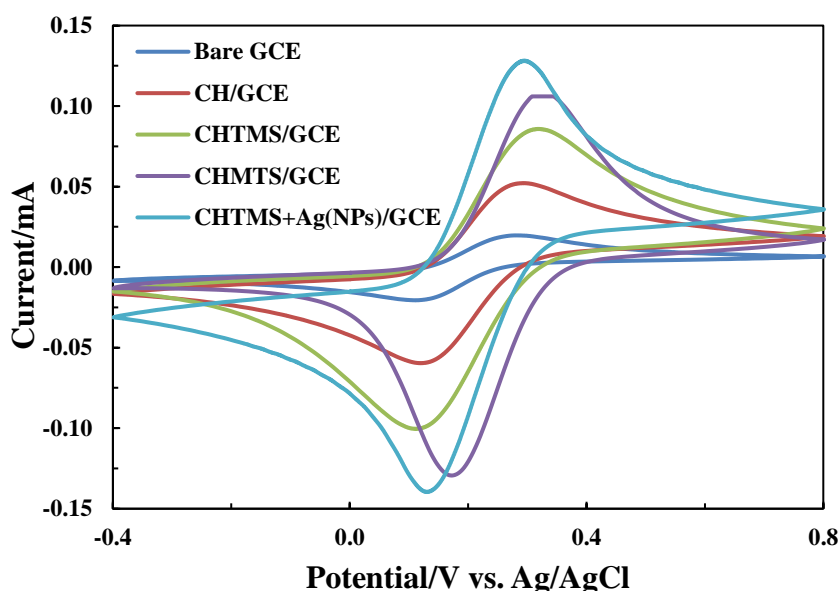
**Figure 3.7:** TEM micrographs of (a) Chitosan (CH); (b) CHMTS; (c) CHTMS; (d) CHTMS+Ag(NPs); (e) d-spacing of Ag(NPs); and (f) Average particle size distribution using the histogram for CHTMS+Ag(NPs) solid.

## 3.2. ELECTROCHEMICAL CHARACTERISATION OF FABRICATED GLASSY CARBON ELECTRODES

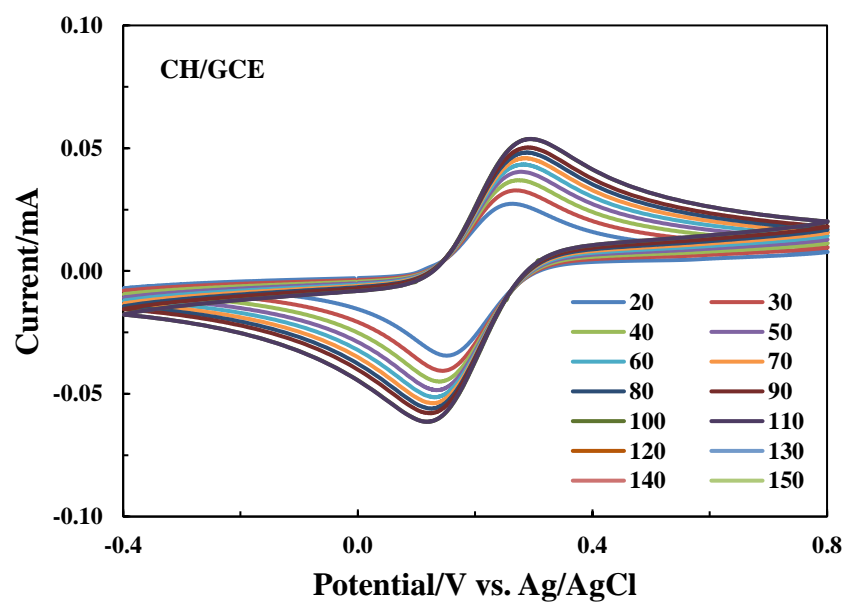
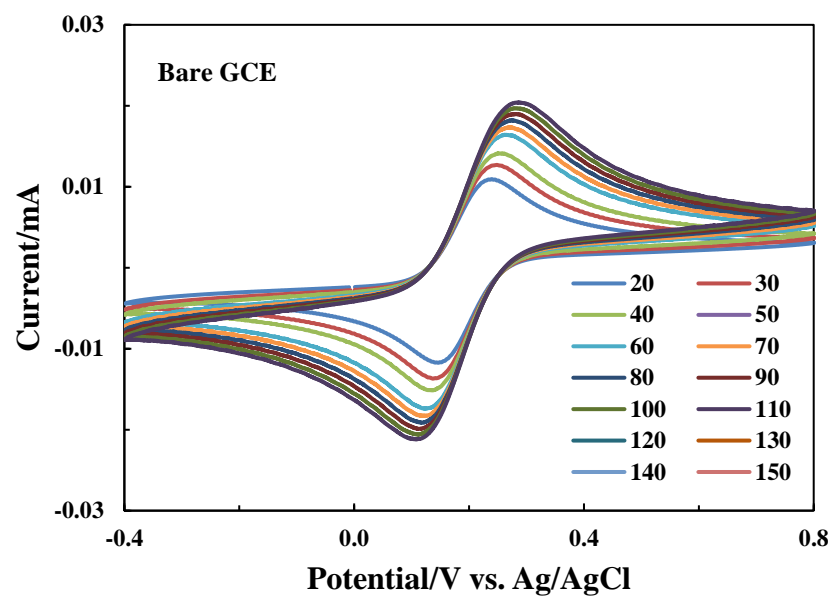
### 3.2.1. Cyclic voltammetry (CV) studies

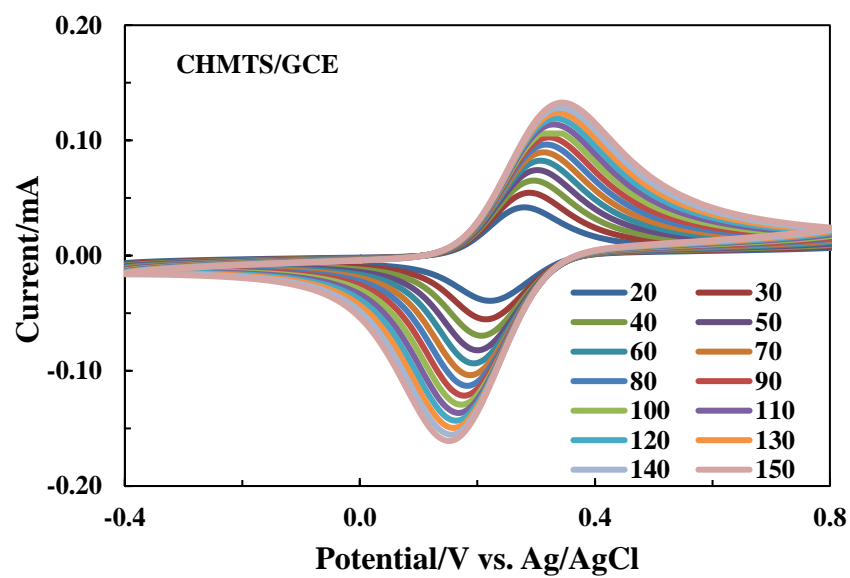
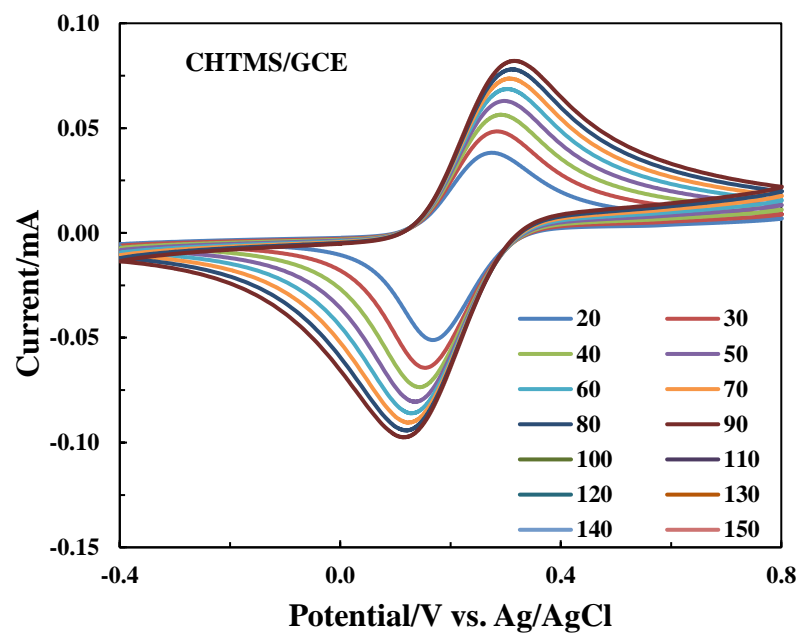
Electrochemical characterisation of bare glassy carbon electrode and fabricated glassy carbon electrodes viz., chitosan (CH/GCE), CHTMS/GCE, CHMTS/GCE and CHTMS+Ag(NPs)/GCE was carried out using the cyclic voltammetry technique. The cyclic voltammograms were collected using the standard redox probe of 0.002 M  $[\text{Fe}(\text{CN})_6]^{3-/4-}$  in 0.1 M acetate buffer at pH 4.5. The CV was collected at the scan rate of 100 mV/s and with the excitation potential window of -0.5 to 1.0 V and results are returned in Figure 3.8. The intense redox peak currents ( $I_p$ ) for  $[\text{Fe}(\text{CN})_6]^{3-/4-}$  redox couples were observed using the CH/GCE, CHMTS/GCE, CHTMS/GCE and CHTMS+Ag(NPs)/GCE. However, the bare GCE show less prominent redox peak currents. The increase in peak currents using the CH/GCE is due to amino and hydroxyl group present in chitosan, which facilitated the sorption of iron ions onto the electrode surface, hence an enhanced redox peak current was recorded. Moreover, the CHMTS/GCE, CHTMS/GCE and CHTMS+Ag(NPs)/GCE show much increased peak currents, which is primarily due to the grafting of silane with chitosan matrix, which provides additional siloxane sites for binding of iron ions along with amino and hydroxyl groups of chitosan resulted with enhanced electron transfer between the electrode surface and solution. The heparin/chitosan/reduce graphene oxide modified GCE showed significantly increased redox peak currents compared to the bare GCE, which was attributed that the heparin macromolecule contained with high electron charge density caused faster electron transfer reactions between the electrode and the analyte solution (Priya *et al.*, 2017). It is worth to be noted that the redox current was significantly increased using the CHTMS+Ag(NPs)/GCE compared to other electrodes. This increase in redox currents is attributed due to the combined effect of amino and hydroxyl group in chitosan along with siloxane site (from grafting of silane) and availability of free energy charge of  $\text{Ag}^0$  resulting in catalytic activity or enhancement of electron transfer reactions with enhanced surface selectivity between electrode surface and the redox couple  $[\text{Fe}(\text{CN})_6]^{3-/4-}$  (Prakash *et al.*, 2012; Zahran *et al.*, 2021)

Furthermore, comparison of voltammograms using different electrodes i.e., bare GCE, CH/GCE, CHMTS/GCE, CHTMS/GCE and CHTMS+Ag(NPs)/GCE the peak to peak separation was reduced using the composite or nanocomposite electrodes. More quantitatively, the calculated  $\Delta E$  value for CHTMS+Ag(NPs), CHMTS/GCE, CHTMS/GCE, CH/GCE, and GCE, was found 0.16, 0.18, 0.22, 0.23, and 0.26 V, respectively. Lower  $\Delta E$  value inferred for faster electron transfer rate at the electrode surface, which resulted in reduction of overpotential and facilitated the faster electron transfer kinetics. Therefore, significantly low values of  $\Delta E$  for the CHTMS+Ag(NPs)/GCE, CHTMS/GCE and CHMTS/GCE facilitate a rapid electron transfer kinetics. The trichloro(octadecyl)silane grafted bentonite modified carbon paste electrode showed an enhanced electron transfer at the electrode surface compared to the bare bentonite (Lalmalsawmi et al., 2020). Moreover, the trichloro(octadecyl)silane grafted bentonite decorated with Ag(NPs) showed further increase in electron transfer reactions compared to the composite material, which was due to the presence of  $\text{Ag}^0$  on silane grafted bentonite surface (Lalmalsawmi & Tiwari, 2021).



**Figure 3.8:** Cyclic voltammograms of  $[\text{Fe}(\text{CN})_6]^{3-/4-}$  (0.002 M; 0.1 M acetate buffer pH 4.5) obtained at a scan rate of 100 mV/s using the bare GCE, CH/GCE, CHTMS/GCE, CHMTS/GCE and CHTMS+Ag(NPs)/GCE.







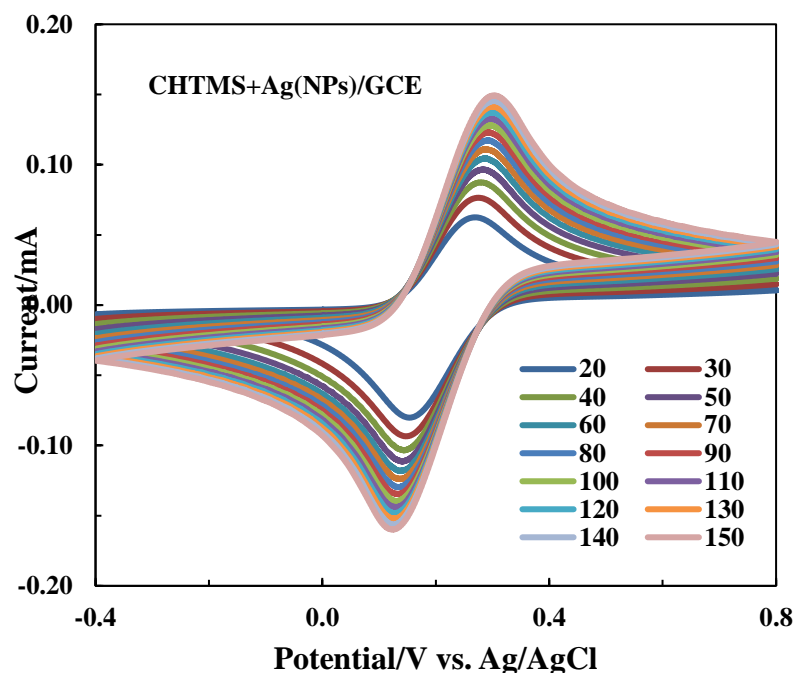


**Figure 3.9:** Scan rate studies for redox couple  $[\text{Fe}(\text{CN})_6]^{3-/4-}$  (0.002 M; 0.1 M acetate buffer; pH 4.5) using the bare GCE, CH/GCE, CHTMS/GCE, CHMTS/GCE and CHTMS+Ag(NPs).

Further, the scan rate study was conducted using these electrodes with the standard redox couple  $[\text{Fe}(\text{CN})_6]^{3-/4-}$ . The scan rate was varied from 20 mV/s to 150 mV/s at a constant concentration of 0.002 M  $[\text{Fe}(\text{CN})_6]^{3-/4-}$  (0.1 M acetate buffer solution pH 4.5). The increase in scan rate from 20 mV/s to 150 mV/s, the peak current was increased linearly with the scan rate (Cf Figure 3.9) for these electrodes i.e., bare GCE, CH/GCE, CHTMS/GCE, CHMTS/GCE and CHTMS+Ag(NPs)/GCE. Further, the oxidative peak current ( $I_p$ ; anodic peak current) vs. square root of scan rate ( $v^{1/2}$ ) was plotted for these electrodes and the linear relationship was obtained (Cf Figure 3.10), which infers that the redox process primarily proceeds through the diffusion-control and follow the Randle-Sevick equation (Zirliannigura et al., 2017). Using Randle-Sevick equation (2.2) electroactive surface area was calculated and return in Table 3.4.



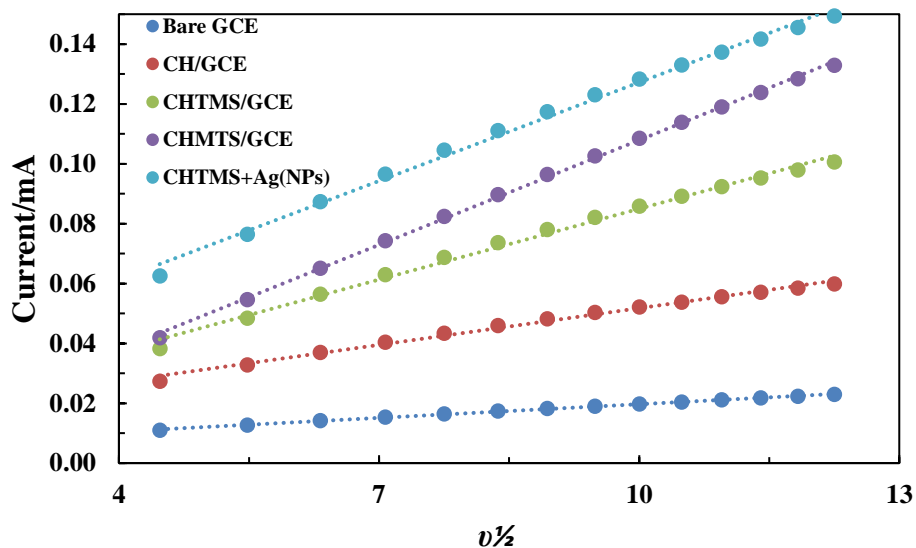


**Figure 3.10:** Plots of scan rate ( $v^{1/2}$ ) vs  $I_p$  (peak current; anodic peak current) using different electrodes i.e., bare GCE, CH/GCE, CHTMS/GCE, CHMTS/GCE and CHTMS+Ag(NPs)/GCE (0.002 M  $[\text{Fe}(\text{CN})_6]^{3-/4-}$  (0.1 M acetate buffer; pH 4.5).

The slope of the straight lines was obtained from the linear plots (*Cf* Figure 3.10), and utilized to obtain the electroactive surface area of employed electrodes ( $A$ ) and returned in Table 3.4. The results clearly indicated that the electroactive surface area of electrodes modified with CHTMS and CHMTS significantly increased compared to the bare GCE. The increase of surface area for the CHTMS and CHMTS was 4 fold and 5 fold higher than the bare GCE. Similarly, a 6 fold increase in electroactive surface area was obtained using the CHTM+Ag(NPs)/GCE compared to the bare GCE. The electroactive surface area of working electrode deduced with this method was reported to relate the amount of electroactive sites available on to the electrode surface (Lalmalsawmi & Tiwari, 2021). Thus, high specific electroactive surface area could provide an enhanced electroactive response and enable for trace detection of the analyte.

**Table 3.4:** Electroactive surface area of GCE, CH/GCE, CHTMS/GCE, CHMTS/GCE and CHTMS+Ag(NPs)/GCE obtained by using the Randle-Sevick equation.

| Employed Electrode | Linear Equation Obtained | $R^2$  | Surface Area Estimated ( $\text{mm}^2$ ) |
|--------------------|--------------------------|--------|------------------------------------------|
| Bare GCE           | $y=0.0015x+0.0049$       | 0.9977 | 0.000895                                 |
| CH/GCE             | $y=0.0038x+0.013$        | 0.9908 | 0.00237                                  |
| CHTMS/GCE          | $y=0.0074x+0.01$         | 0.9918 | 0.003899                                 |
| CHMTS/GCE          | $y=0.0117x-0.0087$       | 0.9992 | 0.00493                                  |
| CHTMS+Ag(NPs)/GCE  | $y=0.011x+0.0174$        | 0.9952 | 0.005827                                 |

### 3.2.2. Electrochemical impedance spectroscopy (EIS) analysis of fabricated electrodes

A standard redox couple 0.002 M  $[\text{Fe}(\text{CN})_6]^{3-/4-}$  with supporting electrolyte (0.1 M acetate buffer; pH 4.5) was employed to study the electron transfer behaviour at the fabricated electrode surface using the EIS technique. The frequency range was applied from 80.0 kHz to 100.0 MHz, while maintaining 6.0 per decade at an employed 10.0 mV peak to peak sinusoidal potential. Nyquist plots (Cf. Figure 3.11) was ascribed by imaginary impedance ( $-I_m(Z)/\text{Ohm}$ ) vs. real impedance ( $R_e(Z)/\text{Ohm}$ ). Best fitted Randles circuit for the Nyquist plots was  $R_s+C_{dl}/(R_{ct}+Z_w)$  (Cf Figure 3.11 inserted), and  $Z_{fit}$  of all the working electrodes is shown in Figure 3.11. The equivalent circuit or Randles circuit indicated that the diffusional element, Warburg ( $Z_w$ ), is connected in series with a resistor ( $R_{ct}$ ), which is measured as the electron transfer resistance (Zainudin et al., 2019). The electrical component ( $R_s$ ) is the solution resistance, wire, or even contact resistance, and double layer capacitance ( $C_{dl}$ ) occur

at electrode surface and electrolyte interface. Electron transfer resistance occurs due to charge (electron) transfer reactions at the electrode and electrolyte interface, while the Warburg diffusion is due to the ionic species diffusion into the bulk solution (Lalmalsawmi et al., 2020). The values obtained for these components show that solution resistance ( $R_s$ ) of the employed electrodes are almost similar for these electrodes *viz.*, bare GCE, CH/GCE, CHTMS/GCE, CHMTS/GCE, CHTMS+Ag(NPs)/GCE (*Cf* Table 3.5). However, a significant decrease in semicircle size of the Nyquist plots for the electrodes CHTMS+Ag(NPs)/GCE and CHMTS/GCE results in significant decrease in  $R_{ct}$  value compared to the bare GCE (*Cf* Table 3.5). The smaller semicircle obtained in CHTMS/GCE and CHMTS/GCE is due to the presence of silane, which further facilitated the electron transfer reactions at the electrode surface. Moreover, a further decrease in semicircle was obtained using the CHTMS+Ag(NPs)/GCE, which is due to the presence of  $Ag^0$  nanoparticles incorporated with silane grafted chitosan. The incorporated  $Ag^0$ (NPs), thus facilitated the electron transfer at the interfacial region. The findings are in line with the cyclic voltammetry results.

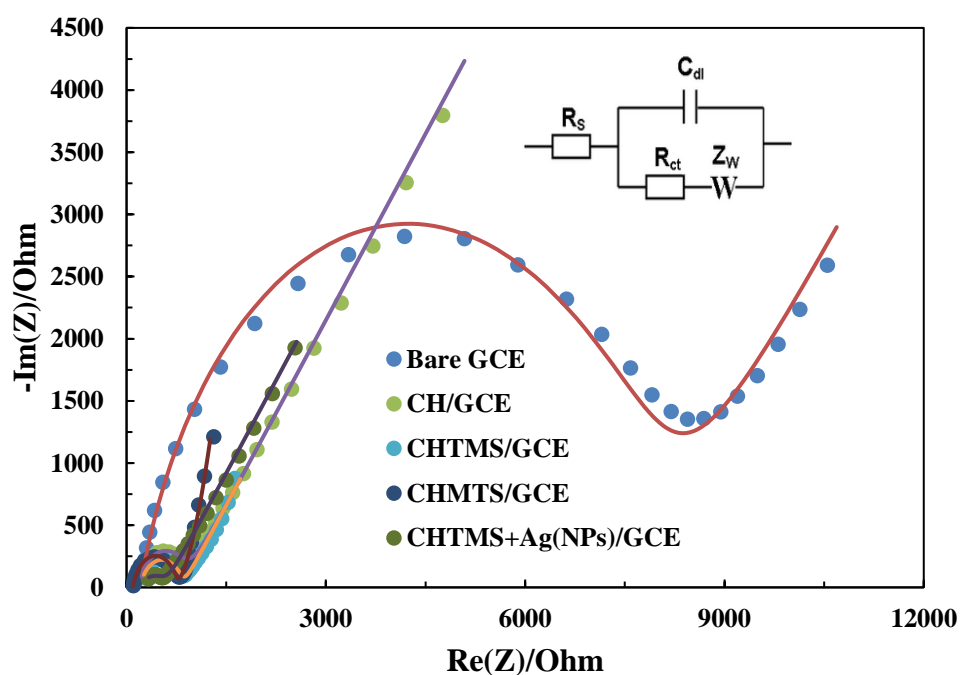


**Figure 3.11:** Nyquist plots of bare GCE, CH/GCE, CHTMS/GCE, CHMTS/GCE and CHTMS+Ag(NPs) with  $Z_{fit}$  modified GCE using the standard probe of  $[Fe(CN)_6]^{3-/4-}$  (0.002 M; 0.1 M acetate buffer at pH 4.5) [Inset: Fitted equivalent circuit].

**Table 3.5:** The optimized EIS parameters for the best fitted electrical circuit model of the Nyquist plots for bare GCE, CH/GCE, CHTMS/GCE, CHMTS/GCE and CHTMS+Ag(NPs)/GCE working electrodes.

| Working Electrode | Parameters    |                  |
|-------------------|---------------|------------------|
|                   | $R_s(\Omega)$ | $R_{ct}(\Omega)$ |
| Bare GCE          | 205.8         | 7746             |
| CH/GCE            | 194.7         | 678.7            |
| CHTMS/GCE         | 197.7         | 646.6            |
| CHMTS/GCE         | 197.3         | 633.7            |
| CHTMS+Ag(NPs)/GCE | 187.7         | 431.6            |

### 3.3. ELECTROCHEMICAL DETERMINATION OF Pb (II) USING CHTMS COMPOSITE MATERIAL

#### 3.3.1. Electrochemical behaviour of Pb (II) at different modified GCE under DPASV

Differential pulse anodic stripping voltammetry (DPASV) was introduced for the analysis of Pb (II) in aqueous solutions. DPASV analysis was carried out using a CHTMS modified GCE in 0.1 M acetate buffer solution (pH 4.5) as a supporting electrolyte with a Pb (II) concentration of 50.0  $\mu\text{g/L}$ . An applied potential of -0.9 V for 180.0 sec. was used for the preconcentration step. The DPASV curves obtained for

the 50.0  $\mu\text{g/L}$  Pb (II) using the bare GCE and CHTMS modified GCE are presented in Figure 3.12. The results show that there is no oxidative peak current using bare GCE, which indicates that the bare GCE possesses insignificant affinity towards the Pb (II) hence, show no or insignificant oxidative peak current. However, using the CHTMS/GCE a prominent oxidative peak current is observed at around *Ca.* -0.35 V. This demonstrates that CHTMS show high affinity for the Pb (II). The presence of amino and hydroxyl groups in chitosan and chelation properties of chitosan towards metal ions in addition the availability of siloxane binding sites enables the efficient binding of Pb (II) at the electrode surface, which results in increase in oxidative peak current. The GCE/Chi-(Bi-CX) (Bismuth doped carbon xerogel and chitosan as substrate material modified glassy carbon electrode) showed an increased sensitivity towards the detection of Pb (II) and Cd (II) compared to the bare GCE. The increased sensitivity was due to the presence of Bi nanoparticles dispersed with the xerogel matrix facilitating the electron transfer reactions on the electrode surface (Fort et al., 2015).

The better performance of the fabricated electrode is due to the crosslinked chitosan with glutaraldehyde, which forms a three-dimensional network structure as shown in the Scheme 3.1. The crosslinking of chitosan with glutaraldehyde was created through the Schiff base reactions (covalent bond formation). In acidic conditions the chitosan network ionization degree increases, which favours the osmotic swelling pressure between the hydrophilic network and acidic solution. This leads to expansion of the gap between the polymer chain making it to hold more water without disintegrating chitosan structure (Rithe, 2014; Song et al., 2018). Furthermore, grafting of silane within the chitosan network, functionalizes the composite materials and shows an enhanced mechanical strength of material (Lalhmunsiam et al., 2016).

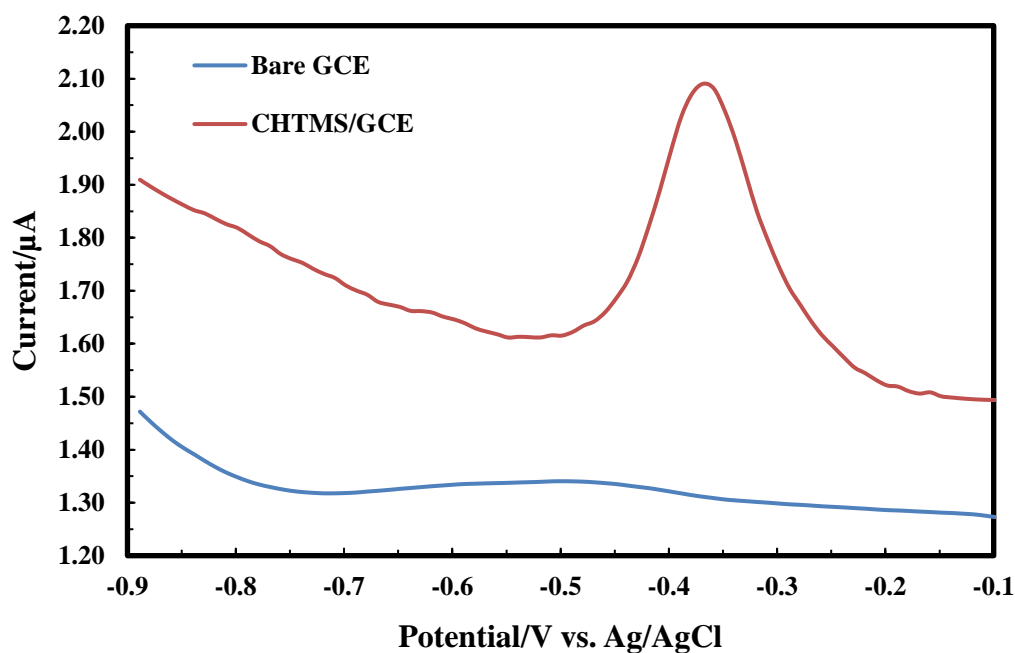
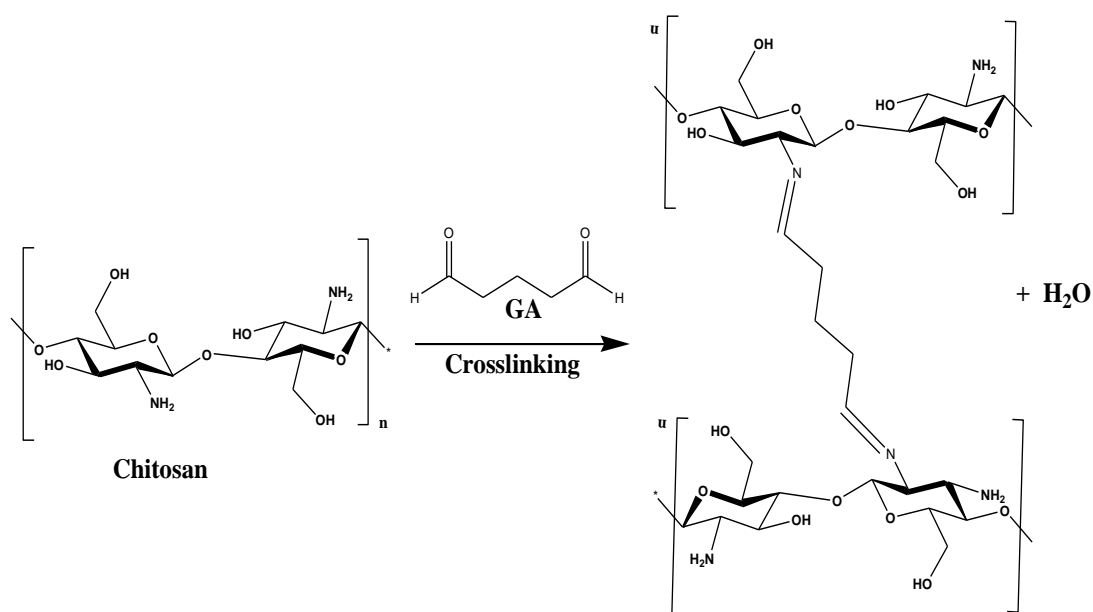


**Figure 3.12:** DPASV curves obtained for Pb (II) (50.0  $\mu\text{g/L}$  at pH 4.5; acetate buffer (0.1 M)) using the bare GCE; and CHTMS/GCE (Deposition potential: -0.9 V; Scan rate: 100 mV/s; and Deposition time: 180.0 sec; Pulse amplitude: 0.05 V; Step potential: 0.0001 V; Modulation time: 0.05 sec; and Time interval: 0.5 sec].



**Scheme 3.1:** Crosslinking of chitosan with 0.1 % glutaraldehyde *via* Schiff base reactions.

### 3.3.2. Optimization of experimental parameters

The optimization of experimental parameters is crucial in electrochemical methods that helps in receiving the sensitive, selective and improved electrochemical signals. An enhanced and distinct signal helps in trace detection of analytes. Therefore, the optimisation of or preconcentration studies were carried out for the parameters *viz.*, effect of pH, deposition potential and deposition time in 50.0  $\mu\text{g/L}$  Pb (II) using 0.1 M acetate buffer solution as supporting electrolyte. Other electronics control such as, Pulse amplitude: 0.05 V; Step potential: 0.0001 V; Modulation time: 0.05 sec.; and time interval: 0.5 sec. remained constant.

### 3.3.3. Effect of pH

The electrochemical behaviour of metal ions is strongly influenced by the solution pH, which is primarily due to protonation/deprotonation and hydrolysis of metal ions. The influence of pH was studied over a pH range from 3.6 to 5.5, while maintaining a constant deposition potential (-0.9 V) and deposition time (180.0 sec.) and a Pb (II) concentration of 50.0  $\mu\text{g/L}$  in 0.1 M acetate buffer. The pH dependent DPASV results are shown in Figure 3.13 (a). Figure 3.13 (a) shows that the stripping peak current ( $I_p$ ) is increased with increasing pH and attains a maximum peak current at pH 4.5. With a further increase in pH ( $\text{pH} > 4.5$ ), the peak current was slightly decreased, which is, perhaps, due to the evolution of  $\text{H}_2$ . The lower peak current response at lower pH is due to the hydrogen ion actively occupying the active sites at the working electrode (Zuo et al., 2017). Moreover, at high pH values the lead is seemingly forming the hydroxides and preventing the sorption at the electrode surface, resulting in decreased peak current. Therefore, pH 4.5 was selected as the optimal pH for the subsequent electrochemical analysis.

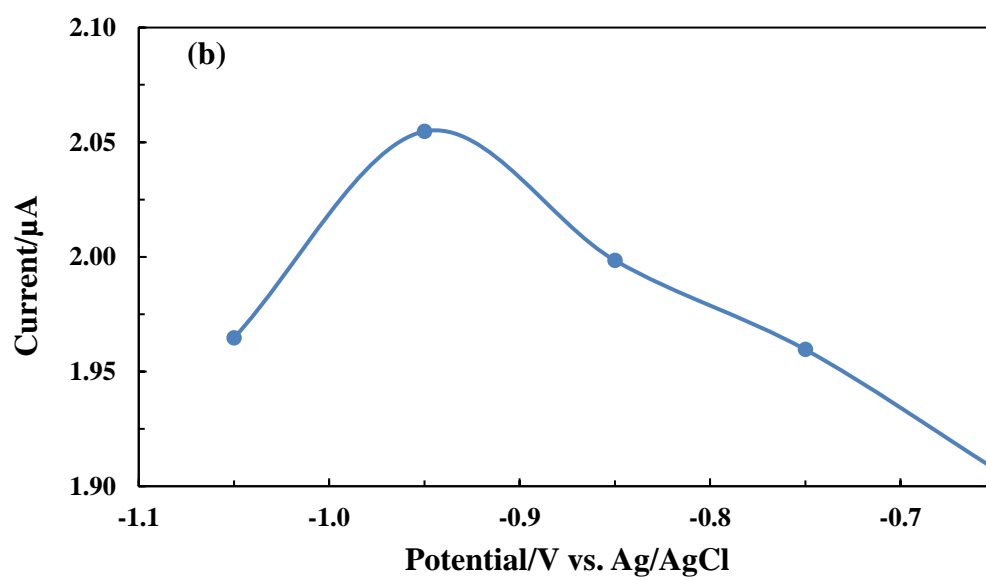
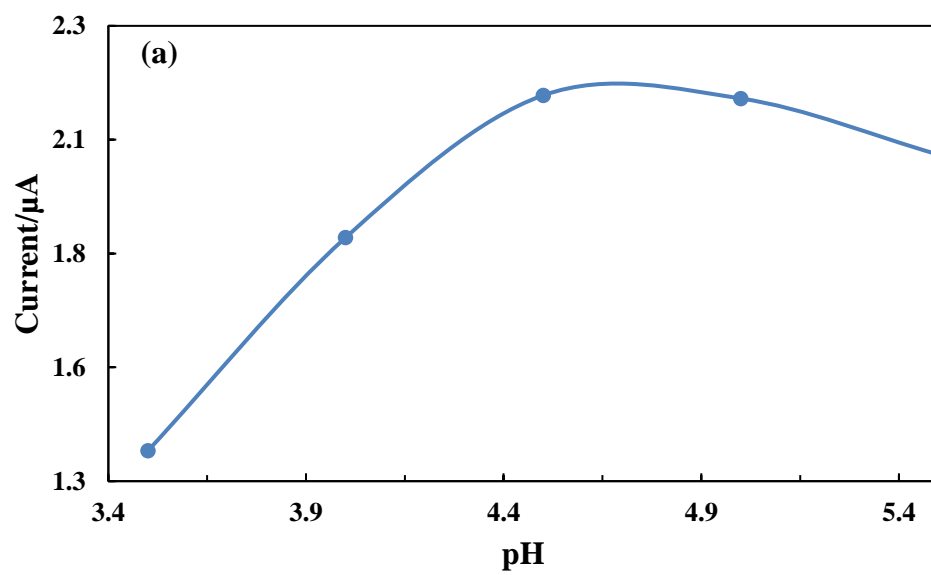
#### 3.3.4. Effect of deposition potential

In the stripping technique, deposition potential is an important parameter that improves the sensitivity of detection. The deposition potential was studied within the potential range of -0.6 to -1.0 V, keeping other parameters constants such as pH (4.5), deposition time (180.0 sec.) and Pb (II) concentration of 50.0  $\mu\text{g/L}$  in 0.1 M acetate buffer solution constant. The deposition potential dependence results are shown in Figure 3.13 (b). Figure 3.13 (b) shows that with an increase in deposition potential from -1.0 to -0.9 V, the stripping peak current ( $I_p$ ) is increased from 1.96 to 2.05  $\mu\text{A}$ , respectively. However, further increase in deposition potential from -0.9 to -0.6 V caused the peak current from 2.05 to 1.91  $\mu\text{A}$ , respectively. The decreased stripping peak current is attributed to the generation of hydrogen gas in the medium at higher applied potentials (Fida et al., 2017). Therefore, a maximum value of peak stripping current ( $I_p$ ) was obtained at an applied potential of -0.9 V.

#### 3.3.5. Effect of deposition time

Similarly, the influence of deposition time was studied at varied deposition time intervals, i.e., from 60.0 sec. to 240.0 sec., while keeping other parameters constant: pH: 4.5, deposition potential: -0.9 V and Pb (II) concentration of 50.0  $\mu\text{g/L}$  in 0.1 M acetate buffer. The results are shown in Figure 3.13 (c). It is evident from the Figure that with an increase in deposition time from 60.0 to 180.0 sec. the stripping  $I_p$  (peak current) is increased from 1.86 to 2.09  $\mu\text{A}$ , respectively. However, a further increase in deposition time (time >180.0 sec), caused a slight decrease in peak current. This decrease in peak current at higher deposition time is due to the saturation of active sites on the surface of the modified GCE (Xiong et al., 2015). Therefore, a deposition time of 180.0 sec. was chosen as an optimal time for the electrochemical detection of Pb (II).





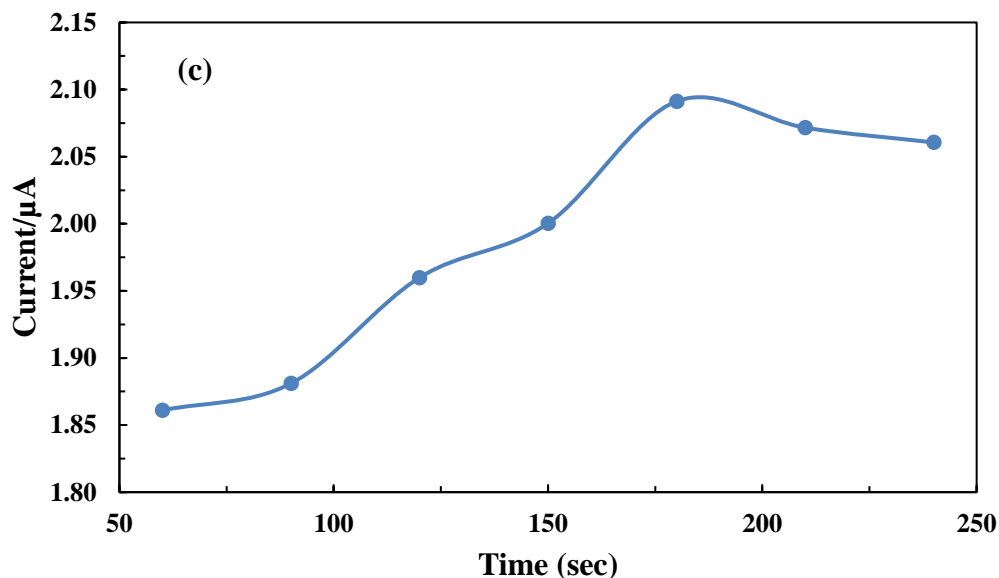


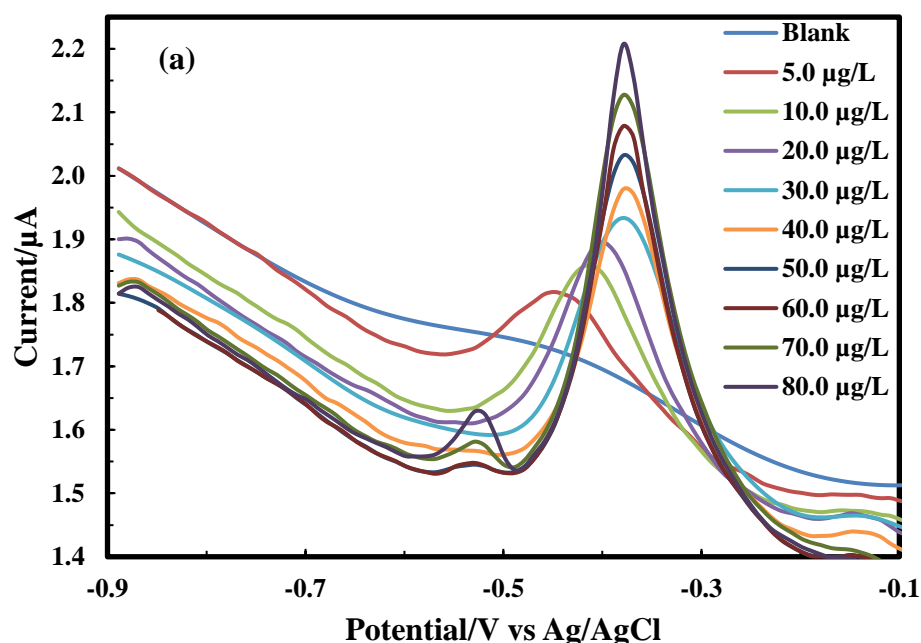
**Figure 3.13:** Parametric studies carried out at 50.0  $\mu\text{g/L}$  Pb (II) (0.1 M acetate buffer; pH 4.5); (a) The oxidative peak current of Pb (II) as a function of pH; (b) The oxidative peak current of Pb (II) as a function of deposition potential; and (c) The oxidative peak current of Pb (II) as a function of deposition time [Pulse amplitude: 0.05 V; Step potential: 0.0001 V; Modulation time: 0.05 sec; and time interval: 0.5 sec].

### 3.3.6. Electrochemical determination of Pb (II)

The optimised parametric values (pH 4.5; deposition potential -0.9 V, and deposition time 180.0 sec.) under the DPASV measurements were used in the detection of Pb (II) in aqueous medium. The oxidative peak currents were recorded at varied concentrations of Pb (II) using CHTMS/GCE. The DPASV results are shown in Figure 3.14 (a). A sharp and distinct oxidative peak for Pb (II) was observed at an applied potential of -0.9 V. Further, it is evident from Figure 3.14 (a) that a gradual increase in peak current was obtained with an increase in concentration of Pb (II). Moreover, the oxidative peak current was slightly shifted towards less negative potential at higher concentration of Pb (II), which was due to the compensation of mass transport from lower to higher concentrations, thus electrochemical system applied more potential for diffusion, resulted in shifting of oxidative peak current position

(Scholz, 2015). Therefore, the oxidative peak current was utilized to obtain the calibration line for the detection of Pb (II).

A good linearity between the oxidative peak against the respective Pb (II) concentrations (5.0 µg/L to 80.0 µg/L) was obtained and the calibration line is shown in Figure 3.14 (b). The calibration line is represented as  $y (\mu\text{A}) = 0.0049 x (\mu\text{g/L}) + 1.7964 (\mu\text{A})$  ( $R^2 = 0.992$ ). Further, the LOD and LOQ values were found to be 2.83 µg/L and 9.43 µg/L, respectively, which are much lower than the permissible limit of lead in drinking water set by the WHO (i.e., 10.0 µg/L). Furthermore, a comparison between the performance of the CHTMS/GCE with other electrodes previously reported are included in Table 3.6. Table 3.6, eventually indicates that the present study enables the detection of Pb (II) at reasonably low levels, which shows the potential use of functionalized material in the trace detection of Pb (II) in aqueous solutions.



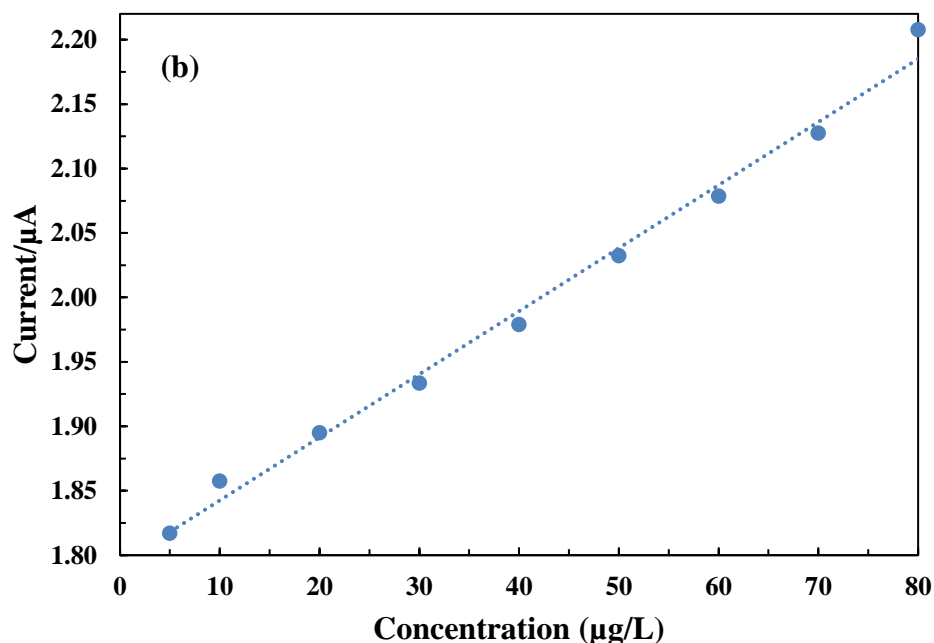


**Figure 3.14:** (a) The DPASV of Pb (II) as a function of Pb (II) concentrations; (b) Calibration line obtained for the oxidative peak current of Pb (II) as a function of Pb (II) concentration (Acetate buffer (0.1 M; pH 4.5); deposition potential: -0.9 V; deposition time: 180.0 sec; Pulse amplitude: 0.05 V; Step potential: 0.0001 V; Modulation time: 0.05 sec; and time interval: 0.5 sec).

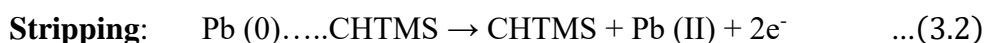
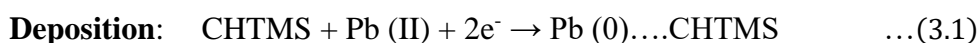
**Table 3.6:** The comparison of LOD obtained for Pb (II) using the CHTMS/GCE with other studies.

| Modified Electrode  | Method | Linear range<br>(µg/L) | LOD<br>(µg/L) | References              |
|---------------------|--------|------------------------|---------------|-------------------------|
| Diacetyldioxime/CPE | DPASV  | 20.7–3105.0            | 2.07          | (Hu et al., 2003)       |
| G/PANI/PS/SPE       | SWASV  | 10.0-500.0             | 3.3           | (Promphet et al., 2015) |

|                                                     |       |            |      |                      |
|-----------------------------------------------------|-------|------------|------|----------------------|
| Fe <sub>3</sub> O <sub>4</sub> -chitosan/ GCE       | SWASV | 20.0-270.0 | 8.74 | (Zhou et al., 2016)  |
| Quasi-spherical Fe <sub>3</sub> O <sub>4</sub> /GCE | SWASV | 60.0–270.0 | 24.6 | (Fan et al., 2016)   |
| Bi-CNT/SPCE                                         | DPASV | 2.0-100.0  | 1.3  | (Hwang et al., 2008) |
| L-cys/GR-CS/GCE                                     | DPASV | 1.04–62.1  | 0.12 | (Zhou et al., 2016)  |
| CHTMS/GCE                                           | DPASV | 5.0-80.0   | 2.83 | <b>This work</b>     |

SWASV- Square wave anodic stripping voltammetry, G/PANI/PS/SPE- Graphene/polyaniline/polystyrene, Bi-CNT/SPCE-Bismuth-carbon nanotube/Screen printed carbon electrode, L-cys/GR-CS/GCE- L-cysteine/graphene/chitosan/glassy carbon electrode

The CHTMS/GCE shows an excellent performance towards Pb (II) detection, which is due to the presence of amino and hydroxyl groups in chitosan and additional siloxane present in the CHTMS material. These functional groups facilitate the sorption of Pb (II) at the electrode surface, resulting in an enhanced electrochemical response (Mourya et al., 2021). Therefore, under the DPASV studies the proposed mechanism of Pb (II) detection is demonstrated in Equations (3.1) and (3.2). This indicates that the Pb (II) shows two electron transfer reactions as shown in the equation below.



### 3.3.7. Effect of Interfering ions

The interference of several cations and anions (each 10-fold to Pb (II)) was studied in 50.0  $\mu\text{g/L}$  Pb (II) solution, and the observed peak currents were compared with that of blank Pb (II) solution. DPASV study was conducted in the presence of several interfering ions, *viz.*, Cd (II), Zn (II), Cr (III), Ni (II), Cu (II), ethylenediaminetetraacetic acid (EDTA), oxalic acid (OA) and glycine (GLY), and the results are shown in Figure 3.15. It is evident from the results that EDTA slightly interferes the determination of Pb (II), which is possibly due to the complexation of Pb (II) with EDTA and the feeble attraction of complexed species by the electrode surface (*Cf* Figure 3.15), hence, leading to a reduced peak current for Pb (II) (Prakash et al., 2012). The remaining cationic or anionic species have no significant effect on the detection of Pb (II). Thus, these studies on interfering ions reveal that the fabricated electrode utilizing the novel functionalized material show potential application in the determination of Pb (II) in the presence of various interfering ions.

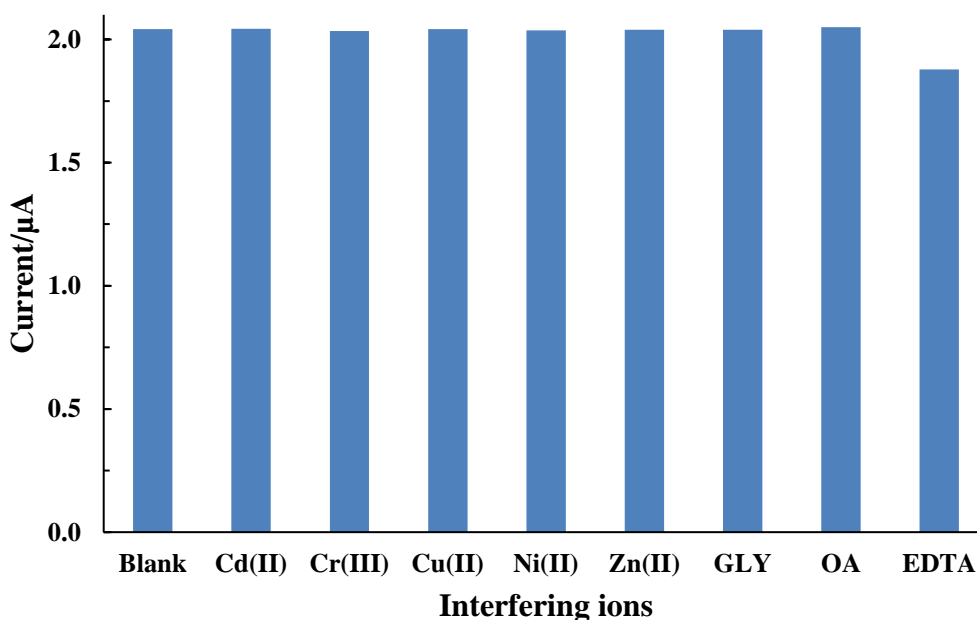


**Figure 3.15:** The detection of Pb (II) in presence of several interfering ions using the CHTMS/GCE ([Pb (II): 50.0  $\mu\text{g/L}$ ; [Interfering ion]: 500.0  $\mu\text{g/L}$ ; acetate buffer (0.1

M; pH 4.5); Pulse amplitude = 0.05 V; Step potential= 0.0001 V; Modulation time= 0.05 sec; and time interval= 0.5 sec).

### 3.3.8. Reproducibility and stability study

A reproducibility/repeatability test performed by 10 repetitive measurements ( $n=10$ ) of Pb (II) (50.0  $\mu\text{g/L}$ ) employing the CHTMS/GCE under the optimized conditions in DPASV measurements. The %RSD (relative standard deviation) was found to be 0.18 %. The low value of %RSD indicated the potential applicability of the fabricated electrode in repetitive determination of Pb (II) from aqueous solution. Further, the stability of the fabricated electrode was also studied in the presence of 50.0  $\mu\text{g/L}$  Pb (II) at different time durations, i.e., 0, 12 hours, 24 hours and 48 hours (5 consecutive detections for each time interval and storage of the prepared electrode at room temperature). Furthermore, the %RSD was calculated at each interval of time. The results obtained are shown in Table 3.7. The results indicate that the fabricated electrode material CHTMS/GCE) exhibits long-term stability for the determination of Pb (II) in aqueous solution (Xu et al., 2019).

**Table 3.7:** Calculation of %RSD (relative standard deviation) in different time duration of prepared electrode in the determination of Pb (II) 50.0  $\mu\text{g/L}$  from aqueous solution.

| Hours | RDS (%) |
|-------|---------|
| 0     | 0.160   |
| 12    | 0.175   |
| 24    | 0.180   |
| 48    | 0.182   |

### 3.3.9. Real sample analysis

To evaluate the applicability of the fabricated electrode in the detection of Pb (II) in natural matrix samples, the study was extended utilizing two different natural water samples. These water samples were collected from two different sources in the Mizoram University campus i.e., ‘Groundwater’ collected through the hand pump and “Spring water”. The collected samples were analysed using different water parameters, and the results are included in Table 3.8. As evident from Table 3.8, both samples contain high concentrations of calcium along with nitrate. The TOC analysis indicated that both samples contain high inorganic carbon, which might be due to the presence of carbonates or bicarbonates. The spring water is having high organic carbon content as well. On the other hand, both water samples are high in calcium. This indicated that both water samples are having relatively high water hardness due to the dissolved calcium bicarbonates (Tiwari et al., 2017). The other metals are almost negligible in both water samples. Prior to conducting the experiment, the water samples were filtered using Whatman filter paper (pore size 11  $\mu\text{m}$ ) to remove any suspended particles and used to prepare 0.1 M acetate buffer pH 4.5. The required concentrations of Pb (II) analyte (5.0  $\mu\text{g/L}$ , 10.0  $\mu\text{g/L}$ , 20.0  $\mu\text{g/L}$ , 30.0  $\mu\text{g/L}$  and 40.0  $\mu\text{g/L}$ ) were prepared using natural water samples, and DPASV experiments were carried out using the optimized experimental parameters, i.e., deposition potential = -0.9 V; accumulation time = 180.0 sec.; pulse amplitude = 0.05 V; step potential= 0.0001 V; modulation time= 0.05 sec.; and time interval= 0.5 sec.].

The DPASV results are illustrated in Figure 3.16 (a & b). The oxidative peak currents for Pb (II) show good linearity with the Pb (II) concentration in both natural water samples (spring water and groundwater). From the calibration curve Figure 3.16 (c & d), the obtained linear equation and correlation coefficients for (c) groundwater and (d) spring water are  $y (\mu\text{A}) = 0.00128 x (\mu\text{g/L}) + 0.5858 (\mu\text{A})$  ( $R^2 = 0.9994$ ) and  $y (\mu\text{A}) = 0.0069 x (\mu\text{g/L}) + 0.675 (\mu\text{A})$  ( $R^2 = 0.9992$ ) respectively. The results indicate that the fabricated electrode using the functionalized material possesses a reasonably good response toward the detection of Pb (II) in natural water samples. Therefore, the fabricated electrode is reliable, and the material has potential with real implications for the low-level detection of Pb (II).



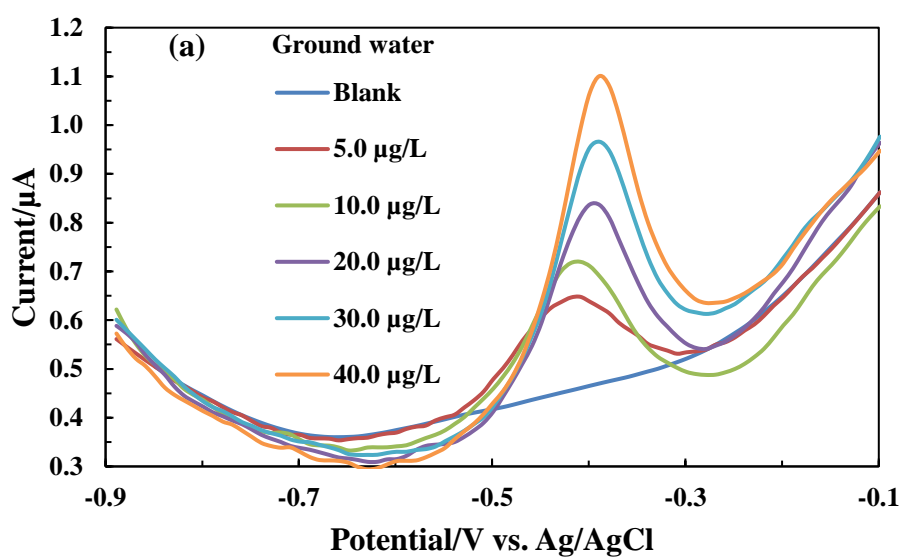
Furthermore, the Pb (II) recovery percentage in both water samples was calculated, and the results are given in Table 3.9. Table 3.9 shows that the calculated concentrations of Pb (II) are very close to the spiked concentrations of Pb (II), even in the presence of several impurities of natural water samples. A promising recovery percentage in both water samples was obtained, i.e., 96.63-102.99% (spring water) and 96.98-104.6% (groundwater). A similar study was previously performed using a clay-based nanoparticles modified glassy carbon electrode in the detection of micropollutants in spring water (Lalmalsawmi & Tiwari, 2021).

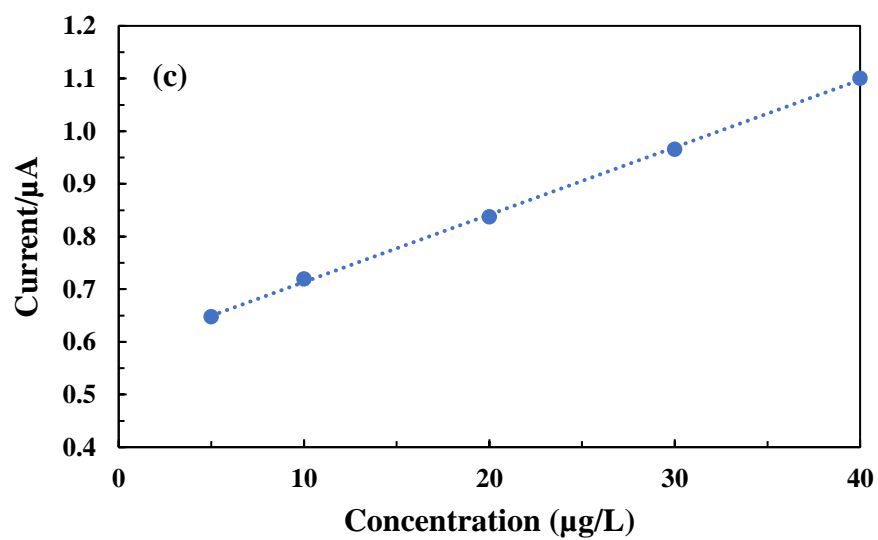
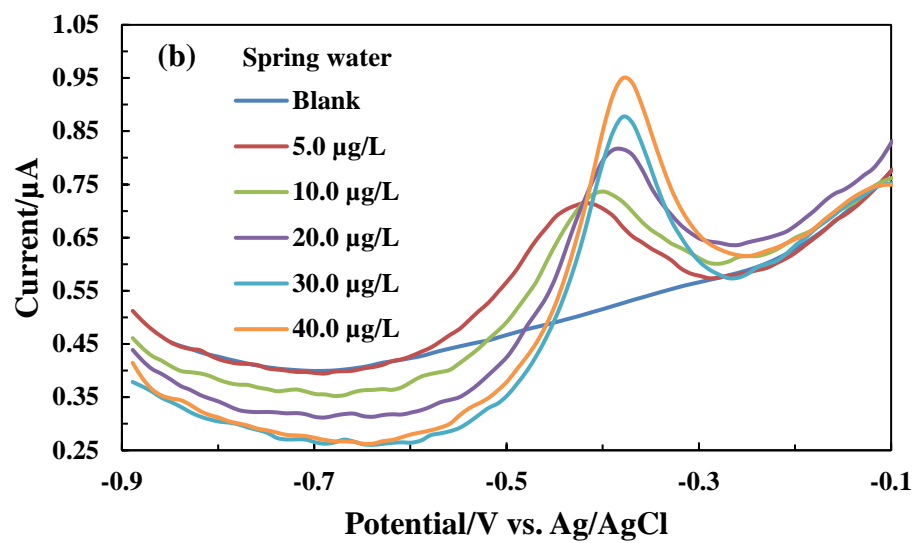
**Table 3.8:** Analysis of real water samples using different analytical methods

| <b>AAS</b>                  | <b>Spring water (mg/L)</b> | <b>Groundwater (mg/L)</b> |
|-----------------------------|----------------------------|---------------------------|
| Copper (Cu)                 | 0.02                       | 0.02                      |
| Calcium (Ca)                | 11.16                      | 12.31                     |
| Zinc (Zn)                   | BDL                        | 0.14                      |
| Lead (Pb)                   | BDL                        | BDL                       |
| Nickle (Ni)                 | BDL                        | BDL                       |
| Iron (Fe)                   | 0.02                       | 0.95                      |
| Manganese (Mn)              | BDL                        | BDL                       |
| <b>TOC</b>                  | <b>(mg/L)</b>              | <b>(mg/L)</b>             |
| NPOC                        | 13.17                      | 1.35                      |
| IC                          | 12.18                      | 11.85                     |
| TC                          | 25.35                      | 13.20                     |
| <b>Multiparameter</b>       |                            |                           |
| Nitrate                     | 6.0 µg/L                   | 8.0 µg/L                  |
| Phosphate                   | 0.03 mg/L                  | 0.06 mg/L                 |
| Sulphate                    | 0.02 mg/L                  | 0.20 mg/L                 |
| <b>Multiparameter Probe</b> |                            |                           |

|              |                                   |                                   |
|--------------|-----------------------------------|-----------------------------------|
| pH           | 7.97                              | 8.21                              |
| OPR          | 6.4 mV                            | 160.7 mV                          |
| Conductivity | 460 $\mu\text{SCm}^{-1}$          | 199 $\mu\text{SCm}^{-1}$          |
| Resistivity  | 0.0022 $\text{m}\Omega\text{ Cm}$ | 0.0045 $\text{m}\Omega\text{ Cm}$ |
| TDS          | 230 mg/L                          | 100 mg/L                          |
| Salinity     | 0.24 PSU                          | 0.10 PSU                          |

BDL: Below detection limit





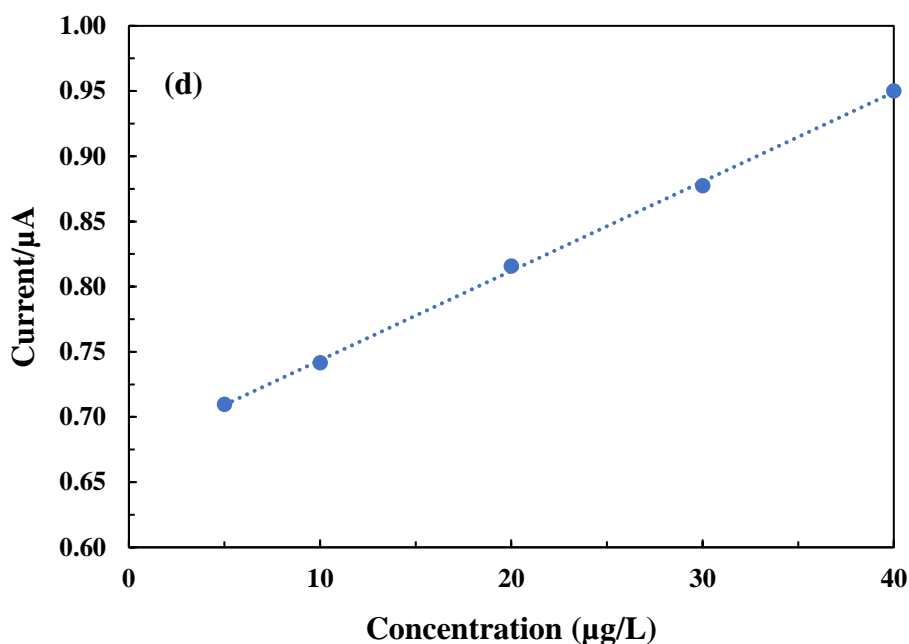


**Figure 3.16:** Real water sample spiked with Pb (II) having concentrations from 5.0 to 40.0  $\mu\text{g/L}$  (Acetate buffer 0.1 M; pH 4.5), (a) DPASV of Pb (II) using the ground water; and (b) DPASV of Pb (II) using spring water; calibration lines obtained for (c) ground water; and (d) spring water samples. [Deposition potential = -0.9 V; Accumulation time = 180.0 sec.; Pulse amplitude = 0.05 V; Step potential= 0.0001 V; Modulation time= 0.05 sec; and time interval= 0.5 sec].

**Table 3.9:** The recovery of Pb (II) in the spiked spring water and ground water using CHTMS/GCE.

| Real sample  | Spiked amount ( $\mu\text{g/L}$ ) | Found ( $\mu\text{g/L}$ ) | Recovery (%) |
|--------------|-----------------------------------|---------------------------|--------------|
| Spring water | 5.0                               | 4.99                      | 99.14        |
|              | 10.0                              | 9.66                      | 96.63        |
|              | 20.0                              | 20.6                      | 102.99       |

|              |      |       |       |
|--------------|------|-------|-------|
| Ground water | 5.0  | 4.85  | 96.98 |
|              | 10.0 | 10.46 | 104.6 |
|              | 20.0 | 19.67 | 98.33 |

### 3.3.10. Conclusion

Electrochemical detection of Pb (II) using CHTMS/GCE was studied under the DPASV technique. The electrochemical response of Pb (II) under DPASV was significantly pronounced compared to the bare GCE. The optimized pH, deposition potential and deposition time was found to be 4.5, -0.9 V and 180 sec., respectively in the efficient detection of Pb (II). The detection of Pb (II) within the concentration range 5.0 µg/L to 80.0 µg/L show a good calibration line with linear equation of  $y (\mu A) = 0.0049 \times (\mu g/L) + 1.7964 (\mu A)$  ( $R^2 = 0.992$ ) with limit of detection of 2.83 µg/L. In the presence of several interfering ions such as Cd (II), Zn (II), Cr (III), Ni (II), Cu (II), EDTA, OA and GLY, where EDTA, which show no significant interference except EDTA. Real matrix study using spring water and ground water show reasonable recovery rate compared to spiked concentrations of Pb (II). Hence, CHTMS/GCE is an efficient and selective material in the trace determination of Pb (II) in aqueous medium.

## 3.4. ELECTROCHEMICAL DETERMINATION OF Pb (II) USING CHTMS+Ag(NPs) NANOCOMPOSITE MATERIAL

### 3.4.1. Electrochemical behaviour of Pb (II) at different modified GCE under DPASV

Electrochemical response of 50.0 µg/L Pb (II) in 0.1 M acetate buffer electrolyte using the bare GC, CHTMS/GCE and CHTMS+Ag(NPs)/GCE under the DPASV is obtained and shown in Figure 3.17. Figure 3.17 (a) reveals that the GCE

showed no oxidation peak current of Pb (II), which implies that the lead shows poor affinity towards the GCE hence, an insignificant oxidation of lead occurs at the electrode surface. However, a pronounced oxidative peak current of Pb (II) at potential *Ca.* -0.37 V is observed using the CHTMS/GCE (*Cf* Figure 3.17 (b)). Moreover, the use of nanocomposite CHTMS+Ag(NPs)/GCE showed significantly enhanced oxidative peak current for Pb (II) at an applied potential of *Ca* -0.35 V (*Cf* Figure 3.17 (c)). The high oxidative peak currents using the CHTMS/GCE or CHTMS+Ag(NPs)/GCE inferred that the Pb (II) is having high affinity towards the nanocomposite materials hence, giving fairly good electrochemical response at the electrode surface. The presence of functional groups of the functionalized material chelating the Pb (II), which enabled the efficient oxidation of Pb (II) at the electrode surface. Similarly, in the CHTMS+Ag(NPs)/GCE, the oxidative peak current was increased by almost 3 fold compared to the CHTMS/GCE and 5 fold compared to the bare GCE. A high oxidative peak current of Pb (II) using the CHTMS+Ag(NPs)/GCE is due to the combined effect i.e., the functionalized composite material and presence of Ag<sup>0</sup>(NPs). The presence of Ag<sup>0</sup>(NPs) catalyses the electron transfer rate, which facilitates faster electron transfer reactions at the electrode surface. Similar report show Ag(NPs)/chitosan synthesized material employed in simultaneous determination of As (III) and Cu (II) where the presence of Ag(NPs) facilitated the current response toward the target pollutants (Prakash et al., 2012)

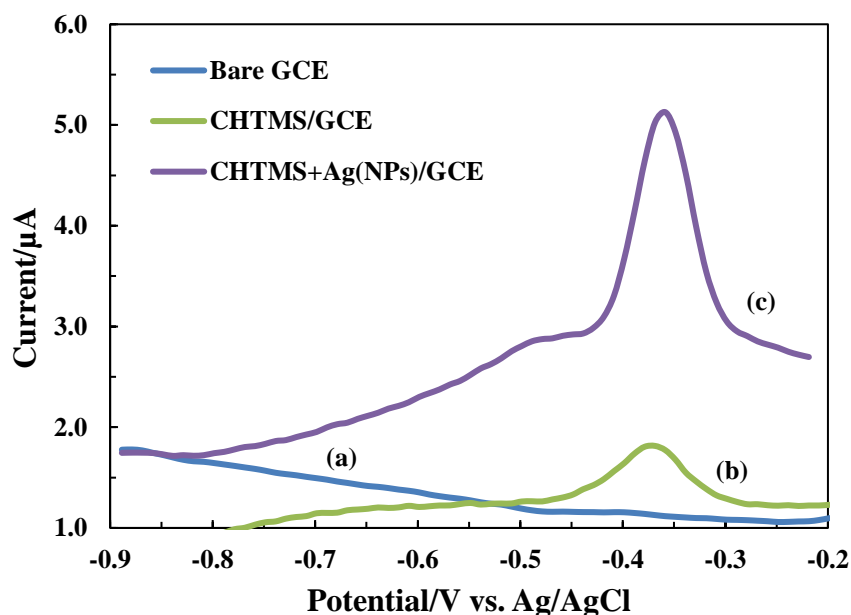


**Figure 3.17:** DPASV curves obtained for Pb (II) (50.0  $\mu\text{g/L}$  at pH 4.5; acetate buffer (0.1 M)) using the (a) bare GCE; (b) CHTMS/GCE; and (c) CHTMS+Ag(NPs)/GCE (Deposition potential: -0.9 V; Scan rate: 100 mV/s; and Deposition time: 180.0 sec; Pulse amplitude: 0.05 V; Step potential: 0.0001 V; Modulation time: 0.05 sec.; and Time interval: 0.5 sec].

### 3.4.2. Optimization of the stripping parameters

Studies at various pH conditions using CHTMS+Ag(NPs)/GCE were carried out in the detection of 50.0  $\mu\text{g/L}$  Pb (II), in acetate buffer (0.1 M). The other parameters were taken as deposition potential -0.9 V (vs. Ag/AgCl), deposition time 180.0 sec. The pH was increased from 3.5 to 5.5 and the corresponding oxidative peak current is shown in Figure 3.18 (a). Figure 3.18 (a) shows that an increase in pH from 3.5 to 4.5 caused a increase in the oxidative peak current from 4.23 to 5.50  $\mu\text{A}$ , respectively. However, further increase in pH from 4.5 to 5.5 caused for decrease in oxidative peak current from 5.50 to 3.95  $\mu\text{A}$ , respectively. A rapid decrease in oxidative peak current at  $\text{pH} > 4.5$  is due to the formation of hydroxy species of lead i.e.,  $\text{Pb}(\text{OH})_x$ , which was not attracted by the electrode surface. Hence restricted the electrooxidation of lead (Eshlaghi et al., 2020). On the other hand, at lower pH conditions  $\text{pH} < 4.5$ , the

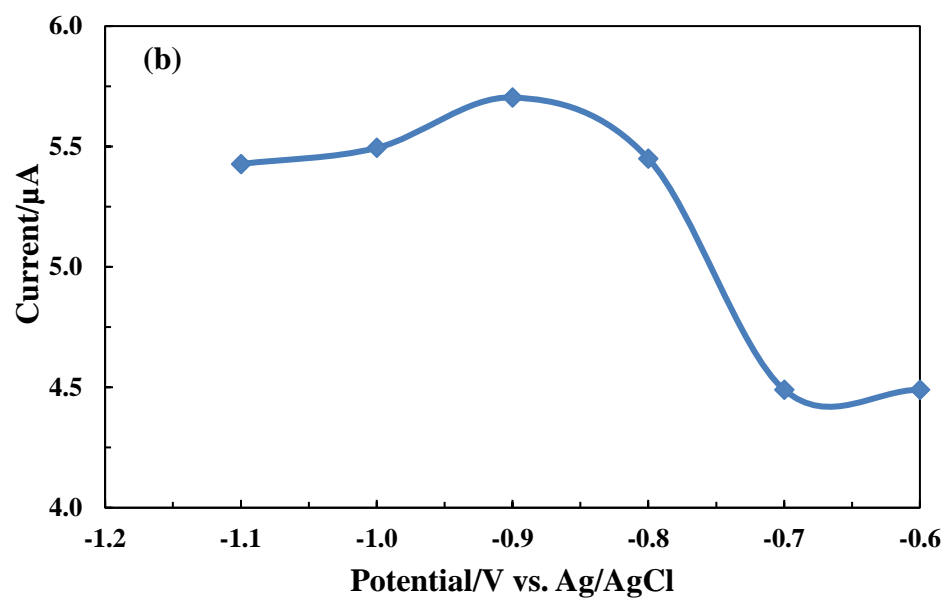
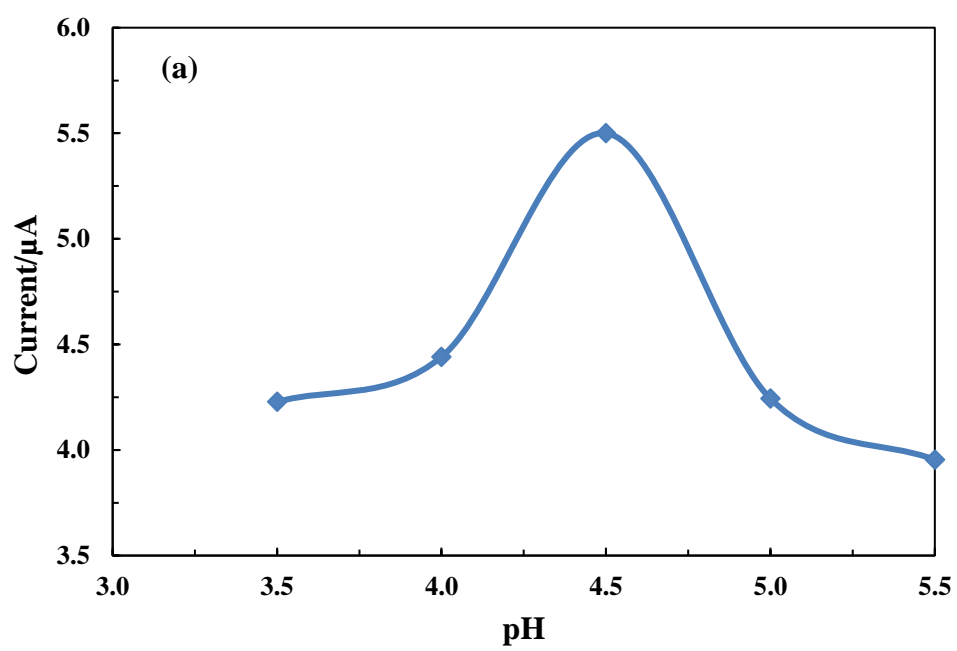
hydrogen ions preferentially occupy the active sites over Pb (II), resulting in the reduced oxidative peak current of Pb (II). Similar observations were reported for Pb (II) determination in various pH conditions using Co<sub>3</sub>O<sub>4</sub>/reduced graphene oxide/chitosan (Co<sub>3</sub>O<sub>4</sub>/rGO/CS) modified glassy carbon electrode (Zuo et al., 2017). Therefore, pH 4.5 was selected for electrochemical detection of Pb (II) in aqueous medium.

The chitosan dissociates in acidic medium, however the crosslinked chitosan matrix with 0.1 percent glutaraldehyde solution having the three-dimensional network structure that remained stable even in acidic conditions as shown previously in Section 3.3.1.

Deposition or the accumulation potential is a crucial parameter in the stripping voltammetry technique since it significantly affects the sensitivity of the working electrode. The deposition potential was varied from -0.6 V to -1.1 V and the corresponding peak current was presented in Figure 3.18 (b). The oxidation peak current was maximum at a deposition potential of -0.9 V. The generation of hydrogen at deposition potential > -0.9 V caused a decrease in peak current. Therefore, the optimum deposition potential for Pb (II) detection was -0.9 V using the nanocomposite fabricated electrode.

The deposition time at various time intervals ranging from 60.0 sec. to 240.0 sec. was conducted and the current response of Pb (II) (50.0 µg/L) is shown in Figure 3.18 (c). An increase in the deposition duration from 60.0 sec. to 180.0 sec. caused a gradual increase in peak current for Pb (II). However, further increase in deposition time from 180.0 to 240.0 sec. caused for almost constant oxidative peak current, which is due to the saturation of electroactive sites at the electrode surface (Cf Figure 3.18 (c)). Therefore, the 180.0 sec. was used as the deposition time for efficient and trace detection of Pb (II) in aqueous medium.





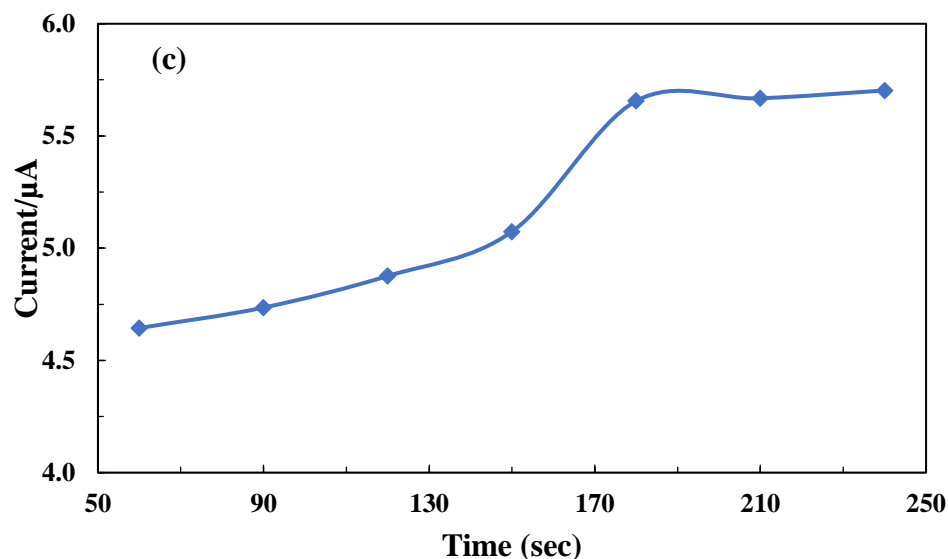


**Figure 3.18:** Parametric studies carried out at 50.0  $\mu\text{g/L}$  Pb (II) (0.1 M acetate buffer; pH 4.5); (a) The oxidative peak current of Pb (II) as a function of pH; (b) The oxidative peak current of Pb (II) as a function of deposition potential; and (c) The oxidative peak current of Pb (II) as a function of deposition time [Pulse amplitude: 0.05 V; Step potential: 0.0001 V; Modulation time: 0.05 sec; and time interval: 0.5 sec].

### 3.4.3. Electrochemical determination of Pb (II)

The DPASV voltammograms of Pb (II) under optimised stripping conditions were recorded using the CHTMS+Ag(NPs)/GCE. Further, the voltammograms at varied Pb (II) concentrations are returned in Figure 3.19 (a). It is evident from the figure that increasing the Pb (II) concentration from 5.0 to 80.0  $\mu\text{g/L}$  caused a gradual increase in the oxidative peak current. Moreover, the oxidative peak current occurred at potential -0.37 V. Further, a calibration line was drawn between the concentration of Pb (II) against the peak current values, which shows a good linear relationship. The calibration line is represented with a linear equation:  $y (\mu\text{A}) = 0.0368 x (\mu\text{g/L}) + 3.5742 (\mu\text{A})$  with  $R^2 = 0.9811$  (Cf Figure 3.19 (b)). The LOD and LOQ were calculated and found to be 1.97  $\mu\text{g/L}$  and 6.58  $\mu\text{g/L}$  for Pb (II) using the CHTMS+Ag(NPs)/GCE. The LOD value is considerably less than the 10.0  $\mu\text{g/L}$  in drinking water, the permissible level suggested by the WHO.

Moreover, the LOD value obtained for Pb (II) in this study is compared with several other electrodes using different materials and returned in Table 3.10. The LOD obtained in this study is quite comparable or lower than many other studies. This pointed to the potential application of nanocomposite material in the trace and efficient detection of Pb (II) in aqueous solutions.

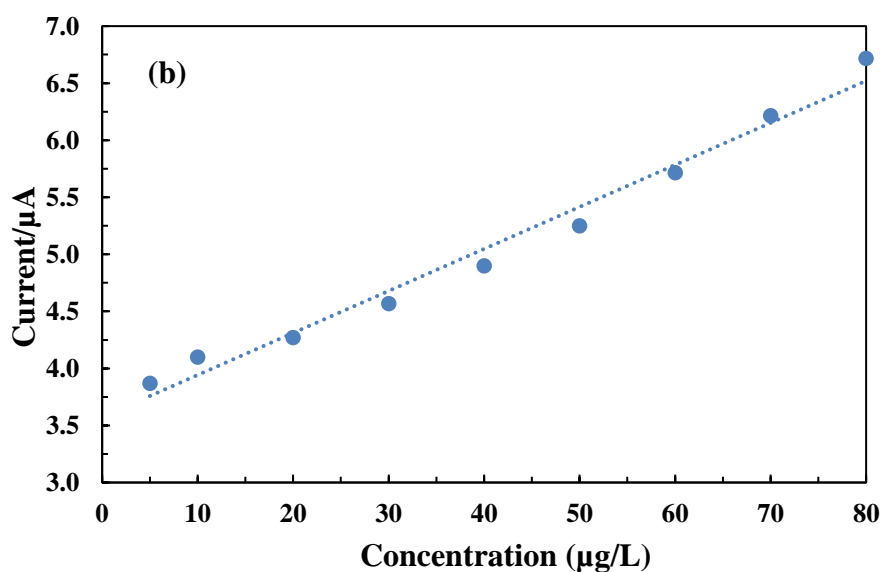
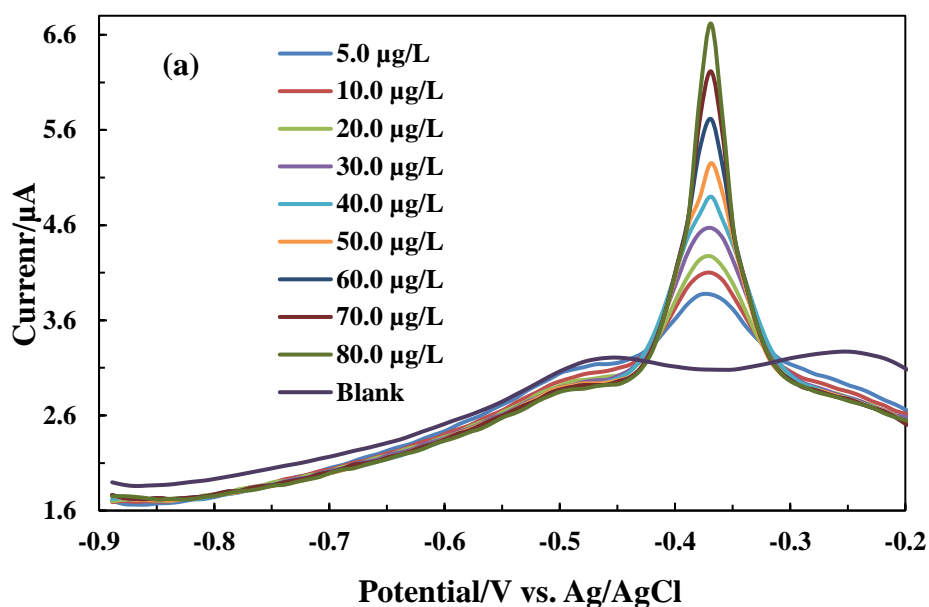


**Figure 3.19:** (a) The DPASV of Pb (II) as a function of Pb (II) concentrations; (b) Calibration line obtained for the oxidative peak current of Pb (II) as a function of Pb (II) concentration (Acetate buffer (0.1 M; pH 4.5); deposition potential: -0.9 V; deposition time: 180.0 sec; Pulse amplitude: 0.05 V; Step potential: 0.0001 V; Modulation time: 0.05 sec; and time interval: 0.5 sec).

**Table 3.10:** The comparison of LOD obtained for Pb (II) using the CHTMS+Ag(NPs)/GCE with other studies.

| Technique employed | Composite material employed                                | Limit of detection (µg/L)<br><br>LOD | Studied concentration range (µg/L) | Ref.                        |
|--------------------|------------------------------------------------------------|--------------------------------------|------------------------------------|-----------------------------|
| SWASV              | GCE/GQDs-NF                                                | 8.49                                 | 20.0–200.0                         | (Pizarro et al., 2020)      |
| DPASV              | 5-Br-PADAP/MWCNT                                           | 0.1                                  | 0.9-114.6                          | (Salmanipour & Taher, 2011) |
| DPASV              | Fe <sub>3</sub> O <sub>4</sub> @PDA@MnO <sub>2</sub> /mGCE | 0.03                                 | 0.1-150.0                          | (Wang et al., 2020)         |
| SWASV              | BEFs                                                       | 2.47                                 | 10.0-100.0                         | (Li et al., 2009)           |

|       |                   |      |          |                     |
|-------|-------------------|------|----------|---------------------|
| SWASV | SPE/SWCNHs        | 0.04 | 1.0-60.0 | (Yao et al., 2019)  |
| DPASV | CHTMS+Ag(NPs)/GCE | 1.97 | 5.0-80.0 | <b>Present work</b> |

\*SWASV - Square wave anodic stripping voltammetry, GC/GQDs-NF- Glassy Carbon Electrode/Graphene Quantum Dots-Nafion, 5-Br-PADAP/MWCNT- 2-(5-bromo-2-pyridylazo)-5-diethylaminophenol/Multiwalled carbon nanotube, PDA-polymer of typical dopamine, BEFs- Bismuth Film Electrodes, SPE/SWCNHs-Screen Printed Electrode/single-walled carbon nanohorns.

#### 3.4.4. Effect of interfering ions in Pb (II) detection

The interference study was conducted using the variety of interfering ions in the detection of 50.0 µg/L Pb (II) under the DPASV measurements using the CHTMS+Ag(NPs)/GCE. The concentration of interfering ions were taken 500.0 µg/L. Cations such as Ni (II), Zn (II), Cr (III), and Cu (II) and anionic species like EDTA, OA and GLY were used as interfering ions. Figure 3.20 shows that the cationic species do not show any significant effect in the determination of Pb (II) from aqueous medium. On the other hand, the anionic species glycine (GLY) and oxalic acid (OA) interferes with the determination of Pb (II). Glycine is contained with the amino and carboxyl groups, which readily oxidise towards the working electrode (Olejnik et al., 2020), and hampers the oxidation of Pb (II) at the working electrode. Therefore, it is caused by relatively less oxidative peak current. GLY also acts as an excellent antioxidant, preventing Pb (II) oxidation at the surface of working electrodes (Alcaraz-Contreras et al., 2011). Similarly, OA shows interference in the Pb (II) determination. OA forms chelate with Pb (II), which restricts the oxidation of Pb (II) and hence, a reduced peak current was recorded. It was reported previously that the Cu (II) detection was interfered in presence of OA using nanoscale hydroxyapatite (nHAP,  $\text{Ca}_{10}(\text{PO}_4)_6(\text{OH})_2$ ) modified electrodes. This interference was due to the formation of strong coordinate bond between the OA and Cu (II), which significantly lowered the free Cu (II) concentration that inhibited the current in the electrochemical detection of

Cu (II) (Wei et al., 2021). However, the coexisting ions do not interfere with the detection of Pb (II) hence, the nanocomposite material is selective in the detection of Pb (II).

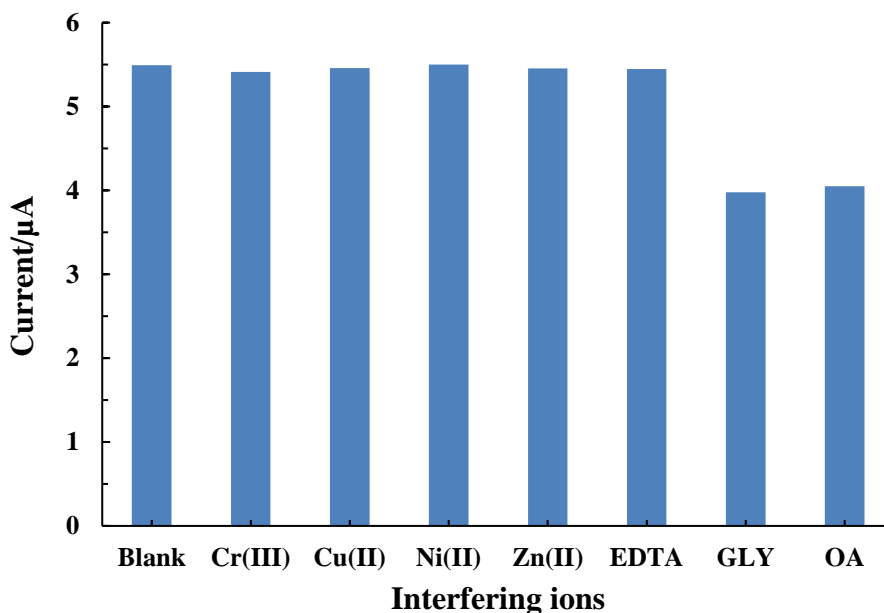


**Figure 3.20:** The detection of Pb (II) in presence of several interfering ions using the CHTMS+Ag(NPs)/GCE ([Pb (II): 50.0 μg/L; [Interfering ion]: 500.0 μg/L; acetate buffer (0.1 M; pH 4.5); Pulse amplitude = 0.05 V; Step potential= 0.0001 V; Modulation time= 0.05 sec; and time interval= 0.5 sec).

### 3.4.5. Reproducibility and stability study

The reproducibility study was conducted under optimised experimental conditions and utilising 50.0 μg/L Pb (II) solution in 0.1 M acetate buffer as supporting electrolyte. The other stripping parameters were taken as mentioned before. The repeatability study was performed in a series of repetitive experiments running the blank sample 10 times and then detected the Pb (II) 5 times. The % relative standard deviation (%RSD) was calculated (n=5) and found always less than 2.43%, which reaffirmed the reproducibility of results using the fabricated electrodes in repeated operations.

Long term stability of the CHTMS+Ag(NPs)/GCE was also investigated in a series of experiments conducted at varied time duration after the fabrication of electrodes, i.e., 0, 12, 24, and 48 hours. Each time the experiment was run for five consecutive times and the electrode was washed with purified water and stored in a closed beaker at room temperature. Further, the RSD% are calculated and presented in Table 3.11. Results show that the RSD% is always less than 5%. Hence, the CHTMS+Ag(NPs)/GCE show reasonably high stability hence, promising in prolonged and efficient use at least for the trace detection of Pb (II).

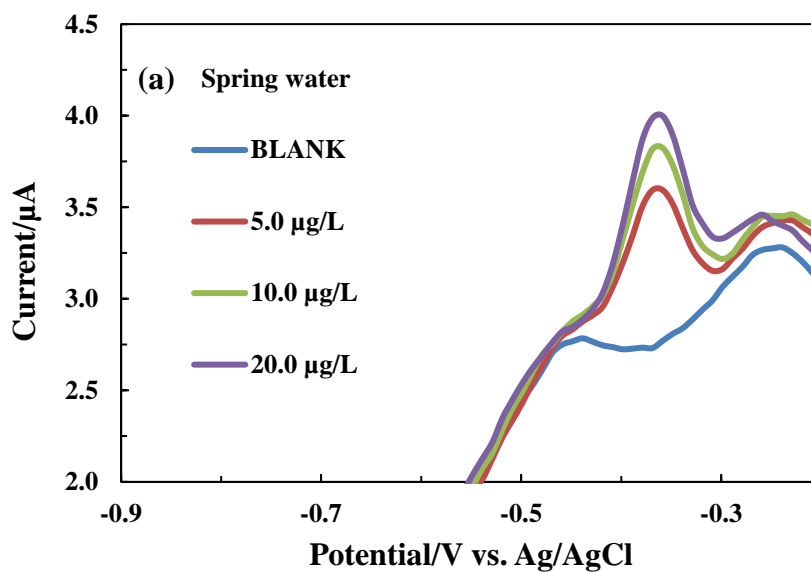
**Table 3.11:** Calculation of %RSD (relative standard deviation) in different time duration of prepared electrode in the determination of Pb (II) 50.0 µg/L from aqueous solution.

| Hours | RSD (%) |
|-------|---------|
| 0     | 2.429   |
| 12    | 2.434   |
| 24    | 2.486   |
| 48    | 2.556   |

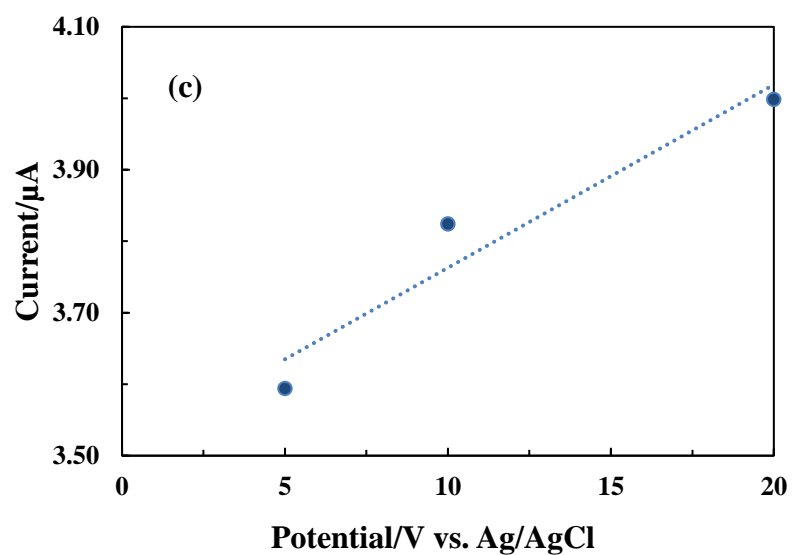
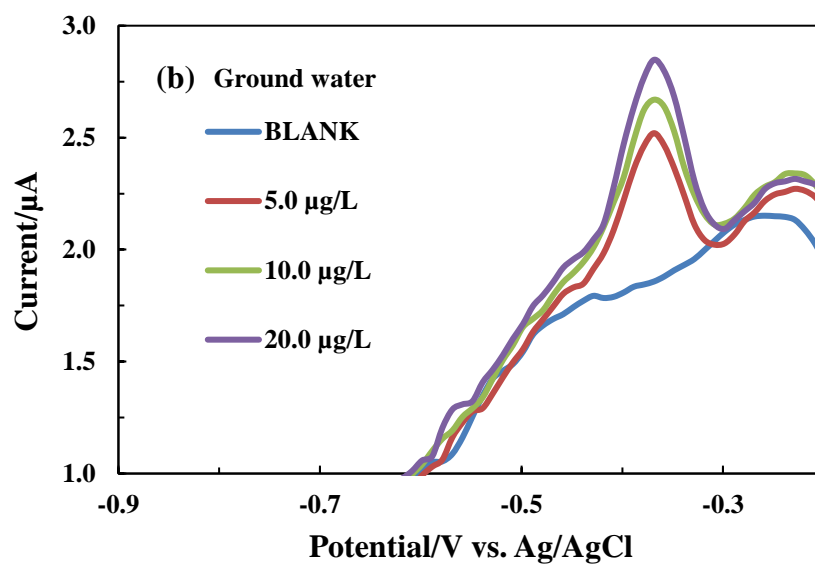
#### 3.4.6. Real sample analysis

The applicability of the CHTMS+Ag(NPs)/GCE in the detection of Pb (II) was performed using the natural water samples as collected previously. The ground and spring water samples were collected from the Mizoram University campus, Tanhril, Aizawl (India). The water parameters were already shown in Table 3.8 and water quality was discussed in Section 3.3.9. The natural water samples were spiked with varied concentrations of Pb (II) i.e., 5.0, 10.0, and 20.0 µg/L of Pb (II) in 0.1 M acetate buffer pH 4.5. The DPASV response for Pb (II) is shown in Figure 3.21 (a & b). It is evident from the DPASV that the Pb (II) showed sharp and distinct oxidative peaks at around the potential of -0.35 V and increasing the concentration of Pb (II) caused for

gradual increase in oxidative peak current. Using the oxidative peak current values, the calibration lines were obtained, which showed a good linear relationship between the concentration of Pb (II) and corresponding peak current values (*Cf* Figure 3.21 (c & d)). The calibration lines were obtained as: for (*Cf* Figure 3.21 (c) spring water:  $y (\mu\text{A}) = 0.0256 \times (\mu\text{g/L}) + 3.5068 (\mu\text{A})$  ( $R^2=0.9292$ ) and  $y (\mu\text{A}) = 0.0213 \times (\mu\text{g/L}) + 2.431 (\mu\text{A})$  ( $R^2=9806$ ) for groundwater (*Cf* Figure 3.21 (d)). The recovery of the spiked concentrations were returned in Table 3.12. The recovery percentage of Pb (II) at natural water samples were between 95.52-96.06% and 92.95-102.57% for spring water and groundwater, respectively. These results inferred that the determination of Pb (II) in natural water samples is not affected and showed promising results, which further show the potential of CHTMS+Ag(NPs)/GCE in the trace, and efficient and selective detection of Pb (II).







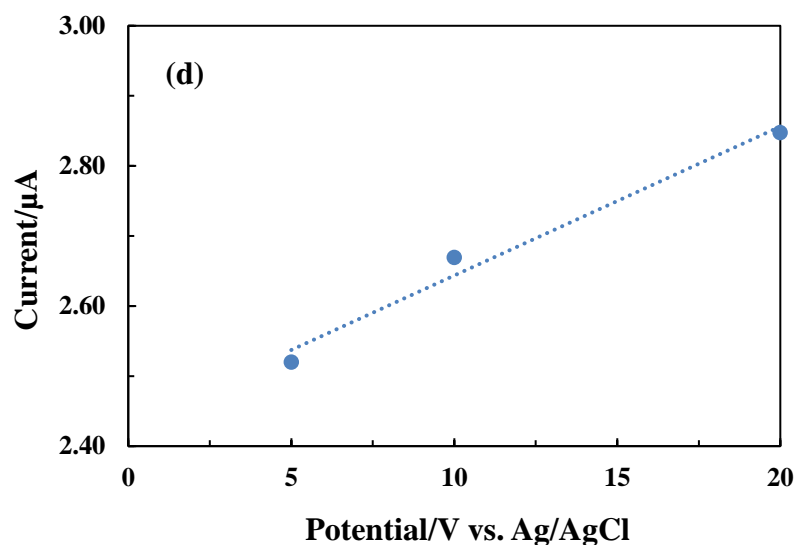


**Figure 3.21:** Real water sample spiked with Pb (II) having concentrations from 5.0 to 20.0  $\mu\text{g/L}$  (Acetate buffer 0.1 M; pH 4.5), (a) DPASV of Pb (II) using the spring water; and (b) DPASV of Pb (II) using ground water; calibration lines obtained for (c) spring water; and (d) ground water samples. [Deposition potential = -0.9 V; Accumulation time = 180.0 sec; Pulse amplitude = 0.05 V; Step potential= 0.0001 V; Modulation time= 0.05 sec; and time interval= 0.5 sec].

**Table 3.12:** The recovery of Pb (II) in the spiked spring water and ground water using CHTMS+Ag(NPs)/GCE.

| Real sample  | Spiked amount ( $\mu\text{g/L}$ ) | Found ( $\mu\text{g/L}$ ) | Recovery (%) |
|--------------|-----------------------------------|---------------------------|--------------|
| Spring water | 5.0                               | 4.78                      | 95.52        |
|              | 10.0                              | 9.66                      | 96.62        |
|              | 20.0                              | 19.21                     | 96.06        |

|              |      |       |        |
|--------------|------|-------|--------|
| Ground water | 5.0  | 4.65  | 92.95  |
|              | 10.0 | 10.26 | 102.57 |
|              | 20.0 | 20.40 | 102.0  |

### 3.4.7. Conclusion

The potential of CHTMS+Ag(NPs)/GCE was studied in the trace, efficient and selective detection of Pb (II). The optimized stripping parameters were pH 4.5, deposition potential -0.9 V and deposition time as 180.0 sec. The free energy charge on the fabricated electrode surface due to the presence of Ag<sup>0</sup>(NPs) synergises the oxidative peak current of Pb (II) due to the fast electron transfer reactions at the surface. Further, the detection of Pb (II) using CHTMS+Ag(NPs)/GCE in aqueous media show limit of detection of 1.97 µg/L in a wide linear range of Pb (II) concentrations i.e., 5.0 µg/L to 80.0 µg/L. The linear equation was found to be  $y (\mu A) = 0.0368 x (\mu g/L) + 3.5742 (\mu A)$  ( $R^2 = 0.9811$ ). The presence of several interfering ions could not affect the detection of Pb (II) except the GLY and OA using the fabricated electrode. The CHTMS+Ag(NPs)/GCE showed relatively high stability and repeatability in the detection of Pb (II). Furthermore, in real matrix study using spring and ground water spiked with different concentrations of Pb (II) showed high recovery percentage of Pb (II). Therefore, silane grafted chitosan decorated with Ag(NPs) is an efficient material in the trace determination of Pb (II) from aqueous medium.

## 3.5. ELECTROCHEMICAL DETERMINATION OF BISPHENOL A (BPA)

### 3.5.1. Electro oxidation of BPA using CHMTS/GCE

Electro oxidation of BPA using CHMTS/GCE under cyclic voltammetry was conducted within a potential window of  $\pm 0.1$  V. The voltammogram of 20.0 mg/L of BPA along with the blank electrolyte i.e., 0.1 M phosphate buffer solution pH 10.0, at scan rate 100 mV/s is shown in Figure 3.22. The Figure indicated that no redox peak current is observed for the blank solution. However, the presence of 20.0 mg/L BPA,

a predominant oxidative peak current was observed at the potential *Ca.* 0.50 V. However, the reverse scan showed no reductive peak, which confirmed the irreversible oxidation of BPA. A similar result was obtained in the oxidation of BPA using the poly(amidoamine)- gold nanoparticles-silk fibroin (PAMAM-AuNPs-SF (Yin *et al.*, 2010). Further, a plausible mechanism of electro-oxidation of BPA is shown in Scheme 3.2. Direct oxidation of phenolic compounds via one electron or two electron transfer resulted with generation of phenoxy radical and quinone, which leads to electro polymerisation at the electrode surface. Further, the dimerization of phenoxy radical or free radical multi step growth polymerization with the monomer or the oxidised monomer initiated by phenoxy radical was suggested (Kuramitz *et al.*, 2001). It is interesting to note that the second or successive cycles of scan, showed no oxidative peak current of BPA using the CHMTS/GCE which further, confirmed the electrooxidation of BPA is resulted with the formation of (4-(2-(4-hydroxyphenyl)propan-2-yl)cyclohexane-2,4-dienone) consequently with the formation of dimer or polymers. These polymers or dimers block the electrode surface and inhibit access of BPA at the electrode surface hence the oxidation of BPA in successive cycles. A similar observation was reported previously in the study of electrochemical oxidation of BPA using cyclic voltammetry (CV), rotating disk electrode (RDE) and controlled potential coulometry (CPC) (Ngundi *et al.*, 2003).

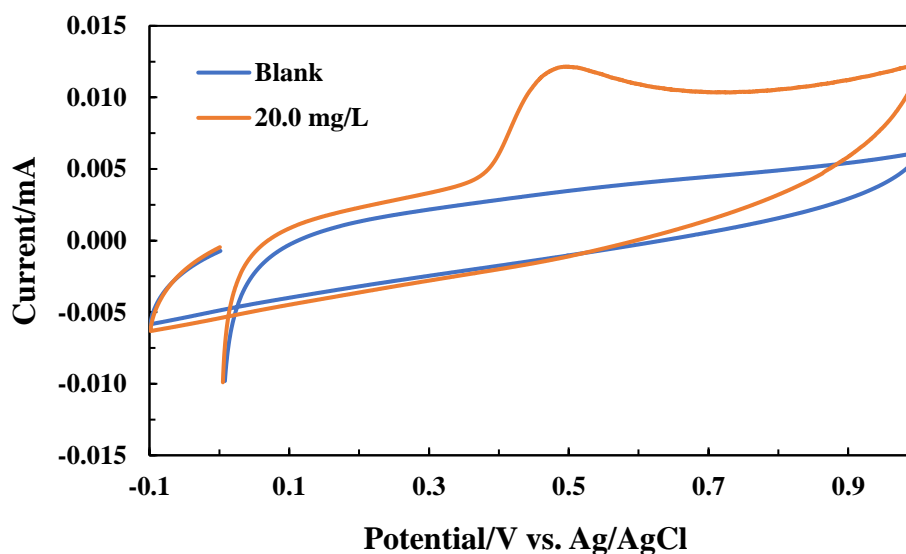
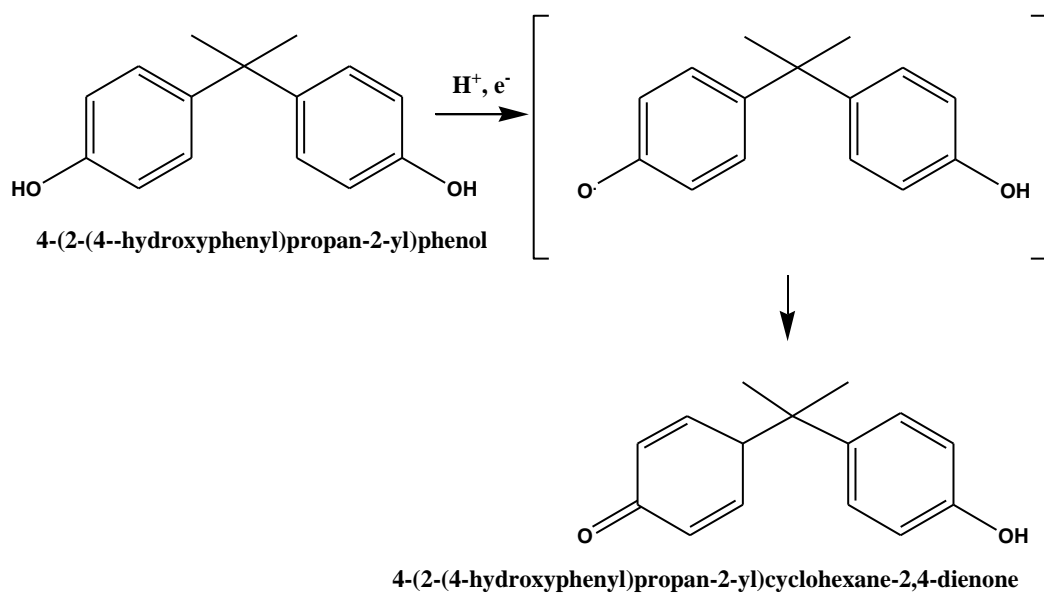


**Figure 3.22:** Cyclic voltammograms of BPA (20.0 mg/L; phosphate buffer (0.1 M); pH 10.0) using the CHMTS/GCE and blank (Scan rate: 100 mV/s).



**Scheme 3.2:** Electro oxidation of (BPA) 4-(2-(4--hydroxyphenyl)propan-2-yl)phenol to 4-(2-(4-hydroxyphenyl)propan-2-yl)cyclohexane-2,4-dienone.

### 3.5.2. Electrochemical behaviour of BPA using the fabricated electrodes under the DPASV studies

The DPASV results of BPA (0.1 M phosphate buffer solution, pH 10.0) using the bare GCE, CH/GCE and CHMTS/GCE at the scan rate of 100 mV/s are shown in Figure 3.23. The DPASV was recorded at the scan rate of 100 mV/s, deposition potential of 0.2 V, deposition time of 180.0 sec., pulse amplitude: 0.05 V, step potential: 0.0001 V, modulation time: 0.05 sec.; and time interval: 0.5 sec. Figure 3.23 reveals that the oxidative peak current of BPA follows the order GCE<CH/GCE<CHMTS/GCE. The bare GCE showed very insignificant oxidative

peak current, which was due to the fact that the BPA molecules were not attracted by the electrode surface hence, the electro oxidation of BPA was not favoured. Moreover, the electron transport to the surface of bare GCE is exceedingly sluggish, which causes lower oxidation of BPA at the GCE (Huang et al., 2014). On the other hand, the CH/GCE showed relatively higher oxidative peak current, which was primarily due to the hydrophobic nature of the chitosan. Moreover, the functional groups viz., amino groups with cationic polysaccharides, possess a net positive charge, enabled to attract the BPA (which has a negative charge in the solution) molecules resulting with an enhanced peak current (Yu et al., 2011).

Furthermore, compared to the CH/GCE, the CHMTS/GCE exhibits much sharper and enhanced oxidative peak current for BPA with a value of 1.28  $\mu\text{A}$  at the potential *Ca* 0.42 V. The higher peak current observed using the composite material modified GCE is due to the synergistic effect using the silane grafted chitosan. The composite material provides an enhanced hydrophobic site which facilitates the sorption of BPA molecules on the electrode surface and undergoes an enhanced oxidation of BPA (Lee et al., 2016).

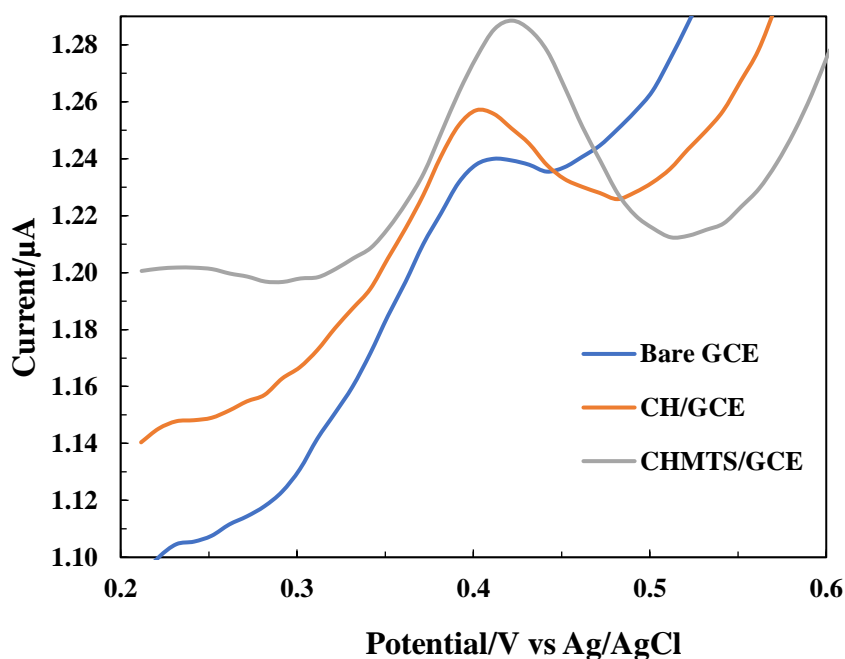


**Figure 3.23:** DPASV curves obtained for BPA (180.0  $\mu\text{g/L}$  at pH 10.0; phosphate buffer (0.1 M)) using the bare GCE, CH/GCE and CHMTS/GCE (Deposition

potential: 0.2 V; Scan rate: 100 mV/s; and Deposition time: 180.0 sec; Pulse amplitude: 0.05 V; Step potential: 0.0001 V; Modulation time: 0.05 sec; and Time interval: 0.5 sec].

### 3.5.3. Optimization of the experimental parameters

The voltammetric method needs the optimization of experimental parameters since these factors provide the optimum sensitivity to the detection of analytes. As a result, several parametric experiments, i.e., effect of pH, deposition potential, and deposition time, were conducted using the composite (CHMTS) thin film electrode in the detection of BPA in an aqueous solution.

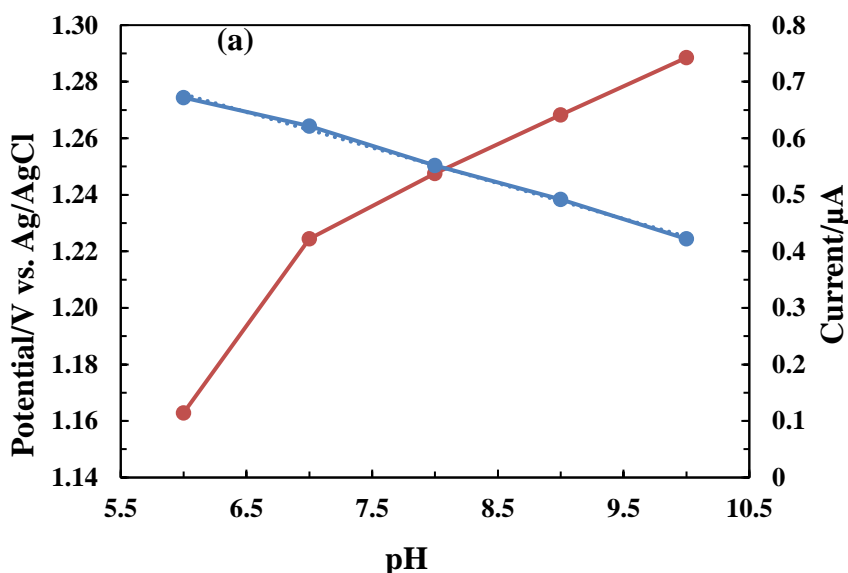
### 3.5.4. Effect of pH

The electrochemical oxidation of BPA was investigated using CHMTS/GCE in 0.1 M phosphate buffer at various pH levels (i.e., from 6.0 to 10.0). The Figure 3.24 (a) (Primary axis) depicts the change in oxidative peak current at various pH values. The oxidative peak current was increased with an increase in the pH, and the maximum oxidative peak current was obtained at pH 10.0. The dissociation constants i.e.,  $pK_a^1$  and  $pK_a^2$  of BPA are 9.9 and 10.2, respectively. Therefore, the speciation of BPA demonstrated that the BPA molecule is almost undissociated throughout a wide range of pH 2.0 to 9.0 (Regueiro et al., 2015; Zheng et al., 2013). The dissociated BPA molecule oxidizes readily at the electrode surface hence, exhibits an increased oxidative current. Moreover, the silane-grafted chitosan possesses hydrophobic and organophilic binding sites that facilitates the sorption of BPA to the electrode surface, and causes enhanced oxidation of BPA. A similar result was observed using thermosensitive molecular imprinted polymers at a higher pH region (Yonten et al., 2016). The BPA was adsorbed onto palygorskite-montmorillonite at pH 12.0, which revealed that the electrostatic attraction was predominant between the solid surface and the dissociated BPA molecules (Berhane et al., 2016). Figure 3.24 (a) (Secondary axis) depicts the relationship between oxidative peak current potential ( $E_p$ ) against the

pH. A linear relationship occurred between the potential and pH (Cf Figure 3.24 (b)). Further, the linear equation is:  $E_p \text{ (V)} = -0.0629 \text{ pH} + 1.0554$  ( $R^2=0.9973$ ), where the slope was found  $0.0629 \text{ pH}^{-1}$ , which is close to the theoretical value of  $0.057 \text{ pH}^{-1}$ . Hence, this infers that the equal number of protons and electrons are involved in the electrode reaction (Akilarasan et al., 2018; Fan et al., 2012).

### 3.5.5. Effect of deposition potential and time

Figure 3.24 (b) indicates increase in accumulation potential from 0.15 V to 0.20 V, the oxidative peak current was increased from 1.265 to 1.284  $\mu\text{A}$ , respectively. However, further increase in potential from 0.20 to 0.35 V caused a decrease in the peak current from 1.284 to 1.273  $\mu\text{A}$ . Similarly, increasing the accumulation duration from 90.0 to 180.0 sec caused an increase in peak current from 1.263 to 1.283  $\mu\text{A}$ . However, further increase in deposition time i.e., time > 180.0 sec. caused a decrease in peak current values (Cf Figure 3.24 (c)). Therefore, the optimized parameters i.e., pH, accumulation potential, and accumulation time is obtained as pH 10.0, 0.2 V, and 180.0 sec, respectively.





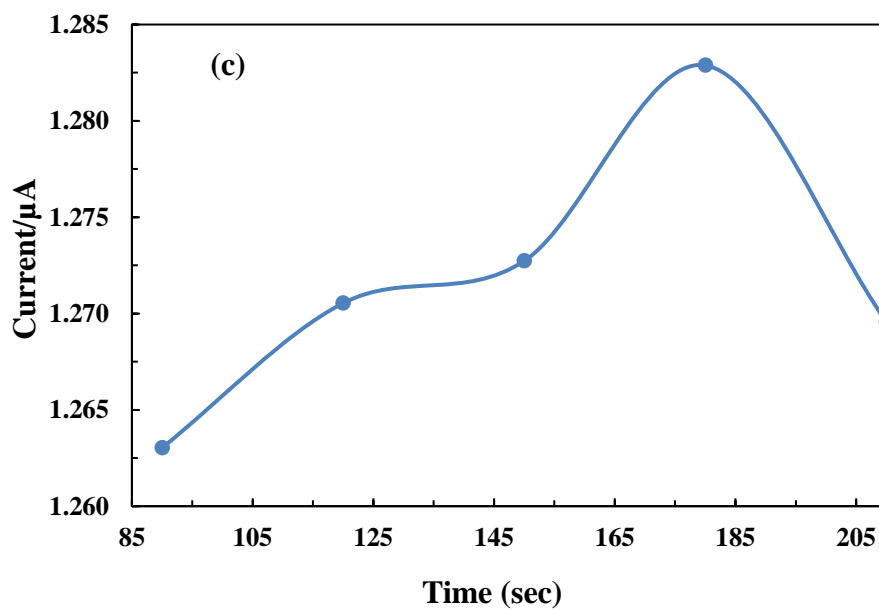
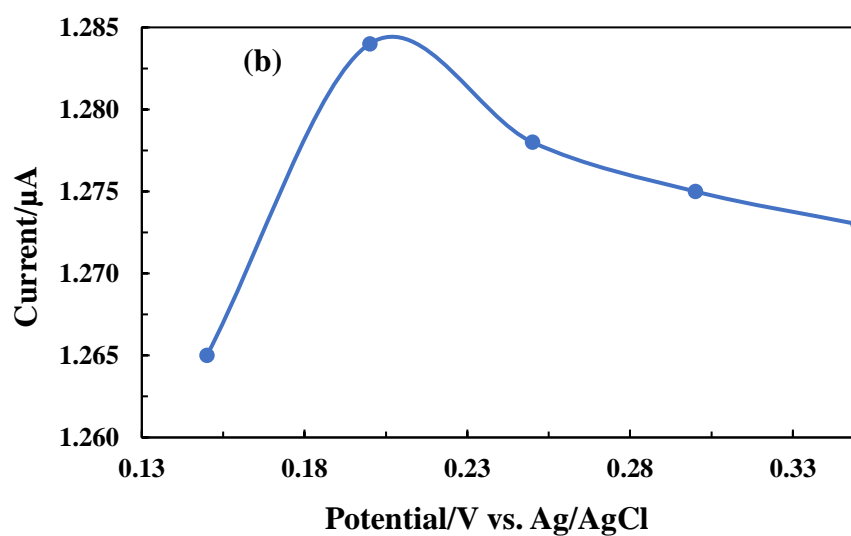


**Figure 3.24:** Parametric studies carried out at 180.0  $\mu\text{g/L}$  BPA (0.1 M phosphate buffer; pH 10.0); (a) The oxidative peak potential (Primary axis) as a function of pH

and the oxidative peak current of BPA at different pH values (Secondary axis); (b) The oxidative peak current of BPA as a function of deposition potential; and (c) The oxidative peak current of BPA as a function of deposition time [Pulse amplitude: 0.05 V; Step potential: 0.0001 V; Modulation time: 0.05 sec; and time interval: 0.5 sec].

### 3.5.6. Electrochemical determination of BPA

The electrochemical detection of BPA at various concentrations of BPA (140.0 µg/L to 200.0 µg/L) utilising CHMTS/GCE are shown in Figure 3.25 (a). The oxidative peak current of BPA (0.1 M phosphate buffer at pH 10.0) was obtained at an applied potential of 0.42 V. The other parameters such as deposition potential: 0.2 V, deposition time: 180.0 sec, pulse amplitude: 0.05 V, Step potential: 0.0001 V, Modulation time: 0.05 sec., and time interval: 0.5 sec. were maintained as constant throughout the experiments. The oxidative peak current of BPA was gradually increased with an increase in BPA concentration (Cf Figure 3.25 (a)). The calibration line between the oxidative peak current and BPA concentration was obtained and shown in Figure 3.25 (b). The straight line equation is:  $y (\mu\text{A}) = 0.0008 x (\mu\text{g/L}) + 1.1337 (\mu\text{A})$  ( $R^2=0.9723$ ). Hence, reasonably a good linearity was obtained between the BPA concentration and peak current. Further, the LOD and LOQ found to be 5.61 µg/L and 18.70 µg/L respectively.

Table 3.13 shows a comparison of the fabricated electrode to other reported modified electrodes in terms of LOD obtained in the detection of BPA from aqueous medium. Table 3.13 revealed that the fabricated electrode possessed reasonably low LOD compared to several other electrodes fabricated using different materials. Therefore, the current investigation demonstrated a useful sensing platform for the low level detection of BPA.

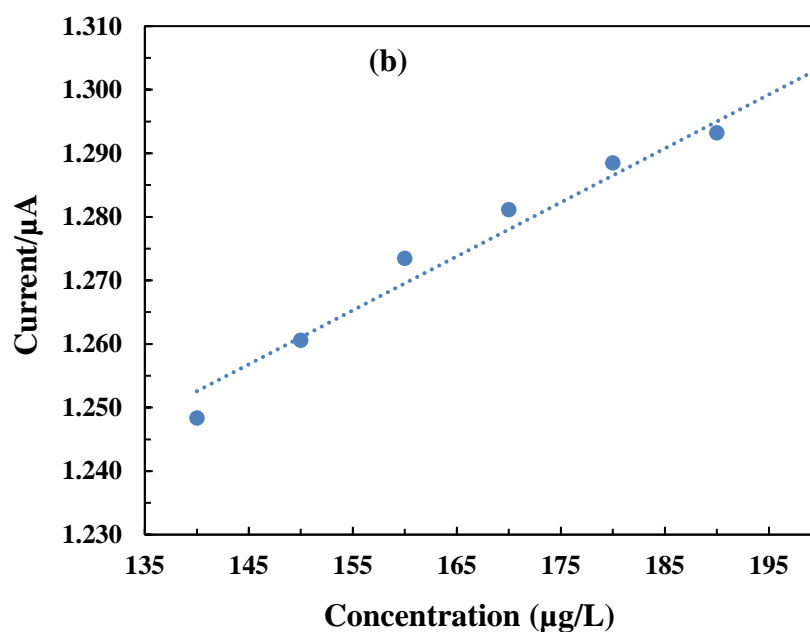
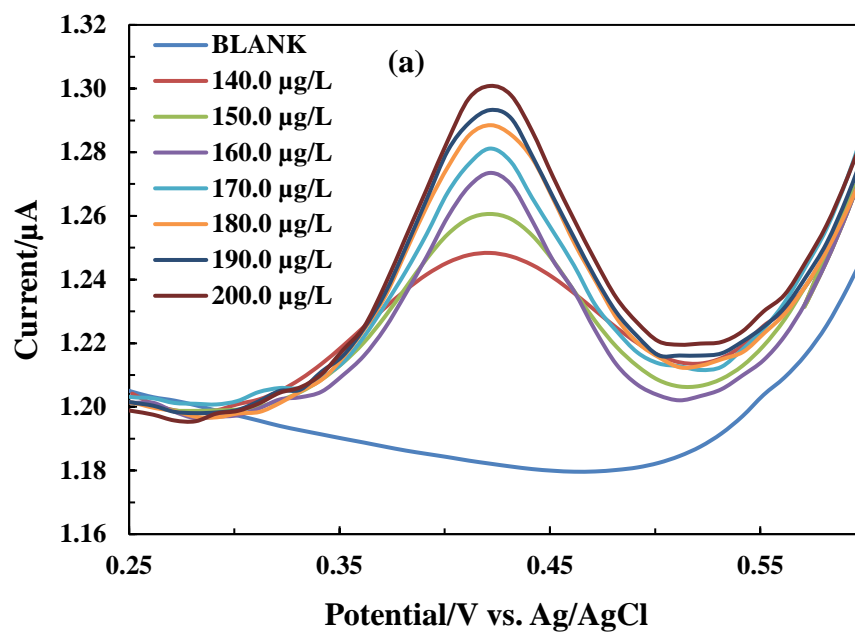


**Figure 3.25:** (a) The DPASV of BPA as a function of BPA concentrations; (b) Calibration line obtained for the oxidative peak current of BPA as a function of BPA concentration (Phosphate buffer (0.1 M; pH 10.0); deposition potential: 0.2 V;

deposition time: 180.0 sec; Pulse amplitude: 0.05 V; Step potential: 0.0001 V; Modulation time: 0.05 sec; and time interval: 0.5 sec).

**Table 3.13:** The comparison of LOD obtained for BPA using the CHMTS/GCE with other studies.

| Electrode material employed | Method      | Concentration range/ linear range ( $\mu\text{mol/L}$ )           | LOD ( $\mu\text{mol/L}$ )       | Ref.                          |
|-----------------------------|-------------|-------------------------------------------------------------------|---------------------------------|-------------------------------|
| MIP-NG/GCE                  | Amperometry | 8.0 to 60000.0                                                    | 0.14                            | (Huang <i>et al.</i> , 2011)  |
| CAS-CG/GCE                  | LSV         | 0.49 to 24.0                                                      | 0.25                            | (Jodar <i>et al.</i> , 2019)  |
| RGO-Ag/PLL/GCE              | DPASV       | 1.0 to 80.0                                                       | 0.54                            | (Li <i>et al.</i> , 2017)     |
| NiNPs/NCN/CS/GCE            | DPASV       | 0.1 to 15.0                                                       | 0.05                            | (Wang <i>et al.</i> , 2020)   |
| CB/AuSNPs/SNGCE             | DPASV       | 0.5 to 50.0                                                       | 0.06                            | (Jebril <i>et al.</i> , 2021) |
| CHMTS/GCE                   | DPASV       | 0.61 to 0.88<br>(140.0 $\mu\text{g/L}$ to 200.0 $\mu\text{g/L}$ ) | 0.02<br>(5.61 $\mu\text{g/L}$ ) | <b>This work</b>              |

LSV – Linear sweep voltammetry, MIP-NG/GCE-Molecularly imprinted polymers and gold nanoparticles/glassy carbon electrode, CAS-CG/GCE - Casein and Carbon Black/glassy carbon electrode, RGO-Ag/PLL/GCE- Reduced graphene oxide-silver/poly-L-lysine nanocomposites/glassy carbon electrode, NiNPs/NCN/CS/GCE- Nickel nanoparticle/nitrogen-doped carbon nanosheet/chitosan/glassy carbon electrode, CB/AuSNPs/SNGCE- green gold sononanoparticles and carbon black nanocomposite.

### 3.5.7. Effect of co-existing ions

Several coexisting ions viz.,  $\text{Na}^+$ ,  $\text{Mg}^{2+}$ ,  $\text{Cl}^-$ ,  $\text{NO}_3^-$ , oxalic acid (OA), ethylene diamine tetraacetic acid (EDTA), and glycine (GLY), along with the phenolic compounds, such as phenol (PH), and hydroquinone (HQ), are investigated in the electrochemical detection of BPA. The concentrations of co-existing ions were kept at 1.8 mg/L, and the BPA concentration was 180.0  $\mu\text{g/L}$ . The peak current was measured in presence of this co-existing ions and compared with the blank value using the CHMTS/GCE under the DPASV measurements (*Cf* Figure 3.26). Figure 3.26, reveals that the presence of these co-existing ions even at the level of 1.8 mg/L had no effect on BPA detection using the composite modified GCE. They inferred that the CHMTS/GCE showed very high selectivity and sensitivity towards the detection of BPA. This enhances the applicability of the material in miniaturized device development for detection of BPA. Similarly molecularly imprinted polymer-modified multiwalled carbon nanotube paste electrode ((MIP-MWNPE) also showed an enhanced sensitivity and selectivity toward the detection of 5.0  $\mu\text{M}$  BPA (Chen et al., 2014)

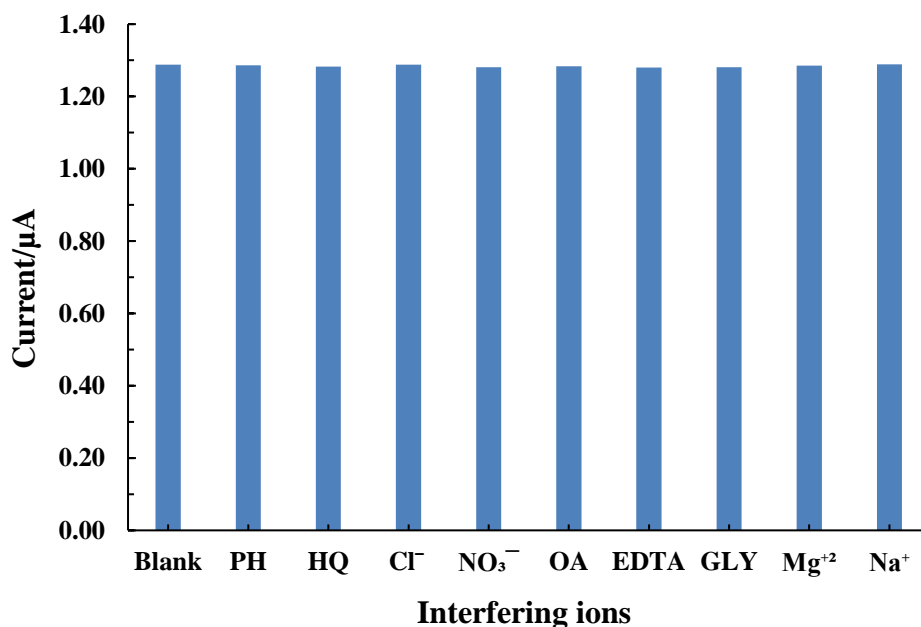


**Figure 3.26:** The detection of BPA in presence of several interfering ions using the CHMTS/GCE ([BPA: 180.0  $\mu\text{g/L}$ ; [Interfering ion]: 1.8. mg/L; phosphate buffer (0.1

M; pH 10.0); Pulse amplitude = 0.05 V; Step potential= 0.0001 V; Modulation time= 0.05 sec; and time interval= 0.5 sec).

#### **3.5.8. Reproducibility and stability study**

The stability of fabricated electrodes was ascertained with the repeated and prolonged use of electrodes in the detection of BPA. The experiments were conducted using 180.0  $\mu\text{g/L}$  BPA (0.1 M phosphate buffer solution at pH 10.0). Similarly, the other parameters in DPASV measurements were taken as deposition period (180.0 sec.), and deposition potential (0.2 V) were unchanged. The CHMTS/GCE was used for 10 times in blank electrolyte, then washed with purified water and again run 5 times in BPA (180.0  $\mu\text{g/L}$ ) analyte, and the oxidative peak current of BPA is shown in Figure 3.27 (a). Further the %RSD (relative standard deviation) was calculated ( $n=5$ ) and found to be 0.35%. The low value of %RSD indicated that CHMTS/GCE is reasonably stable for repeated operations in the determination of BPA.

Similarly, the study was extended to assess the long-term stability of the fabricated CHMTS/GCE. Figure 3.27 (b) showed the current response of BPA (180.0  $\mu\text{g/L}$ ) at a prolonged detection till 48 hrs. At varied time intervals, i.e., from 0 to 48 hours, the CHMTS/GCE response towards BPA detection ( $n=3$ ) was maintained to 99.42% up until the 48 hrs of duration. The stability and reproducibility of CHMTS/GCE showed that the fabricated electrode is reasonably stable and showed long-term applicability for detection of BPA in an aqueous solution.

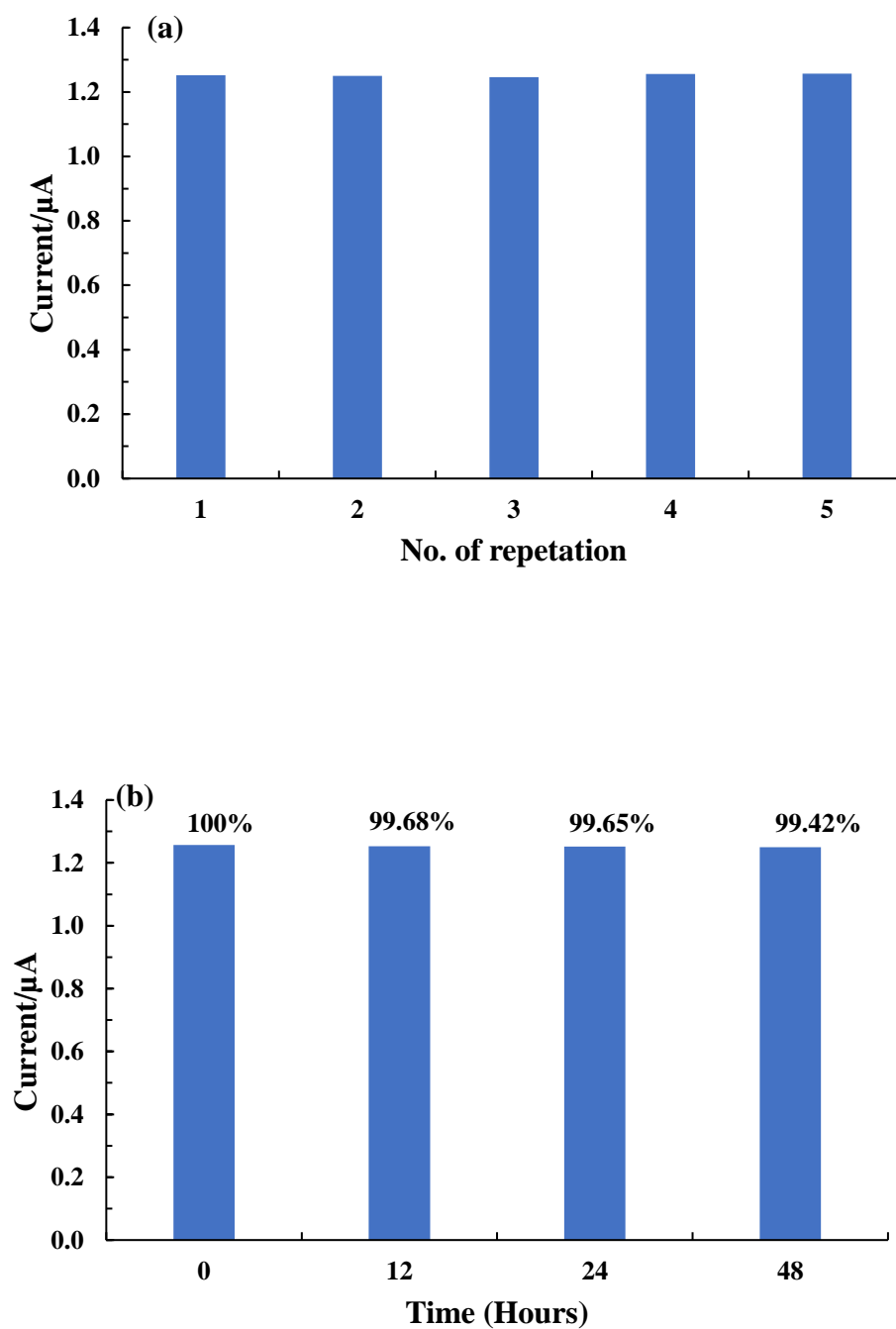


**Figure 3.27:** (a) Reproducibility studies using the CHMTS/GCE at 180.0  $\mu\text{g/L}$  BPA, for repeated detection of BPA; and (b) Stability of fabricated CHMTS/GCE at varied duration of time i.e., from 0 to 48 hrs.

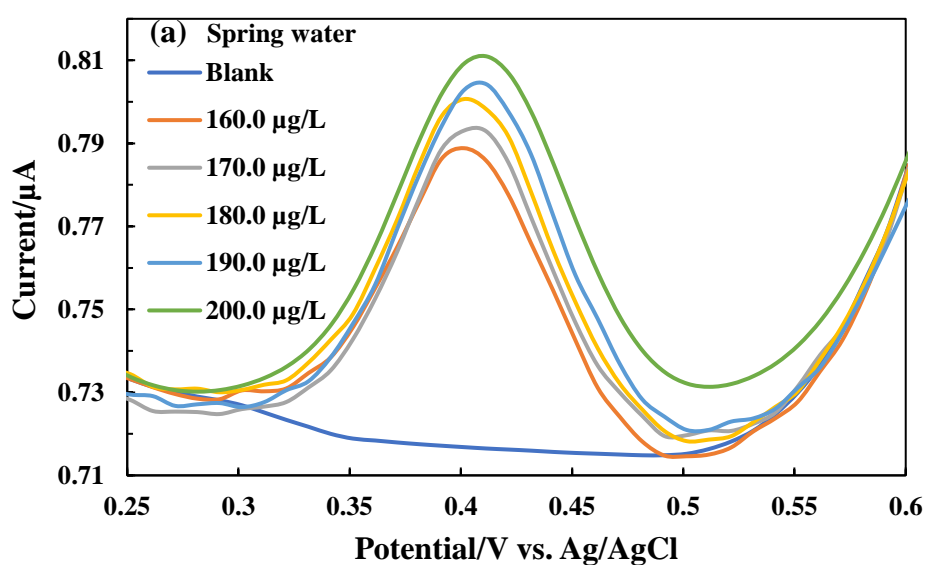
### 3.5.9. Real water implications

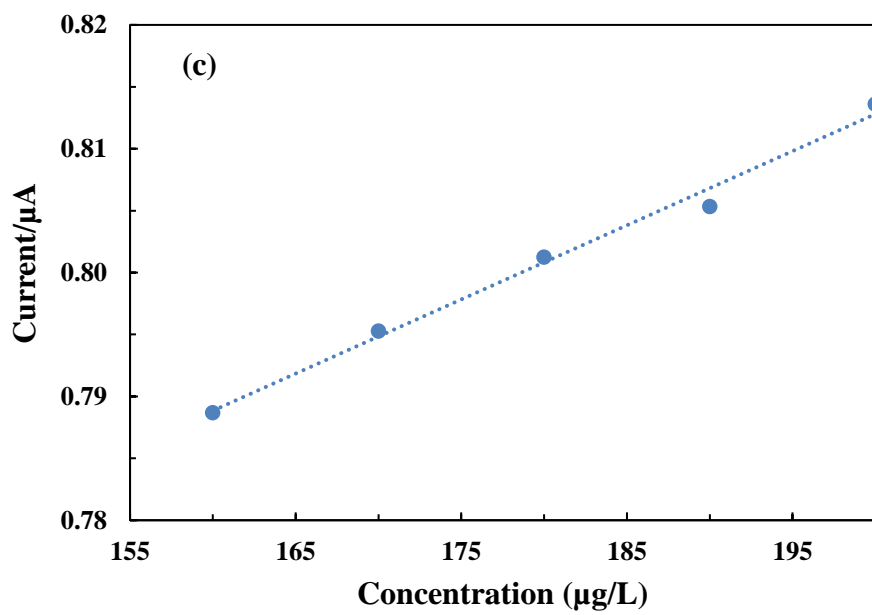
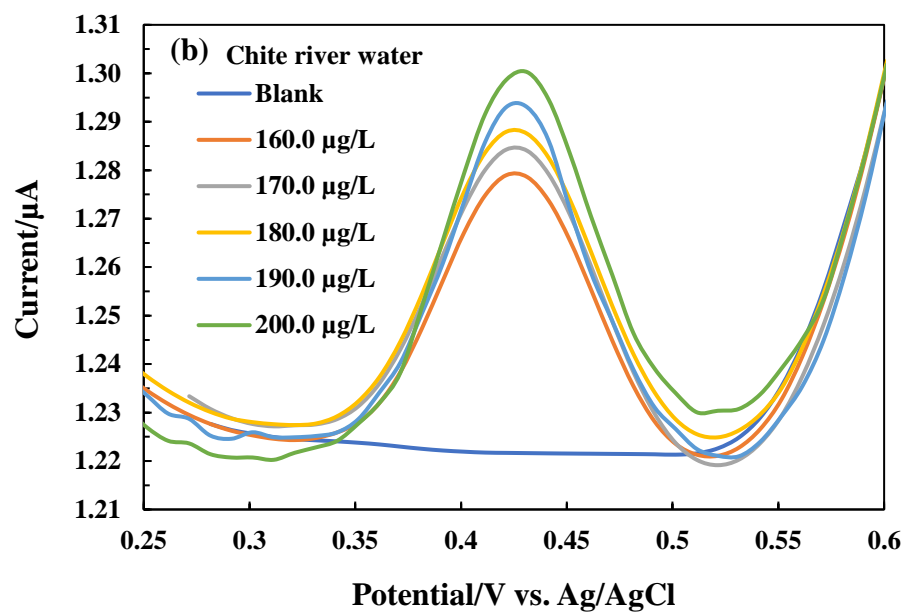
BPA was detected in natural water samples using the fabricated electrode (CHMTS/GCE) under the DPASV measurements. Natural water samples were collected from the Mizoram University campus in Aizawl, Mizoram, India (Springwater) and Chite river water, Aizawl, Mizoram, India (Chite river water). The water samples were first filtered using Whatman filter paper (pore size 11 m) to eliminate the suspended particles. Table 3.14 includes the water quality analysis performed for these two water samples. AAS results showed that spring water contained relatively higher concentration of calcium (1.12 mg/L). However, the other elements viz., are either not detected or minimal in both the water samples. The TOC analysis revealed that both water samples are contained with relatively high value of inorganic carbon (IC). This indicated that the water is having the dissolved carbonates or bicarbonates. Moreover, these samples are having minimal NPOC value. Other impurities viz., the phosphate, nitrate, sulphate, and fluoride are present to their low values in both the water samples. The natural water sample was spiked with varied concentrations of BPA (160.0 µg/L to 200.0 µg/L) in 0.1 M phosphate buffer at pH 10.0. The DPASV experiments were carried out for the determination of spiked BPA under the optimized conditions and DPASV curves are shown in Figure 3.28 (a & b). Figure reveals that increase in BPA concentration caused an increase in oxidative peak current of BPA in both the water samples. Further, the plot of peak current against spiked BPA concentrations is drawn and shown in Figure 3.28 (c & d). Reasonably good straight lines were obtained between the BPA concentration and the peak current values. The straight lines were obtained as:  $y (\mu A) = 0.0006 (\mu g/L) + 0.693 (\mu A)$  ( $R^2=0.991$ ) and  $y (\mu A) = 0.0005 (\mu g/L) + 1.1968 (\mu A)$  ( $R^2=0.9913$ ), respectively for the spring water and Chite river water samples. These results suggested that the CHMTS/GCE possessed reasonably fair applicability in the electrochemical determination of BPA in the real matrix samples.

In addition, the recovery percentage of BPA was estimated and presented in Table 3.15. The recoveries were estimated using three different spiked concentrations of BPA in each water samples i.e., 160.0 µg/L, 170.0 µg/L, and 180.0 µg/L. The results revealed that reasonably a high recovery of BPA is achieved in the detection process. The recovery percentage in the springwater sample was varied from 99.7% to 100.2%,



whereas it varied from 102.4% to 102.9% in the Chite river water sample. The CHMTS/GCE showed a significantly high recovery percentage in the real water samples. This inferred that the fabricated electrode has potential in real-world applications, at least in the trace detection of BPA. The fabricated electrode is, perhaps, a miniaturized device development.





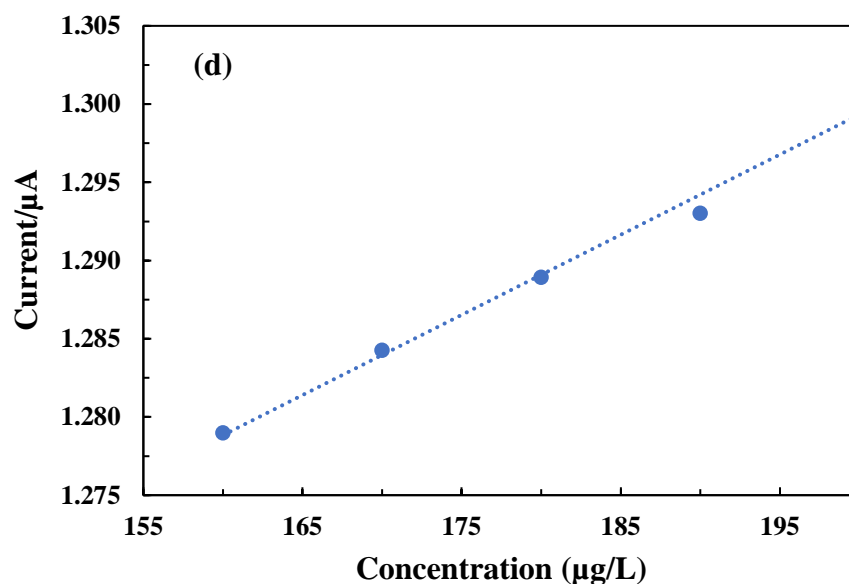


**Figure 3.28:** Real water sample spiked with BPA having concentrations from 160.0 to 200.0  $\mu\text{g/L}$  (Phosphate buffer 0.1 M; pH 10.0), (a) DPASV of BPA using the spring water; and (b) DPASV of BPA using Chite river water; calibration lines obtained for (c) spring water; and (d) Chite river water samples. [Deposition potential = 0.2 V; Accumulation time = 180.0 sec.; Pulse amplitude = 0.05 V; Step potential= 0.0001 V; Modulation time= 0.05 sec; and time interval= 0.5 sec].

**Table 3.14:** Analysis of real water samples using different analytical methods.

| Elemental Analysis | Spring water (mg/L) | Chite river water (mg/L) |
|--------------------|---------------------|--------------------------|
| Copper (Cu)        | 0.01                | BDL                      |
| Calcium (Ca)       | 1.12                | 0.02                     |
| Zinc (Zn)          | BDL                 | BDL                      |
| Lead (Pb)          | BDL                 | BDL                      |

|                                |               |               |
|--------------------------------|---------------|---------------|
| Nickle (Ni)                    | BDL           | 0.01          |
| Iron (Fe)                      | 0.01          | BDL           |
| Manganese (Mn)                 | BDL           | BDL           |
| <b>TOC Analysis</b>            | <b>(mg/L)</b> | <b>(mg/L)</b> |
| NPOC                           | 1.16          | 2.89          |
| IC                             | 15.21         | 14.49         |
| TC                             | 16.37         | 17.38         |
| <b>Other contents Analysed</b> |               |               |
| Nitrate                        | 4.00 µg/L     | 3.70 mg/L     |
| Phosphate                      | 0.01 mg/L     | 0.02 mg/L     |
| Sulfate                        | 0.03 mg/L     | 11 mg/L       |
| Fluoride                       | 0.01 mg/L     | 0.09 mg/L     |

BDL: Below detection limit

**Table 3.15:** The recovery of BPA in the spiked spring water and Chite river water using CHMTS/GCE.

| <b>Real sample</b> | <b>Spiked amount<br/>(µg/L)</b> | <b>Found (µg/L)</b> | <b>Recovery (%)</b> |
|--------------------|---------------------------------|---------------------|---------------------|
| Spring water       | 160.0                           | 159.48              | 99.7                |
|                    | 170.0                           | 170.46              | 100.2               |
|                    | 180.0                           | 180.38              | 100.2               |
|                    | 160.0                           | 164.36              | 102.7               |

|                   |       |        |       |
|-------------------|-------|--------|-------|
| Chite River water | 170.0 | 174.92 | 102.9 |
|                   | 180.0 | 184.28 | 102.4 |

### 3.5.10. Conclusion

3-mercaptopropyl trimethoxysilane grafted chitosan matrix (CHMTS) material was used in fabricating GCE for electrochemical determination of BPA from aqueous medium. The irreversible oxidation of BPA occurred around the potential of 0.50 V. Similarly, the DPASV results showed that the oxidative peak current followed the order GCE<CH/GCE<CHTMS/GCE. Further, the optimized parameters in the DPASV measurements for efficient detection of BPA were: pH 10.0; deposition potential 0.2 V and deposition time 180.0 sec. The BPA concentration (140.0 µg/L to 200.0 µg/L) dependence study showed a good linearity between the BPA concentration against the oxidative peak current values. The linear equation was obtained as:  $y (\mu\text{A}) = 0.0008 \times (\mu\text{g/L}) + 1.1337 (\mu\text{A})$  ( $R^2=0.9723$ ) and the LOD was 5.61 µg/L. Presence of several several coexisting ions ( $\text{Na}^+$ ,  $\text{Mg}^{+2}$ ,  $\text{Cl}^-$ ,  $\text{NO}_3^-$ , OA, EDTA, PH and HQ) were not affected by the detection of BPA using the CHTMS/GCE. Moreover, the CHTMS/GCE showed fairly high stability in terms of repeated and prolonged operations in the detection of BPA. The real matrix implications showed that a high recovery percentage of BPA was obtained as: 99.7 to 100.2 % in spring water and 102.7 to 102.9 % in river water samples. Therefore, the fabricated CHMTS/GCE showed a good sensing platform in the detection of BPA in aqueous medium and, perhaps, showed potential in developing the miniaturized device.

### 3.6. ELECTROCHEMICAL DETERMINATION OF TRICLOSAN (TCS)

#### 3.6.1. *Electro oxidation of TCS toward CHMTS/GCE under CV study*

Figure 3.29, shows the voltammograms of TCS (20.0 mg/L). TCS shows a distinct oxidative peak current at an applied potential of *Ca.* 0.61 V. However, reductive peak current does not appear in the reverse scan of the voltammogram, which shows irreversible oxidation of TCS at the electrode surface. The results follow the previous reports (Zheng et al., 2018). Oxidation of the phenolic hydroxyl group of TCS gives the oxidative peak current. On the other hand, in the absence of TCS (Blank), no redox peak current appeared, indicating the oxidative peak current occurred due to the oxidation of TCS molecules. Further, it is interesting to observe that the successive scans caused a gradual decrease in oxidation peak current values. This is due to the deposition of oxidized TCS species on the surface of CHMTS/GCE forming a polymeric product that blocks the access of TCS for further oxidation at the electrode surface (Yola et al., 2015; Santana & Spinelli, 2020).

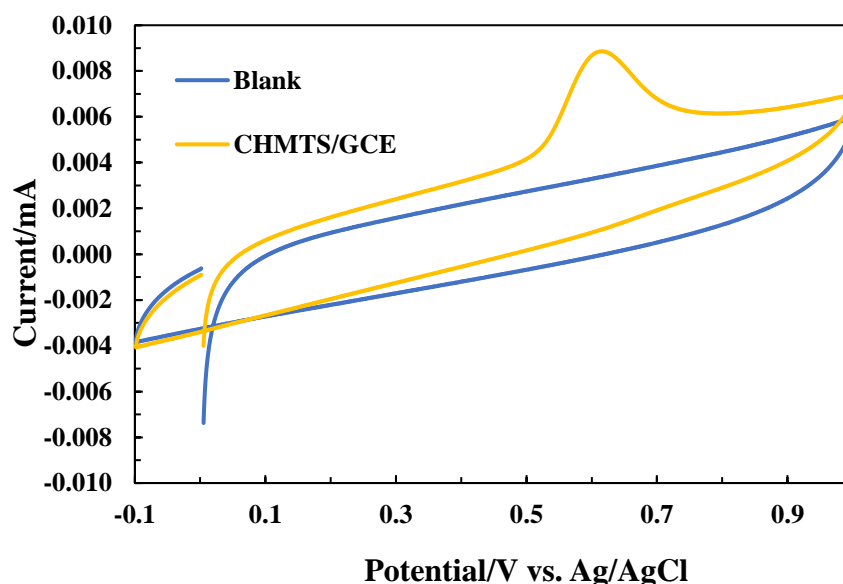


**Figure 3.29.** Cyclic voltammograms of TCS (20.0 mg/L; phosphate buffer (0.1 M); pH 8.0) using the CHMTS/GCE and blank (Scan rate: 100 mV/s).

### 3.6.2. Differential Pulse Anodic Stripping Voltammetry (DPASV) study of triclosan

Voltammograms of TCS (200.0  $\mu\text{g/L}$ ) (0.1 M phosphate buffer; pH 8.0, applied potential: 0.2 V (Ag/AgCl) and deposition time: 180.0 sec.) using different electrodes are shown in Figure 3.30. The redox peak current was observed within the potential of about 0.6 V to 0.64 V, which might be due to the electro-oxidation of the phenolic group in the structure of TCS (Wu et al., 2017b). The results (Cf Figure 3.30) demonstrated that no noticeable peak current was seen in the bare GCE, pointing to the use of the bare GCE for slow electron flow (Dai et al., 2012b). Significant enhanced oxidative peak current was observed using the CH/GCE, CHMTS/GCE, due to the enhanced hydrophobicity of materials that attracted the phenol on the surface of electrodes (Wu et al., 2017b). Furthermore, the CHMTS/GCE showed a well-defined and enhanced oxidative peak current of 1.99  $\mu\text{A}$  at an applied potential of 0.64 V due to the synergistic effect of organophilic and additional siloxane sites favored the sorption of phenol molecules onto the solid surface that showed excellent sensing properties for TCS (Saljooqi et al., 2020).

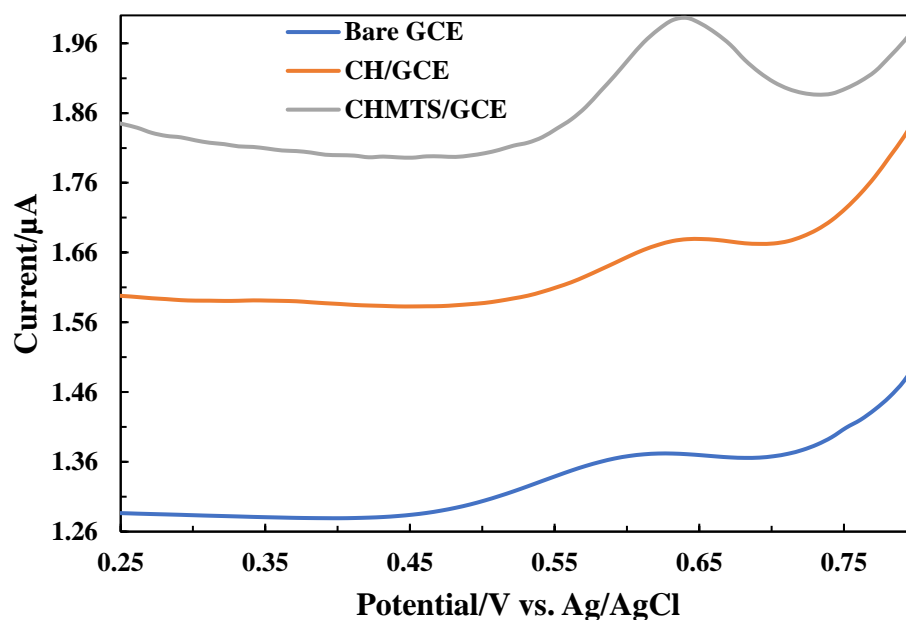


**Figure 3.30:** DPASV curves obtained for TCS (200.0  $\mu\text{g/L}$  at pH 8.0; phosphate buffer (0.1 M)) using the bare GCE, CH/GCE and CHMTS/GCE (Deposition potential: 0.2

V; Scan rate: 100 mV/s; and Deposition time: 180.0 sec; Pulse amplitude: 0.05 V; Step potential: 0.0001 V; Modulation time: 0.05 sec; and Time interval: 0.5 sec].

### **3.6.3. Experimental parameters Optimization**

Various voltammetric studies were conducted to develop selective and sensitive electrochemical sensors, and various parameters (pH, deposition potential, and time) were optimized using the CHMTS/GCE to detect 200.0 µg/L TCS.

### **3.6.4. Effect of pH**

Using CHMTS/GCE, the influence of pH on TCS (200.0 µg/L) detection was investigated. The pH of the 0.1 M phosphate buffer solution was changed from 6.0 to 10.0 (Deposition potential: 0.2 V, Deposition duration: 180.0 sec.). In Figure 3.31 (a), the orange plot shows the electro-oxidation of TCS and electroactive (Wu et al., 2017b). The oxidative peak current rose as pH increased, reaching its maximum value at 8.0. The limiting peak current decreased when the pH level rose further due to the phenolic moiety's dissociation into the corresponding anions (Zheng et al., 2018). As a result, pH 8.0 was chosen as the best pH for the sensitive detection of TCS.

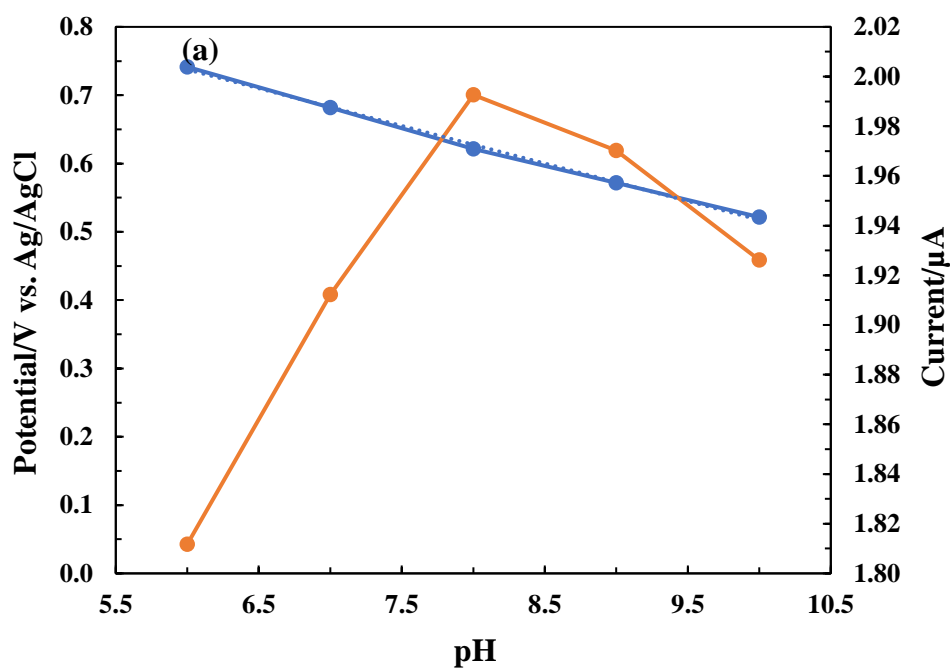
Figure 3.31 (a) shows the effect of pH in peak potential ( $E_p$ ) (blue plot). These results show that the oxidative peak current potential was shifted from higher to lower potential linearly with the increase in pH, which implies an excellent sensing property of CHMTS/GCE towards TCS. Linear relationship of  $E_p$  (V) =  $-0.055 \text{ pH} + 1.0678$  ( $R^2=0.9977$ ) was obtained from Figure 3.31 (a) where slope of this relationship was  $0.055 \text{ pH}^{-1}$ , which approximates the standard value  $0.059 \text{ pH}^{-1}$ . This result demonstrated the same number of protons and electrons involved in the reaction process (Saljooqi et al., 2020).

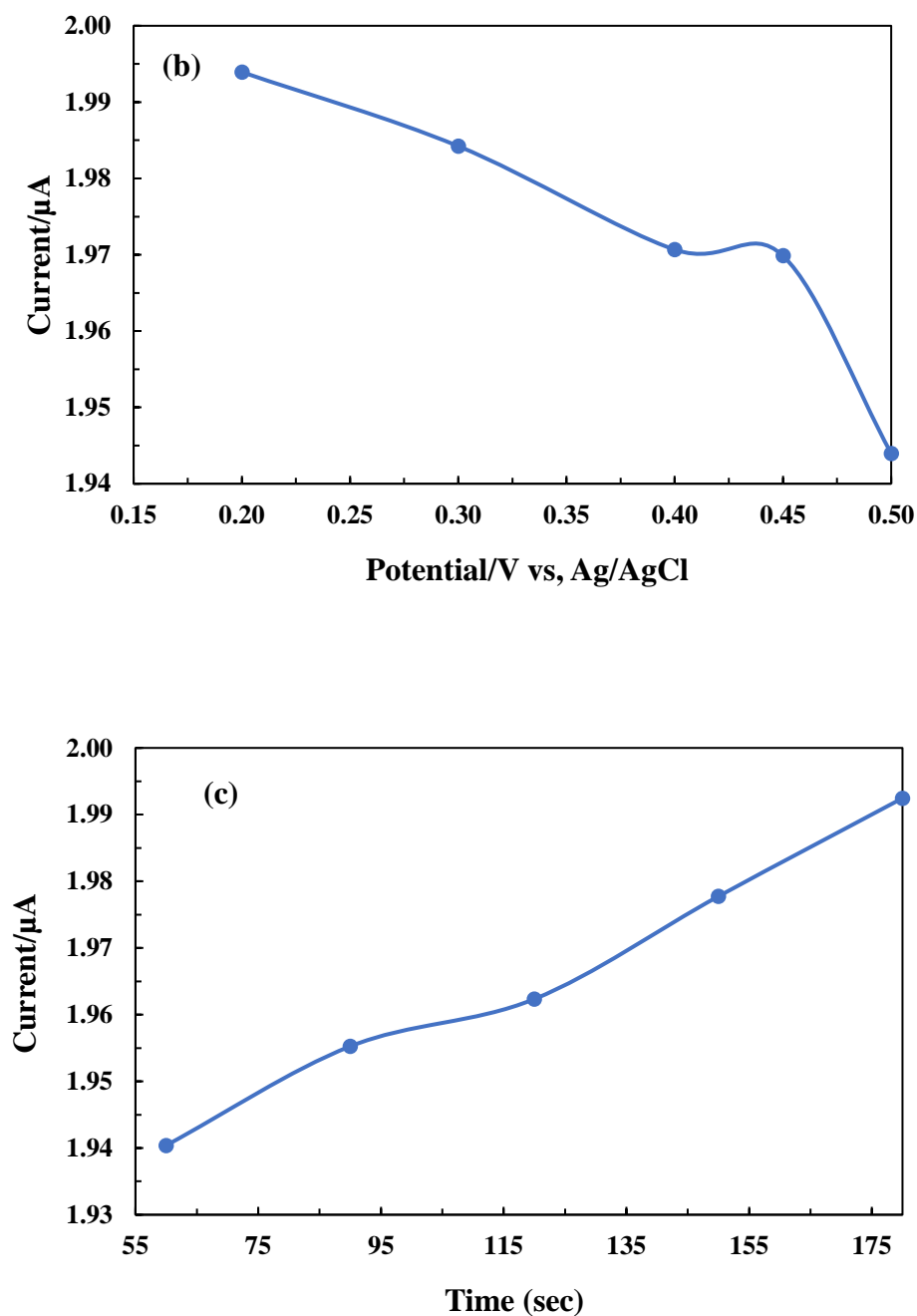
### **3.6.5. Effect of deposition potential and time.**

Optimizing deposition potential and time are critical parameters for developing sensitive electrochemical sensors. The voltammograms of 200.0 µg/L TCS (0.1 M phosphate buffer, pH 8.0) are obtained at varied deposition potential (Cf Figure 3.31



(b)). The 0.2 V (vs. Ag/AgCl) deposition potential gave a relatively higher oxidative peak current. However, further, an increase in potential causes a gradual decrease in oxidative peak. Similarly, the deposition time was increased from 60.0 sec. to 180.0 sec. for peak current values of TCS (Cf Figure 3.31 (c)). Increasing deposition duration favors the oxidative peak current and attains a maximum at 180.0 sec. Therefore, 180.0 sec. is considered an optimum deposition time for sensitive determination of TCS.

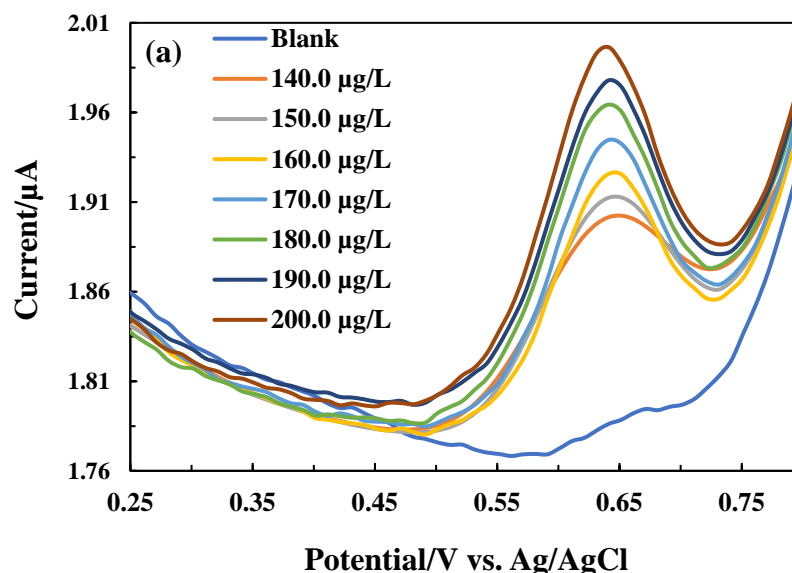




**Figure 3.31:** Parametric studies carried out at 200.0  $\mu\text{g/L}$  TCS (0.1 M phosphate buffer; pH 8.0); (a) The oxidative peak potential (Primary axis) as a function of pH and the oxidative peak current of TCS at different pH values (Secondary axis); (b) The oxidative peak current of TCS as a function of deposition potential; and (c) The oxidative peak current of TCS as a function of deposition time [Pulse amplitude: 0.05 V; Step potential: 0.0001 V; Modulation time: 0.05 sec; and time interval: 0.5 sec].

### 3.6.6. Concentration dependence studies

Low-level determination of TCS was studied under well-optimized experimental conditions, utilizing CHMTS/GCE with a concentration of TCS ranging from 140.0 to 200.0  $\mu\text{g/L}$ , as shown in Figure 3.32 (a). The oxidation of TCS occurs at the potential of *Ca.* 0.64 V. *Ca.* 0.64 V. Further, the obtained oxidative peak current was plotted against the TCS concentration, which resulted in a good linear relation. Therefore, the calibration line was obtained and shown in Figure 3.32 (b). The obtained linear regression equation is:  $y (\mu\text{A}) = 0.0016 x (\mu\text{g/L}) + 1.6724 (\mu\text{A})$  with the correlation coefficient  $R^2=0.993$ . Further, LOD and LOQ were calculated and found out to be 9.49  $\mu\text{g/L}$  and 31.65  $\mu\text{g/L}$ . Furthermore, the performance of the CHMTS/GCE toward TCS detection and the previously reported study were compared in Table 3.16. Table 3.16 showed that the performance of CHMTS/GCE is relatively efficient and found a relatively lower LOD value compared to similar other studies for TCS detection. Therefore, the synthesized CHMTS material showed a good sensing property and was found promising in developing an electrochemical sensor for TCS.



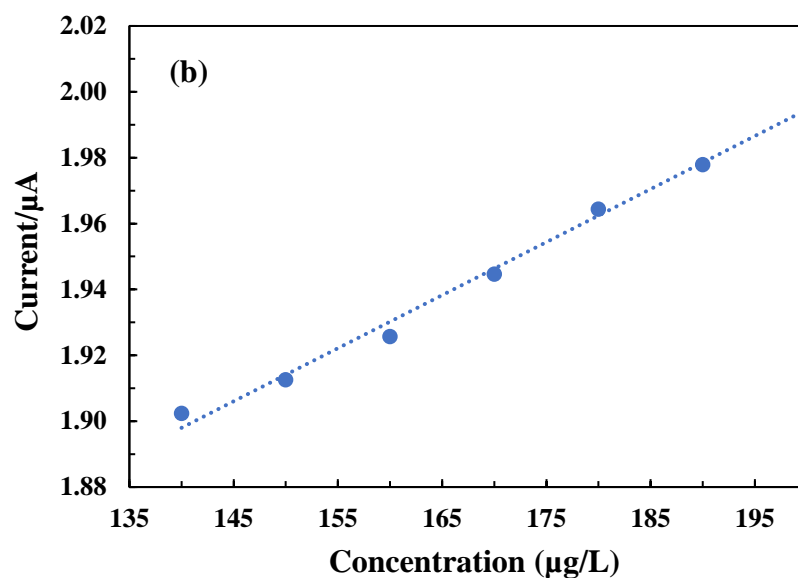


**Figure 3.32:** (a) The DPASV of TCS as a function of TCS concentrations; (b) Calibration line obtained for the oxidative peak current of TCS as a function of TCS concentration (Phosphate buffer (0.1 M; pH 8.0); deposition potential: 0.2 V; deposition time: 180.0 sec; Pulse amplitude: 0.05 V; Step potential: 0.0001 V; Modulation time: 0.05 sec; and time interval: 0.5 sec).

**Table 3.16:** The comparison of LOD obtained for TCS using the CHMTS/GCE with other studies.

| Electrode material employed | Method             | Concentration range/ linear range | LOD                       | Ref.                 |
|-----------------------------|--------------------|-----------------------------------|---------------------------|----------------------|
| Carbon nanoparticles/GCE    | Cyclic voltammetry | 1.0 to 120.0 µmol/L               | 10.0 µmol/L (or 2.3 mg/L) | (Vidal et al., 2008) |

|                                            |                    |                                                     |                                               |                                  |
|--------------------------------------------|--------------------|-----------------------------------------------------|-----------------------------------------------|----------------------------------|
| iPPD/GCE (MIP)                             | Cyclic voltammetry | $2.0 \times 10^{-7}$ to $3.0 \times 10^{-6}$ mol/L  | $8.0 \times 10^{-8}$ mol/L (0.08 $\mu$ mol/L) | (Liu <i>et al.</i> , 2009)       |
| Multiwall carbon nanotube (MWCNT) film/GCE | DPV                | 50.0 $\mu$ g/L to 1.75 mg/L                         | 16.5 $\mu$ g/L                                | (Yang <i>et al.</i> , 2009)      |
| $\beta$ -CD/GNP                            | DPV                | 2.0 to 100.0 $\mu$ mol/L                            | 0.6 $\mu$ mol/L                               | (Li <i>et al.</i> , 2014)        |
| C-PS and C-PC                              | DPV                | 1.0 to 100.0 $\mu$ mol/L                            | 0.49 $\mu$ mol/L and 0.25 $\mu$ mol/L         | (Libansk y <i>et al.</i> , 2014) |
| <b>CHMTS/GCE</b>                           | DPV                | 140.0 to 200.0 $\mu$ g/L (0.48 to 0.69 $\mu$ mol/L) | 9.49 $\mu$ g/L (0.03 $\mu$ mol/L)             | <b>This work</b>                 |

\*iPPD- Imprinted poly-o-phenylenediamine (PPD),  $\beta$ -CD/GNP-  $\beta$ -cyclodextrin/graphene nano platelets, GQD- graphene quantum dots, C-PS- graphitic carbon particles with polystyrene and C-PC- is with polycarbonate

### 3.6.7. Interfering ion study

The reliability of the CHMTS/GCE electrochemical sensor was evaluated in the presence of several cations and anions along with some phenolic compounds. The interfering co-ions chosen were  $\text{Cl}^-$ ,  $\text{NO}_3^-$ ,  $\text{Na}^+$ ,  $\text{Mg}^{2+}$ , EDTA (ethylene diamine tetra acetic acid), OA (oxalic acid), HQ (hydroquinone), PH (phenol), and GLY (glycine).

The concentration of these species was taken 10-fold (2000.0  $\mu\text{g/L}$  or 2.0  $\text{mg/L}$ ) to the analyte (TCS) concentration, i.e., 200.0  $\mu\text{g/L}$  (Blank). Figure 3.33, shows the interfering ions results in the detection of TCS. It is interesting to observe that these species show no effect in the detection of TCS. Therefore, the CHTMS/GCE showed fairly good selectivity for the low-level determination of TCS. Therefore, the results indicated that the selectivity of the material is good, at least for the detection of triclosan in aqueous media. Similarly, glassy carbon electrodes modified with carbon nanodots and chitosan (CNDs-CS/GCE) show selective and sensitive determination of TCS in presence of several interfering ions (Dai et al., 2012).

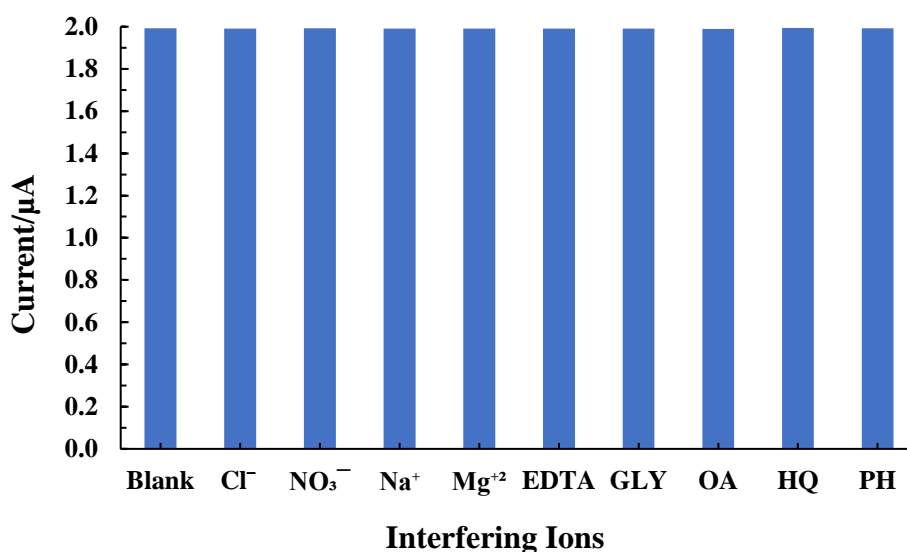
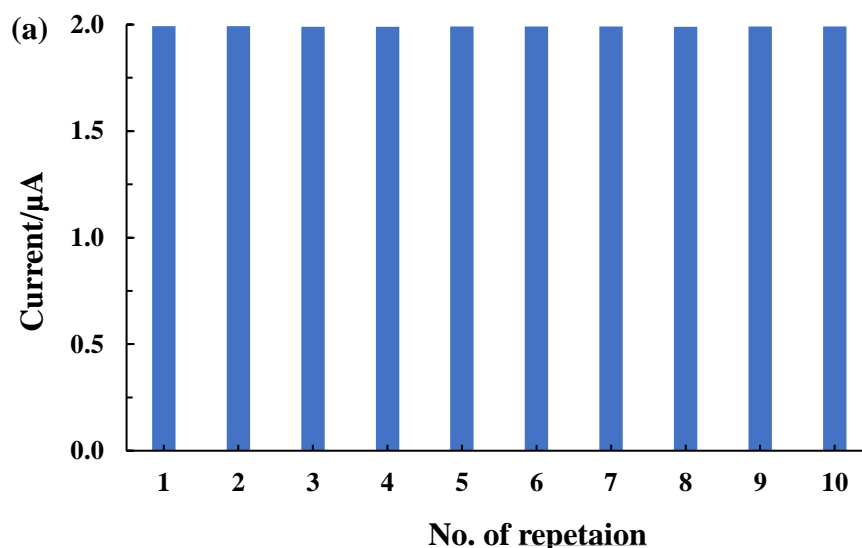


**Figure 3.33:** The detection of TCS in presence of several interfering ions using the CHMTS/GCE ([TCS: 200.0  $\mu\text{g/L}$ ; [Interfering ion]: 2000.0  $\mu\text{g/L}$ ; phosphate buffer (0.1 M; pH 8.0); Pulse amplitude = 0.05 V; Step potential= 0.0001 V; Modulation time= 0.05 sec; and time interval= 0.5 sec.).

### 3.6.8. Reproducibility and stability of fabricated electrode

A reproducibility study was conducted for the CHMTS/GCE to determine TCS 200.0  $\mu\text{g/L}$  under optimized experimental conditions. The detection study was conducted 10 consecutive times. As shown in Figure 3.34 (a), the CHMTS/GCE showed a similar response. The obtained current values were considered for relative standard deviation (RSD) calculation, and found out to be 0.044%. The low value of RSD obtained in the TCS determination inferred that the employed CHMTS/GCE possessed relatively high reproducibility and repeatability in determining the TCS in aqueous media.

Similarly, the stability of the employed CHMTS/GCE was studied for long-term detection of TCS (200.0  $\mu\text{g/L}$ ), and the study was conducted for a prolonged duration, i.e., the time was varied from 0 hours to 48 hours, keeping the electrode at room temperature under ambient conditions. The current response toward TCS is shown in Figure 3.34 (b), and the finding suggests that a variation of time duration peak current maintains the constant value. This inferred that CHMTS/GCE possessed long-term stability for analyte detection.



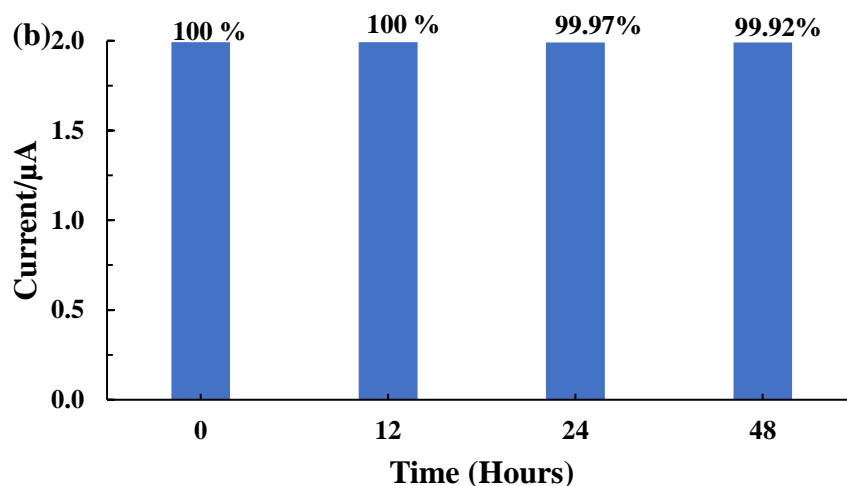


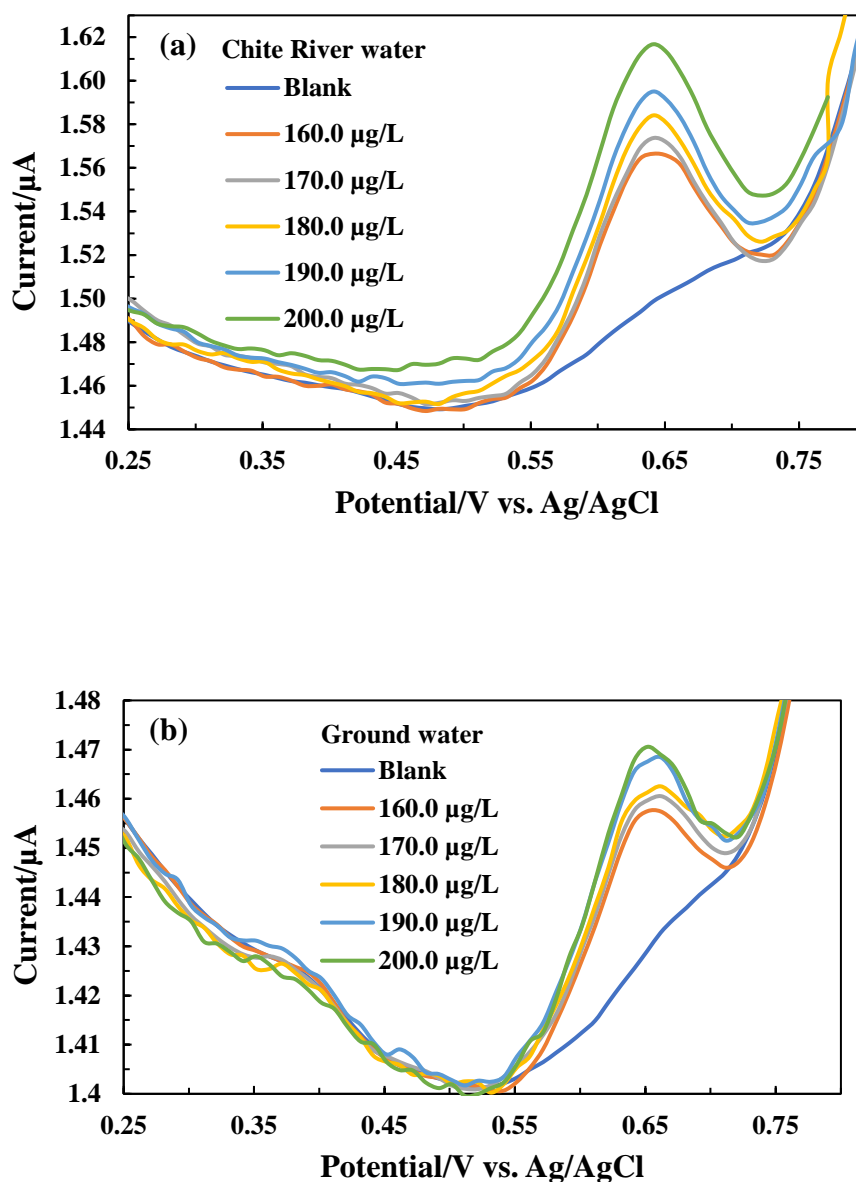
**Figure 3.34:** (a) Reproducibility studies using the CHMTS/GCE at 200.0  $\mu\text{g/L}$  TCS, for repeated detection of TCS; and (b) Stability of fabricated CHMTS/GCE at varied duration of time i.e., from 0 to 48 hrs.

### 3.6.9. Real implication and recovery rate study

For practical application of the CHMTS working electrode which was implemented in detecting TCS real ground water sample which was collected from the Mizoram University Campus, Aizawl, Mizoram, India, While the river water collected from Chite river at Falkland Veng, Mizoram, Aizawl, India. Before water analysis, water samples were filtered utilising whatman filter paper to get rid of any suspended particles or organisms. Real water sample was analyzed using different analytical methods, then returned in Table 3.14 (Chite River water) and Table 3.8 (Ground water). For the practical implications, varying concentrations of TCS were spiked in both the water samples ranging from 160.0-200.0  $\mu\text{g/L}$ , while the electrolyte solution 0.1 M phosphate buffer (pH 8.0) was prepared using the collected water sample. DPASV was employed for TCS detection of spiked concentration in both the water sample and the experiment was carried out under optimised experimental conditions. Other parameters [Pulse amplitude = 0.05 V; Step potential= 0.0001 V; Modulation time= 0.05 sec.; and time interval= 0.5 sec] remain constant and the results are shown in Figure 3.35. The results implies that while increasing the concentration of spiked TCS the peak current increases linearly in both the water sample (groundwater and Chite river water). Further, the calibration line was drawn between the concentration



of TCS against the oxidative peak currents and shown in Figure 3.35 (c & d). The obtained linear equation and correlation coefficient are represented as:  $y (\mu\text{A}) = 0.001 (\mu\text{g/L}) x + 1.4019 (\mu\text{A})$  ( $R^2=0.9932$ ) for Chite river water and  $y (\mu\text{A}) = 0.0004 (\mu\text{g/L}) x + 1.3929 (\mu\text{A})$  ( $R^2=0.9921$ ) for groundwater samples. These results indicated that the response of TCS toward CHMTS/GCE was reasonably good even though other impurities were in high concentration in both the water samples. Therefore, the material has shown potential determination of TCS at trace level in real water samples.



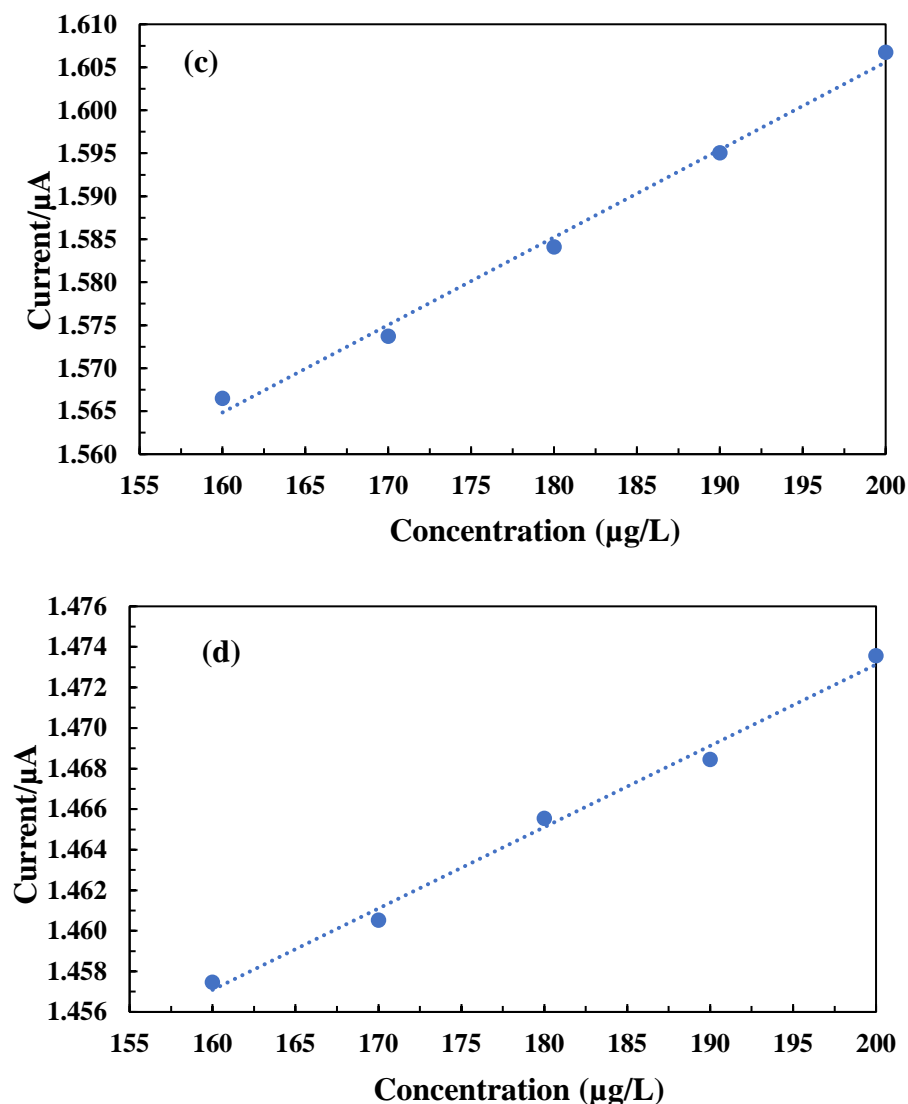


**Figure 3.35:** Real water sample spiked with TCS having concentrations from 160.0 to 200.0  $\mu\text{g/L}$  (Phosphate buffer 0.1 M; pH 8.0), (a) DPASV of TCS using the Chite river water; and (b) DPASV of TCS using ground; calibration lines obtained for (c) Chite river water; and (d) Ground water samples. [Deposition potential = 0.2 V; Accumulation time = 180.0 sec.; Pulse amplitude = 0.05 V; Step potential = 0.0001 V; Modulation time = 0.05 sec.; and time interval = 0.5 sec.].

Furthermore, a recovery percentage study was obtained, and the results are returned in Table 3.17. The spiked concentrations and the recovered concentrations of TCS were calculated. Hence, the recovery percentage was calculated. The experiments

were conducted within the concentration ranging from 160.0-180.0  $\mu\text{g/L}$  of TCS, which is shown in Table 3.17 for both the water samples. Interestingly, the river water percentage recovery is much higher i.e., 101.1% to 102.8%, whereas the groundwater sample showed a recovery percentage of 99.4% to 100.8%. The high recovery percentage of TCS using the CHMTS/GCE inferred the promising detection of TCS even in real matrix analysis; hence, the electrode has potential for device development. A similar response was also reported in real water recovery rate study using novel nanocomposite material coated with silver and gold nanoparticle (Lalmalsawmi et al., 2022)

**Table 3.17:** The recovery of TCS in the spiked Chite river water and ground water using CHMTS/GCE.

| Water sample      | Spiked<br>( $\mu\text{g/L}$ ) | Found<br>( $\mu\text{g/L}$ ) | % Recovery |
|-------------------|-------------------------------|------------------------------|------------|
| Chite river water | 160.0                         | 164.5                        | 102.8      |
|                   | 170.0                         | 171.8                        | 101.1      |
|                   | 180.0                         | 182.2                        | 101.2      |
| Ground water      | 160.0                         | 161.4                        | 100.8      |
|                   | 170.0                         | 169.1                        | 99.4       |
|                   | 180.0                         | 181.6                        | 100.8      |

### 3.6.10. Conclusion

Electrochemical low-level determination of TCS was conducted using CHMTS/GCE. Under CV study for electrooxidation of TCS was irreversible and electrochemical behaviour of TCS toward bare GCE, CH/GCE and CHMTS/GCE show that CHMTS/GCE show enhanced oxidative peak current as it has siloxane and hydrophobic character of CHMTS material. Optimisation experiments show that pH 8.0, deposition potential 0.2 V and deposition time 180.0 sec. was the suited parameter for efficient determination of analyte. Concentration study from 140.0  $\mu\text{g/L}$  to 200.0  $\mu\text{g/L}$  of TCS show increase in peak current with increase in concentration and obtain a good linearity of  $y (\mu\text{A}) = 0.0016 x (\mu\text{g/L}) + 1.6724 (\mu\text{A})$ , and the LOD of 9.49  $\mu\text{g/L}$ . In presence of high concentration of interfering ions such as  $\text{Cl}^-$ ,  $\text{NO}_3^-$ ,  $\text{Na}^+$ ,  $\text{Mg}^{2+}$ , EDTA, GLY, OA, HQ and PH, CHMTS/GCE show sensitivity and selectivity toward TCS. Reproducibility and stability study show CHMTS/GCE long term stability and repeatability till 48 hrs. The fabricated GCE with CHMTS showed practical implacability in the real water samples (groundwater and Chite river water samples) TCS analysis. Therefore, CHMTS fabricated GCE shows potential and promising electrodes in the trace and efficient detection of TCS in aqueous media and possibly a more extensive application in miniature device development.

## **CHAPTER 4**

### **CONCLUSIONS**

#### 4. CONCLUSION

The novel nanocomposite materials were synthesized and introduced in fabricating the glassy carbon electrode (GCE) for development of electrochemical sensor in the detection of Pb (II) and micropollutants *viz.*, bisphenol A (BPA) and triclosan (TCS). A facile and robust synthetic route was adopted synthesising the materials precursor to the chitosan and different silanes. Moreover, the silver nanoparticles were obtained using the natural phytochemicals and *in situ* decorated with the composite materials.

The chitosan (Degree of deacetylation  $\geq 75\%$ ) chitosan (CH) was grafted with trimethoxyoctylsilane (TMS) and 3-mercaptopropyl trimethoxysilane (MTS) in simple one step facile process to obtain the CHTMS and CHMTS composite materials. The composite materials (CHTMS and CHMTS) were used in fabricating the GCEs and employed in the detection of Pb (II), BPA and TCS. Moreover, the CHTMS was decorated with silver nanoparticles (Ag(NPs)) to obtain the nanostructured material *viz.*, CHTMS+Ag(NPs). The silver nanoparticles (Ag<sup>0</sup>) were obtained *in situ* using the *Psidium guajava* leaf extract which act as reducing agent and stabilizing the nanoparticles as capping agent as well. The synthesized composite and nanocomposite materials were characterised by several analytical tools *viz.*, BET, FT-IR, UV- visible, SEM-EDX, TEM and XRD. The N<sub>2</sub> adsorption/desorption isotherms indicated that all the materials follow type IV isotherm with an H3-type loop, which consists of mesopores with slit-shaped pores. Further, the BET specific surface area of composite materials was increased significantly compared to the bare chitosan. On the other hand, the pore size and pore volume was 35.12 nm and 0.0057 cm<sup>3</sup>/g (for CHTMS), 35.21 nm and 0.0097 cm<sup>3</sup>/g (for CHMTS). The FT-IR analysis of CH, CHMTS, CHTMS and CHTMS+Ag(NPs) shows that stretching vibrations of alkyl appeared around the wavenumbers of 2870 cm<sup>-1</sup> and 2924 cm<sup>-1</sup>. Similarly, the amide bond vibrational peaks occurred at 1651 cm<sup>-1</sup> and 1566/1558 cm<sup>-1</sup>. Moreover, the -C-O-C- glycosidic linkage was obtained around the wavenumbers of 1100 cm<sup>-1</sup> to 1000 cm<sup>-1</sup>. It is further observed that the FT-IR peaks were slightly shifted with composite and nanocomposite materials i.e., the amide peak was shifted from 1558 cm<sup>-1</sup> to 1544 cm<sup>-1</sup> in CHMTS, 1558 cm<sup>-1</sup> to 1543 cm<sup>-1</sup> for CHTMS and 1543 cm<sup>-1</sup> to 1566 cm<sup>-1</sup> in CHTMS+Ag(NPs).

The stretching vibration of N-H and O-H was observed around  $3000\text{ cm}^{-1}$  to  $3500\text{ cm}^{-1}$  for chitosan (CH). However, the peaks were almost diminished with composite and nanocomposite materials, which was due to grafting of silane with chitosan matrix. Furthermore, the additional FT-IR bands were observed in composite and nanocomposite materials around  $1000\text{--}1100\text{ cm}^{-1}$ ,  $900\text{--}950\text{ cm}^{-1}$  and  $700\text{--}800\text{ cm}^{-1}$ , which were ascribed to the Si-O-Si, Si-OH and Si-O-Si stretching vibrations. The UV-visible spectrum of nanocomposite material (CHTMS+Ag(NPs)) shows a surface plasmon resonance (SPR) peak at  $440\text{ nm}$ , which infers the formation of Ag(NPs) within the composite material (CHTMS). The SPR peak appears due to formation of  $\text{Ag}^0$  by the phytochemicals. The SEM micrograph of CH shows a heterogeneous surface contained with randomly distributed pores on the surface. The surface of CHTMS is relatively compact and dense and silane is visible on the surface. The pores are occupied with the grafted silanes. Similarly, the CHMTS solid shows heterogeneous and dense surface morphology. On the other hand, the nanocomposite material (CHTMS+Ag(NPs)) shows heterogeneous surface morphology and the Ag(NPs) are randomly distributed on the surface of solid. The EDX spectra show that prominent peaks of C, N, O, S elements appeared in all these materials. Whereas, an additional Si peak appeared with the CHTMS, CHMTS and CHTMS+Ag(NPs) solids, which confirmed the grafting of silanes with the chitosan in these materials. Further, the CHTMS+Ag(NPs) solid shows EDX peak of silver indicating the presence of silver in the solid. The formation of Ag(NPs) in the silane grafted chitosan matrix was supported by the TEM images, and the Ag(NPs) are dispersed on the substrate surface with slight variation in nanoparticle sizes. Moreover, the nanoparticles were not agglomerated on the surface. The calculated mean diameter of Ag(NP) was found to be  $22.32\text{ nm}$  and the d-spacing was  $0.37\text{ nm}$ . The X-ray diffraction pattern of CHTMS and CHTMS+Ag(NPs) were obtained and the CHTMS+Ag(NPs) material showed additional diffraction peaks at  $2\theta$  values of  $38.38$ ,  $46.59$ ,  $64.79$  and  $77.43$  around, which corresponds to the diffraction planes of (111), (200), (220) and (311), respectively of Ag(NPs) (JCPDS card no. 04-0783). Further, the crystallite size was found to be  $28.17\text{ nm}$ .

The working electrodes were fabricated using the composite or nanocomposite materials. The electrochemical characterisation of the fabricated electrodes was

conducted by the cyclic voltammetry and electro impedance spectroscopy employing the standard  $[\text{Fe}(\text{CN})_6]^{3-/4-}$  (0.002 M; prepared in 0.1 M acetate buffer) redox couple. The fabricated GCEs showed characteristic redox peaks of  $[\text{Fe}(\text{CN})_6]^{3-/4-}$ . Moreover, increase in scan rate caused an increase in redox peak currents and the redox process was diffusion controlled. The electroactive surface area obtained using the Randles-Sevcik equation was found to be 0.000895 mm<sup>2</sup>, 0.00237 mm<sup>2</sup>, 0.003899 mm<sup>2</sup>, 0.00493 mm<sup>2</sup> and 0.005827 mm<sup>2</sup> for the bare GCE, CH/GCE, CHTMS/GCE, CHMTS/GCE and CHTMS+Ag(NPs)/GCE. Furthermore, the  $\Delta E$  value was lowered for composite and nanocomposite materials compared to the bare GCE or CH/GCE. On the other hand, the EIS data is fitted well to the Nyquist plots. In Nyquist plots the estimated  $R_{ct}$  (Charge transfer resistance) value was decreased significantly using the composite or nanocomposite materials i.e., 6.46  $\Omega$ , 633.7  $\Omega$  and 431.6  $\Omega$  for CHTMS, CHMTS and CHTMS+Ag(NPs).

Electrochemical behaviour of Pb (II) was studied using bare GCE and CHTMS/GCE under the DPASV technique. The oxidation peak current was significantly increased using the CHTMS/GCE compared to the bare GCE. The detection of Pb (II) was optimized for several parameters under the DPASV measurements. The pH 4.5, deposition potential: -0.9 V, deposition time: 180.0 sec was optimized for the efficient detection of Pb (II). The CHTMS/GCE enabled to obtain a low detection limit (2.83  $\mu\text{g/L}$ ) studied for a concentration range from 5.0  $\mu\text{g/L}$  to 80.0  $\mu\text{g/L}$ . A good linear calibration line was obtained as  $y$  ( $\mu\text{A}$ ) = 0.0049  $x$  ( $\mu\text{g/L}$ ) + 1.7964 ( $\mu\text{A}$ ) ( $R^2 = 0.992$ ). Interfering ion study shows that the EDTA slightly interfere in the detection of Pb (II), which is due to complex formation with Pb (II) and feeble attraction of the complexed species toward the electrode surface resulting in reducing the oxidative peak current of Pb (II). However, the other ions (viz., Cd (II), Cr (III), Cu (II), Ni (II), Zn (II), GLY and OA) do not interfere with the determination of Pb (II). Reproducibility and stability studies show that the fabricated electrode shows repeatability of results with reasonably low %RSD value (0.18%). The long term stability i.e., till 48 hours of use shows that the electrode is quite stable with 0.18% of %RSD value. Additionally, the fabricated electrode is seemingly employed in the real matrix detection of Pb (II). The spring water and ground water samples were



spiked with the Pb (II) and the recovery percentage ranged from 96.63 to 102.99 % in spring water, and it ranged from 96.98 to 104.6% for ground water samples.

Similarly under optimised experimental conditions CHTMS+Ag(NPs) was employed in Pb (II) detection. The DPASV study shows that electro oxidation occurs faster in CHTMS+Ag(NPs) compared to CHTMS composite material with 3 fold increase in oxidative peak current. A linear increase in oxidative peak current is obtained by increasing the concentration of Pb (II) from 5.0 µg/L to 80.0 µg/L under the DPASV measurement. The straight line equation is obtained as:  $y (\mu A) = 0.0368 x (\mu g/L) + 3.5742 (\mu A)$  with a correlation coefficient ( $R^2$ ) of 0.9811 and the calculated LOD was 1.97 µg/L. Interfering study shows that glycine and oxalic acid interferes the detection of Pb (II) whereas the presence of other such as Cr (III), Cu (II), Ni(II), Zn (II) and EDTA are not affecting the Pb (II) detection. The detection of Pb (II) in spiked real waters showed a high percentage recovery with a value of 95.52-96.06 % for spring water and 92.95-102.57 % for ground water. Similarly, the fabricated electrodes are reasonably stable in repeated and prolonged operations at least in the efficient detection of Pb (II).

The novel fabricated electrodes were also employed in the detection of some of the emerging micropollutants viz., bisphenol A triclosan. An irreversible electrooxidation of BPA was obtained at the CHMTS/GCE under the cyclic voltammetric studies. Moreover, the different modified GCEs were employed viz., bare GCE, CH/GCE and CHMTS/GCE to analyse their electrochemical performance towards the BPA and around an applied potential of 0.42 V a characteristic oxidative peak current of BPA was observed. The oxidative peak current follows the order: CHMTS/GCE>CH/GCE>GCE. The DPASV study is optimized for the efficient detection of BPA (200 µg/L), and the optimised conditions are as: pH 10.0, deposition potential 0.2 V, deposition time 180.0 sec. Furthermore, the CHMTS/GCE was employed in the determination of BPA at a wide concentration range of 140.0 µg/L to 200.0 µg/L. A good linear equation of oxidative peak current as a function of BPA concentration is obtained with linear equation:  $y (\mu A) = 0.0007 x (\mu g/L) + 1.1673 (\mu A)$  ( $R^2=0.9947$ ) with LOD of 5.61 µg/L. The presence of several co-existing ions viz., PH, HQ, Cl<sup>-</sup>, NO<sub>3</sub><sup>-</sup>, Na<sup>+</sup>, Mg<sup>+2</sup>, OA, EDTA, GLY could not influence the detection of BPA using the fabricated thin film electrode. Real water analysis show that spiked and found

concentration is almost close to each other with the recovery percentage in spring water is ranged from 99.7-102.7% and for Chite river water is from 102.4 to 102.7%. Similarly, the TCS determination was carried out using the CHMTS/GCE at pH 8.0 using the phosphate buffer (0.1 M). A good linear relationship of TCS concentration and oxidative peak current is obtained with the straight line equation:  $y (\mu\text{A}) = 0.0017 x (\mu\text{g/L}) + 1.648 (\mu\text{A})$ , with the correlation coefficient  $R^2=0.9968$ . The calculated LOD was found to be 9.49  $\mu\text{g/L}$ . No apparent inference was observed in presence of several cations and anions in the detection of TCS using the fabricated micro-electrode. The real water sample analysis using TCS spiked Chite river water and ground water show high recovery of TCS. The stability of fabricated electrode for repeated and prolonged operations ascertain the practical applicability of electrodes in real implications.

Overall the limit of detection (LOD) for Pb (II), BPA and TCS using the composite (CHTMS, CHMTS) and nanocomposite (CHTMS+Ag(NPs)) materials modified glassy carbon electrode are compiled and returned in Table 4.1 The LOD values are compared to the permissible maximum contamination level (MCL) put down by the World Health Organisation or United States Environmental Protection Agency (US EPA) in drinking water (Cf Table 4.1). Table 4.1 clearly inferred that the obtained LOD values are significantly lower than the standard values which further indicated the potential of these electrodes in the device development. The laboratory findings are useful input data for the development of miniaturized devices to efficiently detect these potential water contaminants.

**Table 4.1:** LOD values of several contaminants obtained with modified electrodes compared to MCL levels established by WHO and the US-EPA.

| Sl. No. | Working Electrode | Pollutant | LOD (µg/L) | MCL (µg/L)             |
|---------|-------------------|-----------|------------|------------------------|
| 1       | CHTMS/GCE         | Pb (II)   | 2.83       | 10 (WHO)<br>15 (USEPA) |
| 2       | CHTMS+Ag(NPs)/GCE | Pb (II)   | 1.97       | 10 (WHO)<br>15 (USEPA) |
| 3       | CHMTS/GCE         | BPA       | 5.61       | No fixed<br>MCL        |
| 4       | CHMTS/GCE         | TCS       | 9.49       | No fixed<br>MCL        |

## **REFERENCES**

## References

- Abdel Moneim, A. E., Dkhil, M. A., Al-Quraishy, S., (2011). The protective effect of flaxseed oil on lead acetate-induced renal toxicity in rats. *J. Hazard. Mater.*, **194**: 250–255.
- Adeyemi, Stephen, O., Akanji, A. M., Oguntoye, A. S., (2009). Ethanolic leaf extract of *Psidium guajava*: Phyto-chemical and trypanocidal activity in rats infected with *Trypanosoma brucei brucei*. *J. Med. Plants Res.*, **3(5)**: 420–423.
- Agrawal, P., Strijkers, G. J., Nicolay, K., (2010). Chitosan-based systems for molecular imaging. *Adv. Drug Deliv. Rev.*, **62(1)**, 42–58.
- Akilarasan, M., Kogularasu, S., Chen, S.-M., Chen, T.-W., Lou, B.-S., (2018). A novel approach to iron oxide separation from e-waste and bisphenol A detection in thermal paper receipts using recovered nanocomposites. *RSC Adv.*, **8(70)**: 39870–39878.
- Alcaraz-Contreras, Y., Garza-Ocañas, L., Carcaño-Díaz, K., Ramírez-Gómez, X. S., (2011). Effect of Glycine on Lead Mobilization, Lead-Induced Oxidative Stress, and Hepatic Toxicity in Rats. *J. Toxicol.*, **2011**: 430539.
- Allmyr, M., Harden, F., Toms, L.-M. L., Mueller, J. F., McLachlan, M. S., Adolfsson-Erici, M., Sandborgh-Englund, G., (2008). The influence of age and gender on triclosan concentrations in Australian human blood serum. *Sci. Total Environ.t*, **393(1)**: 162–167.
- An, H., Park, B., Kim, D., (2001). Crab Shell for the Removal of Heavy Metals from Aqueous Solution. *Water Res.*, **35**: 3551–3556.
- Anderson, S. E., Meade, B. J., Long, C. M., Lukomska, E., Marshall, N. B., (2016). Investigations of immunotoxicity and allergic potential induced by topical application of triclosan in mice. *J. Immunotoxicol.*, **13(2)**: 165–172.
- Awual, Md. R., (2016). Assessing of lead(III) capturing from contaminated wastewater using ligand doped conjugate adsorbent. *Chem. Eng. J.*, **289**: 65–73.
- Bansod, B., Kumar, T., Thakur, R., Rana, S., Singh, I., (2017). A review on various electrochemical techniques for heavy metal ions detection with different sensing platforms. *Biosens. Bioelectron.*, **94**: 443–455.

- Batra, B., Pundir, C. S., (2013). An amperometric glutamate biosensor based on immobilization of glutamate oxidase onto carboxylated multiwalled carbon nanotubes/gold nanoparticles/chitosan composite film modified Au electrode. *Biosens. Bioelectron.*, **47**: 496–501.
- Berhane, T. M., Levy, J., Krekeler, M. P. S., Danielson, N. D., (2016). Adsorption of bisphenol A and ciprofloxacin by palygorskite-montmorillonite: Effect of granule size, solution chemistry and temperature. *Appl. Clay Sci.*, **C(132–133)**: 518–527.
- Bhargava, H. N., & Leonard, P. A., (1996). Triclosan: Applications and safety. *Am. J. Infect. Control*, **24(3)**: 209–218.
- Bindler, R., (2011). Contaminated lead environments of man: Reviewing the lead isotopic evidence in sediments, peat, and soils for the temporal and spatial patterns of atmospheric lead pollution in Sweden. *Environ. Geochem. Hlth.*, **33(4)**: 311–329.
- Biswas, B., Rogers, K., McLaughlin, F., Daniels, D., Yadav, A., (2013). Antimicrobial Activities of Leaf Extracts of Guava (*Psidium guajava* L.) on Two Gram-Negative and Gram-Positive Bacteria. *Int. J. Microbiol.*, **2013**: 746165.
- Bolong, N., Ismail, A. F., Salim, M. R., Matsuura, T., (2009). A review of the effects of emerging contaminants in wastewater and options for their removal. *Desalination*, **239(1)**: 229–246.
- Calafat, A. M., Ye, X., Wong, L.-Y., Reidy, J. A., Needham, L. L., (2008). Urinary Concentrations of Triclosan in the U.S. Population: 2003–2004. *Environ. Health Perspect.*, **116(3)**: 303–307.
- Campanale, C., Massarelli, C., Losacco, D., Bisaccia, D., Triozzi, M., Uricchio, V. F., (2021). The monitoring of pesticides in water matrices and the analytical criticalities: A review. *TrAC Trends Analyt. Chem.*, **144**: 116423.
- Cao, C., Xiao, L., Chen, C., Cao, Q., (2015). Magnetically separable Cu<sub>2</sub>O/chitosan–Fe<sub>3</sub>O<sub>4</sub> nanocomposites: Preparation, characterization and visible-light photocatalytic performance. *Appl. Surf. Sci.*, **333**: 110–118.
- Casadidio, C., Peregrina, D. V., Gigliobianco, M. R., Deng, S., Censi, R., Di Martino, P., (2019). Chitin and Chitosans: Characteristics, Eco-Friendly Processes, and Applications in Cosmetic Science. *Mar. Drugs*, **17(6)**: 369.

- Chai, W., Handa, Y., Suzuki, M., Saito, M., Kato, N., Horiuchi, C., (2005). Biodegradation of Bisphenol A by Fungi. *Appl. Biochem. Biotechnol.*, **120**: 175–182.
- Chandraker, S. K., Lal, M., Ghosh, M. K., Tiwari, V., Ghorai, T. K., Shukla, R., (2020). Green synthesis of copper nanoparticles using leaf extract of *Ageratum houstonianum* Mill. And study of their photocatalytic and antibacterial activities. *Nano Express*, **1**(1): 010033.
- Chen, Q., Jiang, H., Ye, H., Li, J., Huang, J., (2014). Preparation, Antibacterial, and Antioxidant Activities of Silver/Chitosan Composites. *J. Carbohydr. Chem.*, **33**(6): 298–312.
- Chen, Z., Tang, C., Zeng, Y., Liu, H., Yin, Z., Li, L., (2014). Determination of Bisphenol A Using an Electrochemical Sensor Based on a Molecularly Imprinted Polymer-Modified Multiwalled Carbon Nanotube Paste Electrode. *Anal. Lett.*, **47**(6): 996–1014.
- Ciftçi, H., Tamer, U., Metin, A., Alver, E., Kizir, N., (2014). Electrochemical copper (II) sensor based on chitosan covered gold nanoparticles. *J. Appl. Electrochem.*, **44**
- Cladière, M., Gasperi, J., Lorgeoux, C., Bonhomme, C., Rocher, V., Tassin, B., (2013). Alkylphenolic compounds and bisphenol A contamination within a heavily urbanized area: Case study of Paris. *Environ. Sci. Pollu. Res. Int.*, **20**(5): 2973–2983.
- Colin, A., Bach, C., Rosin, C., Munoz, J.-F., Dauchy, X., (2014). Is drinking water a major route of human exposure to alkylphenol and bisphenol contaminants in France? *Arch. Environ. Contam. Toxicol.*, **66**(1): 86–99.
- Crini, G., Badot, P.-M., (2008). Application of chitosan, a natural aminopolysaccharide, for dye removal from aqueous solutions by adsorption processes using batch studies: A review of recent literature. *Prog. Polym Sci.*, **33**(4): 399–447.
- Cullinan, M. P., Palmer, J. E., Carle, A. D., West, M. J., Seymour, G. J., (2012). Long term use of triclosan toothpaste and thyroid function. *Sci. Total Environ.*, **416**: 75–79.

- Dai, H., Xu, G., Gong, L., Yang, C., Lin, Y., Tong, Y., Chen, J., Chen, G., (2012a). Electrochemical detection of triclosan at a glassy carbon electrode modifies with carbon nanodots and chitosan. *Electrochim. Acta*, **80**: 362–367.
- Dai, H., Xu, G., Gong, L., Yang, C., Lin, Y., Tong, Y., Chen, J., Chen, G., (2012b). Electrochemical detection of triclosan at a glassy carbon electrode modifies with carbon nanodots and chitosan. *Electrochim. Acta*, **80**: 362–367.
- Daughton, C. G., Ruhoy, I. S., (2009). Environmental footprint of pharmaceuticals: The significance of factors beyond direct excretion to sewers. *Environ. Toxicol. Chem.*, **28(12)**: 2495–2521.
- Deng, J., Peng, Y., He, C., Long, X., Li, P., Chan, A. S. C., (2003). Magnetic and conducting Fe<sub>3</sub>O<sub>4</sub>–polypyrrole nanoparticles with core-shell structure. *Polym. Int.*, **52(7)**: 1182–1187.
- Duruibe, J., C, O., Ekwurugwu, J., (2007). Heavy Metal Pollution and Human Biotoxic Effects. *Int. J. Phys. Sci.*, **2**: 112–118.
- Eshlaghi, M. A., Kowsari, E., Ehsani, A., Akbari-Adergani, B., Hekmati, M., (2020). Functionalized graphene oxide GO-[imi-(CH<sub>2</sub>)<sub>2</sub>-NH<sub>2</sub>] as a high efficient material for electrochemical sensing of lead: Synthesis surface and electrochemical characterization. *J. Electroanal. Chem.*, **858**: 113784.
- Ettinger, A. S., Leonard, M. L., Mason, J., (2019). CDC’s Lead Poisoning Prevention Program: A Long-standing Responsibility and Commitment to Protect Children From Lead Exposure. *J. Public Health Manag. Prac.*, **25**(Suppl 1 LEAD POISONING PREVENTION): S5–S12.
- Fan, H., Li, Y., Wu, D., Ma, H., Mao, K., Fan, D., Du, B., Li, H., Wei, Q., (2012). Electrochemical bisphenol A sensor based on N-doped graphene sheets. *Anal. Chimica Acta*, **711**: 24–28.
- Fan, H.-L., Zhou, S.-F., Gao, J., Liu, Y.-Z., (2016). Continuous preparation of Fe<sub>3</sub>O<sub>4</sub> nanoparticles through Impinging Stream-Rotating Packed Bed reactor and their electrochemistry detection toward heavy metal ions. *J. Alloys Compd.*, **671**: 354–359.
- Fent, K., Weston, A. A., Caminada, D. (2006). Ecotoxicology of human pharmaceuticals. *Aquat. Toxicol. (Amsterdam, Netherlands)*, **76(2)**: 122–159.



- Fida, H., Zhang, G., Guo, S., Naeem, A., (2017). Heterogeneous Fenton degradation of organic dyes in batch and fixed bed using La-Fe montmorillonite as catalyst. *J. Colloid Interface Sci.*, **490**: 859–868.
- Flint, S., Markle, T., Thompson, S., & Wallace, E., (2012). Bisphenol A exposure, effects, and policy: A wildlife perspective. *J. Environ. Manag.*, **104**: 19–34.
- Flora, G., Gupta, D., Tiwari, A., (2012). Toxicity of lead: A review with recent updates. *Interdiscip. Toxicol.*, **5(2)**: 47–58.
- Fort, C. I., Cotet, L. C., Vulpoi, A., Turdean, G. L., Danciu, V., Baia, L., Popescu, I. C., (2015). Bismuth doped carbon xerogel nanocomposite incorporated in chitosan matrix for ultrasensitive voltammetric detection of Pb(II) and Cd(II). *Sens. Actuators B Chem.*, **220**: 712–719.
- Gao, Y., Ierapetritou, M. G., Muzzio, F. J., (2013). Determination of the Confidence Interval of the Relative Standard Deviation Using Convolution. *J. Pharm. Innov.*, **8(2)**: 72–82.
- Gidlow, D. A., (2004). Lead toxicity. *Occup. Med.*, **54(2)**: 76–81.
- Gilbert, S. G., Weiss, B., (2006). A rationale for lowering the blood lead action level from 10 to 2 microg/dL. *Neurotoxicol.*, **27(5)**: 693–701.
- Gleick, P., (2002). The New Economy of Water: The Risks and Benefits of Globalization and Privatization of Fresh Water. *Pacific Institute*. 654 13<sup>th</sup> Street, Preservation Park Oakland, California 94612.
- Gong, T., Liu, J., Liu, X., Liu, J., Xiang, J., Wu, Y., (2016). A sensitive and selective sensing platform based on CdTe QDs in the presence of l-cysteine for detection of silver, mercury and copper ions in water and various drinks. *Food Chem.*, **213**: 306–312.
- Government of Canada, E. C. C. C., (2010, January 27). *ARCHIVED - Environment and Climate Change Canada—Screening Assessment for The Challenge for Phenol, 4,4' -(1-methylethylidene)bis- (Bisphenol A)—CAS No. 80-05-7*.
- Govindan, S., Nivethaa, E. A. K., Saravanan, R., Narayanan, V., Stephen, A. (2012). Synthesis and characterization of chitosan–silver nanocomposite. *Appl. Nanosci.*, **2(3)**: 299–303.

- Greenlee, L. F., Lawler, D. F., Freeman, B. D., Marrot, B., Moulin, P., (2009). Reverse osmosis desalination: Water sources, technology, and today's challenges. *Water Res.*, **43**(9): 2317–2348.
- Gugoasa, L. A. D., (2019). Review—Electrochemical Sensors for Determination of the Endocrine Disruptor, Bisphenol A. *J. Electrochem. Soc.*, **167**(3): 037506.
- Gumpu, M. B., Sethuraman, S., Krishnan, U. M., Rayappan, J. B. B., (2015). A review on detection of heavy metal ions in water – An electrochemical approach. *Sens. Actuators B Chem.*, 213: 515–533.
- Guo, Z., Li, D., Luo, X.-K., Li, Y.-H., Zhao, Q.-N., Li, M.-M., Zhao, Y.-T., Sun, T.-S., Ma, C., (2017). Simultaneous determination of trace Cd(II), Pb(II) and Cu(II) by differential pulse anodic stripping voltammetry using a reduced graphene oxide-chitosan/poly-l-lysine nanocomposite modified glassy carbon electrode. *J. Colloid Interface Sci.*, **490**: 11–22.
- Gupta, V. K., Rastogi, A., (2008). Biosorption of lead from aqueous solutions by green algae *Spirogyra* species: Kinetics and equilibrium studies. *J. Hazard. Mater.*, **152**(1): 407–414.
- Hassan, Z. K., Elobeid, M. A., Virk, P., Omer, S. A., ElAmin, M., Daghestani, M. H., AlOlayan, E. M., (2012). Bisphenol A induces hepatotoxicity through oxidative stress in rat model. *Oxid. Med. Cell. Longev.*, **2012**: 194829.
- Hernberg, S., (2000). Lead poisoning in a historical perspective. *Am. J. Industrial Med.*, **38**(3): 244–254.
- Hossain, M., (2015). WATER: THE MOST PRECIOUS RESOURCE OF OUR LIFE. *Glob. J. Adv. Res.*, **2**: 1436–1445.
- Hu, C., Wu, K., Dai, X., Hu, S., (2003). Simultaneous determination of lead(II) and cadmium(II) at a diacetyldioxime modified carbon paste electrode by differential pulse stripping voltammetry. *Talanta*, **60**(1): 17–24.
- Huang, J., Zhang, X., Liu, S., Lin, Q., He, X., Xing, X., Lian, W. (2011). Electrochemical sensor for bisphenol A detection based on molecularly imprinted polymers and gold nanoparticles. *J. Appl. Electrochem.*, **41**(11): 1323.
- Huang, K.-J., Liu, Y.-J., Liu, Y.-M., Wang, L.-L., (2014). Molybdenum disulfide nanoflower-chitosan-Au nanoparticles composites based electrochemical

- sensing platform for bisphenol A determination. *J. Hazard. Mater.*, **276**: 207–215.
- Huff, J., Lunn, R. M., Waalkes, M. P., Tomatis, L., & Infante, P. F., (2007). Cadmium-induced Cancers in Animals and in Humans. *Int. J. Occup. Environ. Hlth.*, **13**(2): 202–212.
- Hwang, G. H., Han, W. K., Park, J. S., Kang, S. G. (2008). Determination of trace metals by anodic stripping voltammetry using a bismuth-modified carbon nanotube electrode. *Talanta*, **76**(2): 301–308.
- Indian standards referred in government regulations—Bureau of Indian Standards.* (n.d.). Retrieved 29 July 2022.
- Ishibashi, H., Matsumura, N., Hirano, M., Matsuoka, M., Shiratsuchi, H., Ishibashi, Y., Takao, Y., Arizono, K., (2004). Effects of triclosan on the early life stages and reproduction of medaka *Oryzias latipes* and induction of hepatic vitellogenin. *Aquat. Toxicol.*, **67**(2): 167–179.
- Iso, T., Watanabe, T., Iwamoto, T., Shimamoto, A., Furuichi, Y., (2006). DNA damage caused by bisphenol A and estradiol through estrogenic activity. *Biol. Pharm. Bull.*, **29**(2): 206–210.
- Jackson, E. N., Rowland-Faux, L., James, M. O., Wood, C. E., (2018). Administration of low dose triclosan to pregnant ewes results in placental uptake and reduced estradiol sulfotransferase activity in fetal liver and placenta. *Toxicol. Lett.*, **294**: 116–121.
- Jebril, S., Cubillana-Aguilera, L., Palacios-Santander, J. M., Dridi, C., (2021). A novel electrochemical sensor modified with green gold sononanoparticles and carbon black nanocomposite for bisphenol A detection. *Mater. Sci. Eng. B.*, **264**: 114951.
- Jiménez-Gómez, C. P., Cecilia, J. A., (2020). Chitosan: A Natural Biopolymer with a Wide and Varied Range of Applications. *Molecules*, **25**(17)
- Jung, E.-M., An, B.-S., Choi, K.-C., Jeung, E.-B., (2012). Potential estrogenic activity of triclosan in the uterus of immature rats and rat pituitary GH3 cells. *Toxicol. Lett.*, **208**(2): 142–148.

- Kalainila, P., Subha, V., Ravindran, R. S. E., Renganathan, S., (2014). Effect of Green Synthesized Silver Nanoparticles Incorporated with Gelatin for Sustained Drug Release. *Int. J. Chem. Tech. Res.*, **6(10)**: 974-4290.
- Kalaivani, R., Maruthupandy, M., Muneeswaran, T., Hameedha Beevi, A., Anand, M., Ramakritinan, C. M., Kumaraguru, A. K., (2018). Synthesis of chitosan mediated silver nanoparticles (Ag NPs) for potential antimicrobial applications. *Front. Lab. Med.*, **2(1)**: 30–35.
- Kim, H. S., Kim, Y. J., Seo, Y. R., (2015). An Overview of Carcinogenic Heavy Metal: Molecular Toxicity Mechanism and Prevention. *Journal of Cancer Prevention*, **20(4)**: 232–240.
- Kim, M.-K., Zoh, K.-D., (2016). Occurrence and removals of micropollutants in water environment. *Environ. Eng. Res.*, **21(4)**: 319–332.
- Krishna, A. K., Govil, P. K., (2004). Heavy metal contamination of soil around Pali Industrial Area, Rajasthan, India. *Environ. Geo.*, **47(1)**: 38–44.
- Kucka, M., Pogrmic-Majkic, K., Fa, S., Stojilkovic, S. S., Kovacevic, R., (2012). Atrazine acts as an endocrine disrupter by inhibiting cAMP-specific phosphodiesterase-4. *Toxicol. Appl. Pharmacol.*, **265(1)**: 19–26.
- Kuramitz, H., Nakata, Y., Kawasaki, M., Tanaka, S., (2001). Electrochemical oxidation of bisphenol A. Application to the removal of bisphenol A using a carbon fiber electrode. *Chemosphere*, **45(1)**: 37–43.
- Lalchhingpuii, Tiwari, D., Lalhmunsiam, Lee, S. M., (2017). Chitosan templated synthesis of mesoporous silica and its application in the treatment of aqueous solutions contaminated with cadmium(II) and lead(II). *Chem. Eng. J.*, **328**: 434–444.
- Lalhmunsiam, Lalchhingpuii, Nautiyal, B. P., Tiwari, D., Choi, S. I., Kong, S.-H., Lee, S.-M., (2016). Silane grafted chitosan for the efficient remediation of aquatic environment contaminated with arsenic(V). *J. Colloid Interface Sci.*, **467**, 203–212.
- Lalhmunsiam, Lee, S.-M., Lalchhingpuii, Tiwari, D., (2016). Functionalized hybrid material precursor to chitosan in the efficient remediation of aqueous solutions contaminated with As(V). *J. Environ. Chem. Eng.*, **4(2)**: 1537–1544.

- Lalmalsawmi, J., Tiwari, D., (2021). Facile Synthesized Novel Nanocomposites Modified Electrodes in the Trace Detection of Sulfamethoxazole. *J. Electrochem. Soc.*, **168**(12): 126504.
- Lalmalsawmi, J., Tiwari, D., Lee, S.-M., Kim, D.-J., Kim, H., (2022). Efficient electrochemical sensor for trace detection of sulfamethazine in spring water: Use of novel nanocomposite material coated with Ag or Au nanoparticles. *Microchem. J.*, 179: 107520.
- Lalmalsawmi, J., Zirliannigura, Z., Tiwari, D., Lee, S.-M., (2020). Low cost, highly sensitive and selective electrochemical detection of arsenic (III) using silane grafted based nanocomposite. *Environ. Eng. Res.*, **25**(4): 579–587.
- Landry, K. A., Boyer, T. H., (2013). Diclofenac removal in urine using strong-base anion exchange polymer resins. *Water Res.*, **47**(17): 6432–6444.
- Lankester, J., Patel, C., Cullen, M. R., Ley, C., Parsonnet, J., (2013). Urinary Triclosan is Associated with Elevated Body Mass Index in NHANES. *PLOS ONE*, **8**(11): 80057.
- Lee, C.-C., Jiang, L.-Y., Kuo, Y.-L., Hsieh, C.-Y., Chen, C. S., Tien, C.-J., (2013). The potential role of water quality parameters on occurrence of nonylphenol and bisphenol A and identification of their discharge sources in the river ecosystems. *Chemosphere*, **91**(7): 904–911.
- Lee, S. M., Lalchhingpuii, Lalmunsiamia, Tiwari, D., (2016). Synthesis of functionalized biomaterials and its application in the efficient remediation of aquatic environment contaminated with Cr(VI). *Chem. Eng. J.*, **296**: 35–44.
- Ley, C., Pischel, L., Parsonnet, J., (2017). Triclosan and triclocarban exposure and thyroid function during pregnancy – a randomized intervention. *Reprod. Toxicol. (Elmsford, N.Y.)*, **74**: 143–149.
- Li, B., Qiu, Z., Wan, Q., Liu, Y., Yang, N., (2014).  $\beta$ -cyclodextrin functionalized graphene nano platelets for electrochemical determination of triclosan. *Phys. Status Solidi (a)*, **211**(12): 2773–2777.
- Li, G., Zu, L., Wong, P.-K., Hui, X., Lu, Y., Xiong, J., An, T., (2012). Biodegradation and detoxification of bisphenol A with one newly-isolated strain *Bacillus* sp. GZB: Kinetics, mechanism and estrogenic transition. *Bioresour. Technol.*, **114**: 224–230.

- Li, J., Zhang, J., Wei, H., Wang, E., (2009). Combining chemical reduction with an electrochemical technique for the simultaneous detection of Cr(VI), Pb(II) and Cd(II). *Analyst*, **134**(2): 273–277.
- Li, Y., Wang, H., Yan, B., Zhang, H., (2017). An electrochemical sensor for the determination of bisphenol A using glassy carbon electrode modified with reduced graphene oxide-silver/poly-l-lysine nanocomposites. *J. Electroanal. Chem.*, **805**: 39–46.
- Libansky, M., Zima, J., Barek, J., Dejmekova, H., (2014). Construction of an Electrochemical Cell System Based on Carbon Composite Film Electrodes and its Application for Voltammetric Determination of Triclosan. *Electroanalysis*, **26**(9): 1920–1927.
- Lin, J.-L., Lin-Tan, D.-T., Hsu, K.-H., Yu, C.-C., (2003). Environmental lead exposure and progression of chronic renal diseases in patients without diabetes. *N. Engl. J. Med.*, **348**(4): 277–286.
- Lin, K. Y., Chu, W., (2011). Simulation and quantification of the natural decay of a typical endocrine disrupting chemical Atrazine in an aquatic system. *J. Hazard. Mater.*, **192**(3): 1260–1266.
- Ling, S., Yuan, R., Chai, Y., Zhang, T., (2009). Study on immunosensor based on gold nanoparticles/chitosan and MnO<sub>2</sub> nanoparticles composite membrane/Prussian blue modified gold electrode. *Bioproc. Biosyst. Eng.*, **32**(3): 407–414.
- Liu, Y., Song, Q.-J., Wang, L., (2009). Development and characterization of an amperometric sensor for triclosan detection based on electropolymerized molecularly imprinted polymer. *Microchem. J.*, **91**(2): 222–226.
- Losev, V. N., Buyko, O. V., Trofimchuk, A. K., Zuy, O. N., (2015). Silica sequentially modified with polyhexamethylene guanidine and Arsenazo I for preconcentration and ICP–OES determination of metals in natural waters. *Microchem. J.*, **123**: 84–89.
- Louati, I., Dammak, M., Nasri, R., Belbahri, L., Nasri, M., Abdelkafi, S., Mechichi, T., (2019). Biodegradation and detoxification of bisphenol A by bacteria isolated from desert soils. *3 Biotech*, **9**(6): 228.

- Luo, Y., Guo, W., Ngo, H. H., Nghiem, L. D., Hai, F. I., Zhang, J., Liang, S., Wang, X. C., (2014). A review on the occurrence of micropollutants in the aquatic environment and their fate and removal during wastewater treatment. *Sci. Total Environ.*, **473–474**: 619–641.
- Lütfi Yola, M., Atar, N., Eren, T., Karimi-Maleh, H., Wang, S., (2015). Sensitive and selective determination of aqueous triclosan based on gold nanoparticles on polyoxometalate/reduced graphene oxide nanohybrid. *RSC Adv.*, **5(81)**: 65953–65962.
- Mailoa, M. N., Mahendradatta, M., Laga, A., Djide, N., (2014). Antimicrobial Activities Of Tannins Extract From Guava Leaves (*Psidium Guajava* L) On Pathogens Microbial. *Int. J. Sci. Tec. Res.*, **3(1)**: 7.
- Marken, F., Neudeck, A., Bond, A. M., (2002). Cyclic Voltammetry. In F. Scholz (Ed.), *Electroanalytical Methods: Guide to Experiments and Applications* (pp. 51–97). Springer.
- Martinez, V. D., Vucic, E. A., Becker-Santos, D. D., Gil, L., Lam, W. L., (2011). Arsenic Exposure and the Induction of Human Cancers. *J. Toxicol.* **2011**: 431287.
- Masiol, M., Harrison, R. M., (2014). Aircraft engine exhaust emissions and other airport-related contributions to ambient air pollution: A review. *Atm. Environ. (Oxford, England : 1994)*, **95**: 409–455.
- Miao, Y., Chia, L. S., Goh, N. K., Tan, S. N., (2001). Amperometric Glucose Biosensor Based on Immobilization of Glucose Oxidase in Chitosan Matrix Cross-Linked with Glutaraldehyde. *Electroanalysis*, **13(4)**: 347–349.
- Miao, Y., Tan, S. N., (2000). Amperometric hydrogen peroxide biosensor based on immobilization of peroxidase in chitosan matrix crosslinked with glutaraldehyde. *The Analyst*, **125(9)**: 1591–1594.
- Michałowicz, J., (2014). Bisphenol A--sources, toxicity and biotransformation. *Environ. Toxicol. Pharmacol.*, **37(2)**: 738–758.
- Mielke, H., Reagan, P., (1998). Soil Is an Important Pathway of Human Lead Exposure. *Environ. Hlth. Perspect.*, **106**: 217–229.

- Montaseri, H., Forbes, P. B. C., (2016). A review of monitoring methods for triclosan and its occurrence in aquatic environments. *TrAC Trends Anal. Chem.*, **85**: 221–231.
- Morrall, D., McAvoy, D., Schatowitz, B., Inauen, J., Jacob, M., Hauk, A., Eckhoff, W. (2004). A field study of triclosan loss rates in river water (Cibolo Creek, TX). *Chemosphere*, **54(5)**: 653–660.
- Motia, S., Tudor, I. A., Ribeiro, P. A., Raposo, M., Bouchikhi, B., El Bari, N., (2019). Electrochemical sensor based on molecularly imprinted polymer for sensitive triclosan detection in wastewater and mineral water. *Sci. Total Environ.*, **664**: 647–658.
- Mourya, A., Mazumdar, B., Sinha, S. K., (2021). Application of CeO<sub>2</sub>-MWCNTs nanocomposite for heavy metal ion detection in aqueous solutions by electrochemical technique. *Cleaner Mater.*, **2**: 100021.
- Murugan, K., Anitha, J., Suresh, U., Rajaganesh, R., Panneerselvam, Dr. C., Althbyani, A., Tseng, L.-C., Kalimuthu, K., AlSalhi, M., S., D., Nicoletti, M., Sarkar, S., Benelli, G., Hwang, J.-S., (2017). Chitosan-fabricated Ag nanoparticles and larvivorous fishes: A novel route to control the coastal malaria vector *Anopheles sundaicus*. *Hydrobiologia*, **797**: 1–16.
- Murugananthan, M., Yoshihara, S., Rakuma, T., Shirakashi, T., (2008). Mineralization of bisphenol A (BPA) by anodic oxidation with boron-doped diamond (BDD) electrode. *J. Hazard. Mater.*, **154(1–3)**: 213–220.
- Narain, V., (2009). Water as a Fundamental Right: A Perspective from India. *Vt. L. Rev.*, **34**: 917.
- Nasution, T. I., Asrosa, R., Nainggolan, I., Balyan, M., Indah, R., Wahyudi, A., (2018). Sodium tripolyphosphate cross-linked chitosan based sensor for enhancing sensing properties towards acetone. *IOP Conf. Ser.: Mater. Sci. Eng.*, **309**: 012083.
- Ndlovu, T., Arotiba, O. A., Sampath, S., Krause, R. W., Mamba, B. B., (2012). An Exfoliated Graphite-Based Bisphenol A Electrochemical Sensor. *Sensors*, **12(9)**: 11601–11611.



- Ngundi, M. M., Sadik, O. A., Yamaguchi, T., Suye, S., (2003). First comparative reaction mechanisms of  $\beta$ -estradiol and selected environmental hormones in a redox environment. *Electrochem. Commun.*, **5**(1): 61–67.
- Niu, X., Yang, W., Wang, G., Ren, J., Guo, H., Gao, J., (2013). A novel electrochemical sensor of bisphenol A based on stacked graphene nanofibers/gold nanoparticles composite modified glassy carbon electrode. *Electrochim. Acta*, **98**: 167–175.
- Nodehi, M., Baghayeri, M., Veisi, H., (2021). Preparation of GO/Fe<sub>3</sub>O<sub>4</sub>@PMDA/AuNPs nanocomposite for simultaneous determination of As<sup>3+</sup> and Cu<sup>2+</sup> by stripping voltammetry. *Talanta*, **230**: 122288.
- Ntsendwana, B., Mamba, B. B., Sampath, S., Arotiba, O. A., (2012). Electrochemical Detection of Bisphenol A Using Graphene- Modified Glassy Carbon Electrode. *Int. J. Electrochem. Sci.*, **7**: 12.
- Olejniak, A., Karczewski, J., Dołęga, A., Siuzdak, K., Grochowska, K., (2020). Novel approach to interference analysis of glucose sensing materials coated with Nafion. *Bioelectrochem.*, **135**: 107575.
- Oprea, T. I., (2002). 2002b) Current trends in lead discovery: Are we looking for the appropriate properties. *J. Computer-Aided Mol. Des.*, **16**: 325–334.
- Park, B. K., Gonzales, E. L. T., Yang, S. M., Bang, M., Choi, C. S., Shin, C. Y., (2016). Effects of Triclosan on Neural Stem Cell Viability and Survival. *Biomol. Therapeut.*, **24**(1): 99–107.
- Phillips, D. H., Arlt, V. M., (2009). Genotoxicity: Damage to DNA and its consequences. *EXS*, **99**, 87–110.
- Pizarro, J., Segura, R., Tapia, D., Navarro, F., Fuenzalida, F., Jesús Aguirre, M., (2020). Inexpensive and green electrochemical sensor for the determination of Cd(II) and Pb(II) by square wave anodic stripping voltammetry in bivalve mollusks. *Food Chem.*, **321**: 126682.
- Po, H. N., Senozan, N. M., (2001). The Henderson-Hasselbalch Equation: Its History and Limitations. *J. Chem. Edu.*, **78**(11): 1499.
- Prakash, S., Chakrabarty, T., Singh, A. K., Shahi, V. K., (2012). Silver nanoparticles built-in chitosan modified glassy carbon electrode for anodic stripping analysis of As(III) and its removal from water. *Electrochim. Acta*, **72**, 157–164.

- Praveen, S., Arjun, A. R., Prince, S. E., (2020). Toxic effects of bisphenol-A. *Int. J. Med. Toxicol. legal Med.*, **23(3,4)**, 285–295.
- Promphet, N., Rattanasarat, P., Rangkupan, R., Chailapakul, O., Rodthongkum, N., (2015). An electrochemical sensor based on graphene/polyaniline/polystyrene nanoporous fibers modified electrode for simultaneous determination of lead and cadmium. *Sens. Actuators B Chem.*, **207**: 526–534.
- Pruden, A., Pei, R., Storteboom, H., Carlson, K. H., (2006). Antibiotic Resistance Genes as Emerging Contaminants: Studies in Northern Colorado. *Environ. Sci. Technol.*, **40(23)**: 7445–7450.
- Quinn, D. M. (1987). Acetylcholinesterase: Enzyme structure, reaction dynamics, and virtual transition states. *Chem. Rev.*, **87(5)**: 955–979.
- Raafat, D., von Bargen, K., Haas, A., Sahl, H.-G. (2008). Insights into the Mode of Action of Chitosan as an Antibacterial Compound. *Appl. Environ. Microbiol.*, **74(12)**: 3764–3773.
- Rajmohan, K. S., Chandrasekaran, R., Varjani, S., (2020). A Review on Occurrence of Pesticides in Environment and Current Technologies for Their Remediation and Management. *Indian J. Microbiol.*, **60(2)**: 125–138.
- Rattanachaikunsopon, P., Phumkhachorn, P., (2010). Contents and antibacterial activity of flavonoids extracted from leaves of *Psidium guajava*. *J. Med. Plants Res.*, **4(5)**: 393–396.
- Regueiro, J., Breidbach, A., Wenzl, T., (2015). Derivatization of bisphenol A and its analogues with pyridine-3-sulfonyl chloride: Multivariate optimization and fragmentation patterns by liquid chromatography/Orbitrap mass spectrometry. *Rapid Commun. Mass Spectrom.*, **29(16)**: 1473–1484.
- Rithe. (2014). Preparation and analysis of novel hydrogels prepared from the blend of guar gum and chitosan: cross-linked with gluteraldehyde. *Adv. Mater. Sci. Eng. An Int. J.*, **1**.
- Roda, A., Rauch, P., Ferri, E., Girotti, S., Ghini, S., Carrea, G., Bovara, R., (1994). Chemiluminescent flow sensor for the determination of Paraoxon and Aldicarb pesticides. *Anal. Chim. Acta*, **294(1)**: 35–42.
- Rodricks, J. V., Swenberg, J. A., Borzelleca, J. F., Maronpot, R. R., Shipp, A. M., (2010). Triclosan: A critical review of the experimental data and development

- of margins of safety for consumer products. *Crit. Rev. Toxicol.*, **40(5)**: 422–484.
- Ruiz-Manríquez, A., Magaña, P. I., López, V., Guzmán, R., (1998). Biosorption of Cu by *Thiobacillus ferrooxidans*. *Bioproc. Eng.*, **18(2)**: 113–118.
- Rusmin, R., Sarkar, B., Liu, Y., McClure, S., Naidu, R., (2015). Structural evolution of chitosan–palygorskite composites and removal of aqueous lead by composite beads. *Appl. Surf. Sci.*, **353**: 363–375.
- Saljooqi, A., Shamspur, T., Mostafavi, A., (2020). A Sensitive Electrochemical Sensor Based on Graphene Oxide Nanosheets Decorated by Fe<sub>3</sub>O<sub>4</sub>@Au Nanostructure Stabilized on Polypyrrole for Efficient Triclosan Sensing. *Electroanalysis*. **32**: 1-8.
- Salmanipour, A., Taher, M. A., (2011). An electrochemical sensor for stripping analysis of Pb(II) based on multiwalled carbon nanotube functionalized with 5-Br-PADAP. *J. Solid State Electrochem.*, **15(11)**: 2695–2702.
- Sankoda, K., Matsuo, H., Ito, M., Nomiya, K., Arizono, K., Shinohara, R., (2011). Identification of Triclosan Intermediates Produced by Oxidative Degradation Using TiO<sub>2</sub> in Pure Water and Their Endocrine Disrupting Activities. *Bull. Environ. Contam. Toxicol.*, **86(5)**: 470.
- Santana, E. R., Spinelli, A., (2020). Electrode modified with graphene quantum dots supported in chitosan for electrochemical methods and non-linear deconvolution of spectra for spectrometric methods: Approaches for simultaneous determination of triclosan and methylparaben. *Microchim. Acta*, **187(4)**: 250.
- Sarikokba, S., Tiwari, D., Prasad, S. K., Kim, D. J., Choi, S. S., Lee, S.-M., (2020). Bio-Composite Materials Precursor to Chitosan in the Development of Electrochemical Sensors: A Critical Overview of Its use with Micro-Pollutants and Heavy Metals Detection. *Appl. Chem. Eng.*, **31(3)**: 237–257.
- Scholz, F., (2015). Voltammetric techniques of analysis: The essentials. *ChemTexts*, **1(4)**: 17.
- Schwarzenbach, R. P., Escher, B. I., Fenner, K., Hofstetter, T. B., Johnson, C. A., von Gunten, U., Wehrli, B. (2006). The Challenge of Micropollutants in Aquatic Systems. *Science*, **313(5790)**: 1072–1077.

- Shukla, S. K., Mishra, A. K., Arotiba, O. A., Mamba, B. B., (2013). Chitosan-based nanomaterials: A state-of-the-art review. *Int. J. Bio. Macromol.*, **59**: 46–58.
- Silva, S. S., Ferreira, R. A. S., Fu, L., Carlos, L. D., Mano, J. F., Reis, R. L., Rocha, J., (2005). Functional nanostructured chitosan–siloxane hybrids. *J. Mater. Chem.*, **15(35–36)**: 3952–3961.
- Sitko, R., Janik, P., Zawisza, B., Talik, E., Margui, E., Queralt, I., (2015). Green Approach for Ultratrace Determination of Divalent Metal Ions and Arsenic Species Using Total-Reflection X-ray Fluorescence Spectrometry and Mercapto-Modified Graphene Oxide Nanosheets as a Novel Adsorbent. *Anal. Chem.*, **87(6)**: 3535–3542.
- Song, J., Zhou, H., Gao, R., Zhang, Y., Zhang, H., Zhang, Y., Wang, G., Wong, P. K., Zhao, H., (2018). Selective Determination of Cr(VI) by Glutaraldehyde Cross-Linked Chitosan Polymer Fluorophores. *ACS Sens.*, **3(4)**: 792–798.
- Steenland, K., Boffetta, P., (2000). Lead and cancer in humans: Where are we now? *Am. j. Ind. Med.*, **38(3)**: 295–299.
- Suh, J. K., Matthew, H. W., (2000). Application of chitosan-based polysaccharide biomaterials in cartilage tissue engineering: A review. *Biomaterials*, **21(24)**: 2589–2598.
- T, Priya., N, D., N, T., (2017). Electrochemical behavior of Pb (II) on a heparin modified chitosan/graphene nanocomposite film coated glassy carbon electrode and its sensitive detection. *Int. J. Bio. Macromol.*, **104(Pt A)**: 672–680.
- Tian, Y., Deng, P., Wu, Y., Li, J., Liu, J., Li, G., He, Q., (2020). MnO<sub>2</sub> Nanowires-Decorated Reduced Graphene Oxide Modified Glassy Carbon Electrode for Sensitive Determination of Bisphenol A. *J. Electrochem. Soc.*, **167(4)**: 046514.
- Tiwari, D., Zirliannigura, Lee, S. M., (2017). Fabrication of efficient and selective total arsenic sensor using the hybrid materials modified carbon paste electrodes. *J. Electroanal. Chem.*, **C(784)**: 109–114.
- Uddin, I., Ahmad, K., Khan, A. A., Kazmi, M. A., (2017). Synthesis of silver nanoparticles using *Matricaria recutita* (Babunah) plant extract and its study as mercury ions sensor. *Sens. Bio-Sens. Res.*, **16**: 62–67.

- Uhrovčík, J., (2014). Strategy for determination of LOD and LOQ values – Some basic aspects. *Talanta*, **119**: 178–180.
- United States. Environmental Protection Agency. (2010). *Bisphenol A Action Plan: (CASRN 80-05-7), [CA Index Name: Phenol, 4,4'-(1-methylethylidene)bis-]*. U.S. Environmental Protection Agency, Office of Pollution, Pesticides, and Toxic Substances.
- U.S. Environmental Protection Agency. (2010). *Bisphenol A Action Plan*. 22.
- Vaidyanathan, G., Kiruba, D., (2014). Preliminary phytochemical analysis of leaf powder extracts of *Psidium guajava* L. *Int. J. Pharmacogn. Phytochem. Res.*, **6**: 332–334.
- Vakili, M., Deng, S., Li, T., Wang, W., Wang, W., Yu, G., (2018). Novel crosslinked chitosan for enhanced adsorption of hexavalent chromium in acidic solution. *Chem. Eng. J.*, **347**: 782–790.
- Valko, M., Morris, H., Cronin, M. T. D., (2005). Metals, toxicity and oxidative stress. *Curr. Med. Chem.*, **12(10)**: 1161–1208.
- Vandenberg, L. N., Chahoud, I., Heindel, J. J., Padmanabhan, V., Paumgarten, F. J. R., Schoenfelder, G., (2012). Urinary, circulating, and tissue biomonitoring studies indicate widespread exposure to bisphenol A. *Cien. Saude Colet.*, **17(2)**: 407–434.
- Vandenberg, L. N., Hauser, R., Marcus, M., Olea, N., Welshons, W. V., (2007). Human exposure to bisphenol A (BPA). *Reprod. Toxicol.*, **24(2)**: 139–177.
- Vidal, L., Chisvert, A., Canals, A., Psillakis, E., Lapkin, A., Acosta, F., Edler, K. J., Holdaway, J. A., Marken, F. (2008). Chemically surface-modified carbon nanoparticle carrier for phenolic pollutants: Extraction and electrochemical determination of benzophenone-3 and triclosan. *Anal. Chim. Acta*, **616(1)**: 28–35.
- Vieira Jodar, L., Orzari, L. O., Storti Ortolani, T., Assumpção, M. H. M. T., Vicentini, F. C., Janegitz, B. C., (2019). Electrochemical Sensor Based on Casein and Carbon Black for Bisphenol A Detection. *Electroanalysis*, **31(11)**: 2162–2170.
- Wang, L., Lei, T., Ren, Z., Jiang, X., Yang, X., Bai, H., Wang, S., (2020). Fe<sub>3</sub>O<sub>4</sub>@PDA@MnO<sub>2</sub> core-shell nanocomposites for sensitive

- electrochemical detection of trace Pb(II) in water. *J. Electroanal. Chem.*, **864**: 114065.
- Wang, Y., Yin, C., Zhuang, Q., (2020). An electrochemical sensor modified with nickel nanoparticle/nitrogen-doped carbon nanosheet nanocomposite for bisphenol A detection. *J. Alloys Compd.*, **827**: 154335.
- Wani, A. L., Ara, A., Usmani, J. A., (2015). Lead toxicity: A review. *Interdiscip. Toxicol.*, **8(2)**: 55–64.
- Wei, W., Han, X., Shao, Y., Xie, W., Zhang, Y., Yao, Y., Zhao, W., Han, R., Li, S., Zhang, Y., Zheng, C., (2021). Comparing the effects of humic acid and oxalic acid on Pb(II) immobilization by a green synthesized nanocrystalline hydroxyapatite. *Chemosphere*, **285**: 131411.
- Wetherill, Y. B., Akingbemi, B. T., Kanno, J., McLachlan, J. A., Nadal, A., Sonnenschein, C., Watson, C. S., Zoeller, R. T., Belcher, S. M., (2007). In vitro molecular mechanisms of bisphenol A action. *Reprod. Toxicol.*, **24(2)**: 178–198.
- World Health Organization. (2008). *Guidelines for drinking-water quality [electronic resource]: Incorporating 1st and 2nd addenda, Vol.1, recommendations*. World Health Organization.
- Wu, T., Li, T., Liu, Z., Guo, Y., Dong, C., (2017a). Electrochemical sensor for sensitive detection of triclosan based on graphene/palladium nanoparticles hybrids. *Talanta*, **164**: 556–562.
- Wu, T., Li, T., Liu, Z., Guo, Y., Dong, C., (2017b). Electrochemical sensor for sensitive detection of triclosan based on graphene/palladium nanoparticles hybrids. *Talanta*, **164**: 556–562.
- Xing, H., Wang, X., Sun, G., Gao, X., Xu, S., Wang, X., (2012). Effects of atrazine and chlorpyrifos on activity and transcription of glutathione S-transferase in common carp (*Cyprinus carpio* L.). *Environ. Toxicol. Pharmacol.*, **33(2)**: 233–244.
- Xiong, S., Yang, B., Cai, D., Qiu, G., Wu, Z., (2015). Individual and Simultaneous Stripping Voltammetric and Mutual Interference Analysis of Cd<sup>2+</sup>, Pb<sup>2+</sup> and Hg<sup>2+</sup> with Reduced Graphene Oxide-Fe<sub>3</sub>O<sub>4</sub> Nanocomposites. *Electrochim. Acta*, **185**: 52–61.

- Xu, Z., Fan, X., Ma, Q., Tang, B., Lu, Z., Zhang, J., Mo, G., Ye, J., Ye, J., (2019). A sensitive electrochemical sensor for simultaneous voltammetric sensing of cadmium and lead based on Fe<sub>3</sub>O<sub>4</sub>/multiwalled carbon nanotube/laser scribed graphene composites functionalized with chitosan modified electrode. *Mater. Chem. Phys.*, **238**: 121877.
- Yan, X., Zhou, C., Yan, Y., Zhu, Y., (2015). A Simple and Renewable Nanoporous Gold-based Electrochemical Sensor for Bisphenol A Detection. *Electroanalysis*, **27(12)**: 2718–2724.
- Yang, J., Wang, P., Zhang, X., Wu, K., (2009). Electrochemical Sensor for Rapid Detection of Triclosan Using a Multiwall Carbon Nanotube Film. *J. Agric. Food Chem.*, **57(20)**: 9403–9407.
- Yao, Y., Wu, H., Ping, J., (2019). Simultaneous determination of Cd(II) and Pb(II) ions in honey and milk samples using a single-walled carbon nanohorns modified screen-printed electrochemical sensor. *Food Chem.*, **274**: 8–15.
- Yazdankhah, S. P., Scheie, A. A., Høiby, E. A., Lunestad, B.-T., Heir, E., Fotland, T. Ø., Naterstad, K., Kruse, H. (2006). Triclosan and Antimicrobial Resistance in Bacteria: An Overview. *Microb. Drug Resist.*, **12(2)**: 83–90.
- Yi, Y., Zhu, G., Liu, C., Huang, Y., Zhang, Y., Li, H., Zhao, J., Yao, S., (2013). A Label-Free Silicon Quantum Dots-Based Photoluminescence Sensor for Ultrasensitive Detection of Pesticides. *Anal. Chem.*, **85(23)**: 11464–11470.
- Yin, H., Zhou, Y., Ai, S., Han, R., Tang, T., Zhu, L.-S., (2010). Electrochemical behavior of bisphenol A at glassy carbon electrode modified with gold nanoparticles, silk fibroin, and PAMAM dendrimers. *Microchim. Acta*, **170**: 99–105.
- Yonekubo, J., Hayakawa, K., Sajiki, J., (2008). Concentrations of bisphenol a, bisphenol a diglycidyl ether, and their derivatives in canned foods in Japanese markets. *J. Agric. Food Chem.*, **56(6)**: 2041–2047.
- Yonten, V., Ince, M., Tanyol, M., Yildirim, N., (2016). Adsorption of bisphenol A from aqueous solutions by *Pleurotus eryngii* immobilized on Amberlite XAD-4 using as a new adsorbent. *Desalin. Water Treat.*, **57(47)**: 22362–22369.

- Yu, C., Gou, L., Zhou, X., Bao, N., Gu, H., (2011). Chitosan–Fe<sub>3</sub>O<sub>4</sub> nanocomposite based electrochemical sensors for the determination of bisphenol A. *Electrochim. Acta*, **56(25)**: 9056–9063.
- Yuan, Y., Chesnutt, B. M., Haggard, W. O., Bumgardner, J. D., (2011). Deacetylation of Chitosan: Material Characterization and in vitro Evaluation via Albumin Adsorption and Pre-Osteoblastic Cell Cultures. *Materials*, **4(8)**: 1399–1416.
- Yueh, M.-F., Tukey, R. H., (2016). Triclosan: A Widespread Environmental Toxicant with Many Biological Effects. *Annu. Rev. Pharmacol. Toxicol.*, **56(1)**: 251–272.
- Zahran, M., Khalifa, Z., A.-H. Zahran, M., Azzem, M. A., (2021). Recent advances in silver nanoparticle-based electrochemical sensors for determining organic pollutants in water: A review. *Mater. Adv.*, **2(22)**: 7350–7365.
- Zainudin, S. N. F., Abdullah, H., Markom, M., (2019). Electrochemical studies of tin oxide based-dye-sensitized solar cells (DSSC): A review. *J. Mater. Sci. Mater. Electron.*, **30(6)**: 5342–5356.
- Zavareh, S., Zarei, M., Darvishi, F., Azizi, H., (2015). As(III) adsorption and antimicrobial properties of Cu–chitosan/alumina nanocomposite. *Chem. Eng. J.*, **273**: 610–621.
- Zhang, W., Chu, P. K., Ji, J., Zhang, Y., Fu, R. K. Y., Yan, Q., (2006). Antibacterial properties of plasma-modified and triclosan or bronopol coated polyethylene. *Polymer*, **47(3)**: 931–936.
- Zhang, W., Xiong, B., Chen, L., Lin, K., Cui, X., Bi, H., Guo, M., Wang, W., (2013). Toxicity assessment of *Chlorella vulgaris* and *Chlorella protothecoides* following exposure to Pb(II). *Environ. Toxicol. Pharmacol.*, **36(1)**: 51–57.
- Zhao, J.-L., Zhang, Q.-Q., Chen, F., Wang, L., Ying, G.-G., Liu, Y.-S., Yang, B., Zhou, L.-J., Liu, S., Su, H.-C., Zhang, R.-Q., (2013). Evaluation of triclosan and triclocarban at river basin scale using monitoring and modeling tools: Implications for controlling of urban domestic sewage discharge. *Water Res.*, **47(1)**: 395–405.
- Zheng, J., Zhang, M., Ling, Y., Xu, J., Hu, S., Hayat, T., Alharbi, N. S., Yang, F., (2018). Fabrication of one dimensional CNTs/Fe<sub>3</sub>O<sub>4</sub>@PPy/Pd magnetic



- composites for the accumulation and electrochemical detection of triclosan. *J. Electroanal. Chem.*, **818**: 97–105.
- Zheng, S., Sun, Z., Park, Y., Ayoko, G., & Frost, R. (2013). Removal of bisphenol A from wastewater by Ca-montmorillonite modified with selected surfactants. *Chem. Eng. J.*, **234**, 416–422.
- Zhou, S.-F., Han, X.-J., Liu, Y.-Q., (2016). SWASV performance toward heavy metal ions based on a high-activity and simple magnetic chitosan sensing nanomaterials. *J. Alloys Compd.*, **684**: 1–7.
- Zhou, W., Li, C., Sun, C., Yang, X., (2016). Simultaneously determination of trace  $\text{Cd}^{2+}$  and  $\text{Pb}^{2+}$  based on l-cysteine/graphene modified glassy carbon electrode. *Food Chem.*, **192**: 351–357.
- Zirlianggura, Tiwari, D., Ha, J.-H., Lee, S.-M., (2017). Efficient Use of Porous Hybrid Materials in a Selective Detection of Lead(II) from Aqueous Solutions: An Electrochemical Study. *Metals*, **7(4)**: 124.
- Ziv-Gal, A., Craig, Z. R., Wang, W., Flaws, J. A., (2013). Bisphenol A inhibits cultured mouse ovarian follicle growth partially via the aryl hydrocarbon receptor signaling pathway. *Reprod. Toxicol.*, **42**: 58–67.
- Zuo, Y., Xu, J., Jiang, F., Duan, X., Lu, L., Xing, H., Yang, T., Zhang, Y., Ye, G., Yu, Y., (2017). Voltammetric sensing of Pb(II) using a glassy carbon electrode modified with composites consisting of  $\text{Co}_3\text{O}_4$  nanoparticles, reduced graphene oxide and chitosan. *J. Electroanal. Chem.*, **801**: 146–152.

## **BIO-DATA**

- 1. NAME** : Sarikokba  
**2. DATE OF BIRTH** : 20<sup>th</sup> October, 1988.  
**3. FATHER'S NAME** : Kaluba  
**4. PERMANENT ADDRESS** : Kumpani ward, Mangkolemba-798604  
**5. EDUCATIONAL QUALIFICATIONS** : M.Sc. (Chemistry)

| <b>Qualification</b> | <b>Year of Passing</b> | <b>Board/University</b>            | <b>Subjects</b>                                                    | <b>% Of Marks</b> | <b>Div.</b> |
|----------------------|------------------------|------------------------------------|--------------------------------------------------------------------|-------------------|-------------|
| HSLC                 | 2005                   | Nagaland Board of School Education | Mathematics, Science, Social Science, English, Alternative English | 42.4              | Third       |
| HSSLC                | 2008                   | Nagaland Board of School Education | Physics, Chemistry, Biology, Mathematics, English, Alternative     | 42.8              | Third       |

|                      |      |                        |                                                                                                                                                       |       |        |
|----------------------|------|------------------------|-------------------------------------------------------------------------------------------------------------------------------------------------------|-------|--------|
|                      |      |                        | ve<br>English                                                                                                                                         |       |        |
| B.Sc.<br>(General)   | 2012 | Nagaland<br>University | Chemistr<br>y,<br>Botany,<br>Geograp<br>hy                                                                                                            | 51.36 | Second |
| M.Sc.<br>(Chemistry) | 2015 | Mizoram<br>University  | Organic<br>Chemistr<br>y<br>(Speciali<br>sation),<br>Analytic<br>al<br>Chemistr<br>y,<br>Inorgani<br>c<br>Chemistr<br>y,<br>Physical<br>Chemistr<br>y | 67.6  | First  |

## LIST OF PUBLICATIONS

### A. Journals (Published)

1. **Sarikokba**, Jongte Lalmalsawmi, Shailesh Kumar Prasad, Diwakar Tiwari. (2022). Development of a novel sensor with high sensitivity for electroanalytical determination of bisphenol A based on chitosan-3-mercaptopropyl trimethoxysilane modified glassy carbon electrode. *Microchemical Journal*, 181: 107748.
2. **Sarikokba**, Jongte Lalmalsawmi, Seung Mok Lee, Diwakar Tiwari, (2022). Highly Efficient Functionalized Chitosan in the Development of Electrochemical Sensor for Trace Detection of Pb (II). *Journal of The Electrochemical Society*, 169: 066513.
3. Jongte Lalmalsawmi, **Sarikokba Sarikokba**, Diwakar Tiwari, Dong-Jin Jin Kim (2022). Simultaneous detection of  $\text{Cd}^{2+}$  and  $\text{Pb}^{2+}$  by differential pulse anodic stripping voltammetry: Use of highly efficient novel  $\text{Ag}^0(\text{NPs})$  decorated silane grafted bentonite material. *Journal of Electroanalytical Chemistry*, 918: 116490.
4. Malsawmdawngzela, R., **Sarikokba**, Thanhmingliana, Tiwari, D., Lee, S.M., (2021). Hybrid materials precursor to natural bentonite in the decontamination of Alizarin Yellow from aqueous solutions. *Environmental Engineering Research*, 27(6): 210104.
5. **Sarikokba**, Diwakar Tiwari, Shailesh Kumar Prasad, Dong Jin Kim, Suk Soon Choi and Seung-Mok Lee, (2020). Bio-Composite Materials Precursor to Chitosan in the Development of Electrochemical Sensors: A Critical Overview of Its use with Micro-Pollutants and Heavy Metals Detection. *Applied Chemistry for Engineering*, 31(3): 237-257.

## **B. Journals (Communicated)**

1. **Sarikokba**, Lalhmunsiam, Jongte lalmalsawmi, and Diwakar Tiwari, Seung Mok Lee and Jae-Kyu Yang, Greener synthesis of novel nanocomposite material for efficient and selective trace detection of Pb (II): Insights of stability and real implication studies. *Environmental Engineering Research (Accepted)*.
2. **Sarikokba**, Lalhmunsiam, Dong-Jin Kim, Seung Mok Lee, Diwakar Tiwari. Novel composite material thin film electrode for trace and efficient detection of triclosan: Stability of electrode and real matrix analyses. *Analytical and Bioanalytical Research (Communicated)*.

## **CONFERENCES AND SEMINAR**

1. **Sarikokba** and Diwakar Tiwari. Development of green nanocomposite material for electrochemical sensor: determination of Pb (II) from aqueous medium. International Conference on Emerging Trends in Nanomaterials Science and Technology (ICETNMST-2022) during 27<sup>th</sup> – 29<sup>th</sup> January, 2022, organised by the Department of Science and Humanities, National Institute of Technology Nagaland, India.
2. **Sarikokba** and Diwakar Tiwari. Use of nanocomposite material in the development of electrochemical sensor: Efficient determination of arsenic. 2<sup>nd</sup> Annual convention of North East (India) Academy of Science and Technology (NEAST) And International Seminar on Recent Advance in Science and Technology (ISRAST) during 16<sup>th</sup> – 18<sup>th</sup> November 2020 (Virtual) organized by NEAST, Mizoram University, Aizawl- 796004, Mizoram (India).
3. **Sarikokba**, Ralte Malsawmdawngzela and Diwakar Tiwari. Efficient use of hybrid material in the remediation of aquatic environment contaminated with alizarin yellow dye. National Conference on Functional Materials and Applications (NCFMA - 2019), Organised by Department of BS and HSS

(Physic), National Institute of Technology Mizoram, Aizawl, Mizoram, India-796012, during 22<sup>nd</sup> – 23<sup>rd</sup> November, 2019.

4. **Sarikokba** and Diwakar Tiwari. Efficient use of hybrid material in the remediation of aqueous solutions contaminated with antibiotic tetracycline. National Conference on Emerging Trends In Environmental Research – (NACETER) 2019, Organised by Department of Environmental Science, Pachhunga University College, Aizawl during 31<sup>st</sup> October – 2<sup>nd</sup> November, 2019.

Volume 181, October 2022  
ISSN 0026-265X

# Microchemical JOURNAL

Devoted to the Application of  
Microtechniques in all branches  
of Chemistry

EDITOR-IN-CHIEF:  
MIGUEL DE LA GUARDIA



Contents lists available at ScienceDirect

Microchemical Journal

journal homepage: [www.elsevier.com/locate/microc](http://www.elsevier.com/locate/microc)

# Development of a novel sensor with high sensitivity for electroanalytical determination of bisphenol A based on chitosan-3-mercaptopropyl trimethoxysilane modified glassy carbon electrode

Sarikokba<sup>a</sup>, Jongte Lalmalsawmi<sup>a</sup>, Shailesh Kumar Prasad<sup>b</sup>, Diwakar Tiwari<sup>a,\*</sup>

<sup>a</sup> Department of Chemistry, School of Physical Sciences, Mizoram University, Aizawl 796004, India

<sup>b</sup> Department of Chemistry, National Institute of Technology, Jamshedpur 831043, India

## ARTICLE INFO

### Keywords:

Functionalized material  
Highly efficient and selective fabricated electrode  
Differential pulse anodic stripping voltammetry  
Real matrix analysis  
Trace detection of bisphenol A

## ABSTRACT

In a facile synthesis process, a novel functionalized composite material was synthesized as precursors to the chitosan and 3-mercaptopropyl trimethoxysilane (CHMTS). The materials, chitosan (CH) and CHMTS were characterized using Fourier-transform infra-red, scanning electron microscope/energy dispersive X-rays, transmission electron microscopy, and Brunauer-Emmett-Teller surface area analyser techniques. The cyclic voltammetry (CV) studies showed that a 6-fold increase in oxidative peak current was recorded in CHMTS/GCE compared to bare GCE and 3-fold increase in peak current compared to CH/GCE. Similarly, EIS Nyquist plots showed a significant decrease in a semicircle for the CHMTS/GCE compared to the bare GCE and CH/GCE with the  $R_{ct}$  value of 10814.0  $\Omega$ , 2639.0  $\Omega$ , and 663.7  $\Omega$ , respectively for the CHMTS/GCE, CH/GCE, and GCE. Further, the electrochemical behaviour of bisphenol A (BPA) showed an irreversible 2-electron process. Moreover, the differential anodic stripping voltammetry is found sensitive and selective for the trace detection of BPA under optimized experimental parameters such as pH 10.0, deposition potential 0.2 V (vs. Ag/AgCl), and deposition time 180 sec. The determination of BPA showed good linearity with BPA concentration against the oxidation peak current, within the studied concentration range of 140.0  $\mu\text{g/L}$  to 200.0  $\mu\text{g/L}$ , and the calculated limit of detection is 5.61  $\mu\text{g/L}$ . The 10-fold increase in several co-existing ions not affect the detection of BPA, indicating the selectivity and sensitivity of the CHMTS/GCE toward BPA. The fabricated electrode showed reasonably good reproducibility with an RSD value of 0.35%. Furthermore, CHMTS/GCE showed long-term stability since the peak current was retained at 99.42% even after 48 hrs of repeated use. Real water samples using spring water and river water revealed the recovery percentage of Ca. 100% in the detection of BPA, which showed the practical applicability of the fabricated electrode.

## 1. Introduction

Bisphenol A is a potential endocrine disturbing chemical (EDCs) and is regarded as an emerging contaminant in the natural water bodies. BPA is often detected in surface water, groundwater, and landfill leachates. Several methods such as nanofiltration [1], UV/H<sub>2</sub>O<sub>2</sub> and reverse osmosis [2], and advanced oxidation process [3] membrane bioreactor [4] are demonstrated for efficient removal of bisphenol A from wastewater. These methods showed good removal efficiency for BPA at higher concentrations. However, it is not removed efficiently at low-level concentrations.

Moreover, the existing conventional treatment plants are also not

efficient enough to remove the BPA altogether; hence, it is detected at low concentrations in the water bodies. Hence, detecting the BPA at trace levels in an aqueous medium is a prerequisite. A review well demonstrated the electrochemical biosensors and sensors for the detection of various environmental contaminants using various materials [5]. Advance instruments, including spectroscopic and chromatographic techniques, are known. However, they mostly lacked the costly and complicated instrumentations, the need for highly trained operators, and mostly off-site detection is feasible [6]. On the other hand, the electrochemical technique gives advantages over those sophisticated instruments. However, it showed drawbacks like selectivity, limited linear range, stability issues, and required limit of detection (LOD) [7].

\* Corresponding author.

E-mail address: [diw.tiwari@yahoo.com](mailto:diw.tiwari@yahoo.com) (D. Tiwari).

<https://doi.org/10.1016/j.microc.2022.107748>

Received 13 April 2022; Received in revised form 29 June 2022; Accepted 30 June 2022

Available online 8 July 2022

0026-265X/© 2022 Elsevier B.V. All rights reserved.



# JES

Journal of The  
Electrochemical  
Society




The Electrochemical Society  
[www.electrochem.org](http://www.electrochem.org)

#### JOURNAL INFORMATION

1902-present  
Journal of The Electrochemical  
Society  
doi: 10.1149/issn.1945-7111  
Online ISSN: 1945-7111  
Print ISSN: 0013-4651



## Highly Efficient Functionalized Chitosan in the Development of Electrochemical Sensor for Trace Detection of Pb (II)

Sarikokba Sarikokba,<sup>1</sup> Jongte Lalmalsawmi,<sup>1</sup> Seung Mok Lee,<sup>2,\*</sup> and Diwakar Tiwari<sup>1,2</sup> 

<sup>1</sup>Department of Chemistry, School of Physical Sciences Mizoram University, Aizawl-796004, India

<sup>2</sup>Department of Health & Environmental Engineering, Catholic Kwandong University Gangneung 210-701, Republic of Korea

Fabrication of a working electrode with silane grafted chitosan (CHTMS) employed in the sensitive detection of Pb(II) in aqueous media is presented. Several advanced analytical methods have extensively characterized the nanocomposite material. The prepared material was subsequently employed for modification of a glassy carbon electrode (GCE) and characterized using cyclic voltammetry (CV) and electrochemical impedance spectroscopy (EIS), which show a 3-fold enhancement in surface area compared with the bare GCE, and a charge transfer resistance of 678.7  $\Omega$ . The modified electrode was employed in the sensitive determination of Pb(II) in aqueous media using differential pulse anodic stripping voltammetry (DPASV), where optimization of experimental parameters such as pH, deposition time and deposition potential was carried out. Under optimized conditions, the linear regression and correlation coefficient were obtained, which show that Pb(II) can be detected over a wide concentration range with a calculated limit of detection (LOD) of 2.83  $\mu\text{g l}^{-1}$ , which is lower than the permissible limit set by the WHO. For practical applicability, reproducibility and stability tests as well as real water sample analyses were further performed, with the obtained recovery rates showing promising results.

© 2022 The Electrochemical Society ("ECS"). Published on behalf of ECS by IOP Publishing Limited. [DOI: 10.1149/1945-7111/ac77c4]

Manuscript submitted March 8, 2022; revised manuscript received June 2, 2022. Published June 21, 2022.

Supplementary material for this article is available [online](#)

Heavy metal toxic ions pose serious environmental threats due to their toxicity, bioaccumulation, non-biodegradability and persistence in the environment.<sup>1,2</sup> The accumulation of these toxic ions leads to serious issues concerning human health and imbalances in natural ecosystems.<sup>3</sup> Natural activities contribute significantly to the occurrence of toxic ions in the environment in addition to several anthropogenic activities. The rapid industrialization and disposal of partly treated wastes into the aquatic environment has led to the entry of contaminants into the food chain.<sup>4</sup>

Pb(II) is one of the most toxic and persistent non-essential heavy metals that causes numerous health effects, mainly affecting the central nervous system.<sup>5,6</sup> Pb(II) accumulates readily in the bones, muscles and kidney.<sup>7</sup> It reaches water bodies through pipes with Pb (II) layering, leading to the contamination of drinking water. The World Health Organization (WHO) has set the permissible limit of Pb(II) in drinking water to as low as 10  $\mu\text{g l}^{-1}$ .<sup>5</sup> Therefore, to safeguard human health, there is an urgent need to develop robust and miniaturized devices for Pb(II) detection at trace levels. Many sophisticated techniques are known for the low-level detection of Pb (II), including atomic absorption spectroscopy (AAS),<sup>8</sup> inductively coupled plasma-mass spectrometry/optical emission spectroscopy (ICP-MS/OES),<sup>9</sup> atomic fluorescence spectroscopy (AFS),<sup>10</sup> surface-enhanced Raman scattering (SERS),<sup>11</sup> and X-ray fluorescence spectrometry (XRF).<sup>12</sup> Although these sophisticated techniques are advantageous in the low-level detection of Pb(II), these techniques lack on-site detection and require trained personnel to operate the instruments. On the other hand, electrochemical techniques, viz., stripping voltammetry, provide numerous advantages, such as simplicity, sensitivity, selectivity, stability, easy operation, and cost effectiveness, and, most importantly, devices can be employed for on-site analyte detection.<sup>6</sup> Among various electrochemical techniques, DPASV (differential pulse anodic stripping voltammetry) has drawn greater interest because of its high sensitivity and selectivity toward several heavy metal toxic ions.<sup>13</sup>

Furthermore, the sensitivity and selectivity of analytes by electrochemical methods greatly depend on the electrode surface and can be significantly improved by suitable modification using advanced materials. Nanoparticles, nanocomposites, carbon nanotubes, graphene-based composites, polymers, biological compounds,

etc., are often employed as electrode modifiers for the low-level determination of various metal ions.<sup>14–20</sup> Recently, electrodes modified with polymers such as polyaniline and PEDOT (poly 3,4-ethylenedioxythiophene) have shown promise due to their physiological robustness, chemical stability, adsorptive ability, versatility for introducing various functional groups, and relatively inexpensive and robust synthesis.<sup>21,22</sup> However, recent research efforts have focused on developing biocompatible, non-toxic, easy, and environmentally friendly processes for material production. Hence, biopolymers are promising precursor materials for synthesizing suitable advanced materials.<sup>23</sup> The combination of film forming capabilities, high stability, bioactivity, high water permeability, low toxicity, good mechanical strength, and susceptibility to chemical changes makes biopolymers ideal for electrochemical applications.<sup>24</sup> It has been reported that chitosan is a useful biopolymer for the extraction of chemicals and for metal determination.<sup>25</sup>

Chitosan is a natural polymer with a variety of interesting and impressive properties, viz., good adsorption ability, low-cost, abundance and ready chelation of heavy metal ions.<sup>26,27</sup> Moreover, chitosan is biocompatible, non-toxic, biodegradable, and cost effective, with film forming, swelling, adhesion properties, etc. For these reasons, chitosan has found applications in many research areas.<sup>28</sup> It is derived from the deacetylation of chitin and obtained from the exoskeleton of insect cuticles, shrimp and crabs.<sup>2</sup> The  $\beta$ -glycosidic linkages of chitosan show similarities with cellulose, where two units of chitosan are linked together through glycosidic linkages, i.e., 2-acetamido-d-glucose and 2-amino-d-glucose, as shown in Fig. 1.<sup>29</sup>

Despite several unique and useful properties of chitosan, the use of bare chitosan has several limitations, including weak mechanical strength, settling problems and pH sensitivity, since, at lower pH, it is readily soluble and dissociates from its structural indiginity.<sup>30,31</sup> However, the functional groups present in chitosan enable the modification of chitosan with suitability and selectivity as a natural engineered material. The chemical modification of chitosan has been primarily conducted via crosslinking with glutaraldehyde. Furthermore, the modified material shows good selectivity toward the detection of Cr (VI), glucose and hydrogen peroxide.<sup>32–34</sup> Furthermore, the diepoxy compound [1,2:7,8-diepoxyoctane (DEO)] was crosslinked with chitosan and found suitable for the adsorption of Cr(VI) under acidic conditions;<sup>35</sup> sodium tripolyphosphate (TPP) and gloxal are also

\*E-mail: leesm@cku.ac.kr; diw\_tiwari@yahoo.com



Volume 921

15 September 2022

ISSN 1572-6657

# Journal of Electroanalytical Chemistry

An International Journal  
also devoted to  
All Physicochemical Aspects of  
Fundamental and Applied Electrochemistry

Editor-in-Chief:  
X.H. Xia

Editors:  
M. Opallo  
R. Torresi  
T. D. Chung  
G. Xu

Available online at [www.sciencedirect.com](http://www.sciencedirect.com)

**ScienceDirect**

In collaboration with  
the International Society  
of Electrochemistry





Contents lists available at ScienceDirect

Journal of Electroanalytical Chemistry

journal homepage: [www.elsevier.com/locate/jelechem](http://www.elsevier.com/locate/jelechem)

# Simultaneous detection of $\text{Cd}^{2+}$ and $\text{Pb}^{2+}$ by differential pulse anodic stripping voltammetry: Use of highly efficient novel $\text{Ag}^0(\text{NPs})$ decorated silane grafted bentonite material

Jongte Lalmalsawmi<sup>a</sup>, Sarikokba<sup>a</sup>, Diwakar Tiwari<sup>a,\*</sup>, Dong-Jin Kim<sup>b,\*</sup><sup>a</sup> Department of Chemistry, School of Physical Sciences, Mizoram University, Aizawl-796004, India<sup>b</sup> Department of Environmental Sciences & Biotechnology, Institute of Energy and Environment, Hallym University, Chuncheon 24252, Korea

## ARTICLE INFO

## Keywords:

Green synthesis  
Simultaneous trace detection  
Nanomaterial  
Real matrix analysis  
 $\text{Cd}^{2+}$  and  $\text{Pb}^{2+}$

## ABSTRACT

Novel and highly efficient nanomaterials were synthesized using relatively greener routes, and these materials were utilized in the trace and simultaneous detection of  $\text{Cd}^{2+}$  and  $\text{Pb}^{2+}$  in aqueous solutions. Silver nanoparticles ( $\text{AgNP}$ ) were synthesized by using the *Persea Americana* leaf extract, and the  $\text{AgNP}$  were in situ decorated with the silane grafted bentonite ( $\text{AgNP@Bt/TC}$ ). The structure/morphology of the synthesized materials was characterized by scanning electron microscopy/energy-dispersive X-ray (SEM/EDX), transmission electron microscopy (TEM), and X-ray photoelectron spectroscopy (XPS). Nanomaterial was utilized to modify the glassy carbon electrode surface. For the first time, the fabricated electrode was employed for the single and simultaneous trace detection of lead and cadmium in aqueous solutions using the differential pulse anodic stripping voltammetry (DPASV). Extensive parametric studies viz., pH, depositional potential, time, and potentially interfering ions were studied. Fairly good calibration lines were obtained to detect these two ions with a detection limit (LOD) of 0.79  $\mu\text{g/L}$  for  $\text{Cd}^{2+}$  and 0.88  $\mu\text{g/L}$  for  $\text{Pb}^{2+}$ . The detection method was utilized in the simultaneous detection of the metal ions in real matrix samples, which gave the recovery of 93 to 108% for cadmium and 99 to 113% for lead detection.

## 1. Introduction

The non-essential heavy metal ions (HMI's) such as As, Pb, Cd, Hg, etc. are highly toxic and non-biodegradable, causing significant environmental hazards. These toxic ions are readily accumulated in the body's tissues and cause serious health problems affecting the nervous system, skin, liver, kidneys, bones, etc. [1–3]. Humans are greatly exposed to lead and cadmium through contaminated food items or even drinking water. Given its toxicity, the United States Environmental Protection Agency (US-EPA) and World Health Organization (WHO) have set 3.0–5.0  $\mu\text{g/L}$  and 10.0  $\mu\text{g/L}$  as maximum intake limits for cadmium and lead, respectively, in drinking water [4]. Although the US-EPA regulates the maximum contamination level of these two ions, many countries imposed non-occurrence of these ions even at trace levels. Many industrial activities, including mining, agriculture, metal-plating, manufacturing of batteries, alloys, paints, dyes, etc. are vast contributors of the heavy metals released to the aquatic and terrestrial ecosystems, which eventually enter into the bio-environment [5,6]. Consequently, efforts are made to monitor and assess

heavy metal contamination in aquatic environments properly. The analysis of heavy metals are mostly carried out by standard spectroscopic techniques such as atomic absorption spectroscopy [7,8], inductively coupled plasma-mass spectroscopy [9] and inductively coupled plasma-optical emission spectroscopy [10]. Nonetheless, the requirement of expensive and sophisticated instruments with cumbersome operational procedures are the known disadvantages of utilizing these methods. Moreover, the methods are limited to off-site measurements only. Thus, the alternative techniques that offer a simple, cost-effective setup with user-friendly operation and apply to on-site detection of toxic heavy metal ions have been considerably encouraged in the recent past [11,12]. Many detection strategies based on miniaturized devices have recently emerged as viable alternatives in the efforts of robust, portable, and low-cost detection methods. These devices eventually overcome the shortcomings of conventional methods, viz., fluorescence [13], colorimetry [14], surface-enhanced Raman scattering [15], electrochemistry [16], and surface plasmon resonance [17]. Electrochemical methods are recognized as promising tools to fulfil the demands. They are inexpensive, portable, and rapid, hence providing

\* Corresponding authors.

E-mail addresses: [diw.tiwari@yahoo.com](mailto:diw.tiwari@yahoo.com) (D. Tiwari), [dongjin@hallym.ac.kr](mailto:dongjin@hallym.ac.kr) (D.-J. Kim).<https://doi.org/10.1016/j.jelechem.2022.116490>

Received 1 April 2022; Received in revised form 28 May 2022; Accepted 1 June 2022

Available online 06 June 2022

1572-6657/© 2022 Elsevier B.V. All rights reserved.



# Hybrid materials precursor to natural bentonite in the decontamination of Alizarin Yellow from aqueous solutions

Ralte Malsawmdawngzela<sup>1</sup>, Sarikokba<sup>1</sup>, Thanhmingliana<sup>2</sup>, Diwakar Tiwari<sup>1\*</sup>, Seung Mok Lee<sup>3</sup>

<sup>1</sup>Department of Chemistry, School of Physical Sciences, Mizoram University, Aizawl-796004, India

<sup>2</sup>Department of Chemistry, Pachhunga University College, Mizoram University, Aizawl-796001, India

<sup>3</sup>Department of Environmental Engineering, Catholic Kwandong University, Gangneung 25601, Republic of Korea

## ABSTRACT

The present study aims to investigate the insights of Alizarin Yellow removal by hybrid materials precursor to natural bentonite. The hybrid materials employed are bentonite modified with hexadecyltrimethylammonium bromide (HDTMA) (BnH) and aluminium pillared HDTMA bentonite (BnAH). Surface morphology of materials are obtained with scanning electron microscopy-Energy dispersive X-ray analysis (SEM-EDX). The batch reactor operations conducted in the removal of Alizarin Yellow by these solids for various parametric studies which enabled to deduce the mechanism involved at solid/solution interface. Sorption capacity and selectivity was increased significantly using hybrid materials in the removal of AY. Hybrid materials showed very high removal capacity of AY and apparently unaffected at varied pH (4.0–10.0) and sorptive concentrations 1.0 to 25.0 mgL<sup>-1</sup>. Kinetic studies indicated that an apparent equilibrium occurred within 5–10 min of contact and the kinetic data was better fitted to the pseudo-second-order kinetic model. The percent removal of AY was not affected by increasing the background electrolyte (NaCl) concentration to 0.1 molL<sup>-1</sup> and in presence of several co-existing ions. It is revealed that the hybrid materials are found more organophilic and AY molecule bound with strong forces at the surface of hybrid materials.

**Keywords:** Alizarin Yellow, Hybrid materials, Organophilic materials, Pillared materials, Sorption mechanism, Strong bonding

## 1. Introduction

Rapid growth of modern textile industries has led to an excessive discharge of wastes containing dyes and pigments. A report stated that around 10–15% of the dye produced is lost annually during the textile dyeing process and final processes [1]. Dye compounds are non-biodegradable, persistent in nature, stable to light thereby disturbing the process of photosynthesis in the aquatic environment and are difficult to eliminate because of aromatic structure from water bodies [2–8]. More than 5,000 years, natural dyes, for instance, indigo have been employed for coloring but due to the low cost and availability of new colors, natural dyes are being replaced by the synthetic dyes [9]. Alizarin Yellow, an azo dye, 5-(3-Nitrophenylazo) salicylic acid sodium salt is produced by the diazo coupling reaction and readily soluble in water. It is used in wool, leather, paper, fibers, leather, plastics, food, pharmaceuticals, paints and lacquers industries [9–11]. Several biological and physicochemical treatments such as oxidation, coagulation, acti-

vated sludge processes, filtration, photocatalysis, membrane filtration and adsorption are employed in the removal of dye compounds from wastewaters. However, some of these methods are expensive, generate even more toxic by-products and sometimes show limited efficiency [12–14]. Therefore, adsorption is a common and viable method to be employed for the removal of dyes from wastewaters due to its low-cost, easy process and effective since no hazardous by-products are formed in the overall process [15–20].

Clay minerals are natural adsorbent and are found useful in the remediation of aquatic environments contaminated with a variety of water pollutants. The presence of exchangeable cations, electrical charge, micro-porosity and surface functional groups makes clay mineral a good natural adsorbent. However, clay minerals show less efficiency towards several anionic and organic contaminants. Therefore, to increase its sorption capacity towards such pollutants, modification of clay minerals with suitable organic molecules, grafting, treating with acid and alkali, pillaring with poly(hydroxo-metal) cations and cross-linking are interesting alter-



This is an Open Access article distributed under the terms of the Creative Commons Attribution Non-Commercial License (<http://creativecommons.org/licenses/by-nc/3.0/>) which permits unrestricted non-commercial use, distribution, and reproduction in any medium, provided the original work is properly cited.

Copyright © 2022 Korean Society of Environmental Engineers

Received February 26, 2021 Accepted November 17, 2021

\* Corresponding author

E-mail: diw\_tiwari@yahoo.com

Tel: +91-9862323015 Fax: +91-389-2330834

ORCID: 0000-0002-9177-9704



## Bio-Composite Materials Precursor to Chitosan in the Development of Electrochemical Sensors: A Critical Overview of Its use with Micro-Pollutants and Heavy Metals Detection

Sarikokba, Diwakar Tiwari<sup>†</sup>, Shailesh Kumar Prasad\*, Dong Jin Kim\*\*, Suk Soon Choi\*\*\*, and Seung-Mok Lee\*\*\*\*,†

*Department of Chemistry, School of Physical Sciences, Mizoram University, Aizawl-796004, India*

*\*Department of Chemistry, National Institute of Technology, Jamshedpur-831043, India*

*\*\*Department of Environmental Science & Biotechnology, Hallym University, Chuncheon 24252, Republic of Korea*

*\*\*\*Department of Biological and Environmental Engineering, Senyung University, Jecheon 27136, Republic of Korea*

*\*\*\*\*Department of Health and Environment, Catholic Kwandong University, Gangneung 25601, Republic of Korea*

*(Received May 12, 2020; Revised May 15, 2020; Accepted May 19, 2020)*

### Abstract

The role of nano bio-composites precursor to chitosan are innumerable and are known for having different applications in various branches of physical sciences. The application to the sensor development is relatively new, where only few literature works are available to address the specific and critical analysis of nanocomposites in the subject area. The bio-composites are potential and having greater affinity towards the heavy metals and several micro-pollutants hence, perhaps are having wider implications in the low or even trace level detection of the pollutants. The nano-composites could show good selectivity and suitability for the detection of the pollutants as they are found in the complex matrix. However, the greater challenges are associated using the bio-composites, since the biomaterials are prone to be oxidized or reduced at an applied potential and found to be a hinderance for the detection of target pollutants. In addition, the materials could proceed with a series of electrochemical reactions, which could produce different by-products in analytical applications, resulting in several complex phenomena in electrochemical processes. Therefore, this review addresses critically various aspects of an evaluation of nano bio-composite materials in the electrochemical detection of heavy metals and micro-pollutants from aqueous solutions.

**Keywords:** *Electrochemical sensor, Bio-composite materials, Chitosan, Detection limit, Glassy carbon electrode, Heavy metals, Micro-pollutants*

### 1. Introduction

The presence of micro-pollutants in the aquatic environment can lead to serious environmental issues. These micro-pollutants are persistence and relatively toxic in nature and are found to be emerging as water contaminants. It includes a variety of anthropogenic and natural occurring substances. Anthropogenic substances are those which include day to day consumables viz., cosmetics, pharmaceutical products, pesticides used by cultivators and variety of industrial wastes emanating from chemical industries. These pollutants are detected in water bodies at very low level in concentrations (ng/L to µg/L) hence, it makes difficult to detect and complicates the process further in regards to treating these compounds in the wastewater treatment plants (WWTPs)[1]. Since these micro-pollutants are persistence hence, it is removed/degraded partly in the WWTPs and escaped through the WWTPs.

Therefore, it resulted a continuous introduction of these pollutants into the aquatic environment[2]. Micro-pollutants which escape through WWTPs in an aquatic environment becomes a serious threat to human and other living beings because of its long- or short-term toxicity, endocrine disrupting effects and antibiotic resistance. In this respect, since there are no intended guidelines laid down by the regulatory bodies for discharge of these micro-pollutants into the water bodies, there will be problems going forward related to this issue[1]. However, many of these contaminants are toxic to living beings as well and need to be continually monitored and researched to preserve human health outcomes in the future.

It is known that the pharmaceuticals/drugs which are administered to the human body could metabolize only up to 30% hence, and therefore the major pharmaceutical compounds are either unmetabolized or metabolized as by-products, and are excreted through urine or faeces which eventually enters into the receiving waste water treatment plants (WWTPs)[3-5]. Micro-pollutants are included with the endocrine disrupting chemicals (EDCs) which is known to be a serious health hazard. It is therefore, responsible of disrupting the endocrine system as well as nervous system of living organisms[1]. Apart from pharmaceuticals, the prolonged usage of pesticides in agricultural lands for controlling crops damaging insects, fungus etc. also contributes a sig-

<sup>†</sup> Corresponding Author: Catholic Kwandong University,  
Department of Health and Environment, Gangneung 25601, Republic of Korea  
Tel: +82-33-649-7535 e-mail: leesm@cku.ac.kr

<sup>‡</sup> Corresponding Author: Mizoram University,  
Department of Chemistry, School of Physical Sciences, Aizawl-796004, India  
Tel: +91-9862323015 e-mail: diw\_tiwari@yahoo.com

## **PARTICULARS OF THE CANDIDATE**

|                                       |                                                                                                                                                                 |
|---------------------------------------|-----------------------------------------------------------------------------------------------------------------------------------------------------------------|
| <b>NAME OF CANDIDATE</b>              | : Sarikokba                                                                                                                                                     |
| <b>DEGREE</b>                         | : Doctor of Philosophy (Ph.D.)                                                                                                                                  |
| <b>DEPARTMENT</b>                     | : Chemistry                                                                                                                                                     |
| <b>TITLE OF THESIS</b>                | : Nanocomposite materials precursor to chitosan in the development of sensors: Detection of micro-pollutants and heavy metal toxic ions from aqueous solutions. |
| <b>DATE OF ADMISSION</b>              | : 9 <sup>th</sup> August, 2018                                                                                                                                  |
| <b>APPROVAL OF RESEARCH PROPOSAL:</b> |                                                                                                                                                                 |
| 1. B.O.S.                             | :16 <sup>th</sup> October 2018                                                                                                                                  |
| 2. SCHOOL BOARD                       | : 25 <sup>th</sup> October 2018                                                                                                                                 |
| 3. MZU REGN. NO.                      | : 2010616                                                                                                                                                       |
| 4. Ph.D. REGISTRATION NO.& DATE       | :MZU/Ph.D./1176 of 25.10.2018                                                                                                                                   |
| 5. EXTENSION                          | : NA                                                                                                                                                            |

Head

Department of Chemistry

## **ABSTRACT**

# **NANOCOMPOSITE MATERIALS PRECURSOR TO CHITOSAN IN THE DEVELOPMENT OF SENSORS: DETECTION OF MICRO-POLLUTANTS AND HEAVY METAL TOXIC IONS FROM AQUEOUS SOLUTIONS**

**AN ABSTRACT SUBMITTED IN PARTIAL FULFILMENT OF  
THE  
REQUIREMENTS FOR THE DEGREE OF DOCTOR OF  
PHILOSOPHY**

**SARIKOKBA**

MZU REGISTRATION NUMBER: 2010616

Ph.D. REGISTRATION NUMBER: MZU/Ph.D./1176 OF 25.10.2018



**DEPARTMENT OF CHEMISTRY  
SCHOOL OF PHYSICAL SCIENCES  
SEPTEMBER, 2022**



## ABSTRACT

NANOCOMPOSITE MATERIALS PRECURSOR TO CHITOSAN IN  
THE DEVELOPMENT OF SENSORS: DETECTION OF MICRO-  
POLLUTANTS AND HEAVY METAL TOXIC IONS FROM  
AQUEOUS SOLUTIONS

BY  
SARIKOKBA  
Department of Chemistry

Under the supervision of  
Prof. DIWAKAR TIWARI

Submitted  
In partial fulfilment of the requirement of the Degree of Doctor of  
Philosophy in  
Chemistry of Mizoram University, Aizawl.

## Abstract

The rapid increase in population, urbanisation, and industrialisation have led to consequences such as polluting the aquatic environment through municipal waste, discharge from industries and mining areas, chemical runoff, and other non-biodegradable pollutants that are released without proper treatment. Some heavy metals are recognized for being important in human bodies in minute quantity, yet exceeding the required quantity has negative consequences. Some non-essential heavy metals ions such as As, Pb, Cd, Hg etc. are highly toxic toward living beings and are non-biodegradable, causing serious threat to the human health and environment. Among the heavy metal toxic ions, Pb (II) is a non-essential toxic metal but having varied applications in diverse areas. The release of lead into the environment is eminent and polluting the environment. Pb (II) readily bio-accumulated in bones and kidney, and causes serious damage to central nervous system, renal function. The World Health Organization (WHO) has set a maximum tolerable level of 10  $\mu\text{g/L}$  in drinking water. On the other hand, widespread use of synthetic chemicals, pharmaceuticals, and personal care products caused elevated levels of these compounds in the aquatic environment. These compounds are known to be emerging water pollutants because they are very persistent, and escape through waste water treatment plants. The tenacious nature of these contaminants causes a significant danger of bioaccumulation and aid in the development of bacteria antibiotic resistance. A variety of contaminants are detected in drinking water, surface water, ground water, sludge and streams with pollutants, which includes bisphenol A (BPA) and triclosan (TCS). These pollutants are emerging endocrine disturbing chemicals (EDC) as well. These compounds are having wide applications in the manufacture of bottles, containers, pipes, etc, which contain BPA, and TCS is employed in various personal care products. BPA behaves as estrogen-17- $\beta$  estradiol, which mimics the normal estrogen-17- $\beta$  estradiol function and binds with estrogen receptors and disrupts the entire estrogen function. TCS discharge into the environment results in greater contamination and is detected in river lake and wastewater. TCS degradation under UV irradiation produces more toxic dioxin-type compounds that lead to greater

contamination and is regarded as carcinogenic to humans in aqueous solutions as demonstrated by the USEPA (United States Environmental Protection Agency).

Although advance analytical techniques such as atomic absorption spectroscopy (AAS), inductively coupled plasma, mass spectroscopy (ICP-MS), X-ray fluorescence spectrometry (XRF), gas chromatography-mass spectrometry (GC-MS) and high-performance liquid chromatography (HPLC) etc. are highly efficient, however; showed several limitations such as high instrument cost, complicated in operation, sometimes time consuming and most importantly only off-site analysis is possible. As a result, an efficient, robust and miniaturized device is a need of the hour, which could be employed for on-site detection of these pollutants. This could enable a proper monitoring of the pollutants in aquatic environments. The electrochemical methods based on efficient sensing electrodes have attracted greater attention in the recent past. The electrochemical methods, in general, user-friendly, robust, efficient, rapid with high precision and cost effective, hence; are useful alternatives for detection of analytes in aqueous medium.

The introduction of newer advanced materials in the fabrication of working electrodes allows the efficient detection of a variety of pollutants in water bodies. The sensitivity and selectivity of electrochemical detection methods are largely dependent on the electrode materials and type of fabrication. The composite and nanocomposite materials precursor to the natural chitosan showed enhanced applications in the diverse area of research.

Furthermore, the greener route of material synthesis has attracted interest in material synthesis since this provides an alternate and environmentally friendly route in addition to being cost effective. The green synthetic approaches involve phytochemicals from plant leaves extract, which efficiently reduces metal precursor ions to zero valent metals and also acts as a capping agent for nanoparticles and stabilizes the nanoparticle from aggregation. Therefore, these phytochemicals serve as an alternative for toxic reducing agents, which minimised the use of toxic chemicals in traditional nanoparticle synthesis. Chitosan is a natural biopolymer having numerous applications due to their intriguing properties such as film forming ability,

adsorption capacity, swelling ability, and chelation toward metal ions. The availability of amino groups in chitosan is suitable for chemical modification and functionalization of polymeric chains using different organic compounds.

Chitosan (CH) was grafted with 3-mercaptopropyl trimethoxysilane (MTS) and trimethoxyoctyl silane (TMS) for synthesizing composite material (CHMTS and CHTMS) and CHTMS was later decorated with Ag(NPs) in *in situ* process to obtain the (CHTMS+Ag(NPs)) nanocomposite material. The synthesized material was employed in efficient and trace detection of Pb (II) and micro-pollutants viz., BPA and TCS from aqueous medium. *Psidium guajava* leaf extract was used to synthesize silver nanoparticles in the nanocomposite materials. The UV-Vis spectra from the synthesized nanocomposite show surface plasmon resonance (SPR) peak at 440 nm, reaffirmed the formation of Ag nanoparticles within the composite material. The synthesized composite and nanocomposite materials were characterised by the FT-IR, SEM-EDX, TEM, XRD and BET analytical tools. Composite and nanocomposite materials were utilised in surface modification of GCE and employed in the determination of Pb (II), TCS and BPA. The fabricated electrodes were characterised electrochemically using CV (Cyclic Voltammetry) and EIS (Electro Impedance Spectroscopy) using the standard redox couple  $[\text{Fe}(\text{CN})_6]^{3-/4-}$ . The electrochemical determination of Pb (II), BPA and TCS were conducted under DPASV (Differential Pulse Anodic Stripping Voltammetry) methods. Various parametric studies were conducted viz., pH, deposition potential, deposition time, influence of interference to demonstrate the deduce the insights of detection methods. Further, the stability and selectivity of fabricated electrodes were extensively conducted in the laboratory experimentations.

The cyclic voltammetric studies were carried out at varied scan rates from 20 to 150 mV/s, and the redox peak currents of  $[\text{Fe}(\text{CN})_6]^{3-/4-}$  were obtained using different fabricated electrodes. A linear relationship was obtained between the square root of scan rate vs the oxidative peak currents for these electrodes inferred that the redox reactions at the electrode surface are diffusion controlled. Moreover, the linear equations were used in calculating the electroactive surface area for all these electrodes using the known Randles-Sevcik equation. The calculated electroactive surface area

of the electrodes is: 0.000895, 0.00237, 0.00493, 0.003899, 0.005827 mm<sup>2</sup> for Bare GCE, CH/GCE, CHMTS/GCE, CHTMS/GCE and CHTMS+Ag(NPs)/GCE, respectively. The EIS study shows that  $R_{ct}$  values decreases significantly for composite and nanocomposite materials as compared to bare GCE, i.e., 7746  $\Omega$  (bare GCE), 663.7  $\Omega$  (CHMTS), 646.6  $\Omega$  (CHTMS) and 431.6  $\Omega$  (CHTMS+Ag(NPs)).

Electrochemical behaviour of the analyte towards different modified GCE was studied under DPAVS technique and the increased oxidative current was obtained using composite and nanocomposite materials modified GCE. The electrochemical determination of Pb (II) was conducted using CHTMS/GCE under optimised experimental condition (pH:4.5, deposition potential: -0.9 V and deposition time: 180.0 sec) at varied concentration of Pb (II) from 5.0  $\mu\text{g/L}$  to 80.0  $\mu\text{g/L}$ . The detection limit of Pb (II) was found to be 2.83  $\mu\text{g/L}$ . Similarly, using the CHTMS+Ag(NPs)/GCE enabled to achieve the LOD of 1.97  $\mu\text{g/L}$ . Furthermore, the micropollutants viz., BPA and TCS was studied using composite material modified GCE (CHMTS/GCE) at the optimised experimental conditions as: pH: 10.0 (BPA) and pH: 8.0 (TCS), deposition potential: 0.2 V and deposition time: 180.0 sec for both the pollutants. The detection of BPA and TCS were studied within the concentration range of 140.0 to 200.0  $\mu\text{g/L}$ . Further, the LOD of these two micropollutants was found to be 5.61  $\mu\text{g/L}$  for BPA and 9.49  $\mu\text{g/L}$  for TCS.

Electrochemical determination of analytes were studied under high concentrations (i.e., 500  $\mu\text{g/L}$  interfering ions for Pb (II) study; 1800  $\mu\text{g/L}$  interfering ions for BPA study; and 2000  $\mu\text{g/L}$  interfering ions for TCS study) of several interfering ions (i.e., Cd (II), Cr (III), Cu (II), Zn (II), Ni (II), GLY, OA, EDTA, PH, HQ, Cl<sup>-</sup>, NO<sub>3</sub>, Mg<sup>2+</sup>, Na<sup>+</sup>) as to demonstrate the selectivity of electrode materials for low level detection of these pollutants in aqueous medium. The detection of Pb (II) using CHTMS/GCE was affected in presence of EDTA. On the other hand, using the CHTMS+Ag(NPs)/GCE, the determination of Pb (II) was hampered in presence of glycine and oxalic acid. Similarly, the detection of TCS and BPA in the presence of these interfering ions was not affected significantly using the CHMTS/GCE.

The stability of these electrodes was ascertained with prolonged (0 to 48 hrs) and repeated operations (10 cycles). Further, the real implications were conducted using the real water samples (collected from Mizoram University's campus groundwater and spring water, and from Aizawl city river water). The collected water sample were filtered before electrochemical measurement to remove impurities and sediments. The water samples were analysed for physico-chemical parametric studies viz., pH, conductivity, salinity, resistivity, oxidation reduction potential and total dissolved solids, IC (inorganic carbon), TC (total carbon) and NPOC (Non-purgeable organic carbon). Several metals were analyzed using the AAS (Atomic absorption spectroscopy). The real water samples were spiked with known concentrations of these pollutants (i.e., Pb (II), TCS and BPA) and analyzed using the fabricated electrodes under the optimized electrochemical conditions. The %recovery of these analytes were then obtained. The recovery of Pb (II) using the CHTMS/GCE was obtained from 99.14 to 102.99% in spring water and 96.98 to 98.33% in ground water. Similarly, utilizing the CHTMS+Ag(NPs), the % recovery of Pb (II) was within 95.52 to 96.06% for spring water and 92.95 to 102.00% for ground water. On the other hand, the micropollutant recovery rate was obtained in real water samples using CHMTS/GCE. The spiked concentrations of TCS or BPA was increased from 160 to 180  $\mu\text{g/L}$ . The BPA percentage recovery was varied from 99.70 to 100.20% in spring water and 102.70 to 102.40% in river water samples. Similarly, the % recovery of TCS varied from 101.1 to 102.8% in river water and from 99.4% to 100.8% in ground water. The high recovery percentage of these pollutants viz., Pb (II), BPA and TCS in real water samples showed greater applicability of fabricated electrodes in real implications. Overall, the laboratory findings are useful input data for the development of miniaturized devices to efficiently detect these potential water contaminants.